A STUDY OF PRE-EQUILIBRIUM PHENOMENA IN PHOTO-NUCLEAR REACTIONS

Thesis submitted by

SHAHRIAR BAYEGAN

for the degree of

DOCTOR OF PHILOSOPHY

University of Edinburgh

August, 1983.

To my parents

ABSTRACT

The aim of this study was to propose a new model calculating pre-compound photo-induced nucleon and α-particle energy spectra at energies below the meson production threshold.

It is assumed that the dominant process above giant resonance would be photo-interaction with two correlated nucleons. The interaction contributions from different shells have been calculated assuming that the basic strength of interaction is related to the photo-disintegration of the deuteron. From this assumption the "pseudo-Levinger constant" for individual shells is theoretically evaluated.

The final state interactions for the two nucleons are based on the pre-compound quasi-free scattering model (Q.F.S.). The idea is that by using the Q.F.S. model the subsequent secondary interaction of particles with the rest of the nucleus, following the initial photo-nucleus interaction, can be taken into consideration.

This new approach is applied to ^{60}Ni where the energy spectra for (γ, p) and (e, α) are calculated. The calculated results are compared to the experimental data giving productive conclusions, where the advantages and disadvantages of the proposed model have been discussed.

ACKNOWLEDGEMENTS

I will always be grateful to my supervisor, Dr. A.C. Shotter, for his valuable advice, forbearance and encouragement throughout my study. Also I am obliged to Dr. D. Branford, especially for introducing me to the Edinburgh Nuclear Structure Group.

I would like to thank Mr. B. Murdoch of Edinburgh Regional Computing Centre for his advice on computing matters and Drs. J.C. McGeorge, A.G. Flowers, M.R. Sene and I. Anthony for their direct or indirect assistance. I am indebted to Mrs. Chester for her elegant and excellent typing of this thesis. My thanks also go to some friends for their moral support, enabling me to accomplish this work.

Last but not least I am grateful and indebted to my parents for their moral and financial support, encouragement and patience.

C O N T E N T S

C O N T E N T S (Contd).

CONTENTS (Contd.)

CONTENTS (Contd.)

CONTENTS (Contd.)

CHAPTER I

INTRODUCTION TO THE THESIS

1.1.Ø Pre-compound Emission in Photo-nuclear Reactions

The study of pre-compound particle decay has been continued with increasing effort in the last few years, both by experiment and in theory. However most of these investigations have been applied to obtain and to interpret data for pre-compound effects arising from nucleon-induced reactions. In recent years there have been numerous experimental efforts to use electromagnetic probes, photons and electrons, to investigate pre-compound particle emission. For instance, measurements of photon-induced pre-compound complex-particle decay have been carried out for medium-weight and heavy nuclei[1,2]. The energy spectra of the α-particle in Figures 1.1 and 1.2 represent examples of electron-induced pre-compound effects for ^{60}Ni and ^{197}Au nuclei.

There are two well-marked energy regions in these spectra; the low energy region which exhibits the shape expected for compound nucleus reactions, the medium energy region characterised by its continuous shape which declines with respect to increasing energy of outgoing particles. Of course there is a high energy region characterised by peaks corresponding to the excitation of particular low-lying states in the target by direct processes. However the latter region has not been covered by these figures.

The interpretation of the mechanisms involved in photo-induced pre-compound particle decay has been described by several attempts[3,4].

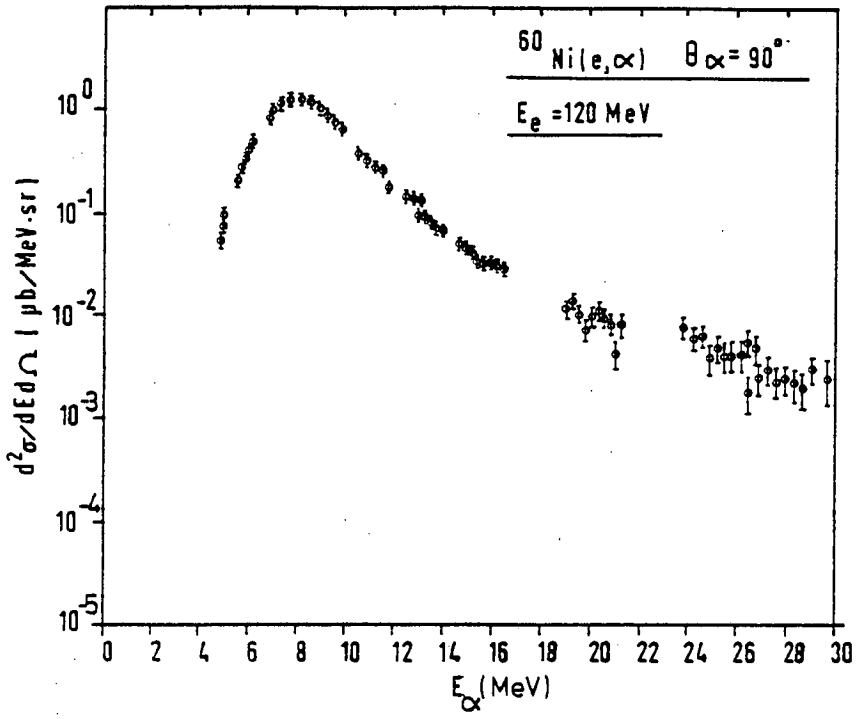

Figure 1.1: The measured energy spectra for ^{60}Ni at $\theta_\alpha = 90^\circ$, $E_e = 120$ MeV, is shown by empty circles (ref. 1).

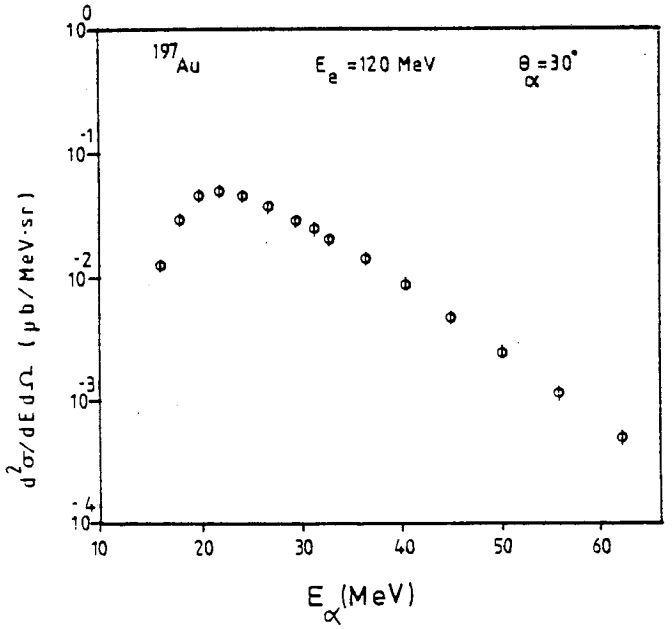

Figure 1.2: The measured energy spectra for ^{197}Au at $\theta_\alpha = 30^\circ$, $E_e = 120$ MeV is shown by empty circles (ref. 1).

These theoretical works have basically assumed that the process of absorbing a real or virtual photon by the nucleus can be dominantly proceeded by an interaction with a correlated neutron and proton in the energy region above giant resonance. The primary generated neutron and proton subsequently interact with the rest of the nucleus. This final state interaction is particularly important for medium and heavy nuclei.

An attempt based on Monte Carlo Cascade calculations was the first theoretical work suggested[3] to produce the photo-induced pre-compound nucleon emissions. This approach used the Levinger model of quasi-deuteron[5] to generate primary neutron and proton, then the final state interactions were calculated by using the intra-nuclear cascade model (Fig. 1.3), (see section 1.3.2). Although photo-induced cascade reaction models were successful in producing experimental data, these models are inapplicable for interpretation of photo-induced cluster emission processes.

The second approach proposed by Wu and Chang[4] was intended to describe photo-induced pre-compound nucleon and cluster emissions. This approach was based on a similar idea of producing primary neutrons and protons using the quasi-deuteron model. However, the final state interactions were taken into account by use of the pre-compound exciton model (see section 1.3.2). Although this synthetic approach produced surprisingly encouraging results (Figures 1.4 and 1.5) for photo-induced pre-compound cluster emissions, it should be noted that the dynamics of the nucleon-nucleon and nucleon-α-particle were ignored in this type of exciton model. Furthermore, the photonuclear reactions were assumed to take place on stationary neutron-proton pairs and consequently the momentum distribution of a correlated neutron-proton was not taken into account.

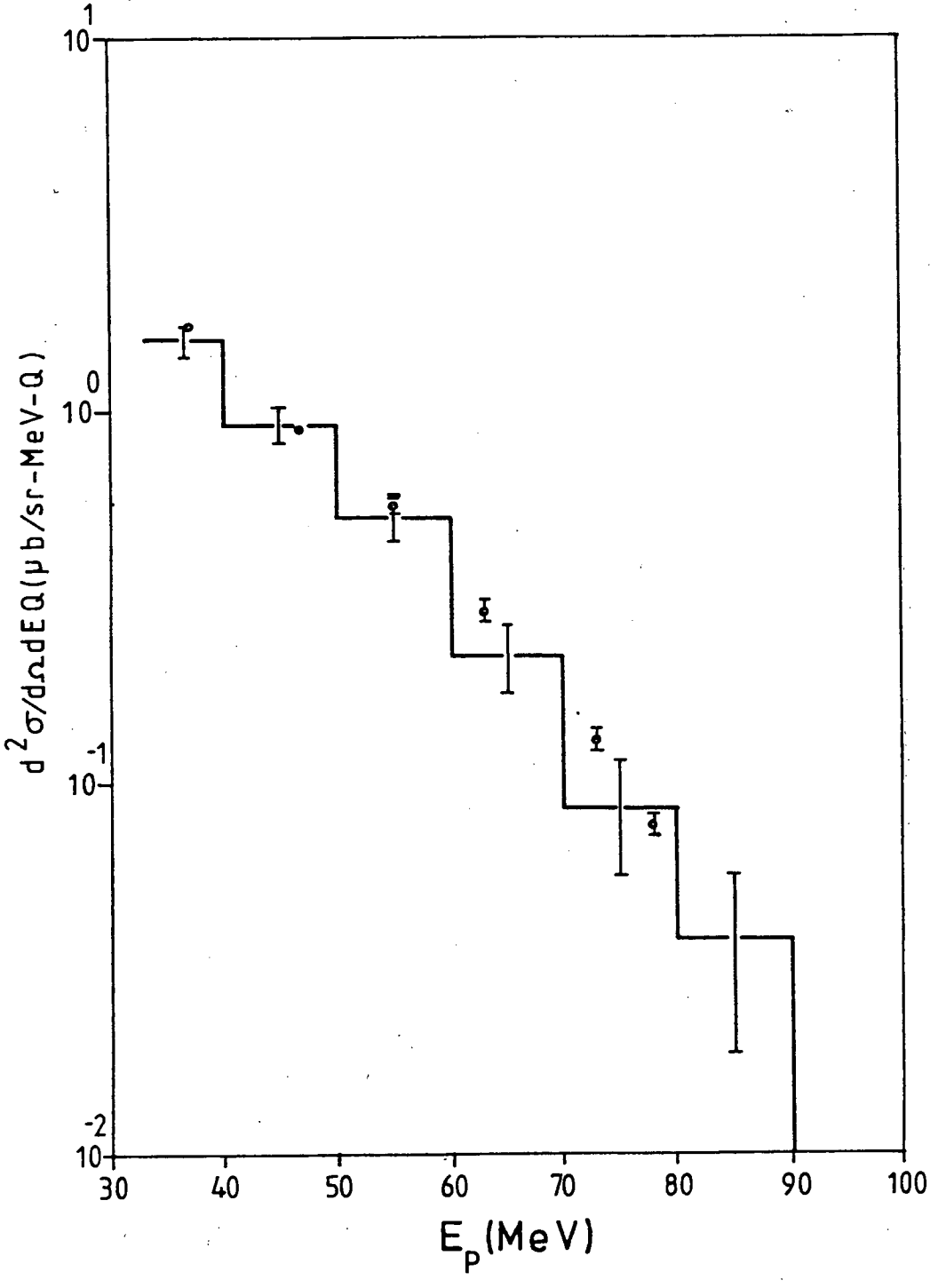

Figure 1.3: The calculated proton differential cross-section at 51.4^o resulting from 110 MeV Bremsstrahlung photons on ^{12}C. Empty circles: experimental data (Ref. 3). Solid curve: modified intra-cascade calculation (Ref. 3).

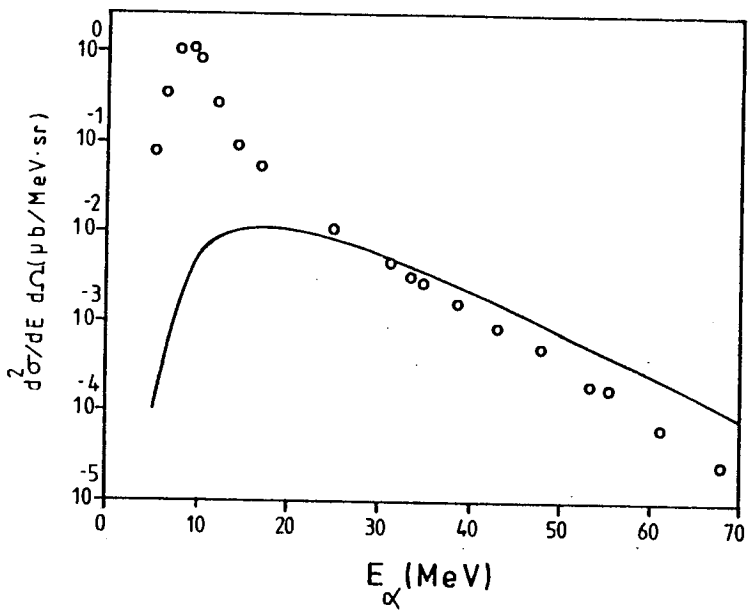

Figure 1.4:

The measured energy spectra compared[1] to modified exciton model calculation for alpha particles. Empty circles: experimental data (Ref. 1). Solid line is the modified exciton model result. Alpha particle energy spectra is at $\theta_\alpha = 30^\circ$ for $E_e = 120$ MeV.

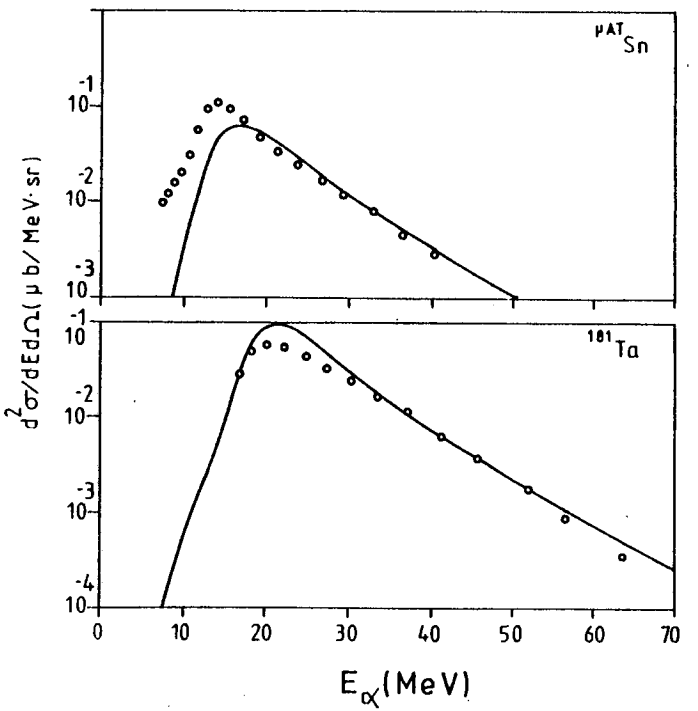

Figure 1.5:

The measured energy spectra compared[2] to modified exciton model calculation for alpha particles. Empty circles: experimental data (Ref. 2). Solid line is the modified exciton model result.

In the present study a new approach will be suggested for the calculation of nucleon and α-particle energy spectra resulting from photonuclear reactions at energies below the meson production threshold. This approach basically uses the idea of photon absorption by a correlated neutron and proton and effectively considers the momentum distribution of correlated pairs. Furthermore, shell model configurations will be used in contrast to the Fermi gas model states adapted in the quasi-deuteron model of Levinger. Therefore the photo-induced cross-sections will be separately calculated for different shells.

In the quasi-deuteron model the Levinger constant (see section 1.2.2) is theoretically evaluated. However there is wide disagreement on the value of this constant and it is often left as a floating parameter in fitting data. A range of values between 2 - 15 can be found in the literature for the Levinger constant. The present study, however, considers the variation of the Levinger constant for different shells by theoretically evaluating it.

The problem of the final state interactions for the primary generated protons and neutrons will then be considered by incorporating the pre-compound model of quasi-free scattering[6] (see section 1.3.2 and Chapter III). This pre-compound model has been proposed to explain the interaction mechanism of (N,N') and (N,α) reactions where the dynamics of nucleon-nucleon and nucleon-alpha scattering inside the nucleus have been taken into consideration.

Thus, the present study intends to synthesise two models, the quasi-deuteron model and the quasi-free scattering model to investigate the energy spectrum of reactions of type $(\gamma \nearrow \begin{matrix} n' \\ p' \end{matrix} \searrow p)$ and $(e \nearrow \begin{matrix} n \\ p \end{matrix} \searrow \alpha)$ or generally (γ,p) and (e,α) reactions.

In this chapter, firstly the photonuclear reactions at the energy region above giant resonance and below pion threshold will be reviewed (section 1.2.Ø). Then the problem of the final state interactions and the different models proposed for pre-compound process will be considered (section 1.3.Ø). Finally, the objectives of the present study will be explained (1.4.Ø).

In Chapter II the quasi-deuteron model will be re-examined and the formalism for calculating double differential cross-sections of primary generated neutrons and protons will be constructed. The pre-compound model of quasi-free scattering will be discussed in Chapter III, where the formalism for evaluating the probabilities of final state interactions will be considered. In Chapter IV the task of bringing the quasi-deuteron and pre-compound quasi-free scattering models together will be fulfilled and the combined model will be compared with the experimental data. Finally, a conclusion to the present study will be given in Chapter V.

1.2.Ø Survey of Photo-Absorption Mechanism

1.2.1 Introduction

Electromagnetic interactions with nuclei can be grouped into three categories on the basis of the incident photon or virtual photon energies. These are the giant resonance region ($E_\gamma \lesssim 30$ MeV), the region between the giant resonance and the pion threshold ($30 \text{ MeV} \lesssim E_\gamma \lesssim 150$ MeV), and the region above the pion threshold ($E_\gamma \gtrsim 150$ MeV). In each region there is a characteristic type of event. In what will follow, these regions and the corresponding characteristics will be briefly discussed.

In the giant resonance region, the incident photon interacts mainly with the dipole-moment of the target nucleus and the nucleus de-excites by emitting particles or α-rays via the compound nucleus mechanism. It is theoretically interpreted that the main photo-absorption is given by the dipole excitation of the nucleus. This interpretation is supported by the fact that the integrated cross-section, $\int\sigma(E)dE$ for E1 exhausts a large fraction (generally $\geq$ 70%)[7] of the value expected from the dipole sum rule in absence of exchange and velocity dependent nucleon-nucleon potentials. Furthermore, the isovector giant quadrupole resonance is expected to lie in the photon energy between about 25 and 50 MeV. However, the integrated cross-section, $\int\sigma(E)dE$ for E2 strength, is of the order of 10 - 15% of the corresponding sum for the E1 strength.

Although in the energy range between the giant resonance and pion threshold (30 - 150) MeV no detailed neutron-proton coincidence data are available, the measurements[8] of the total photonuclear cross-section $\sigma_{tot}(E_\gamma)$ indicate that the interaction between a photon and a complex nucleus is dominated by the (γ, np) cross-section. A recent measurement[9] of the total photo-absorption cross-section by the Mainz group on ^{12}C or ^{16}O at above 40 MeV indicates that the combined (γ, p) and (γ, n) total cross-sections are much smaller than the (γ, np) total cross-section. More recently[10] cross-sections for heavier nuclei such as Sn, Ce, Ta, U and also ^{16}O have been provided by the Saclay group. According to detailed assessment given by this group, there is strong evidence that for $E_\gamma \geq 45$ MeV the $\sigma_{tot}(E_\gamma)$ is dominated by (γ, np) cross-sections. Furthermore Findlay et al.[11] and Göringer et al.[12a] recently reported comparable magnitudes for the (γ, p_o) and (γ, n_o) cross sections $(\sigma(\gamma, p_o)/\sigma(\gamma, n_o) \leq 1)$. These results have provided

stronger belief that the direct single-nucleon knock-out effect does not give a correct picture of the photo absorption mechanism[12b].

For the region above the pion threshold, the interaction between a photon and the individual nucleon associated with pion production competes with the photon absorption by a neutron-proton pair.

The region of interest in the present investigations is the photon energy region above giant resonance up to pion threshold. In section (1.2.2) a survey of the main theoretical developments concerning the photo-absorption mechanism and in particular the (γ, np) reaction type will be given. Finally, in subsection (1.2.3) the three following questions will be discussed:

(a) Does the dominant mode of absorption of an intermediate-energy photon take place on a correlated proton-neutron pair in the nucleus?

(b) Can the single-particle absorption model largely explain the photo absorption mechanism?

(c) Can the photon be absorbed by a cluster structure within the nucleus such as in a quasi - α-particle model?

1.2.2 Review of Different Models for Photo-Interactions with Nuclei at Intermediate Energies (30 MeV $\leq E_\gamma \leq$ 150 MeV.

The first step towards a theoretical description of photonuclear processes was taken by Levinger [5] in 1951 when he introduced the quasi-deuteron model for the energy region up to several hundred MeV (E_γ > 200 MeV). In this model a link is established between the total photo-nuclear cross-section and photo-disintegration of a free

deuteron. Within the framework of this simple model, the photonuclear absorption cross-section for a $_{Z}A_{N}$ nucleus, extrapolated to photon-energies in the 30 MeV $\lesssim E_\gamma \lesssim$ 150 MeV range, can be expressed as

$$\sigma_{qd}(E_\gamma) = L \frac{NZ}{A} \sigma_d(E_\gamma) \qquad (1)$$

where $\sigma_d(E_\gamma)$ is the photo-disintegration cross-section of the deuteron and L is the Levinger constant. According to this expression, which stresses the importance of correlated neutron-photon pairs in the photoabsorption mechanism, the total photonuclear absorption cross-section is proportional to the total number of neutron-proton pairs NZ and the photodisintegration cross-section $\sigma_d(E_\gamma)$, $(\gamma + D \rightarrow p + n)$. Furthermore, the factor $\frac{L}{A}$ is introduced because the nuclear density is greater than the deuteron density (see Chapter II). However this model did not consider a realistic picture for the correlated proton-neutron pairs inside the real nuclei, i.e., the binding energy and Fermi-motion effects were neglected. Levinger's quasi-deuteron model, therefore, overestimates the cross-sections for photon energies below E_γ = 150 MeV. Thus the calculation of cross-section given by expression (1) can be adjusted by changing the Levinger constant (a range of values (2 - 15) exists in the literature for this constant). The problem of overestimation of the cross-section by expression (1) led Levinger to propose a so-called "modified quasi-deuteron model", which expresses the total photonuclear absorption cross section[13] as

$$\sigma_{mqd}(E_\gamma) = L \frac{NZ}{A} \sigma_d(E_\gamma) \exp\left(\frac{-D}{E_\gamma}\right) \qquad (2)$$

where the factor $\exp\left(\frac{-D}{E_\gamma}\right)$ is essentially introduced for considering the Pauli blocking effect in the final states with D as an arbitrary

constant. Although expression (2) improves fit to the experimental data with respect to the original expression (1), it is quite obvious that the factor $\exp(\frac{-D}{E_\gamma})$ has been arbitrarily introduced. Furthermore, expression (2) like expression (1) has not taken into account the binding energy and Fermi-motion effects. Recently, however, a new approach based on the original formulation of the quasi-deuteron model (Eq. (1)) has been suggested by Laget[10,14]. In this approach the binding energy and Fermi-motion effects for correlated neutron-proton pairs inside the real nuclei has been considered. Here, the photo-absorption mechanism below the pion threshold has been interpreted by considering that the photon interacts with the nucleus through its direct coupling to the exchange currents. This picture indicates that the free deuteron cross-section $\sigma_d(E_\gamma)$ in expression (1) can be replaced by $\sigma_d^{exch}(E_\gamma)$, i.e. the transition amplitude for a virtual meson to be emitted by one nucleon of the deuteron and reabsorbed by the other. Thus this new approach proposes a new expression in the same spirit as that of Levinger's original expression (Eq. (1)), without taking the final state interactions into account.

$$\sigma_{qd}(E_\gamma) = \frac{LNZ}{A} \sigma_d^{exch}(E_\gamma) \quad . \qquad (3)$$

The comparison of the theoretical results obtained from expression (3) with the experimental data confirm that above E_γ = 60 MeV the main photonuclear reaction mechanism is very likely to be the (γ, np) interaction. Moreover this calculation reproduced data reasonably well and this indicates the importance of the meson-exchange current in the reaction mechanism (see Chapter II, subsection 2.2.2.3).

The above mentioned models assume that the photonucleons leave the nucleus intact. While the fact is that these primary generated nucleons may collide with other nucleons before they leave the nucleus, the collided nucleons may fail to escape the nucleus and be reflected from its surface. These final state effects will have an impact on the final cross-sections and they will change the magnitudes and shapes of double differential and photonuclear cross-sections.

The energy and angular distribution of the primary generated photonucleons using the quasi-deuteron model were calculated with the most widely used approach given by Matthews[15]. This successful evaluation of double differential cross-sections considers the momentum distributions of the neutron-proton pairs inside the nucleus. In this approach, however, the treatment of the binding energy of the correlated neutron-proton pairs was arbitrarily introduced (see section 2.2.3). The comparison of double differential cross-section with experimental data produced reasonable agreement. However the Levinger constant was left as a floating parameter. Furthermore the final state interactions were not considered in the Matthews approach.

Another major step in improving the quasi-deuteron model was made by Gottfried[16]. In this approach the nuclear matter model employed by Levinger was replaced by a more realistic model, i.e., the independent-pair model for finite systems. Gottfried assumed the two-particle absorption mechanism to be fundamental. The (γ, np) cross-section was then written for the closed shell nuclei as

$$d\sigma = (2\pi)^{-4} F(K) \sum_{fi} \delta(E_f - E_i) d^3k_p \, d^3k_n \quad . \qquad (4)$$

The cross-section is given by the product of three factors, (1) the available phase space, (2) the momentum distribution F(K) of the centre-of-mass of the neutron-proton pair with total momentum $\vec{K}$ ($\vec{K} = \vec{K}_n + \vec{K}_p - \vec{\omega}$), and (3) a function S_{fi} which depends on the relative momentum of the paired nucleons. The pair momentum distribution F(K), at least in principle, is calculable from the shell model and it is not a significant quantity from a dynamical point of view. It determines, however, the shape of the neutron and proton angular correlation. The quantity S_{fi} contains the nuclear dynamics, e.g. short range correlations, which mainly influence the photon energy dependence and absolute magnitude of the two body photodisintegration cross-section.

In equation (4), Gottfried calculated the quantity S_{fi} by using the deuterium cross-section. The assumption is that if the neutron-proton pair wavefunction, at relative distance (x) much less than the nucleus radius ($x \lesssim 10^{-13}$cm), is to be identical to the free deuteron wavefunction in the same range, one can get the Levinger result. Therefore using $S_{fi} \equiv 3\gamma {}^3D_{fi}$, where γ is a proportionality constant and the transition probability D_{fi} is related to the free deuteron photon-disintegration cross-section in the centre of momentum frame. Equation (4) is applicable for those nuclei which are closed shells (e.g. ^{16}O, ^{40}Ca). But for other targets two complications will arise: (i) the form factor F(K) is no longer a function of $|\vec{K}|$ only. This indicates that F(K) can not be defined as the probability of finding two particles of total momentum $\vec{K}$ and zero separation in the Slater determinant; (ii) S_{fi} contains interference terms. This complication eliminates the possibility of determining S_{fi} from

the photo-effective deuterium as mentioned before.

There are other calculations using the model of independent pairs[17-21]. In these approaches the photon is assumed to be absorbed by a correlated proton-neutron pair and the nucleon-nucleon correlations are treated explicitly in a shell model framework. Whereas in the Gottfried and Levinger approaches the experimental deuteron photo-disintegration cross-sections are used as an input.

Recently the question of validity of quasi-deuteron and the reason for its success has been investigated by the Bochum group[22]. They have discussed the dynamical aspects of photo-nuclear reactions over a wide range of energies from 40 to 400 MeV. The transition amplitude is considered to be made up of three components: (1) shell-model, (2) meson-exchange currents and (3) nucleon-nucleon correlations. The main purpose of Bochum's work is to see at what energies and cross sections the different contributions of shell-model exchange and correlations dominate. In this approach[23] the (γ, np) total cross-section on ^{16}O was calculated and the dominance of the exchange contribution to the transition matrix shows that the (γ, np) process is supposed to be the dominating photonuclear reaction in energy range of $60 \lesssim E_\gamma \lesssim 140$ MeV (see section 1.2.3). With respect to other partial cross-sections like (γ, pp) or (γ, nn), because of vanishing meson exchange contribution for proton-proton and neutron-neutron states the (γ, pp) and (γ, nn) contributions do not contribute (see section 2.2.Ø).

Apart from exchange current, Gari and Hebach[23] also considered the correlation contributions to (γ, np), (γ,nn) and (γ, pp).

However the amounts of these correlations in contrast to exchange current contributions for (γ, np) is about 1%. The remaining contribution is due to pure shell-model. This contribution vanishes, since a one-body operator cannot excite two nucleons at the same time. The work of Gari and Hebach with the recent suggestion by Laget[14,24] emphasise the importance of the meson-exchange current in the reaction mechanism (see sub-section 2.2.2.3). This type of contribution can explain the large enhancement of the total photo-absorption compared with the Thomas-Reiche-Kuhn sum rule which ignores these contributions.

In several papers by Noguchi and Parts[25,26] the quasi-deuteron mechanism has been investigated in connection with (γ, p), (γ, n) and (γ, np) reactions. The calculations presented by Noguchi and Parts differ from Gari and Hebach's calculation. In the Noguchi and Parts approach the use of scattering amplitudes instead of the wavefunctions was emphasised. The quasi-deuteron contribution to the photodisintegration process followed Levinger's method of expressing the quasi-deuteron process in terms of the photodisintegration of a real deuteron, i.e. the deuteron photodisintegration amplitude off the energy shell. Noguchi and Parts developed the quasi-deuteron model of Levinger by calculating the on-the-energy-shell contribution by considering the $^4He(\gamma,pnd)$ reaction. The cross-section for this reaction was found to be in general agreement with experiment. This method uses the $^4He(\gamma,pnd)$ amplitude to calculate the $^4He(\gamma,N)T$ cross-section (where N = proton, or neutron and T = ^3H or ^3He respectively). In this type of calculation Noguchi and Parts concluded that above 60 MeV the quasi-deuteron mechanism in addition to the single nucleon absorption mechanism contribute to the photodisintegration cross-

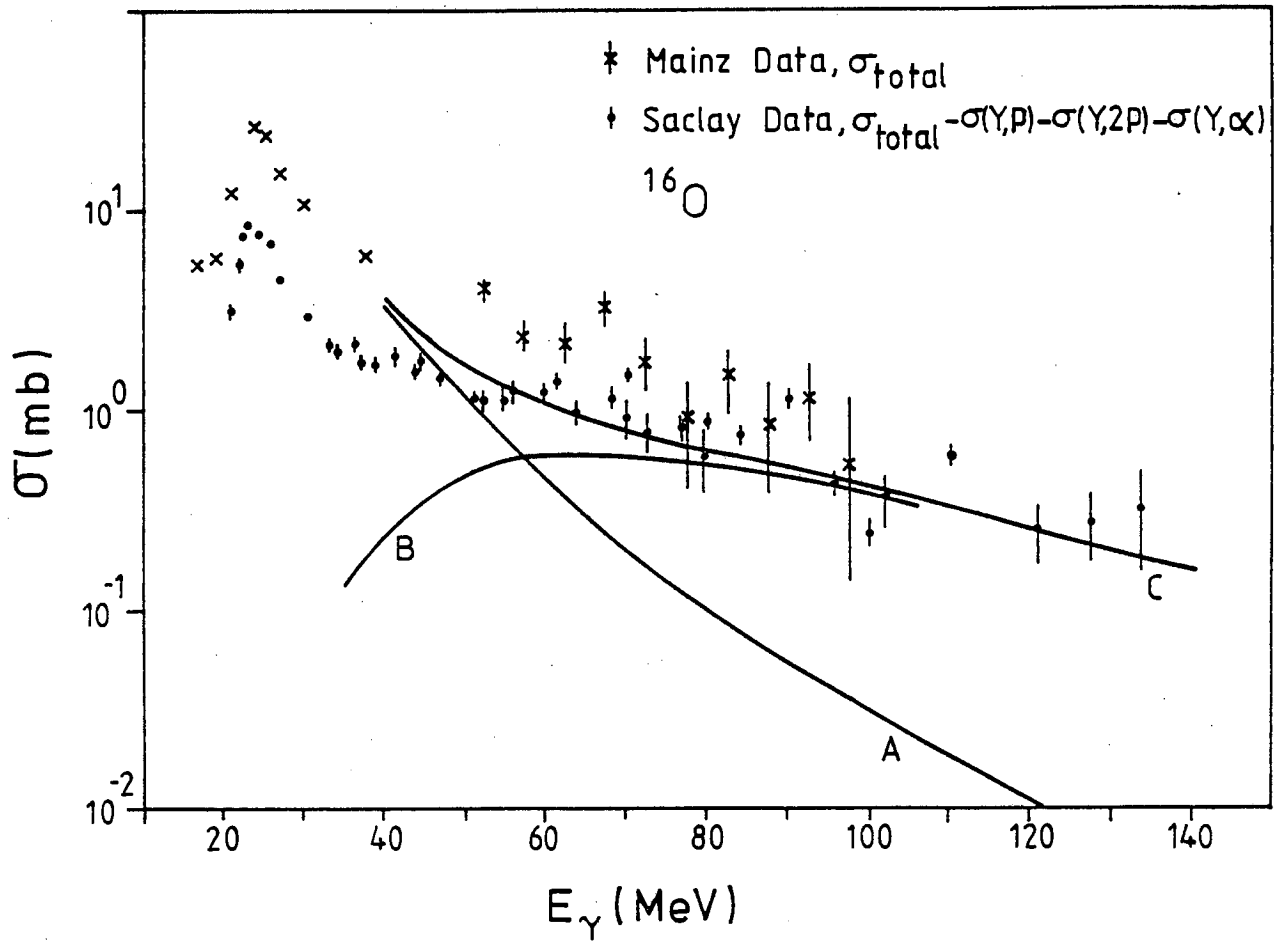

Figure 1.6: Photonuclear cross-sections for ^{16}O. Curve A: calculated total cross section for single-nucleon emission $(\gamma,p) + (\gamma,n)$ from the P-shell. Curve B: calculated total cross section for (γ, pn). Curve C: sum of A and B, i.e. sum of the cross-sections for (γ, pn), (γ, n) and (γ, p). Curves A, B and C are calculated by Gari and Hebach (ref. 23).

section. However, the quasi-deuteron contributions dominate strongly the direct contribution at photon energies around and above 100 MeV. This conclusion was also reached by Gari and Hebach, using the above mentioned alternative approach.

Another alternative method[27-29] of calculating the effect of photo-absorption by a nucleon pair is to extend the independent particle model by including Jastrow-type N-N short-range correlations. It turned out that, if the range of these two-body correlations does not exceed the range of typical hard core or soft core effects, there is no important change of the results obtained within the pure shell model, at least for energies below 100 MeV.

Although the idea underlying the quasi-deuteron model namely the absorption of a photon by a neutron-proton pair, is certainly correct in energy region $E_\gamma > 60$, the contributions due to (γ, p) and (γ, n) reactions should be taken into account. Gari and Hebach[23] in their suggested model calculated the total cross-section for the reactions $^{16}O(\gamma, p)$ and $^{16}O(\gamma, n)$. These calculations (Fig.1.6) indicate that the (γ, np) cross-section is equal to the combined cross-sections of (γ, p) and (γ, n) reactions (for emission from the p-shell of ^{16}O) near 60 MeV photon energy and exceeds them by a factor of ten at 100 MeV.

In analysing the (γ, p_o) and (γ, n_o) reactions in ^{16}O (leaving the residual nucleus in its ground state) the proposed model of Schoch[30] for photo-disintegration cross-section attracted some attention. The expression which Schoch proposed uses the idea of the quasi-deuteron model. This model factorises the cross-section into the deuteron photo-disintegration cross-section $(\frac{d\sigma}{d\Omega})_d$ (to be taken from experiment) and a factor which is determined by the overlap of the nuclear wavefunctions in the initial and final states,

$C(\vec{\omega}, \theta)$:

$$\frac{d\sigma}{d\Omega} = \frac{L}{A} \left(\frac{d\sigma}{d\Omega}\right)_d J P_S C(\vec{\omega}, \theta) \qquad (5)$$

where L is an adjustable constant, J and P_S are Jacobian and phase space factors respectively. $\vec{\omega}$ is photon momentum and θ is the angle of the outgoing particle. The model assumes that in the case of proton detection, the neutron is to be absorbed into the ground state of the (A - 1) nucleus. The results of this calculation are in close agreement with the existing (γ, p_o) and (γ, n_o) data below 100 MeV. In the Schoch calculation, a value of 5.4 has been suggested for the Levinger constant (L). It should be noted that if use has been made only of the exchange part, $\left(\frac{d\sigma}{d\Omega}(E_\gamma)\right)_d^{exch}$, of the deuteron differential cross-section, the Levinger constant ought to be increased. The reason for such replacement of $\left(\frac{d\sigma}{d\Omega}\right)_d$ with $\left(\frac{d\sigma}{d\Omega}\right)_d^{exch}$ could be found in the use of the $(\pi + \rho)$ meson exchange part of the differential cross-section for the deuteron. This idea simply means that the exchange part is the only contribution responsible for the absorption of the photon by a correlated pair and it is a matter for further discussion and investigation.

In the next section a brief assessment of the present section will be given and the questions raised in section (1.2.1) will be answered.

1.2.3 Discussion Related to the Selection of a Model for Photo-Absorption Mechanism.

The questions raised in section (1.2.1) can now be answered, using the review of different models presented in section (1.2.2). The first question was about the dominant mode of absorption of

photons in the intermediate energy. Figure 1.6 taken from Gari and Hebach's calculation[23], clearly indicates that the dominant mode is (γ, np) above E_γ = 60 MeV. This indicates that the model of Levinger, namely, the absorption of a photon by a correlated proton-neutron is indeed correct. However, it should be pointed out that the recent calculations by the Bochum group[23] and Laget[10,14] indicate the interaction of a photon with a nucleus through direct coupling between the photon and the exchange currents. In Chapter IV of this study an attempt will be made to speculate on this point.

The second question in section (1.2.1) was related to the role of the single-particle absorption mechanism. This mechanism is certainly not a dominant process in the region above $E_\gamma > 60$ MeV. However, its contribution to total cross-section is significant about E_γ = 60 MeV (Fig. 1.6).

The third question was concerned with the contribution due to the absorption of photons by clusters, such as three or four particles. For $E_\gamma \lesssim 150$ MeV the wavelength of the photon is $\lambda \gtrsim 1.3$ fm and the probability that three or four nucleons will be present in a nuclear volume of these linear dimensions may not be small in comparison with the probability of finding two nucleons in this volume. Consequently, it must be expected that the multiparticle photo-absorption mechanism will be of definite importance in this energy range, and its importance will increase with decreasing photon-energy. Taran[31] gave a confirmation for the above idea by measuring photo-absorption by ^{12}C at $E_\gamma \lesssim 170$ MeV. An interesting result is that in the region 60 MeV $\lesssim E_\gamma \lesssim$ 100 MeV, the contribution to total cross-section from a multi-particle absorption mechanism is about 6.2 MeV-mb. This indicates that more experimental results and more theoretical investigations are necessary to confirm the role of multi-particle absorption

mechanisms.

In the next section the different models suggested for the pre-compound process will be considered. The purpose of this survey is to see the prospect of using such models for taking into account the final state interactions for photo-nucleons produced by the primary photon-absorption event.

1.3.Ø The Final State Interactions for Photo-Induced Reactions

1.3.1 Introduction

Photo-nucleons produced by the primary photon-absorption process with a neutron-proton pair inside the nucleus may collide with other nucleons before they leave the nucleus, but prior to escape from nucleus they may be reflected from its surface. These effects will reduce the number of neutron-proton coincidences. There are other possibilities which also exist, e.g. the collision of primary photo-nucleons with pre-formed α-particles or other complex particles such as ^{3}He, t and d.

There are two synthesised models for taking into account the final state effects for (γ, np) reactions. These synthesised models are basically based on making a link between the quasi-deuteron model of Levinger and a pre-compound model for nucleon-induced reactions. These synthesised models are:

(i) Monte-Carlo Cascade calculations[3],

(ii) Wu and Chang modified exciton model.[4]

In the introduction to this chapter an assessment of these two synthesised models has been given. However in the following sections a review of different pre-compound models will make clear the advantages and the disadvantages of these models generally, in

particular that type of pre-compound models which were used in the above mentioned synthesised models.

1.3.2 Review of Different Models for Pre-Compound Processes in Nuclear Reactions

Neils Bohr introduced the compound-nucleus model in 1936[32]. The basis of this model is the independence hypothesis. The physical picture of his suggestion was the immediate formation of an intermediate system in the course of interaction of a projectile with a target nucleus. Bohr emphasized that the break up of this intermediate system must in fact be considered as a separate process which has no immediate connection with the first stage of the encounter.

In 1947, Serber's remarks[33] gave indication that the Bohr independence hypothesis can only be justified when the system, i.e. projectile and target nucleus, loses fully the memory of the incident channel. The essence of Serber's idea was that there is a series of direct processes in the form of successive nucleon-nucleon collisions within the nucleus. These are generated by the incident high-energy nucleon which results in the direct emission of some of the nucleons that participate in the consequent collision cascade.

In the early 1960's, experimental measurements[34] confirmed these direct emissions by the observation of a long and continuous region between a compound nucleus and direct interaction (Fig.1.7)[35]. These direct emissions are not accounted for by either the conventional compound-nucleus or the usual direct reaction theory.

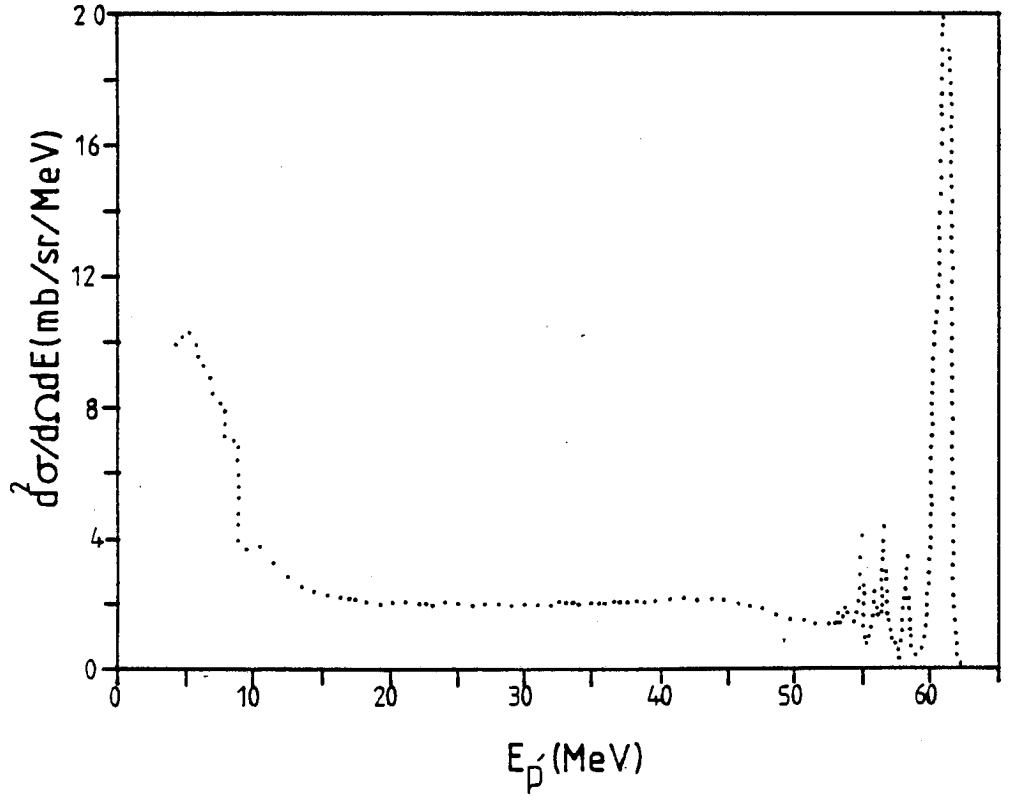

Figure 7: Spectra from the (p,xp') reaction for 62 MeV protons on ^{56}Fe at 37° (ref. 35).

It is also experimentally observed that energy spectra show very similar shapes for different nuclei, i.e. a low energy peak plus an exponential decrease in cross-section, with increasing particle energy. The angular distribution of complex and non-complex particles emitted in a statistical reaction is predicted to be symmetric about 90^{o}. However, if the particles are emitted in some form of direct or pre-equilibrium reaction, a forward peaked angular distribution is predicted.

The problem of continuous spectra was initially investigated theoretically by Griffin[36]. Since this major initiative in 1966, different models have been suggested for the physical processes in this interaction region between compound nucleus and direct interaction processes.

In this section, these models will be reviewed and their underlying theories will be discussed. Five groups of models can be identified:

1) group A (Exciton and Hybrid Models)
2) group B (Cascade type Models)
3) group C (Hot Spot type Models or Cluster Models)
4) group D (Relaxation type Models)
5) group E (Quantum Mechanical Approaches).

1.3.2.1 Group A (Exciton and Hybrid Models) - General Remarks

The first evidence of a smoothly varying background of the particle spectra beyond the evaporation maxima was observed long ago[34]. Griffin successfully attempted to interpret this continuum in particle spectra by suggesting the exciton model[36],

in which it was assumed that equilibration between target and projectile was achieved by a succession of two-body interactions between the projectile and target nucleus.

Models of group (A)[36,40] describe the states of an excited nucleus by characterizing them by a number, n, of excited particles, P, and holes, h, referred to as the excitons (n = h + P). Excitons are defined with respect to the Fermi energy of the target. In the first strike the projectile interacts with a nucleon and excites a particle-hole pair. These states have the characteristic of (2P,1h) and its exciton number is 3. A state of a given n, can decay either by means of a residual two-body interaction to states having a number of excitons $n \pm 2$ or by emitting a particle of a certain energy in the continuum. This indicates that the excitation of the nucleus with n^{th} excitons are more complex than those of the $(n - 2)^{nd}$ excitons and less complex than those of the $(n + 2)^{nd}$ excitons.

The main physical assumption to explain continuous particle spectra is the exciton assumption. If the equilibration time t_{equ} is large in comparison to the decay time t_{dec} of a composite highly excited system of target plus projectile nucleons, pre-equilibrium emission will occur.

Another common feature of all approaches in group (A) is the equation for the cross-section for nucleon emission of type x, although the different quantities are calculated in different ways:

$$\frac{d\sigma}{d\varepsilon} \propto \sum_{\substack{n=n_o \\ \Delta n=2}}^{\bar{n}} \left[f(n,x) \frac{\rho(n-1,\ U)}{\rho(n,\ E)} . g . \lambda_c(\varepsilon) \right] . D_n(E) . T_n(\varepsilon, E) \qquad (6)$$

where the influences of proton-neutron distinguishability are

represented by the quantity $f(n,x)$. The sum is taken over all exciton states (n), starting from the initial condition (n_o) up to the exciton number which denotes thermal equilibrium ($\bar{n}$). The quantities ρ denote the level densities of systems with (n) excitons and excitation energy E or (n-1) excitons and excitation energy $U = E - B - \varepsilon$ (B = binding energy and ε = channel energy of the emitted nucleon). The emission rate into the continuum, $\lambda_c(\varepsilon)$, is derived from detailed balance principle. The single particle density is denoted by g. The dimensionless depletion factor $D_n(E)$ accounts for the reduced population of each state due to particle emission from simpler states with smaller (n) The time $T_n(\varepsilon,E)$ is the quantity which was a matter of controversy[37, 38]. It is in fact a specific time for the system to spend in configuration (n). In the hybrid model $T_n(\varepsilon,E)$ has been calculated, based on the fact that only transitions of one unbound nucleon are to be taken into account. This model neglects the influences due to the properties of the residual excited system, e.g. transitions of excited but bound particles. But in the exciton model each configuration (n) is considered as a quasi-equilibrium one. Accordingly $T_n(\varepsilon,E)$ has been evaluated considering all the possible transitions (excited bound and excited unbound particles). The assumption of quasi-equilibrium [39] however results in an angular distribution which is symmetric about 90^o. Therefore calculations based on exciton formalism are, in fact, a multi-step quasi-equilibrium process. In this terminology the hybrid model can be regarded as a direct multi-step process with a forward peaked angular distribution characteristic.

The most controversial hypothesis of the models of group (A)

is that, every partition of energy for a given exciton number occurred with equal a priori probability during the equilibration process[40]. But, there is firm evidence[41-43] that although this ad hoc assumption provides partial reproduction of nucleon spectra, it fails to predict the shape of α-particle spectra. On the basis of the above mentioned discrepancies about the a priori probability assumption, more elaborate investigations have been carried out to replace this incorrect assumption with a more realistic one[41, 44]. The most natural way of improving the theory beyond hybrid and exciton models consists in substituting, at each stage of the de-exciting cascade, the α-energy distribution in the case of (N,α) reactions, or the nucleon energy distribution in the case of (N,N) reaction (N = proton or neutron). This energy distribution can be evaluated on the basis of the nucleon-nucleon or nucleon- α-particle scattering dynamics. Blann improved the hybrid model by considering these effects and introduced a new model, i.e. Quasi-Free-Scattering Model (see section 1.3.3 and Chapter III for a fuller description of this model).

1.3.2.2 Group B (Cascade Models) - General Remarks

The intranuclear-cascade model of Serber[33] in principle was introduced to describe the interaction of a high energy projectile with a target nucleus. However, the basic idea of using free particle-particle scattering cross-sections to describe data below 100 MeV projectile energy has been accepted in recent years[45,46]. In this model, the trajectory of each nucleon is followed and after a mean free path, it will be assumed that a nucleon-nucleon collision

will take place. Except for limitations due to the Pauli Principle, it is assumed that this collision is identical with the free interaction. The most sophisticated version of the intranuclear-cascade model is the one described by Chen et al.[45]. In this calculation the target nucleus is taken to be a Fermi gas with a step function density distribution chosen to approximate the Fermi distribution and the effect of refraction of the cascade particles as they move through the nucleus has been taken into account. In a further refinement of the calculation, the possibility that particles with enough energy to escape from the nucleus may be reflected back into the interior, has been considered. In another version of the intranuclear-cascade model due to Bertini[46], the inclusion of refractions and reflection effects has been neglected on account of the fact that consideration of these effects suppresses the escape of fast particles to the extent that serious discrepancies are introduced for the elements considered at the lower incident energies and for the heavier elements at all the energies. However, although the neglect of these effects causes no problems in fitting data for protons with a few hundred MeV incident energy, when protons with a few tens of MeV energy have been used, a difficulty was encountered, i.e. the predicated cross-sections fell off too fast as the angle was increased[47]. This discrepancy might be due to the assumption of a straight path between nucleon-nucleon collisions. Thus neglect of the inclusion of the diffraction effect is likely to be the origin of the above mentioned trouble. In conventional versions of the Intra-Cascade Monte Carlo models one takes into account only the interactions that involve excited particles. It has to be mentioned that in a recent version by

Iljinov et al.[48], this shortcoming has been taken into account, although in a rather artificial way.

In a recent calculation by Chiang et al.[49] an attempt has been made to evaluate the inclusive cross-section resulting from the pre-compound process, using a simplified version of the intranuclear cascade model. This model is based on high energy (several 100 MeV) theory[50] where, instead of following the complicated path of the projectile through the nucleus, one follows an average trajectory, namely the straight line in the initial direction and at the impact parameter b. Chiang's initiative has demonstrated a relatively successful reproduction of data for nucleon emission. In particular, the dominance of single scattering for inclusive cross-sections has been confirmed. However, according to the assumptions[50] from which the Chiang model is derived, they are valid for energies above 500 MeV, but for smaller energies, especially below 100 MeV, little is known about their accuracy[51]. The validity of the Chiang model has been further tested by comparing (Fig. 1.8.a) the angular distribution with both the experimental data and the D.W.B.A. calculation by Tamura et al.[52a] (see group E, section 1.3.2.5). The failure of the Chiang model to reproduce data as the angle was increased for $^{209}Bi(P,P')$ and $^{27}A\ell(P,P')$ reactions (the incident energy was kept at 62 MeV, Fig. 1.8), indicates that the wave-bending effect is important. The calculation by Tamura describes this effect quite satisfactorily. Therefore the comparison in Figure 1.8 indicates that the use of free-nucleon-nucleon kinematics for calculation of angular distributions in the Chiang model is likely the origin of the failure to reproduce data.

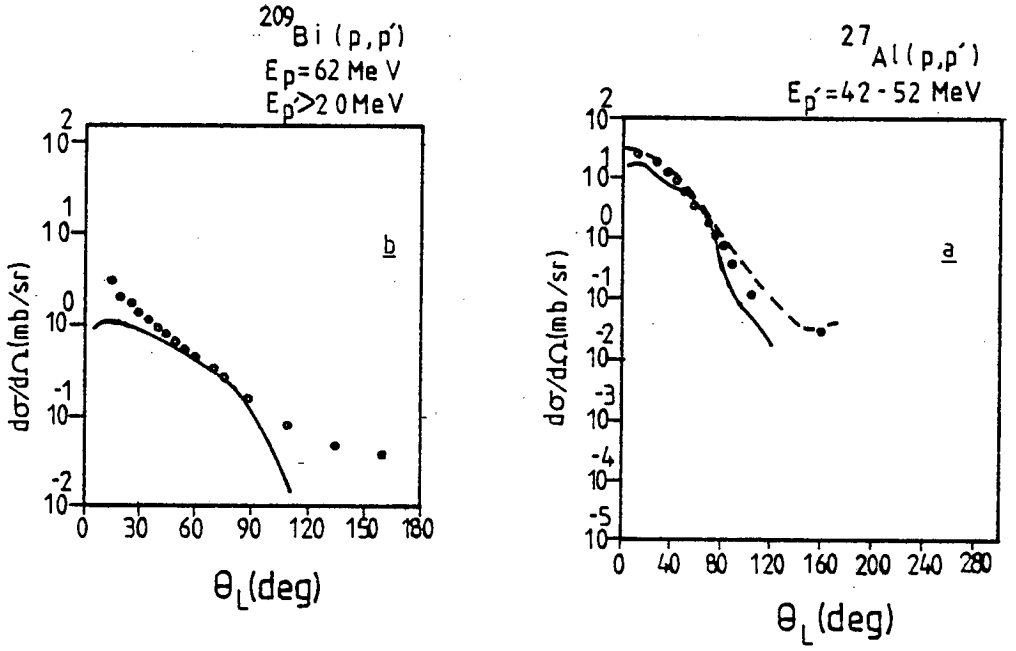

Figure 1.8: The differential cross-section $\frac{d\sigma}{d\Omega}$ for (P,P') reactions as a function of the laboratory angle θ_L of the final nucleon. Empty Points: experimental data (ref.49). Solid lines: Chiang et al. calculation (ref. 49). Broken line: Tamura D.W.B.A. calculation (ref. 52a).

1.3.2.3 Group C (Hot-Spot Models or Cluster Models)- General Remarks

Several years ago a thermodynamical approach describing the pre-equilibrium phenomena was suggested[53]. In this proposal pre-equilibrium is a consequence of a local excitation of the target, predominantly in the peripheral region. Such a local excitation in configuration space is referred to as a "hot-spot". After the establishment of local equilibrium the inhomogeneity of energy density is assumed to spread all over the nucleus according to a diffusion-type process. The local temperatures become measurable by observing the emission particle spectra. Recently[54] the concept of the "hot-spot" model has been developed to consider angular distributions for nucleon-induced pre-compound reactions in nuclear matter. This classical approach appears to reproduce the energy and

angular distribution of the emitted nucleon and α-particle in a quite consistent way. Especially the comparison with (e,α) data[55] provides remarkable agreement for different target nuclei. (Fig. 1.9).

The subject of "hot-spot" had been limited to theoretical discussion only. This situation has changed; there are at present at least three experiments in nuclear physics[56] and one experiment in particle physics[57], each of which in itself can bardly be explained without invoking "hot-spots". This indicates that a strong support is growing for the idea that in nuclear or hadronic matter excitations can be localised in space-time, giving rise to pre-equilibrium phenomena.

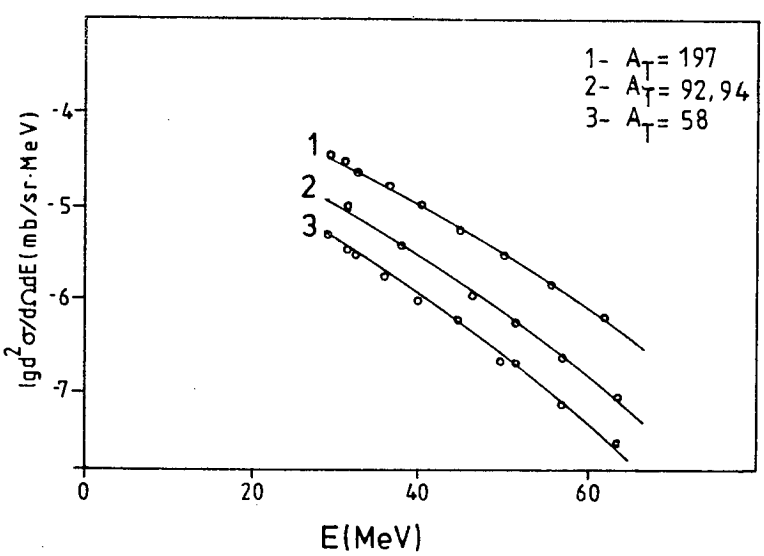

Figure 1.9: Energy distribution of α-particle emitted in the reaction $A_T(e,\alpha)X$ for different target mass numbers A_T at E = 120 MeV and $\theta = 30^o$. Continuous lines represent Stelte hot-spot model prediction (ref. 54). Empty points: experimental data (ref. 55).

1.3.2.4 Group D (Relaxation Models) - General Remarks

One of the approaches for describing the progress of medium-energy reactions is through time development of composite nuclear systems. This intranuclear relaxation process in nucleon-induced reactions has been investigated by Harp and Miller[58] in a Fermi gas model, utilizing kinetic equations for the evolution of single-particle-state occupation numbers. In this model the nucleus is viewed as being composed of independent proton and neutron Fermi gases. Therefore, the proton and neutron occupation numbers for the single-particle states of these gases completely specifies the internal configuration of the nucleus at any time. Further, it is assumed that the mechanism for the equilibration of the gases is through binary nucleon-nucleon collisions, where free nucleon-nucleon cross-sections have been incorporated to evaluate the binary interaction. In contrast to the exciton model[36], the Harp and Miller model spends most of its time calculating the distribution among energy states of the excited particles and holes. However, in the exciton model this distribution is assumed to be known through *ad hoc* assumptions of equal *a priori* probabilities. Furthermore, the internal transition probabilities used in the exciton model are taken as some average quantity, while the Harp and Miller model calculates explicitly this quantity in terms of the assumed two-body interaction.

Another time-dependent formulation of pre-equilibrium reactions has been proposed by Cline and Blann[59] in the framework of the exciton model. This approach has been further developed by Mantzouranis et al.[60,62], by incorporating the direction of

flight of the leading particle.

Recently a model for the relaxation process in a nucleon-induced reaction was developed[63] which is based on the Fermi gas model and uses the generalized transport equations. A comparison (Fig. 1.10) based on calculations using this model with the results of Mantzouranis and the generalized exciton model of Mädler and Reif[64], shows that all of these exciton models give similar results up to reaction angle about 60°. However in the backward angles the exciton model predictions are too small by orders of magnitude. The calculation based on generalised transport equations explains data in the angular range up to about 90° remarkably well, but it over-estimates data in backward angles.

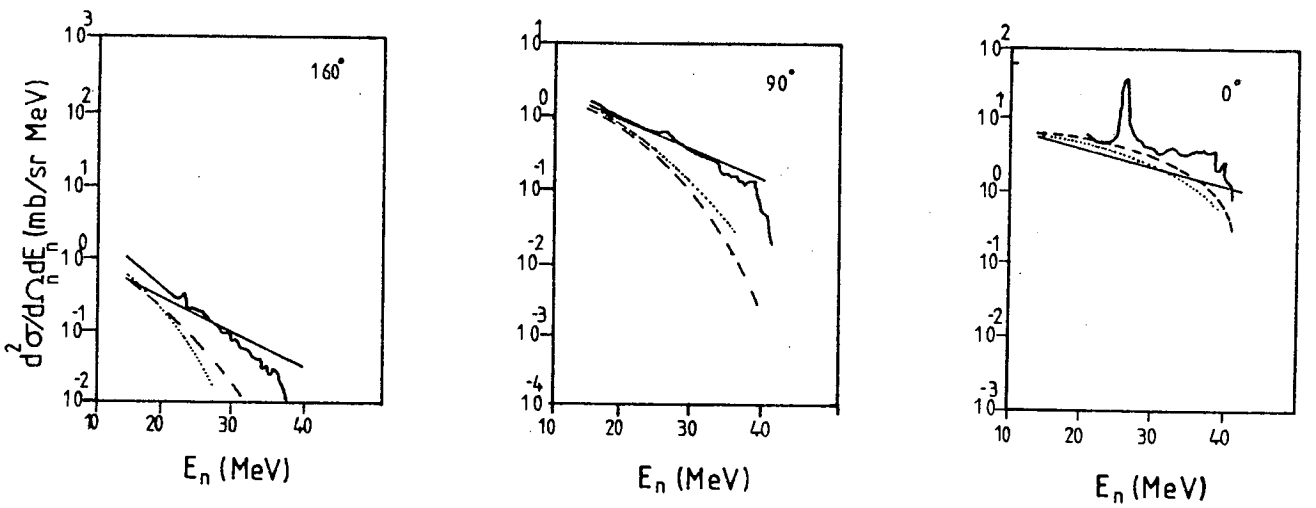

Figure 1.10: Double-differential cross-section of the reaction $^{208}Pb(p,n)$, E_p = 45 MeV. Thick solid curves: experimental data (ref. 47). Solid curves: Mädler and Reif relaxation process (ref. 63). Dashed curves: Mädler and Reif generalized exciton model (ref. 64). Dotted curves: Mantzouranis et al. generalised exciton model (ref. 62).

1.3.2.5 Group E (Quantum Mechanical Approaches) - General Remarks

All the different groups of models which were reviewed in the previous sub-sections provide valuable information about the theoretical interpretation of the mechanism of pre-compound emission in nuclear reactions. One should realise that most of these calculations are mainly based on semi-classical theories and therefore should be treated with caution. The first attempt to provide a quantum mechanical treatment of the reaction mechanism which considers both compound and pre-compound problems was given by Mantzouranis[60,61]. This approach is based on a quantum-statistical master equation and was able to give angular distributions that fit the experimental data with moderate success. One point worthy of mention is that this model has used the free nucleon-nucleon scattering cross-sections, while the Pauli effect has been neglected.

The second initiative was by Tamura et al.[52] who extended the direct reaction method into a new area of continuum transitions in contrast with the usual discrete state transitions. Their work achieves this purpose by assuming that any state in a nucleus is well described by the single-particle shell model. It therefore precludes any configuration mixing. More precisely, the experimental spectrum of the cross-sections, i.e. the continuum cross-section per unit energy, should be interpreted as an energy average of the sum of cross-sections taken over a large number of exciting states. Therefore any configuration mixing contributions will be averaged out and the summed cross-section is thus reduced to what is obtained by assuming a pure single particle shell model.

Finally Feshbach et al.[39] have recently proposed a new way of tackling the pre-compound mechanisms which describe the reaction

mechanism by two very different routes depending on the nature of the excited states in the target nucleus. The excited states are divided into unbound and bound classes. If all the excited particles in the nucleus are bound, the description of the reaction can be based on quasi-equilibrium hypothesis giving rise to statistical multi-step compound emission. On the other hand, if at least one particle is in the continuum the reaction must be treated in a way similar to a direct process giving rise to statistical multi-step direct emission. Recently[65] the multi-step direct method has been compared with data and the results show overall agreement with the measurements.

The approach by Tamura calculates the elementary cross-sections based on the direct reaction theory and it was applied to a finite nucleus. However, the approach by Mantzouranis et al.[60,61] uses the free nucleon-nucleon cross-section and it was applied to an infinite nuclear matter. It is clear from Figure 1.10 that the Mantzouranis et al. approach fits experimental spectra rather well, particularly at the lower energy end. For the higher energy end, however, Mantzouranis et al.'s approach underestimates the experimental cross-sections. This discrepancy is due to the use of infinite matter, because when an infinite matter is assumed, there remains little chance for the higher energy components to survive.

The Tamura and Feshbach approaches for $^{208}Pb(p, n)$ with E_p = 45 MeV show similar predictions. The quality of fit for both approaches are the same and both consider one- and two-step contributions.

1.3.3 Discussion Related to the Selection of a Pre-Compound Model for This Study

In order to proceed with the detailed investigation of the final state interactions a pre-compound model is chosen from models discussed in section (1.3.2), considering the following criteria:

a) The simplicity of the model,

b) The ability to reproduce the data (angular distribution and energy spectra) by this model.

c) The compatibility of this model for the purpose of combining to (γ, np), i.e. considering final state interactions with this pre-compound model.

The models of group (A) are considered to be the simplest. Therefore, refinement of these models in order to take into account the momentum distribution of particles inside the nucleus can make them more realistic, especially for the case of (N, α) reactions. Among the models in group (A), the hybrid model has been developed[6] in order to take the dynamics of (N, α) and (N, N') reactions into account. Recently the exciton model has also been developed[44] to consider the momentum distribution of particles inside the nucleus. Further the models of group (A) reproduce data reasonably well and they are capable of combining with quasi-deuteron model (γ, np). In this group, however, the developed hybrid model has some advantages compared to the developed exciton model (quasi-equilibrium assumption is employed after the first strike in developed exciton models, while in the developed hybrid model there is no such weak assumption).

In group (B), although the Intra Cascade Monte-Carlo models use more complicated formalism, they are not capable of being used

for cluster emission processes, e.g. (N, α). Although the Chiang model reproduces (N, N') data fairly well, for the (N, α) reaction an extra free factor (pre-formation factor) should be introduced with its limitations. Further the underlying assumption of the Chiang model is only valid for high energy projectile (≥500 MeV).

Hot-spot models in group (C) have been used for (e, α) reactions. However the processes of collision of the photon with the nucleon and subsequent interactions are hidden in these models. Furthermore in comparing with experimental data, we shall have to keep in mind that direct reaction contributions have to be subtracted in some way, a procedure which is in no way simple or unique.

The models in group (D) have not been used for complex particle emission. However, the introduction of pre-formation factors in these models certainly creates similar problems to the ones that already exist in group A.

Finally, in group (E), the two models by Tamura and Feshbach have some advantages compared to the third model (Mantzouranis et al.). However, compared to the other groups, Tamura and Feshbach are complete and sophisticated. But for the purpose of (γ, np) final state calculations these models are not suitable.

In this study the developed hybrid model (Quasi-Free-Scattering model) will be used (see Chapter III).

1.4.0 Objectives of the Present Study

The purpose of this research can be divided into two parts:

a) The development of the quasi-deuteron model.

b) The consideration of the effect of the final state interactions.

In what follows, these two main objectives will be briefly explained.

a) The two-body photodisintegration of complex nuclei, or the (γ, pn) reactions, will be investigated using the quasi-deuteron model. The classical quasi-deuteron model of Levinger is a simple model with three major shortcomings, i.e.

I) The Levinger constant has been treated correctly by Levinger; however, the choice of nuclear model (Fermi gas) is not a realistic one and therefore the total photonuclear absorption cross-section will produce uncomparable results with the values $L = 6.4$ or $L = 8$ for $r_o = 1.4$ fm and 1.2 fm, respectively (r_o is the nuclear radius parameter). In this study the Levinger constant will be calculated using shell structure for the nucleus. To this end, a so-called "Pseudo-Levinger" constant will be evaluated for different possibilities. These possibilities are when a photon interacts with (i) two nucleons from a 1S shell, (ii) two nucleons from a 1P shell, (iii) one from a 1P shell, one from a 1S shell and so on. Consequently the study will try to find an answer to the following questions in relation to the Levinger constant;

(1) What is the dependence of the Pseudo-Levinger constant on the shell structure of the nucleus? (See sub-section 2.2.2.4).

(2) Is there any possibility to calculate an accurate value for the Levinger constant? (See sub-section 2.2.2.4).

II) The motion of the centre of mass of the quasi-deuteron reduces the height of the free deuteron cross-section and

broadens it. This effect has been considered for the case of angular distribution and energy spectra in an approximate manner by Levinger. However, in the classical expression for total cross section the effect of Fermi motion has not been taken into account for free-deuterons. Another effect is the binding energy of the correlated neutron-proton pairs which shifts the free deuteron cross-section toward higher energy. Several papers in the past considered these two effects (see section 1.2.Ø). In the present study the calculation of double differential cross section will be carried out considering the Fermi motion of the centre of mass and binding energy of the correlated (np) pairs for different shell's contribution. With respect to the evaluation of double differential cross-section, the following questions arise:

(1) What are the contributions of double differential cross-sections calculated from different shells? (see section 2.4.Ø and Chapter IV).

(2) How do the calculated double differential cross-sections compare with the experimental data? (see section 2.4.Ø and Chapter IV).

III) Levinger's quasi-deuteron model simply link the total photonuclear cross-section to the photodisintegration cross-section of the free deuteron ($\gamma + D \rightarrow n + p$). An emerging physical picture is that below the pion threshold, the photon interacts with the nucleus through its direct coupling to the exchange currents. Therefore in the framework of the quasi-deuteron model, one could ask these two

questions:

(1) What is the underlying reason that the simple model of Levinger overestimates the cross-section for photon energies below E_γ = 150 MeV? (See Chapters IV and V).

(2) Can the free-deuteron cross-section be replaced only by the exchange part of the total photodisintegration cross-section of the deuteron? (See Chapters IV and V).

b) The effect of final state interactions is the other objective of this study. The primary interaction of photon with nucleons (proton and neutron) generates two nucleons. The consideration of chain interactions of these two nucleons with the rest of the nucleons in the nucleus provides necessary information on the pre-compound emission for γ-induced reactions. The consideration of final states will give rise to the questions, as follows:

(1) How would be the success of combined models of quasi-deuteron and pre-compound quasi-free-scattering in explaining the (γ, p) and (e, α) reaction in contrast to similar types of synthesized models? (See Chapter IV and V).

(2) What sort of nuclear structure information can one obtain from (e, α) reaction? (See Chapter IV).

The quasi-deuteron model will be re-examined in Chapter II. Then the model which has been used to consider final state interactions will be discussed in Chapter III. Chapter IV is concerned with the combination of quasi-deuteron and the pre-compound quasi-free-scattering model. This combined model will then be compared with experimental data. Finally, Chapter V provides a conclusion to the present study.

CHAPTER II

QUASI-DEUTERON MODEL

2.1.Ø. Introduction

In this chapter a new method is developed in order to calculate the double differential cross-section for the (γ, np) interaction in the nuclear interior of nuclei. It is assumed that the photo-absorption process is due to the photo-dissociation of a correlated neutron and proton within the nucleus. The neutron and proton absorb the photon energy and may then escape from the nucleus.

The total double differential cross-section for the interaction of γ with the whole nucleus is obtained by, first, summing over the cross-section for the photo-dissociation of all possible neutron-proton pairs in a particular shell, and then summing over all the shells' contributions. This particular shell can be constructed by two nucleons creating a pair. These pairs are either on a similar shell, e.g. 1S-1S shell, or they are on two different shells, e.g. 1S-1P shell.

The basic strength of photo-dissociation of any pair is related to the cross-section of the free deuteron. However, the probability of finding the neutron and proton in the nucleus at a distance within the nucleon force range (which is analogous to the same probability in the free deuteron) is theoretically evaluated for individual shells using two different shell configurations, (a) pure square well and, (b) harmonic oscillator potentials.

In section (2.2.Ø) the basis of the model of correlated neutron and proton will be discussed. The formulation of this model will then be restructured in such a way as to be compatible with a cross-

section evaluation for individual shells (section 2.2.1). A brief summary of a computer programme constructed to calculate (γ, np) double differential cross-section will then be considered in section (2.3.Ø). Finally, section (2.4.Ø) concerns the conclusion to this chapter and an outline of the objectives of the remaining chapters.

2.2.Ø. Principle of the Quasi-Deuteron Model

The two-particle mechanism for the absorption of high energy photons (E_γ > 200 MeV) was put forward[5] with the aim of describing experimental data on photo-nuclear reactions at high energies. However, as was argued in Chapter I, the process of absorption of photons by the two-particle mechanism is also a dominant process at energies above the giant resonance region (E_γ > 40 MeV). The proposed model for photo-absorption is based on two assumptions:

a) the photons are absorbed mainly by nucleon-nucleon pairs in the nucleus,

b) the cross-section for photonuclear reaction in complicated nuclei can be expressed in terms of the photo-disintegration cross-section of the free deuteron.

The first of these two assumptions considers that the nucleus is built up from protons and neutrons only. The electromagnetic interaction is supposed to proceed via the one-body current. This picture cannot be the whole truth because of the presence of mesons in the nucleus. In addition, the nucleons can sometimes be excited to nuclear resonances. This means that the nucleus as a whole is a complicated system of mesons and baryons. Therefore the conventional picture, i.e. nucleonic degrees of freedom, can only be considered as an approximation.

The second assumption can also be justified within the framework of certain definite approximations. These approximations are as follows:

I) Electric dipole moments of neutron-neutron and proton-proton pairs are zero. This approximation can easily be justified by the use of a model suggested by Gari and Hebach[23] (see Chapter I, section 1.2.2). In this model the exchange contribution plays a dominant role at the intermediate photon energies. It has been suggested that these exchange terms are proportional to the isovector operator $(\vec{\tau}_1 \times \vec{\tau}_2)^3$ which acts on two-nucleon states as follows:

$$(\vec{\tau}_1 \times \vec{\tau}_2)^3 |np\rangle = |pn\rangle$$

$$(\vec{\tau}_1 \times \vec{\tau}_2)^3 |pp\rangle = (\vec{\tau}_1 \times \vec{\tau}_2)^3 |nn\rangle = 0.$$

Therefore the contribution to the cross-section due to photo-absorption by (γ, nn) and (γ, pp) are neglected. It is also possible that the (γ, np) cross-section can be calculated from the exchange current contributions for electric dipoles and quadrupoles. However, the dipole contribution to the total (γ, np) cross-section exceeds 90% up to 100 MeV photon energy.[22] Thus higher multiples are not important. This is equivalent to assuming that dipole absorption plays the dominant role.

The contribution to the cross-section of triplet and singlet (np) pairs is assumed equal with the exception of the spin weighting factor. Nevertheless, the contributions of the singlet state can be ignored and the transition due to the triplet state can be considered as the only contributing factor.

II) The wavefunction $\psi_\alpha \equiv \psi_\alpha$ (1,2,3,..., A) for the target nucleus A is represented by the product of the wavefunction $\psi_{K_1K_2}$ for the two isolated nucleons with momenta $\vec{K}_1$ and $\vec{K}_2$ and the wavefunction ψ_β (3,..., A) for the remainder of the nucleus. Moreover, $\psi_{K_1K_2}$ is in the following form ignoring antisymmetric coefficient:

$$\psi_{K_1K_2} = \psi_K(\vec{R})\ \psi_k(\vec{r}) \qquad (1)$$

where $\psi_K(\vec{R})$ is the wavefunction for the motion of the centre-of-mass of the two nucleons and it is taken in the form of a plane wave corresponding to the resultant momentum $\vec{K} = \vec{K}_1 + \vec{K}_2$. $\psi_k(\vec{r})$ is the wavefunction for the relative motion with momentum $\vec{k} = (\vec{K}_1 - \vec{K}_2)/2$ at infinity and describes the unbound S state (in fact $\psi_k(\vec{r})$ is the wavefunction for the corresponding scattering problem). This function is taken in the effective-range approximation for the (np) interaction. Since small distances between the nucleons (less than, say, 1F) are important for the process which is being considered here, $\psi_k(\vec{r})$ can be related to the wavefunction for the free deuteron ψ_d and, in particular, it can be shown[5] that

$$\psi_k(r) \sim \psi_d(r) \quad . \qquad (2)$$

III) It is assumed that the absorption of the photon by the (np) pair in the nucleus does not affect the state of the remaining (A-2) nucleons. At the same time, the nucleon momentum distribution in the nucleus is assumed[5] to be given by the Fermi distribution at zero temperature (the radius is taken to be $R = 1.4A^{1/3}$F).

2.2.1 Formulation of Quasi-Deuteron Model

2.2.1,1 Derivation of the Total Cross-section Using Quasi-Deuteron Hypothesis

By using the above approximations the photo-electric cross-section of the quasi-deuteron was derived by Levinger[5] by means of the following equation (see Appendix A):

$$\frac{\sigma_{qd}}{\sigma_q} = \left[\frac{\psi_k}{\psi_d}\right]^2 = \left[\frac{(4\pi/\nu)^{\frac{1}{2}}(\alpha^2 + k^2)^{-\frac{1}{2}}}{[2\alpha/(1 - \alpha r_o)]^{\frac{1}{2}}}\right]^2 \qquad (3)$$

where σ_{qd} is the photodisintegration cross-section for a quasi-deuteron in which the neutron and proton have wave number k for their relative motion. σ_d is the free deuteron cross-section and is calculated in the dipole approximation in accordance with approximation (I), (section 2.2.Ø). The other parameters are, ν, the volume of the nucleus, α, the scattering length and, r_o, the effective range of the nuclear forces (the essential details of effective range approximation are given in Appendix (A)). In considering the photodisintegration on a finite nucleus expression (3) can be multiplied by a factor NZ which indicates the number of ways of choosing the protons and neutrons for the whole nucleus.

$$\frac{\sigma_{qd}}{\sigma_d} = NZ \frac{2\pi(1 - \alpha r_o)}{\alpha(\alpha^2 + k^2)\nu} \quad . \qquad (4)$$

In order to find an average value for the quantity $(\alpha^2 + k^2)^{-1}$ over all possible values of the wave number $(k = |\vec{k}|)$ in the nucleus, the third approximation can be used (section 2.2.Ø). The average cross-section can therefore be written:

$$\frac{\sigma_{qd}}{\sigma_d} = NZ \frac{2\pi(1 - \alpha r_o)}{\alpha \cdot \nu} \cdot \langle(\alpha^2 + k^2)^{-1}\rangle \qquad (5)$$

The average value of the quantity $(\alpha^2 + k^2)^{-1}$ can be evaluated by means of the following equation:

$$\langle(\alpha^2 + k^2)^{-1}\rangle = \frac{\iint F(K_1)F(K_2)(\alpha^2 + k^2)^{-1}\, d\vec{K}_1\, d\vec{K}_2}{\iint F(K_1)\, F(K_2)\, d\vec{K}_1\, d\vec{K}_2} \qquad (6)$$

where $F(K_1)$ and $F(K_2)$ are the momentum distribution of the neutron and proton respectively. Levinger[5] used a Fermi distribution with the following form:

$$F(K_1)\, d\vec{K}_1 = \left[\frac{3}{k_m^3}\right] K_1^2\, dK_1 , \qquad K_1 \leq k_m \qquad (7)$$

where k_m is the Fermi momentum for wave number $K_1 = |\vec{K}_1|$, and also one can write the same expression for protons with $K_2 = |\vec{K}_2|$.

The value[5] for $\langle(\alpha^2 + k^2)^{-1}\rangle$ evaluated from equation (6) is $4.1\, k_m^{-2}$. This value can be substituted in equation (5) to give:

$$\sigma_{qd} = NZ.\sigma_d \cdot \frac{2\pi(1 - \alpha r_o)}{\alpha\nu(4.1)^{-1} k_m^2} \qquad (8)$$

If ν is taken as, $\nu = \frac{4}{3}\pi R^3$ with $R = 1.4A^{1/3}$, then one can write $\nu = \frac{4}{3}\pi A(1.4)^3$. So, equation (8) takes the form of:

$$\sigma_{qd} = \left[(2.24) \cdot \frac{(1 - \alpha r_o)}{\alpha k_m^2}\right] \cdot \frac{NZ}{A} \cdot \sigma_d \cdot \qquad (9)$$

Levinger substituted experimental values for r_o, α and k_m which enabled him to get the widely used expression for total cross-section of photodisintegration of the nucleus, i.e.,

$$\sigma_{qd} = L \cdot \frac{NZ}{A} \cdot \sigma_d \qquad (10)$$

where L is essentially the ratio of the probabilities of finding the neutron and proton in the nucleus at a distance of, say, less than 1F from each other to the analogous probability in the free deuteron. Thus, L is given equal to:

$$L = (2.24) \cdot \frac{1 - \alpha r_o}{\alpha k_m^2} \quad . \qquad (11)$$

The value of this Levinger constant L was evaluated to be 6.4. However, Levinger found that, in his simple model, L depends on the nuclear radius parameter r_o and hence he had to use values of $L = 6.4$ and $L = 8$ for $r_o = 1.4$ fm and 1.2 fm respectively. On the other hand, a more recent analysis [66] of cross-section data, obtained for light nuclei in the 50-150 MeV photon-energy range by Ahren et al. [67] led them to conclude that L ought to increase with A. Therefore the Levinger constant was suggested to be $L = 6.8 \pm 2.5$ for the ^{16}O case. However, the Ahrens group [10b] itself fitted the very same data on ^{16}O with $L = 4.6$. More recently the Saclay group [10b] used $L = 4.6$ to compare with their experimental results, in spite of the fact that this value for Levinger constant created more discrepancy. It must be pointed out that with the exception of the Levinger evaluated constant, all the other values for this constant have been introduced through fitting to data.

In the following sub-section the Levinger procedure for evaluating the Levinger constant will be discussed and a more realistic approach for calculating this constant will be explained.

2.2.1.2 Discussion Related to Problems Facing the Levinger Constant

From equation (8) it can be noted that the nuclear photoeffect cross-section is obtained by averaging the cross-section for the photo-dissociation of the quasi-deuteron over all possible neutron-proton pairs. This was carried out using the Fermi gas model for the nucleus. However, it is important to realize that in the infinite uniform nuclear matter the system is translationally invariant. Therefore, the energy of a particle cannot depend on its location but may depend on its momentum. On the other hand, in a finite nucleus, there is no translational invariance. With respect to this argument the shell model potential is a function of position and therefore it represents an improvement over the Fermi gas model.

Thus the present study intends to use the shell model configuration to calculate the Levinger constant in contrast to the Fermi gas model used by Levinger[5]. In this procedure the photon interacts with two correlated nucleons which are located on different shells and consequently the Levinger constant will be shell dependent.

In the next section this new procedure will be presented and the results for two different nuclei will be shown.

2.2.2 A New Approach to Calculate Total Photo-Absorption Cross-Section and the Levinger Constant

2.2.2.1 Introduction

In order to evaluate the total cross-section for the photo-absorption process, the shell model approach will be adopted. In this approach the photo-absorption cross-section for different shells will be evaluated. To this end, for these individual

contributions, the Levinger constant will be separately calculated. This procedure uses the momentum distribution for neutron and proton resulting from shell model wavefunctions such as pure square well and harmonic oscillator. The calculated Levinger constant shows a decreasing trend in going from the lower shell to the upper one.

In the next sub-section the procedure for calculating the total cross-section and the Levinger constant will be given with the help of an example (i.e. section 2.2.2.2). Then, it is appropriate to calculate the total cross-section by using this approach. A comparison is made with the experimental data using the suggested Laget formalism[14,24] in sub-section (2.2.2.3). Finally in sub-section (2.2.2.4) a discussion concerning the results and outcomes of the new approach for the calculation of the Levinger constant will be given.

2.2.2.2 The Clarification of the New Approach by Using an Example

The best way to clarify the new approach is to consider the (γ, np) process on a light target, e.g. ^{12}C. The photon interaction for a typical exchange contribution, giving rise to the (γ, np) effect, can be expressed by Figure 2.1, where the basic strength of interaction is related to the photo-disintegration of the deuteron.

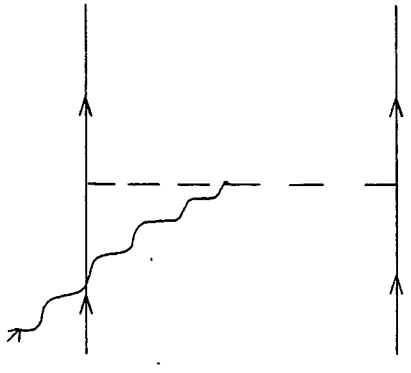

Figure 2.1

The shell model potentials that will be employed are:

a) Square well potential

b) Harmonic oscillator potential.

There are three possible contributions which can contribute to the (γ, np) total cross-section:

1) Contribution from (1S-1S) shells with NZ = 4 possible neutron-proton pairs;

2) Contribution from (1P-1P) shells with NZ = 16 possible neutron-proton pairs;

3) Contribution from (1S-1P) shells with NZ = 8 possible neutron-proton pairs, which must be multiplied by 2 because both neutrons and protons fill 1S and 1P shells.

The Levinger constant for these three contributions will be calculated for the corresponding shell model potentials.

In the following, each of the above mentioned potentials will be separately dealt with. The formalism for calculating the total photo-absorption cross-section as well as the corresponding shell dependent values of the Levinger constant for the two potentials will be given for ^{12}C.

2.2.2.2a Square Well Potential Case

One can calculate the Levinger constant using a square well potential for the three above mentioned possibilities by using eigenfunctions associated with a potential of the form:

$$v(r) = -v_o \quad \text{for} \quad r < R$$
$$v(r) = \infty \quad \text{for} \quad r > R \; . \tag{12}$$

The eigenfunctions are given by:

$$\psi_{n\ell m}(K_{n\ell}r) = A_{n\ell} J_{\ell} (K_{n\ell}r)Y_{\ell m} \tag{13}$$

where $A_{n\ell} = (2R^{-3})^{\frac{1}{2}} \frac{1}{J_{\ell+1}(K_{n\ell}R)}$.

Using these eigenfunctions for the 1P and 1S shells, it is possible to calculate the momentum distribution for individual nucleons in a particular shell by using the Fourier transform:

$$F(K_N) = \left| \int \psi(r)\, e^{-i\vec{K}_N \cdot \vec{r}}\, d\vec{r} \right|^2 \tag{14}$$

where $\psi(r)$ is the special wavefunction and $F(K_N)$ is the momentum distribution of the nucleon $(N = 1, 2)$ with $F(K_1)$ and $F(K_2)$ for neutron and proton respectively. In Figure 2.2A the momentum distribution $F(K_N)$ for wavefunctions associated with square well potential are given.

The quantity $\langle(\alpha^2 + k^2)^{-1}\rangle$ can now be easily calculated by the use of equation (6) for the three different possibilities of photoabsorption by pairs from (1S - 1S), (1P - 1P) and (1P - 1S) shells using nucleon momentum distribution resulting from equation (14). Equation (5) will now be identified with a particular shell combination β.

$$\left[\frac{\sigma_{qd}}{\sigma_d}\right]_\beta = N_\beta Z_\beta \cdot \left[\frac{2\pi(1-\alpha r_o)}{\alpha . \nu_\beta} \cdot \langle(\alpha^2 + k^2)^{-1}\rangle_\beta\right]_\beta \tag{15}$$

and

$$\left[\frac{\sigma_{qd}}{\sigma_d}\right]_\beta = N_\beta Z_\beta \cdot L'_\beta \tag{16}$$

where the subscript β indicates (1S - 1S), (1P - 1P) and (1S - 1P) shells' contributions. The coefficient L'_β is equal to the quantity in the bracket in the right-hand-side of equation (15), i.e.,

$$L'_{\beta} = \left[\frac{2\pi(1 - \alpha_o)}{\alpha . \nu_{\beta}} \cdot \langle(\alpha^2 + k^2)^{-1}\rangle_{\beta} \right]_{\beta} \qquad (17)$$

In the present study L'_{β} will be referred to as the "Pseudo Levinger" constant. The final total cross-section can finally be written by

$$\left[\frac{\sigma_{qd}}{\sigma_d}\right]_F = \Sigma_{\beta}\left[\frac{\sigma_{qd}}{\sigma_d}\right]_{\beta} . \qquad (18)$$

In equation (15), ν_{β} is the overall confinement-volume for the scattering of a neutron and proton in their respective shells. In the case of square well potential, ν_{β} is simply taken to be the volume of the considered nucleus, e.g. ^{12}C, for the three shell combinations. The results concerning the calculated pseudo Levinger constant are given in Table (1). These results show the shell dependent characteristic of the pseudo-Levinger constant.

Square well potential	$1S^2$	1S-1P	$1P^2$	L'_{av}
L'	0.664	0.614	0.460	0.579

Table (1): Pseudo-Levinger Constant (L') calculated for ^{12}C using square well potential. The potential characteristics are shown in Table (9).

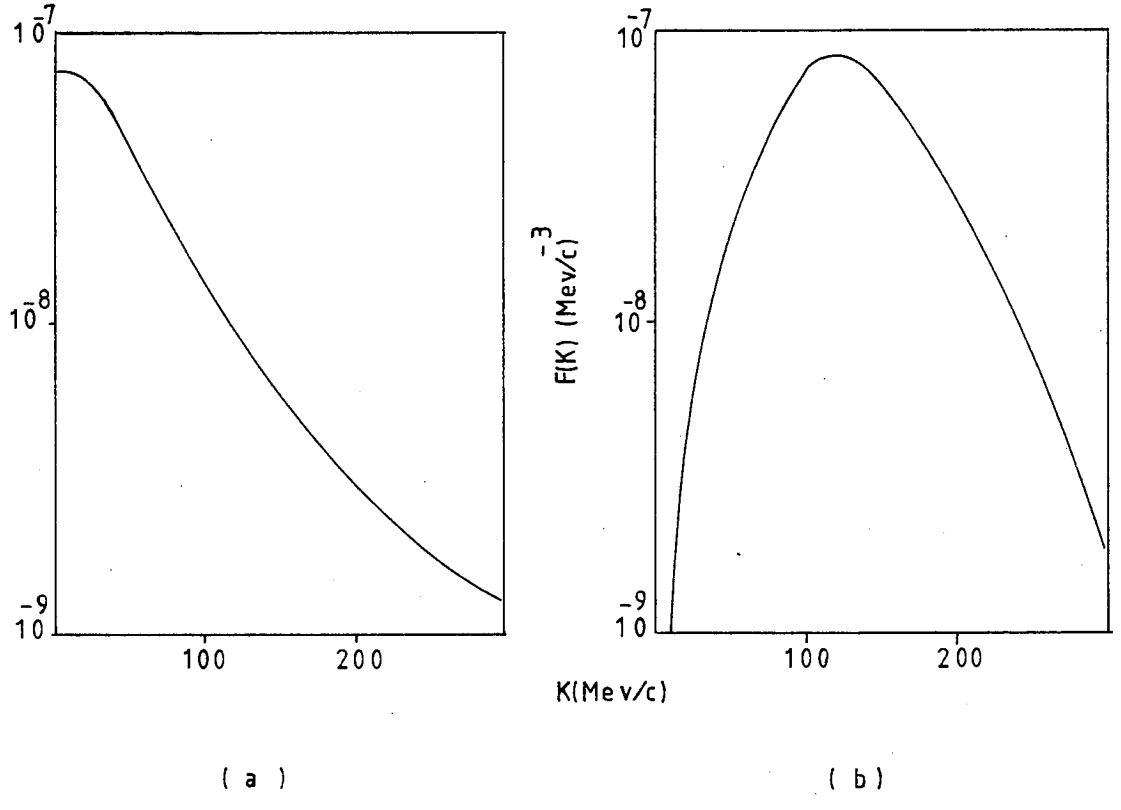

Figure 2.2A: (a) Nucleon momentum distribution $F(K_N)$ for 1S shell.
(b) Nucleon momentum distribution $F(K_N)$ for 1P shell.
For both cases the square well potential is used.

2.2.2.2b Harmonic Oscillator Potential Case

The procedure mentioned in (2.2.2.2a) can be considered using a harmonic oscillator potential with the following form:

$$V(r) = -V_o + \frac{1}{2} m_p \omega^2 r^2 \tag{19}$$

The resulting eigenfunctions are given by

$$\psi_{\ell nm}(r, \theta, \phi) = (-1)^n \sqrt{\frac{2}{(\ell+\frac{1}{2})!} \binom{\ell+n+\frac{1}{2}}{n}} r^{\ell} e^{-\frac{1}{2}\lambda r^2} {}_1F_1(-n, \ell+\tfrac{3}{2}, \lambda r^2) \times Y_{\ell m} \tag{20}$$

where $\lambda = m_p \omega/\hbar$.

These wavefunctions can be used to provide $F(K_N)$ from equation (14) which enables one to calculate the quantity $\langle(\alpha^2 + k^2)^{-1}\rangle_\beta$ where β again can take the three possibilities of (1S-1S), (1P-1P) and (1P-1S). In Figure 2.2B the momentum distributions $F(K_N)$ calculated by using the wavefunctions associated with harmonic oscillator potential are given.

The cross-section can then be evaluated by means of equations (15) and (16). However the remaining point to be made about using the harmonic oscillator potential is that the volume ν_β has to be calculated. The evaluation of a shell's expectation radius can easily be done by the use of the following relation:

$$\langle r^2 \rangle_\beta = \int \psi^*_{\ell' n' m'}(r)\, r^2\, \psi_{\ell nm}(r)\, d\vec{r} \tag{21}$$

where $\langle r^2 \rangle_\beta$ is the expected radius for a particular shell, e.g. β = 1S-1S and so forth. $\psi_{\ell nm}(r)$ is the wavefunction introduced in equation (20) for different shells. It seems reasonable that the volume ν_β, should be given by:

$$\nu_\beta = \frac{4}{3}\pi(\langle r^2\rangle_\beta)^{3/2} \quad . \tag{22}$$

In Table 2 the results concerning the pseudo-Levinger constant are given. These results show the shell dependent characteristic of the pseudo-Levinger constant.

Harmonic oscillator potential	$1S^2$	1S - 1P	$1P^2$	L'_{av}
L'	1.906	1.763	1.322	1.664

Table (2): Pseudo-Levinger constant (L') calculated for ^{12}C using harmonic oscillator potential. The potential characteristics are given in Table 9 .

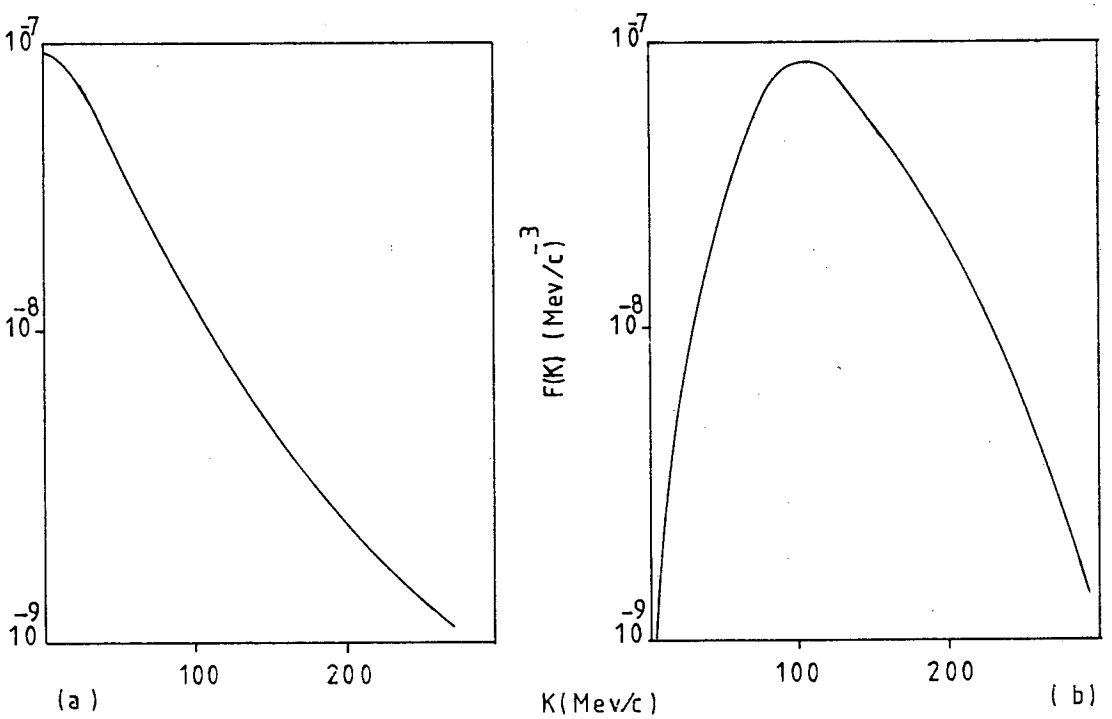

Figure 2.2B: (a) Nucleon momentum distribution $F(K_N)$ for (1S) shell.
(b) Nucleon momentum distribution $F(K_N)$ for (1P) shell.
For both cases the harmonic oscillator potential is used.

2.2.2.3 Comparison of the Total Cross-Section with the Experimental Data

The intention of this subsection is to calculate the total photo-absorption cross-section for a $_{Z}^{A}N$ nucleon. To this end the total cross-section for ^{12}C has been calculated using the two calculated pseudo-Levinger constants (see Tables 1 and 2). However, in order to evalute the total cross-section the averaged values for the pseudo-Levinger constants have been used. Furthermore, the photodisintegration cross-sections σ_d have been taken from the Partovi[69] parameterisation of the free deuteron.

Table 3 shows the result of the total photonuclear absorption cross-section σ_{qd} for ^{12}C obtained using equation (10).

E_γ (MeV)	σ_{qd}(mb) using square well potential with $L'_{av} = 0.58$	σ_{qd}(mb) using Harmonic oscillator potential with $L'_{av} = 1.66$
32	6.738	19.360
64	2.539	7.295
96	1.585	4,556
128	0.665	1.912

Table (3): Quasi-deuteron cross-section computed using equation (10) with $(L'_{av} = \frac{L}{A})$.

It is appropriate to compare the results given in Table 3 with experimental data. Figure 2.3 shows this comparison using the data taken by the Mainz group[9]. As the figure clearly shows, the calculated results lie well above the experimental data. This conclusion however is expected because the simple expression of Levinger (equation (10)), overestimates the cross-sections for photon

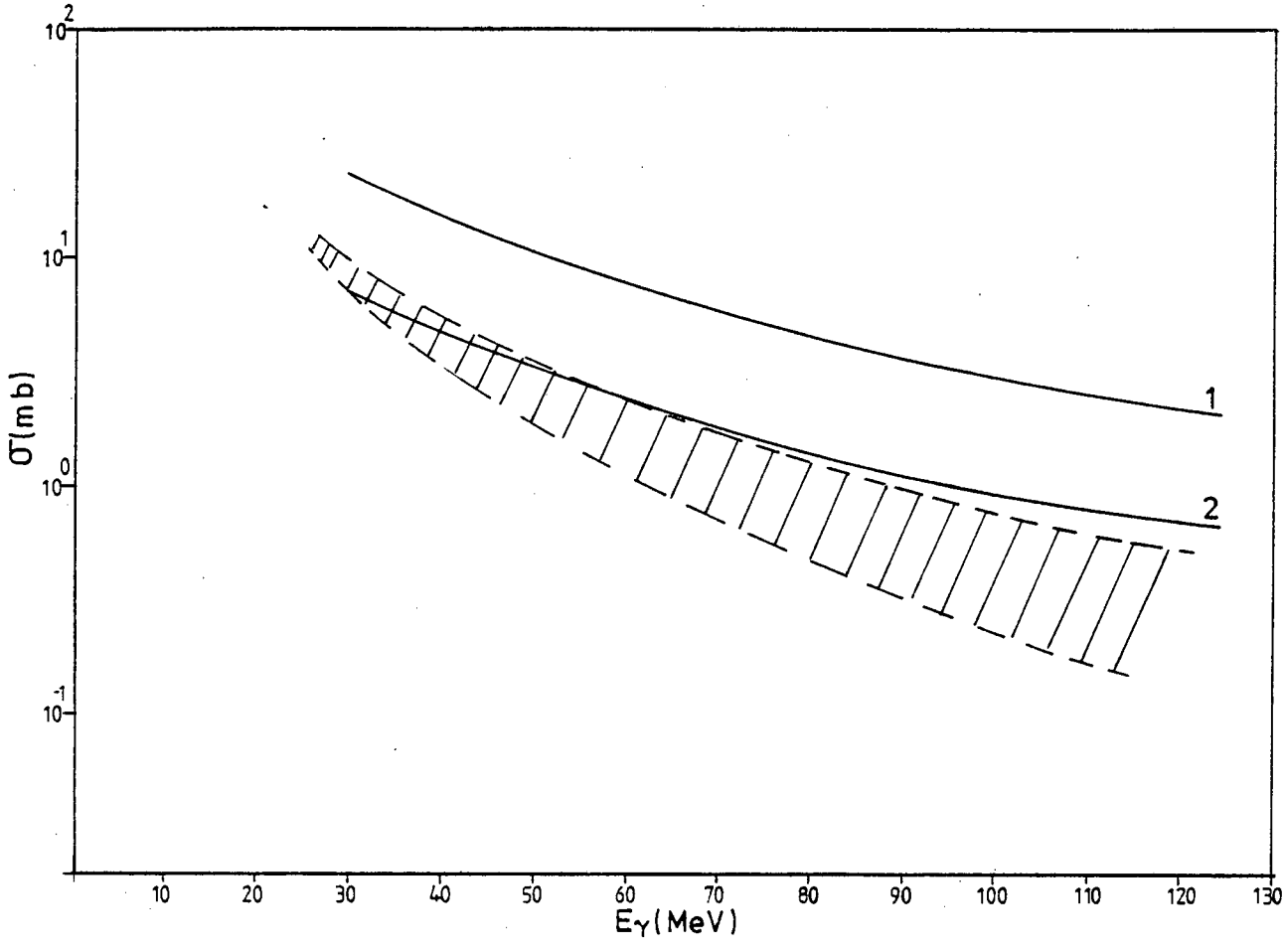

Figure 2.3: Comparison of the calculated total cross-section and experimental data; the shaded area is data for ^{12}C taken from ref. (9), curves (1) and (2) are calculated using no floating parameter (see Table 3). These two curves are calculated using the square well for curve (2) and the harmonic oscillator for curve (1).

energies below E_γ = 150 MeV. The resulting cross-sections however encouraged us to make a further investigation. To this end the recent suggestion by Laget[14, 24, 10] has been considered. Laget, as mentioned in Chapter I, proposed to use the $(\pi+\rho)$ meson exchange part of the deuteron electrodisintegration cross-section $(\gamma+D \rightarrow pn)$. Therefore an improved version of the old quasi-deuteron model with the following expression was introduced:

$$\sigma_{qd} = \frac{L}{A} NZ \, \sigma_d^{exchange} \quad . \tag{23}$$

In the previous attempts, this equation has been used with the floating Levinger constant, while in the present study the averaged pseudo-Levinger constants L'_{av}, given in Tables 1 and 2, are used to calculate the total photonuclear cross-sections.

Table 4 gives the results of this type of calculation and the comparison with experimental data can be seen in Figure 2.4.

E_γ (MeV)	σ_{qd}(mb) using square well potential with $L'_{av} = 0.58$	σ_{qd}(mb) using harmonic oscillator potential with $L'_{av} = 1.66$	$\sigma_d^{exchange}(E_\gamma)$ (μb) taken from Ref. (10a)
32	0.771	2.216	37
64	0.583	1.677	28
96	0.492	1.413	23.6
128	0.439	1.264	21.1

Table (4): Quasi-Deuteron cross-section computed using equation (23) with $(\frac{L}{A})$ replaced by the pseudo-Levinger constant, (L'_{av}).

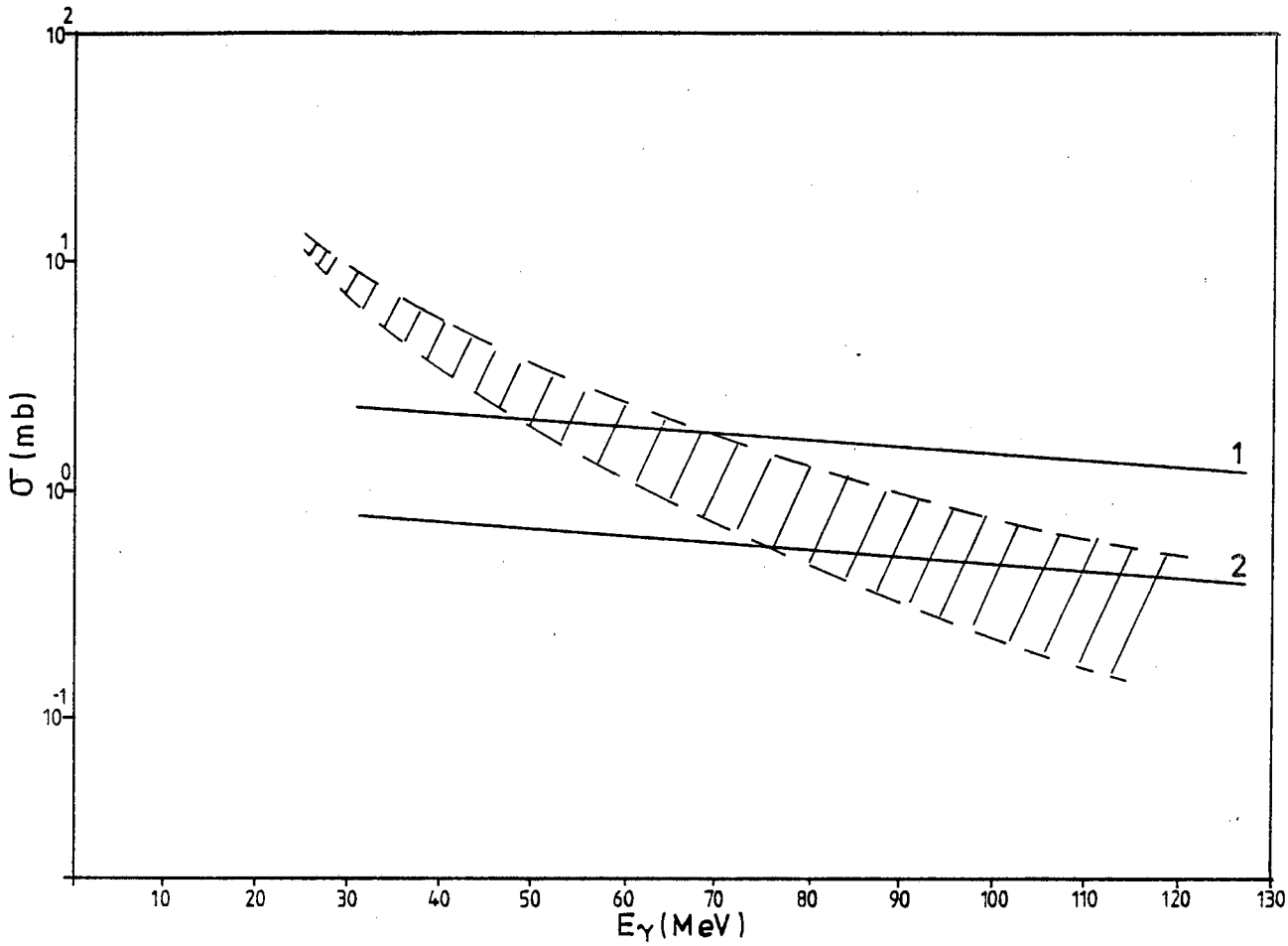

Figure 2.4: Comparison of the calculated total cross-section and experimental data; the shaded area is data for ^{12}C taken from ref. (9), curves (1) and (2) are calculated using no floating parameter (see Table 4). These two curves are calculated using the square well for curve (2) and the harmonic oscillator for curve (1).

More recently Laget[10b] proposed more realistic values for $\sigma_d^{exchange}$ in which the binding energy and Fermi motion effects have been taken into consideration. Table 5 gives the results of the calculated total cross-section, where the proposed averaged pseudo-Levinger constant values and the refinement made by Laget for $\sigma_d^{exchange}$ are used. Then the resulting total cross-sections are compared with the experimental data taken by the Mainz group. The calculated results lie well in the shadded band above 60 MeV (Fig. 2.5).

E_γ (MeV)	σ_{qd}(mb) using square well potential with $L'_{av} = 0.58$	σ_{qd}(mb) using harmonic oscillator with $L'_{av} = 1.66$	$\sigma_d^{exchange}$ (E_γ) μb refined values, Ref. (10b)
32	0	0	0
64	0.166	0.478	8.0
96	0.243	0.700	11.7
128	0.271	0.778	13.0

Table (5): Quasi-Deuteron cross-section for ^{12}C, computed using equation (23) with $(\frac{L}{A})$ replaced by the pseudo-Levinger constant, (L'_{av}). The refined values for $\sigma_d^{ex.}$ are used.

The comparison of calculated results with the experimental data stresses the importance of correlated neutron-proton pairs in the photoabsorption mechanism. The results also show the significance of the photointeraction with the nucleus through its direct coupling to the exchange currents.

Calculation of the total photonuclear cross-section presented

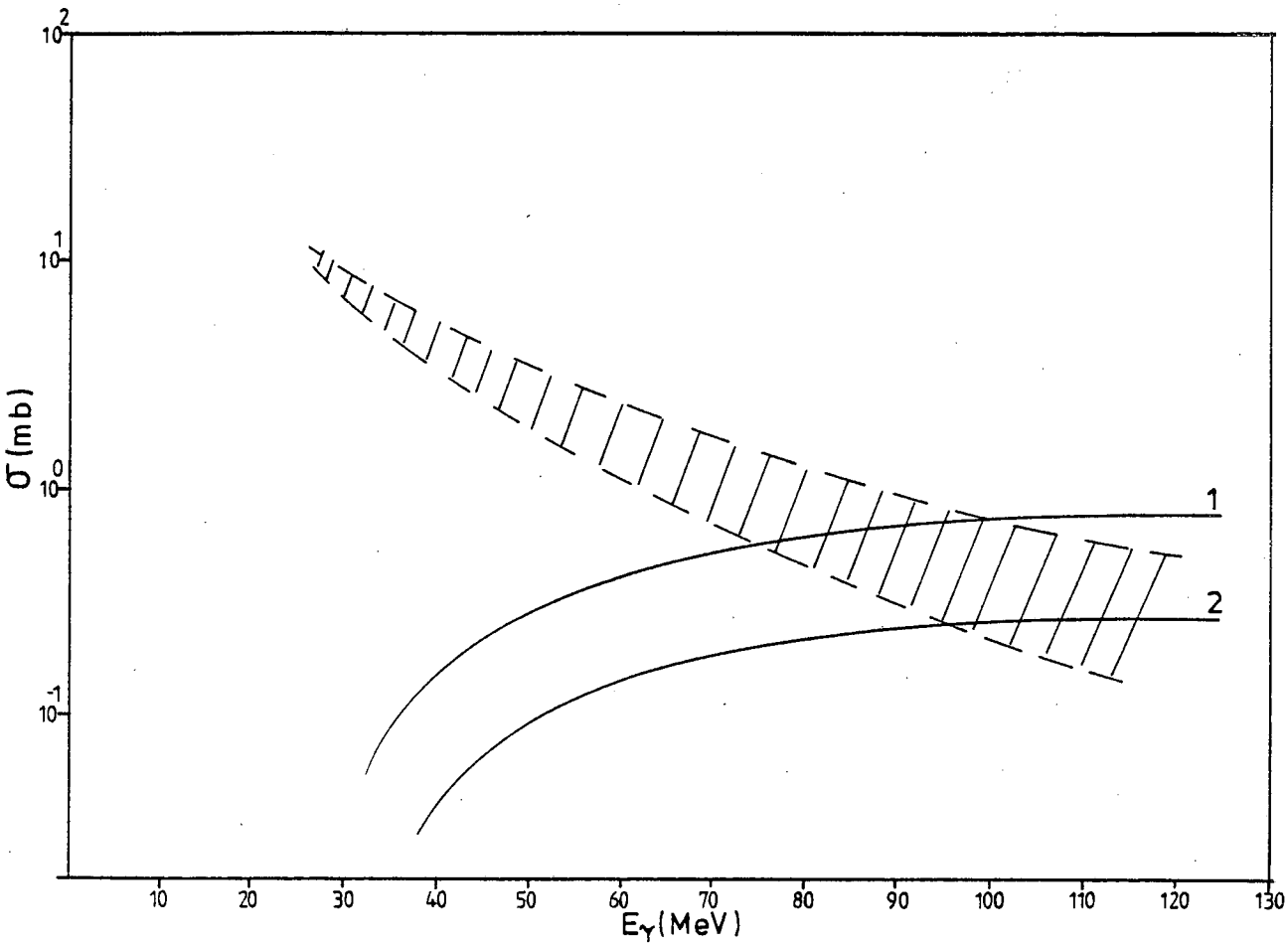

Figure 2.5: Comparison of the calculated total cross-section and experimental data; the shaded area is data for ^{12}C taken from ref. (9). Curves (1) and (2) are calculated using no floating parameter (see Table 5). These two curves are calculated using the square well for curve (2) and the harmonic oscillator for curve (1).

above was achieved without using a floating parameter, i.e. the Levinger constant. Therefore it is appropriate to calculate the photonuclear total cross-section for another target, i.e. ^{16}O. To this end the pseudo-Levinger constant is calculated for two different potentials (square well and harmonic oscillator potentials). The results of this calculation are shown in Tables 6(a) and 6(b).

Square well potential	$1S^2$	1S-1P	$1P^2$	L'_{av}
L'	0.495	0.457	0.343	0.432

Table 6(a): Pseudo-Levinger constant (L') calculated for ^{16}O using square well potential. The potential characteristics are given in Table 9 .

Harmonic oscillator potential	$1S^2$	1S-1P	$1P^2$	L'_{av}
L'	1.426	1.319	0.989	1.245

Table 6(b): Pseudo-Levinger constant (L') calculated for ^{16}O using harmonic oscillator potential. (The potential characteristics are given in Table 9 .

Evaluation of the total cross-sections were carried out using $\sigma_d^{exchange}(E_\gamma)$ for the free deuteron, including the consideration of the binding energy and Fermi motion effects for correlated (n-p) pairs inside the real nuclei. The results of the total photo-absorption cross-section for ^{16}O are shown in Table 7. These results

are compared with the data taken by the Mainz[9] and Saclay[10b] groups (Fig. 2.6). It has been assumed that the values for $\sigma_d^{exchange}$ for ^{12}C can be used for ^{16}O.

E_γ(MeV)	σ_{qd}(mb) using square well potential with $L'_{av} = 0.432$	σ_{qd}(mb) using harmonic oscillator potential with $L'_{av} = 1.245$	$\sigma_d^{exchange}(E_\gamma)$ (μb) refined values Ref. (10b)
32	0	0	0
64	0.220	0.635	8.0
96	0.322	0.931	11.7
128	0.359	1.034	13.0

Table (7): Quasi-Deuteron cross-section for ^{16}O, computed using equation (23) with $(\frac{L}{A})$ replaced by the pseudo-Levinger constant, (L'_{av}). The refined values for $\sigma_d^{ex.}$ have been used.

It became appropriate to compare the results calculated by Gari and Hebach[23] for total photonuclear cross-section of ^{16}O with the results given in Table 7. This comparison can be seen in Figures 2.6a and 2.6b.

The results of the calculation presented in this sub-section indicates that:

a) the calculations of the pseudo-Levinger constant for two different potentials show the significance attributable to the alteration of the free deuteron cross-section arising from a consideration of binding energy and Fermi motion effects.

b) the importance of the idea that a photon interacts with the nucleus through its direct coupling to the exchange currents.

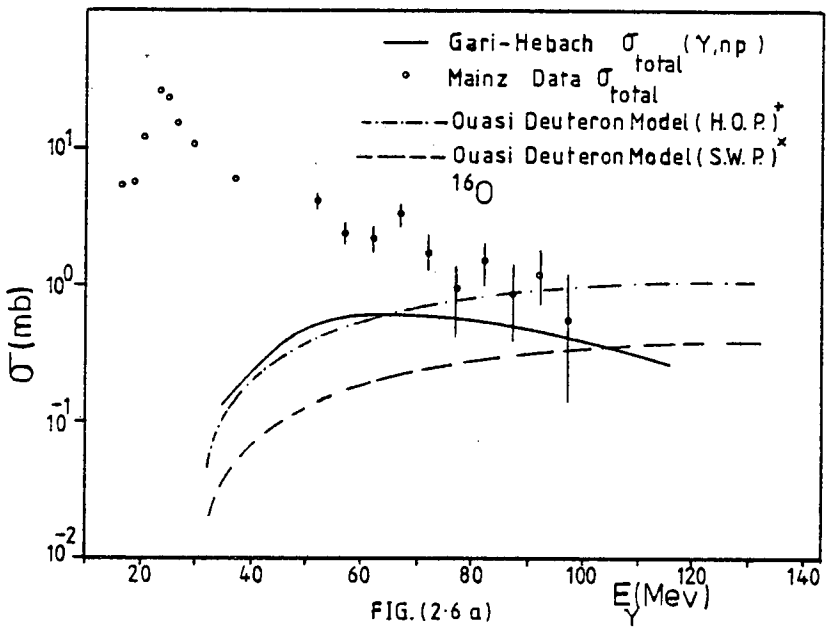

FIG. (2·6 a)

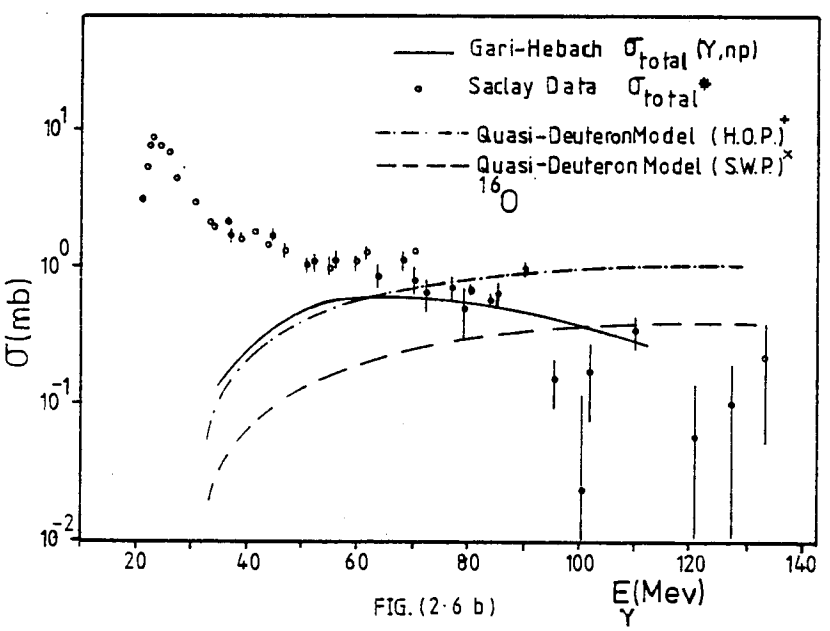

FIG. (2·6 b)

Figure 2.6: Comparison of the calculated total cross-section with experimental data (see Table 7).

\+ : Harmonic oscillator potential used.

x : Square well potential used.

* : $\sigma_{total} = \sigma_{total} - \sigma(\gamma,P) - \sigma(\gamma,2P) - \sigma(\gamma,\alpha)$.

2.2.2.4 Discussion

In section (2.2.2) a new approach to calculate the total photo-absorption cross-section and Levinger constant was introduced. Although the original formulation of the quasi-deuteron model was followed by this new approach, the shell model configuration was used in contrast to the Fermi gas model.

The Levinger constant has been replaced by a so-called pseudo-Levinger constant which is shell dependent. In order to calculate these proposed constants, two potentials, i.e. square well and harmonic oscillator, have been used. The calculations of pseudo-Levinger constants have preliminarily been worked out for two targets, i.e. ^{12}C and ^{16}O. The resulting values for these constants show an increasing trend from upper shell to lower one, for both studied cases. This type of calculation has extended to another nucleus, i.e. ^{60}Ni and the result of this calculation are given in Table 8. The evaluated constants for ^{60}Ni will be used later in Chapter IV for the calculation of (γ, p) and (e, α) energy spectra. For ^{60}Ni a similar trend to ^{12}C and ^{16}O for pseudo-Levinger constants can be observed.

Calculations of the total photo-absorption cross-section by the theoretically calculated pseudo-Levinger constants stress the importance of the Fermi motion and binding energy for correlated p-n pairs inside the real nuclei. Furthermore, these evaluated constants for different shells can be averaged over for the nucleus under consideration $(L'_{av} = \frac{L}{A})$. When using the square potential for ^{12}C and ^{16}O, the obtained $L \sim 7$ while for ^{60}Ni, $L \sim 6$. On the other hand, in the case of harmonic oscillator potential the obtained $L \sim 20$ for ^{12}C and ^{16}O and for ^{60}Ni, $L \sim 19$.

IS's combinations	$1S^2$	1S-1P	1S-1d	1S-2S	1S-2P	1S-1f
L'	0.157	0.131	0.124	0.136	0.131	0.084

IP's combinations	$1P^2$	1P-1d	1P-2S	1P-2P	1P-1f
L'	0.115	0.127	0.131	0.132	0.132

1d's combinations	$1d^2$	1d-2S	1d-2P	1d-1f
L'	0.094	0.086	0.102	0.092

2S's combinations	$2S^2$	2S-2P	2S-1f
L'	0.090	0.080	0.078

1f's combinations	$1f^2$	1f-2P
L'	0.082	0.097

Table 8(a): Pseudo-Levinger constant L' calculated for ^{60}Ni using square well potential. The potential characteristics are given in Table 9 .

1S's combinations	$1S^2$	1S-1P	1S-1d	1S-2S	1S-2P	1S-1f
L'	1.134	0.617	0.420	0.583	0.575	0.220

1P's combinations	$1P^2$	1P-1d	1P-2S	1P-2P	1P-1f
L'	0.388	0.330	0.317	0.331	0.275

1d's combinations	$1d^2$	1d-2S	1d-2P	1d-1f
L'	0.197	0.151	0.148	0.160

2S's combinations	$2S^2$	2S-2P	2S-1f
L'	0.194	0.116	0.113

1f's combinations	$1f^2$	1f-2P
L'	0.123	0.123

Table 8(b): Pseudo-Levinger constant L' calculated for ^{60}Ni using harmonic oscillator potential. The potential characteristics are given in Table 9 .

Table 9

	Potential Characteristics [Sq. Well & H.O.]	
$Z^{A}N$	H.O. Width Par. [$\lambda = m_p w/\hbar$] (Mev/c)	Sq. well Radius (fm)
^{12}C	86.1	2.74
^{16}O	78.2	3.71
^{60}Ni	50.3	4.69

Thus, a realistic potential may well produce a reasonable value for Levinger constant which lies between the two calculated values for ^{12}C, ^{16}O and ^{60}Ni.

Finally, the absorption of the photon (40 MeV to 140 MeV) by quasi-deuteron has been associated only with the exchange part, $\sigma_d^{ex}(E_\gamma)$ in the total photo-disintegration cross section $\sigma_d(E_\gamma)$ of the free deuteron. The importance of meson exchange together with the calculated values for averaged pseudo-Levinger constant indicates a more realistic calculation in contrast to the classical quasi-deuteron model (see Figure 2.6).

The proposed procedure for the calculation of different shell contributions to the final total cross-section can be used for evaluating the energy and angular distribution of outgoing nucleons where the square well and harmonic oscillator potentials will again be employed. The double differential cross-section for the (γ, np) process is then the purpose of investigation in the following section.

2.2.3 Derivation of the Double Differential Cross-Section Using the Quasi-Deuteron Hypothesis

2.2.3.1 Introduction

The energy and angular distribution of the outgoing nucleons after the interaction of a photon with a correlated neutron-proton pair are influenced, compared to the case of the photo-disintegration of the free deuteron, by the momentum of the neutron-proton pairs inside the nucleus and the binding energy of the pairs. If the shell model approach is again employed then there are different quantities which should be evaluated in order to construct the final double differential cross-section. These are:

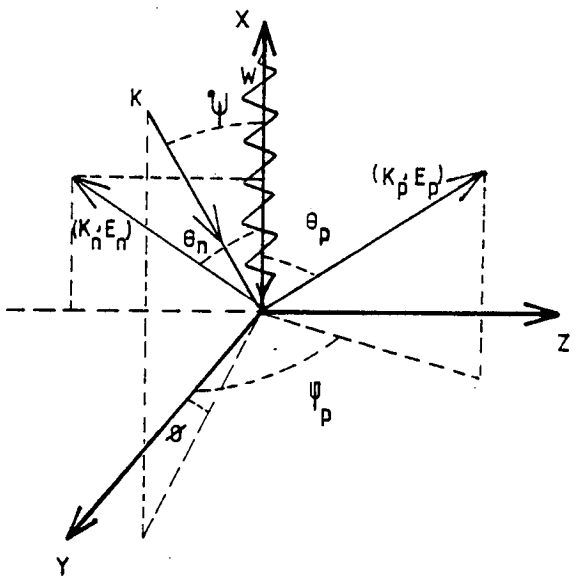
X
W
K
Ψ
(K_p, E_p)
(K_n, E_n)
θ_n
θ_p
Z
φ_p
φ
Y

A

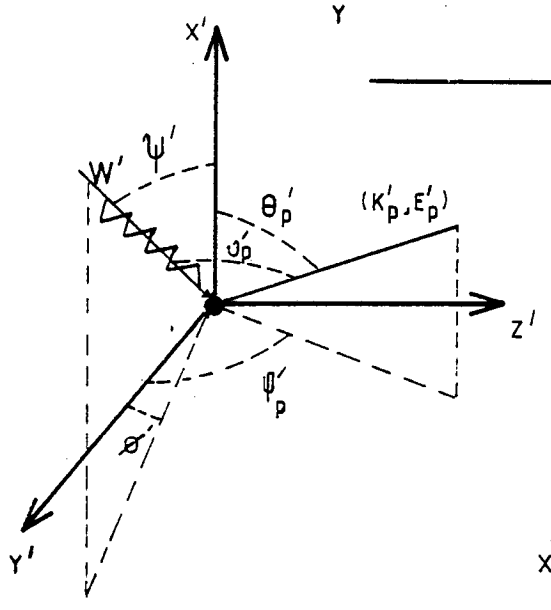
X'
W'
Ψ'
θ_p'
(K_p', E_p')
ϑ_p'
Z'
φ_p'
φ'
Y'

B

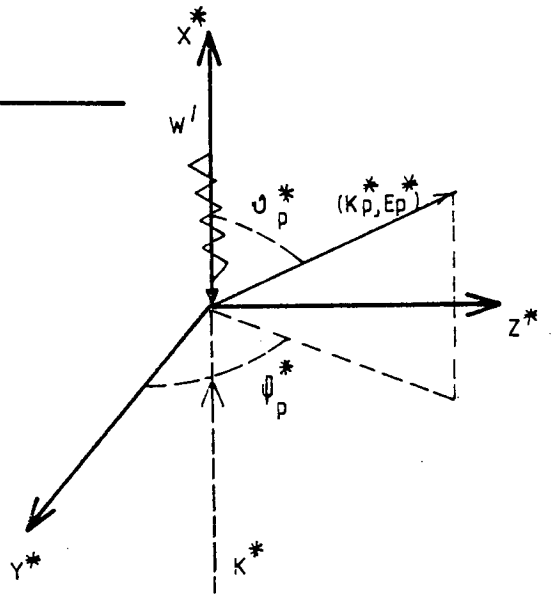
X*
W'
ϑ_p^*
(K_p^*, E_p^*)
Z*
φ_p^*
Y*
K*

C

I) evaluation of a corresponding binding energy of the pair from a specific shell (if the contributions from different shells are separately evaluated),

II) calculation of the shell model wavefunctions (square well or harmonic oscillator) in order to determine the momentum distribution of the quasi-deuteron inside the nucleus.

III) evaluation of the pseudo-Levinger constant and the associated pairs for a particular shell, as has been discussed in section (2.2.2).

The basic idea underlying the present approach and the similar approaches adopted by Kim[68,70] and Matthews[15] are the same. Although the present treatment differs in many respects, obviously the main difference consists in the fact that while the approach adopted by Matthews does not consider the photo-interaction contribution from different shells (Fermi gas model adopted), the one that will be proposed here calculates the different shells' contributions. It must be mentioned that Kim calculated the photo-interaction contribution from different shells for ^{12}C by using an arbitrary momentum distribution for the correlated (p-n) pair and an overall floating factor.

2.2.3.2 Derivation of Double Differential Cross-Section for (γ, np) Reaction

One can start to investigate energy and angular distribution for (γ, np) process by introducing the kinematics of the quasi-deuteron reaction. For this purpose we consider a photon with momentum $\vec{\omega}$, interacting with a neutron-proton pair with momentum $\vec{K}$, within the nucleus, producing a state consisting of one neutron $\vec{K}_n$ and one proton $\vec{K}_p$ before leaving the nucleus (see diagram A). This system of coordinates will be referred to as the Laboratory system and all the quantities referred to it are unprimed.

Conservation of momentum in the quasi-deuteron picture therefore demands:

$$\vec{\omega} + \vec{K} = \vec{K}_n + \vec{K}_p. \tag{24}$$

The momentum $-\vec{K}$ for the remaining (A-2) nucleons is assumed to be the same before and after the reaction. In the following discussion, the top of the nuclear well is chosen as the reference point. For energy conservation one gets:

$$\omega + \frac{K_1^2}{2m_1} + \frac{K_2^2}{2m_2} = E_p + E_n + \bar{Q} \tag{25}$$

where (K_1, m_1) and (K_2, m_2) are momentum and mass of proton and neutron respectively. The energy of the photon is $\omega(\hbar = c = 1)$. E_n and E_p are kinetic energies of the neutron and proton outside the nucleus, as would be measured by particle detectors. The sum of the separation energy for the (γ, np) reaction, the recoil energy of the (A-2) system, and the excitation energy of the (A-2) system is denoted by $\bar{Q}$. Equation (25) can now be re-written in the appropriate form of

$$\omega + \frac{K^2}{2M} + \frac{k^2}{2m} = E_p + E_n + \bar{Q} \tag{26}$$

where $\vec{K} = \vec{K}_1 + \vec{K}_2$ and $\vec{k} = \frac{m_2\vec{K}_1 - m_1\vec{K}_2}{m_1 + m_2}$. Furthermore $M = m_1 + m_2$ and $m = \frac{m_1 m_2}{m_1 + m_2}$. The assumption of $m_1 = m_2 = m'$ will replace the equation (26) with:

$$\omega + \frac{K^2}{4m'} + \frac{k^2}{m'} = E_p + E_n + \bar{Q} \ . \tag{27}$$

Therefore $\frac{K^2}{4m'}$ is the kinetic energy of the centre-of-mass of neutron-proton pair and $\frac{k^2}{m'}$ is the relative energy of the neutron-proton pair. It has been suggested that $\frac{k^2}{m'}$ can take values from 0 to 40 MeV.

Levinger assumed an average value for $\frac{k^2}{m'}$ equal to 12 MeV. Therefore the absorption of a photon by a neutron-proton pair occurs in a state characterised by $\frac{k^2}{m'} = 12$ MeV. However, in the present study the state of the neutron-proton pair has been specified by $\bar{Q}$ as the effective binding energy. Thus equation (27) will take its new form by considering $\frac{k^2}{m'}$ equal to zero.

$$\omega + \frac{K^2}{4m'} = E_p + E_n + \bar{Q} \qquad (28)$$

where in this equation $\bar{Q}$ is assumed to be constant. It depends on the particular shell where the pair will be picked up, and it is distributed equally between protons and neutrons. Furthermore, the direction of momentum does not change when the nucleons leave the nucleus, i.e. no final state interactions. In Chapter IV the interaction of the neutron and proton with the residual nucleus, leading to the emergence of the particles into the laboratory will be considered as a second stage of the calculation for (γ, np) process.

The relation between equations (24) and (28) can be established by writing:

$$E_N = E_N^{\text{inside}} - \frac{1}{2}\bar{Q}$$

where N can be either proton (p) or neutron (n).

The formalism for the photo-induced double differential cross-section can be derived by using the quasi-deuteron hypothesis, i.e. photons are absorbed by a pair of nucleons in the photo-emission of nucleons in complex nuclei (see section 2.2.Ø). On the basis of this hypothesis the double differential cross-section is related to the momentum distribution of the quasi-deuterons and the free deuteron photo-disintegration cross-section for a photon of energy ω by:

$$d\sigma^{\omega} = c \left[\frac{d\sigma(\omega, \theta_p)}{d\Omega_p} \right]_d d\Omega_p \cdot G(K) d\vec{K} \qquad (29)$$

where in this expression $d\sigma^{\omega}$ denotes the cross-section for a monochromatic photon with energy ω. The other terms in expression (29) can be explained as follows:

a) A constant c which will be specified later in this subsection,

b) The term in brackets is the free deuteron photodisintegration cross-section as a function of photon energy ω and the proton angle θ_p.

c) The momentum distribution $G(K)d\vec{K}$ of a correlated proton-neutron pair where $d\vec{K}$ is $d^3K = K^2 dK \sin\psi d\psi d\phi$ and $\vec{K}$ is the total momentum of a pair.

In the expression (29) the term $[d\sigma(\omega, \theta_p)/d\Omega_p]_d$ will be transformed to the system of coordinates where the deuteron is at rest. This system will be referred to as the rest system and all the quantities introduced in it are primed. (See diagram B). The reason for such a transformation is that the free deuteron cross-section generally will be expressed in terms of ω', the photon energy in the rest system of the neutron-proton (diagram B), and ν^*_p, the angle of the proton relative to the photon direction in the photon-deuteron centre of mass system. The angle ν^*_p and the photon-deuteron centre of mass system are shown in diagram C. Therefore the term $(d\sigma(\omega, \theta_p)/d\Omega_p)_d$ can be transferred to the rest system (diagram B) by the transformation of variables (ω, θ_p) to (ω', ν'_p):

$$(d\sigma(\omega, \theta_p)/d\Omega_p)_d = J_o (d\sigma(\omega', \nu'_p)/d\Omega'_p)_d \; ; \qquad (30)$$

$J_o \equiv \dfrac{d(\cos \nu'_p)}{d(\cos \theta_p)}$ is the corresponding Jacobian (all the associated

expressions concerning the Jacobian are given in Appendix B).

Equation (30) will then take the appropriate form by substituting J_o:

$$(d\sigma(\omega, \theta_p)/d\Omega_p)_d = \frac{d(\cos\nu'_p)}{d(\cos\theta_p)} (d\sigma(\omega', \nu'_p)/d\Omega'_p)_d \ . \qquad (31)$$

Thus, expression (29) can be re-written by using equation (31) as

$$d\sigma^{\omega} = c\frac{d(\cos\nu'_p)}{d(\cos\theta_p)} (d\sigma(\omega',\nu'_p)/d\Omega'_p)_d \ d\Omega_p \ G(K)d\vec{K} \ . \qquad (32)$$

The next transformation which must be considered is the transformation of the variables (ω', ν'_p) to (ω', ν^*_p) in the free deuteron cross-section (see diagram C). The corresponding Jacobian takes the following form

$$J_1 \equiv \frac{d(\cos\nu^*_p)}{d(\cos\nu'_p)} \ . \qquad (33)$$

Therefore equation (32) will take the new form of:

$$d\sigma^{\omega} = c\frac{d(\cos\nu'_p)}{d(\cos\theta_p)} \cdot J_1(d\sigma(\omega', \nu^*_p)/d\Omega^*_p)_d \ d\Omega_p . G(K)d\vec{K} \ . \qquad (34)$$

It is convenient to proceed with the calculation of double differential cross-section by considering monochromatic photon energy. By the use of equation (34) the appropriate form for double differential cross-section can be constructed. This approach can then be easily used for a spectrum of photons, i.e. by summing the different monochromatic calculated cross-sections weighted for the corresponding photon intensities in the photon spectrum range. This approach will be discussed further in section (2.2.3.5).

Another approach for dealing with a spectrum of photons is to take into account the independent probability $B(\omega)d\omega$ of

finding an incident photon of energy between ω and $\omega + d\omega$ where the direction of the photon is kept fixed. This approach has been incorporated in the present study. By considering $B(\omega)d\omega$, equation (34) will take its appropriate form:

$$d\sigma = c \frac{d(\cos \nu'_p)}{d(\cos \theta_p)} \cdot J_1 (d\sigma(\omega', \nu^*_p)/d\Omega^*_p)_d \, d\Omega_p \cdot G(K) d\vec{K} \, B(\omega) d\omega \, . \tag{35}$$

It must be pointed out that the differential $d\omega$ is in the laboratory frame (diagram A) and it can be transferred to the differential in nucleon energy dE_p in the same system. However, the process of transformation tends to be difficult. Therefore a more appropriate procedure has been chosen. The differential $d\omega$ will be transformed to the corresponding one in the rest system (diagram B) by:

$$d\omega = \frac{\partial \omega}{\partial \omega'} \, d\omega' \equiv J_2 \, d\omega' \tag{36}$$

where $J_2 \equiv \frac{\partial \omega}{\partial \omega'}$ is the corresponding Jacobian.

The differential $d\omega'$ can then be transferred to differential in nucleon energy in the rest system by:

$$d\omega' = \frac{\partial \omega'(E'_p, \nu_p')}{\partial E'_p} \, dE'_p \equiv J_3 \, dE'_p \tag{37}$$

where $J_3 \equiv \frac{\partial \omega'(E'_p, \nu'_p)}{\partial E'_p}$ is the appropriate Jacobian and it can be evaluated using the rest-system (diagram B) energy-momentum conservation equations which are

$$\begin{cases} \omega' = E'_n + E'_p \\ \vec{\omega}' = \vec{k}'_n + \vec{k}'_p \end{cases} \tag{38}$$

Equation (35) consequently takes the form of

$$d\sigma = c\left[dE'_p \cdot \frac{d(\cos\nu_p')}{d(\cos\theta_p)}\right] \cdot J_1 \cdot J_2 \cdot J_3 (d\sigma(\omega', \nu^*_p)/d\Omega^*_p)_d \, d\Omega_p \cdot$$

$$\cdot G(K) \, d\vec{K} \, B(\omega) \qquad (39)$$

where equations (36) and (37) are used.

The last transformation which must be considered is the transformation of differential dE_p' to the laboratory system (diagram A). However this transformation can be achieved by taking the appropriate steps, i.e. considering the following term in equation (39):

$$dE'_p \cdot \frac{d(\cos\nu'_p)}{d(\cos\theta_p)} = \left[\frac{dE'_p}{dE_p} \cdot dE_p\right] \cdot \left[\frac{d(\cos\nu'_p)}{d(\cos\theta'_p)} \cdot \frac{d(\cos\theta'_p)}{d(\cos\theta_p)}\right] . \qquad (40)$$

In this equation the second bracket has been introduced because as it is obvious from diagram A, the variables (θ_p, ϕ_p) are transformed to variables (ν'_p, ϕ'_p) in diagram B. However this transformation will be achieved by using the chain process, i.e:

$$(\theta_p, \phi_p) \rightarrow (\theta'_p, \phi'_p) \rightarrow (\nu'_p, \phi'_p) \quad . \qquad (41)$$

It is also convenient to write equation (40) in a new form:

$$dE'_p \cdot \frac{d(\cos\nu'_p)}{d(\cos\theta_p)} = dE_p \cdot \left[\frac{dE'_p}{dE_p} \cdot \frac{d(\cos\theta'_p)}{d(\cos\theta_p)}\right] \cdot \frac{d(\cos\nu'_p)}{d(\cos\theta'_p)} . \qquad (42)$$

The term in the bracket is simply equal to $\frac{K_p}{K'_p}$ (see Appendix B). Therefore equation (39) will take its new form by substituting equation (42), bearing in mind the equality of

$$\frac{\partial(E'_p,\ \cos\theta'_p)}{\partial(E_p,\ \cos\theta_p)} = \frac{K_p}{K'_p} :$$

$$d\sigma = c(d\sigma(\omega',\ \nu^*_p)/d\Omega^*_p)_d\ G(K)\ d\vec{K}\ B(\omega)\ J_1.J_2.J_3.J_4\ dE_p\ d\Omega_p \tag{43}$$

where $J_4 \equiv \dfrac{d(\cos\nu'_p)}{d(\cos\theta'_p)} \cdot \dfrac{K_p}{K'_p}$. Finally the double differential cross-section for the (γ, np) process is given by:

$$\frac{d^2\sigma}{dE_p d\Omega_p} = c \int d\vec{K}\ G(K)\cdot(d\sigma(\omega',\ \nu^*_p)/d\omega^*_p).B(\omega).J_{tot} \tag{44}$$

where $d\vec{K} = d^3K = K^2dK\ \sin\psi d\psi d\phi$ and $J_{tot} = |J_1.J_2.J_3.J_4|$.

In equation (44) the integration is over the momentum distribution of the pair. The integration is justified because the undetected nucleon is of course not necessarily coplanar with the detected proton and photon.

An unsolved issue is the matter of constant (c) in equation (44). The calculation of this constant will proceed as follows:

The integration of equation (44) over all energies and angles gives the total cross-section, i.e.

$$\sigma^A_{qd} = \iint \frac{d^2\sigma}{dE_p d\Omega_p}\ dE_p\ d\Omega_p \tag{45}$$

or,

$$\sigma A_{qd} = c\left[\iiint dE_p\ d\Omega_p\ d\vec{K}\ G(K)(d\sigma(\omega',\nu^*_p)\ /d\Omega^*_p)_d.B(\omega).J_{tot}\right] \tag{46}$$

then,

$$\sigma^A_{qd} = c\ \sigma^A_q \tag{47}$$

where σ^A_q is equal to the term in brackets in equation (46) and σ^A_{qd} is the total photonuclear absorption cross-section considering

alteration due to binding-energy and Fermi-motion effect for the correlated proton-neutron pairs inside the real nuclei. On the other hand, the widely used Levinger expression without due consideration to these effects was introduced by:

$$\sigma_{qd} = \frac{L}{A} NZ\ \sigma_d(E_\gamma) \quad . \tag{48}$$

This expression can be weighted by the same photon spectrum as that in equation (46), i.e. $B(\omega)d\omega$, then

$$\sigma_{qd} = \frac{L}{A} NZ\ [\ \int \sigma_d(\omega)\ B(\omega)\ d\omega\ ] \quad . \tag{49}$$

The term in the bracket is total deuteron cross-section and it can be equal to σ_q^A in equation (47) by defining the following relation

$$\sigma_q^A = \frac{1}{c'} \int \sigma_d(\omega)\ B(\omega)\ d\omega \quad . \tag{50}$$

Constant c'^{-1} denotes the reduction of $\int \sigma_q(\omega)\ B(\omega)d\omega$ in order to be equal to σ_q^A . The reason for this reduction is that, σ_{qd} without due consideration to the binding-energy and Fermi-motion effects, overestimates the total photonuclear absorption cross-section for a $_Z^A N$ nucleus.

Therefore the constant c in equation (47) can be defined as:

$$c = \frac{L}{A} NZ. \tag{51}$$

Justification for equation (51) can be fulfilled by the multiplication of σ_q^A in equation (47) by constant c' (defined by equation (50)) which will make equation (47) equal to equation (49).

Thus, equation (44) will take its appropriate form which is suitable for further calculation, i.e.

$$\frac{d^2\sigma}{dE_p d\Omega_p} = \frac{L}{A} NZ \int \vec{dK}\, G(K).(d\sigma(\omega',\nu^*_p)/d\Omega^*_p)_d.B(\omega).J_{tot}. \qquad (52)$$

This is the expression which has been used during the calculation of energy distribution of the primary nucleons. The term nucleon can now be specified by neutron or proton because the calculation of each of them would be completely symmetric if the proton and neutron masses are assumed to be equal.

Equation (52) can be used to calculate the contribution from different shells if one introduces a suitable value for $\overline{Q}$, as a separation energy of the pair picked up from a particular shell in a specific nucleus. However, there are two more terms which must be specified before one can evaluate the shell's contribution. The first term is momentum distribution of pair $G(K)$ and the next one is the pseudo-Levinger constant.

2.2.3.3 Momentum Distribution of Quasi-Deuteron

The pair momentum distribution $G(K)$ has been suggested[71] as a simple Gaussian function of the form:

$$G(K) = A \exp\left(-\frac{K^2}{2\alpha^2}\right) \qquad (53)$$

where α is the width of the Gaussian distribition. Constant A can be evaluated using the normalization condition $(A = 2\pi\alpha^2)^{-3/2}$.

$$\int G(K) d^3K = 1 \; . \qquad (54)$$

For the purpose of evaluation of a shell's contribution to the final cross-section, one needs to derive separately the momentum distribution for each shell. The most powerful expression for closed shell nuclei was suggested by Gottfried[16]

$$G(K) = \sum_{nn'\ell\ell'} \sum_{\rho=|\ell-\ell'|}^{\ell+\ell'} (2\ell+1)(2\ell'+1) \left| <\ell\ell' oo|\rho o> \right|^2 \times$$

$$\times \left| \int_0^\infty R_{n\ell}(r) R_{n'\ell'}(r) j_\rho(Kr) r^2 dr \right|^2 \qquad (55)$$

where $<\ell\ell' oo|\ \rho o>$ is a Clebsch-Gordan coefficient, $R_{n\ell}(r)$ is the radial part of the wavefunction $\psi_{\ell nm}(r)$; and $j_\rho(Kr)$ is the spherical Bessel function of order ρ. In section (2.2.4) a simple example will be given where the construction of $G(K)$ for different shells will be carried out by the use of expression (55).

2.2.3.4 Pseudo-Levinger Constant for Shells' Contribution

The last parameters tc be discussed are the pseudo-Levinger constant and the number of nucleon pairs in each shell. In section (2.2.2) the process of constructing the pseudo-Levinger constant for each shell and the number of nucleon pairs for a particular shell, was discussed. However, in the case of double differential cross-section one can construct the pseudo-Levinger constant for each shell by the use of equation (47), where constant c is defined similar to equation (51), i.e.

$$c = L'_\beta \ N_\beta \ Z_\beta \qquad (56)$$

where use has been made of equations (16) weighted by the same photon spectrum, i.e. $B(\omega)d\omega$.

Therefore the double differential cross-section for a particular shell can then be written as:

$$\left[\frac{d^2\sigma}{d\Omega_p dE_p}\right]_\beta = L'_\beta \ N_\beta \ Z_\beta \int d^3K \ G_\beta(K) \left[\frac{d\sigma}{d\Omega^*_p}\right]_d B(\omega) J_{tot}. \qquad (57)$$

Finally,

$$\left[\frac{d^2\sigma}{d\Omega_p dE_p}\right]_F = \sum_\beta \left[\frac{d^2\sigma}{d\Omega_p dE_p}\right]_\beta \qquad (58)$$

where β can take the forms of β = 1S-1S, 1S-1P and so forth. $N_\beta Z_\beta$ is the number of pairs to be considered for each shell. $G_\beta(K)$ is the momentum distribution for a particular shell under consideration. L'_β is again pseudo-Levinger constant.

In the following subsection, i.e. (2.2.3.5), two different approaches with the intention of calculating double differential cross-section for photo-induced reaction will be discussed. Then, in section (2.2.4), ^{12}C will be used to demonstrate (by a simple example) how the construction of the quantities $\left[\frac{d^2\sigma}{d\Omega_p dE_p}\right]_\beta$ and $\left[\frac{d^2\sigma}{d\Omega_p dE_p}\right]_F$ can be carried out.

2.2.3.5 Discussion Concerning Two Approaches for Deriving the Double Differential Cross-Section for (γ, np) Process.

The derivation of double differential cross-section for (γ, np) was discussed in subsection (2.2.3.2). Equation (52) was derived with the intention of analysing experimental data using the continuous photon-spectrum. As it was mentioned before, it is possible to derive an expression for monochromatic photon induced double differential cross-section. The starting point can be equation (34), i.e.

$$d\sigma^\omega = c \frac{d(\cos\nu'_p)}{d(\cos\theta_p)} \cdot J_1 (d\sigma(\omega', \nu^*)/d\Omega^*_p)_d \, d\Omega . G(K) d\vec{K} \quad . \qquad (59)$$

This equation can be written as follows by writing

$d\vec{K} = K^2 dK \sin\psi d\psi d\phi$, i.e.

$$d\sigma^{\omega} = c \frac{d(\cos\nu'_p)}{d(\cos\theta_p)} \cdot J_1 (d\sigma(\omega',\nu^*)/d\Omega^*_p)_d \frac{dK}{dE'_p} \cdot dE'_p \, d\Omega . G(K) K^2 \sin\psi d\psi d\phi . \tag{60}$$

By using equation (40), equation (60) takes the new form, i.e.

$$\frac{d^2\sigma^{\omega}}{dE_p d\Omega_p} = c \, J_1 . J_4 . J_5 . (d\sigma(\omega',\nu^*)/d\Omega^*_p)_d G(K) K^2 \sin\psi d\psi d\phi \tag{61}$$

where J_4 was introduced before in equation (43) and $J_5 = \frac{dK}{dE'_p}$ in Appendix B. Therefore, equation (61) can be integrated on $d\psi$ and $d\phi$ by:

$$\frac{d^2\sigma^{\omega}}{dE_p d\Omega_p} = c \int G(K) K^2 . J_{tot} . (d\sigma(\omega',\nu^*)/d\Omega^*_p)_d . \sin\psi d\psi d\phi \tag{62}$$

where $J_{tot} = J_1 . J_4 . J_5$. Equation (62) can then be weighted by bremsstrahlung intensity for the purpose of comparing with bremsstrahlung photo-proton data. Using the approach mentioned above needs a careful consideration of the relation between K, ψ and ϕ and further investigation is necessary in order to use this approach in the analysis of experimental data.

2.2.4 The Clarification of Calculation Concerning Double Differential Cross-Section

2.2.4.1 Introduction

In this section the calculation of double differential cross-section for photo-induced reaction will be carried out by the use of the formalism given in section (2.2.3). In this calculation, equation (57) for individual shell contribution and equation (58) for final double differential cross-section as a sum of individual contribution have been

incorporated. Calculation of the total cross-section which was carried out by the use of two types of potentials in section (2.2.2) can now be extended for the evaluation of double differential cross-section.

Thus one can again choose the target ^{12}C for the demonstration of the calculation by using the two following potentials for (γ, np) process.

a) square well potential

b) harmonic oscillator potential.

In the following these two cases will be discussed.

2.2.4.1a. Choice of Square Well Potential

Calculation of the three contributions from 1S-1S, 1S-1P and 1P-1P can easily be done by the use of equation (57). For this equation, calculation of terms such as pseudo-Levinger constant and number of possible pairs was discussed in (2.2.2). The term G(K) is constructed by the means of equation (55) for different shells using the corresponding eigenfunctions of the pure square well. The results of $\left[\frac{d^2\sigma}{d\Omega_p dE_p}\right]_\beta$ and $\left[\frac{d^2\sigma}{d\Omega_p dE_p}\right]_F$ for ^{12}C are given in Figure 2.7 , and are compared with some data[71] for (γ, p) process on ^{12}C using Bremsstrahlung end-point energy of 98.5 MeV. In Figure 2.8, the shape of $G_\beta(K)$ for different shells is demonstrated. Although ^{12}C is not a closed shell nuclei, equation (55) is used with an appropriate weighting factor $(N_\beta Z_\beta)$, which will take into account the reduction of the number of p-shell nucleons in contrast to a closed shell nuclei.

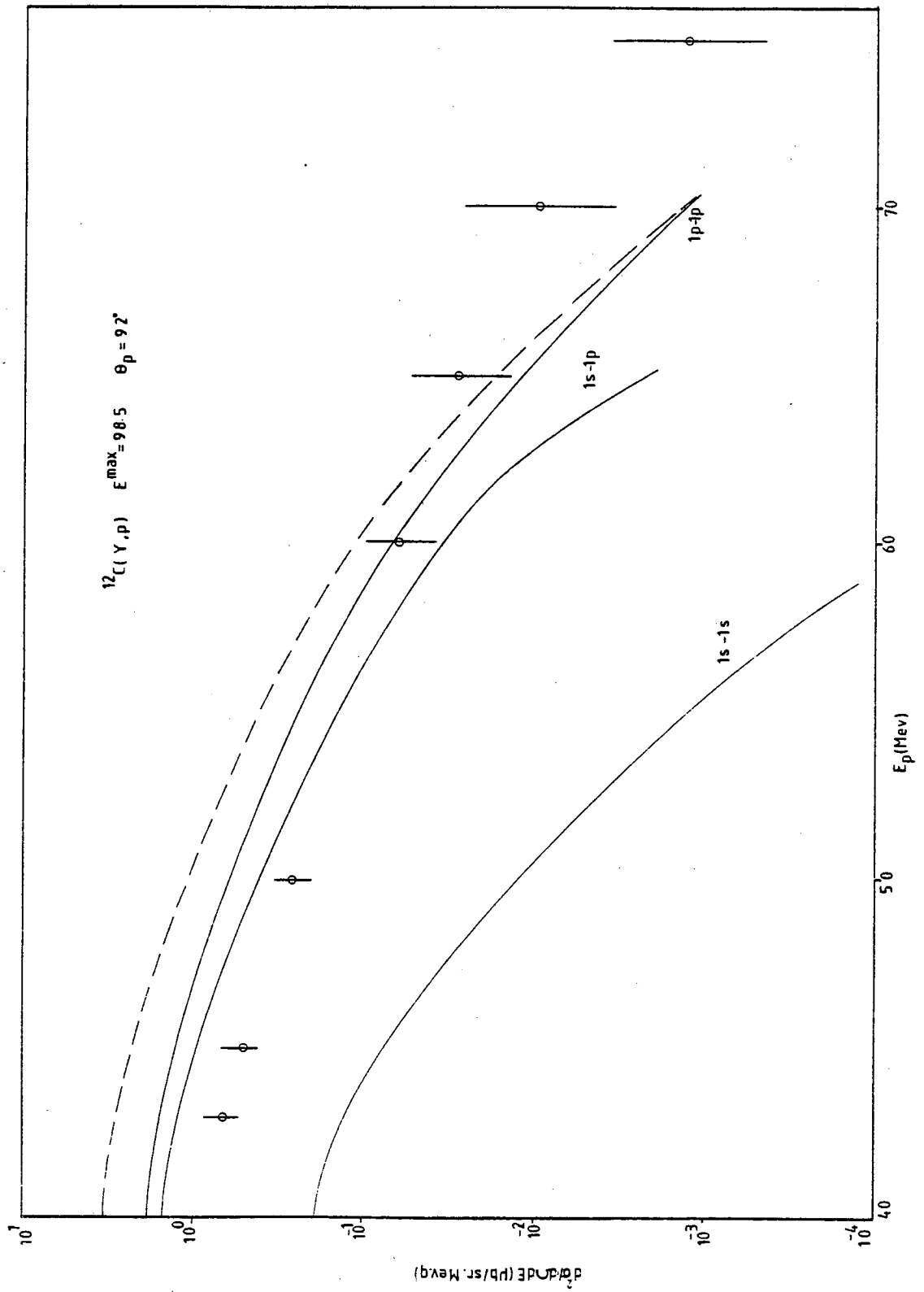

Figure 2.7: Proton double differential cross-sections are calculated using the square well potential and compared with the experimental data[71]. Empty circle: experimental data. Broken curve: sum of shell's contribution. Full curves: contribution from different shells.

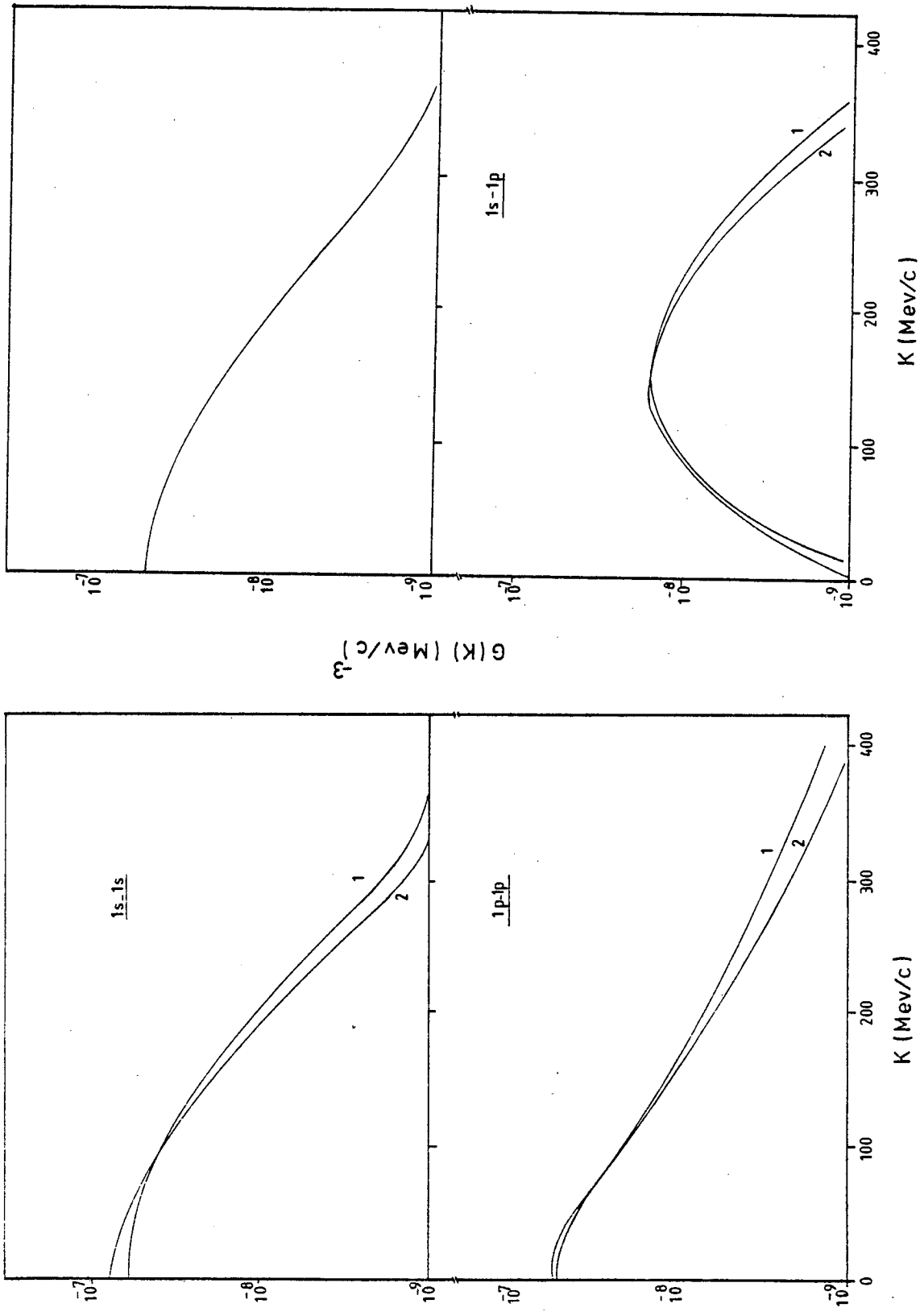

Figure 2.8: Curves (1) and (2) are the quasi-deuteron momentum distribution (^{12}C) using the square well and harmonic oscillator associated wavefunctions, respectively (see section 2.2.4). Top right corner curve is the deuteron momentum distribution using equation (53).

2.2.4.1b Choice of Harmonic Oscillator Potential

For harmonic oscillator potential, the procedure to calculate L'_β and $N_\beta Z_\beta$ which was mentioned in section (2.2.2) will be used. The momentum distribution $G_\beta(K)$ using harmonic oscillator wave-functions can again be structed by means of equation (55). The shapes of $G_\beta(K)$ for 1S-1S, 1P-1P and 1P-1S are shown in Figure 2.8. The double differential cross-sections $\left[\frac{d^2\sigma}{d\Omega_p dE_p}\right]_\beta$ and $\left[\frac{d^2\sigma}{d\Omega_p dE_p}\right]_F$ using ^{12}C are evaluated and the results can be seen in Figure 2.9 (where comparison is made with (γ,p) data taken by Matthews et al.[71]).

2.2.4.2 Discussion Related to the Results of Double Differential Cross-Sections

The results of double differential cross-section for $^{12}C(\gamma,p)$ show that by using square well potential the data lie below the sum of shell's contribution (Fig. 2.7, broken line). On the other hand, the results of calculation of $\left[\frac{d^2\sigma}{d\Omega_p dE_p}\right]$ for the case of harmonic oscillator significantly overestimate the experimental data (Fig. 2.9, broken line). As Figures 2.7 and 2.9 show, the calculated values fall below data in the energy region above 60 MeV. This discrepancy in both cases may be due to other channels contributing to the build-up of cross-section, e.g. direct (γ,p). It must be pointed out that the final state effects have not been considered and the consideration of it may widen further the gap between the calculated and the experimentally taken data.

In the next section a brief summary of the computer programme constructed to calculate double differential cross-sections will be discussed.

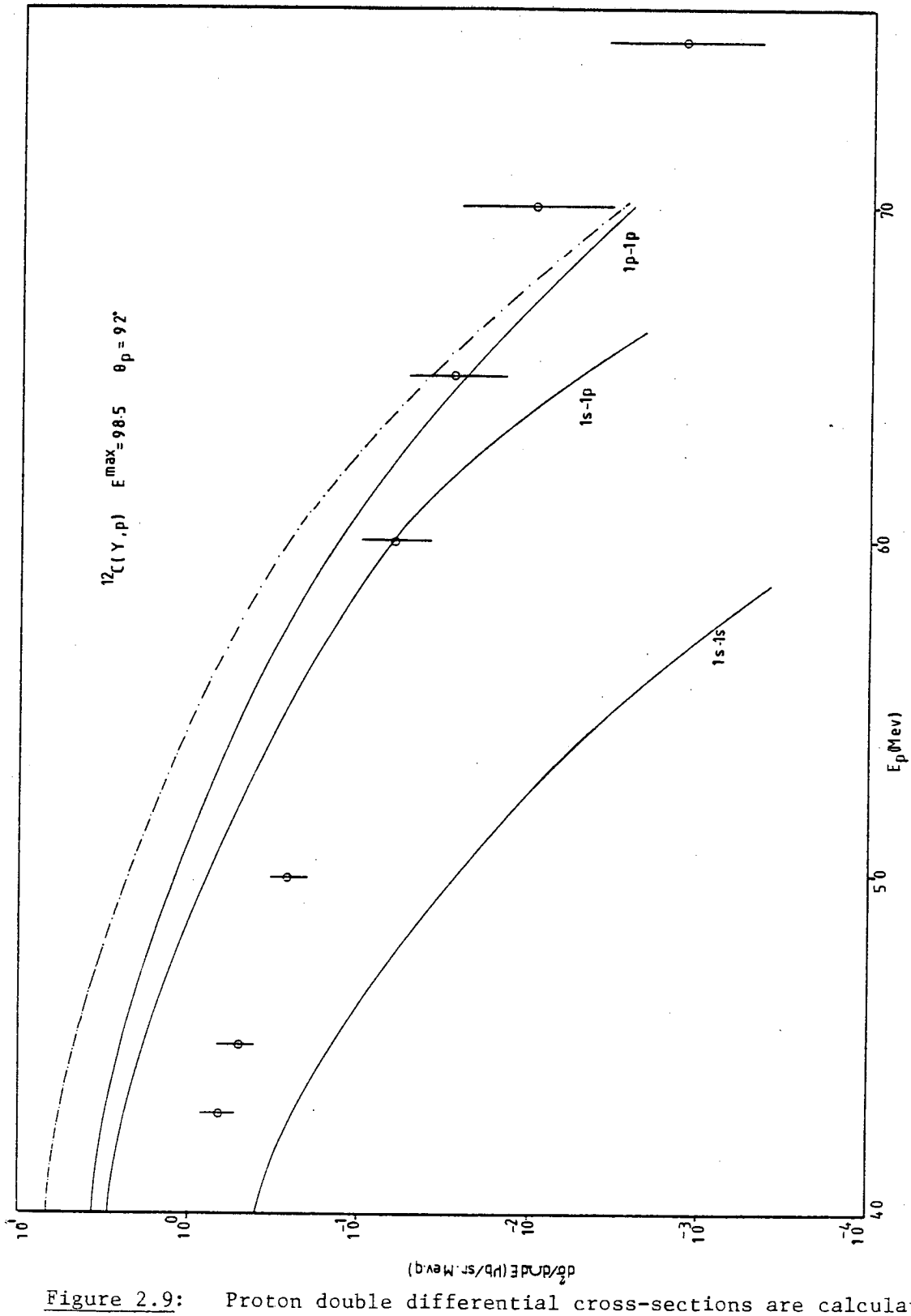

Figure 2.9: Proton double differential cross-sections are calculated using the harmonic oscillator potential and compared with the experimental data[71]. Empty circle: experimental data. Dash-dotted curve: sum of shell's contribution. Full curves: contribution from different shells.

2.3.Ø. The Computer Programme Constructed to Calculate the Double Differential Cross-section for the A(γ,np)A-2 Process

The task of evaluating the double differential cross-sections $\left[\frac{d^2\sigma}{d\Omega_N dE_N}\right]_\beta$ where N denotes the proton or neutron, was carried out by constructing a computer programme capable of performing the integration on the momentum of the pair in equation (57). In section (2.3.1) the procedure to calculate the cross-sections for the photo-disintegration of the deuteron will be given and then in section (2.3.2) the main steps taken in order to calculate equation (57) will be outlined.

2.3.1 Calculation of Deuteron Cross-section (γ+D → n+p)

In a paper by Partovi[69] the following equation was introduced to calculate the cross-sections for photo-disintegration of the deuteron

$$\frac{d\sigma}{d\Omega^*_N}(\omega', \nu^*_N) = a + b\sin^2\nu^* \pm c\cos\nu^* \pm d\sin^2\nu^*\cos\nu^* + e\sin^4\nu^* \quad (63)$$

where the +ve signs apply to proton detection and the -ve signs to neutron detection. All the parameters (a, b, c, d and e) were tabulated for different energies in the Partovi[69] paper. This equation was used for photon energies less than 80 MeV. (N = proton or neutron).

For photon energies above 80 MeV, the least square fits to Kose et al.[72] data were given by themselves. They fitted their measurements with the function:

$$\frac{d\sigma}{d\Omega^*_N}(\omega', \nu^*_N) = A \pm B\cos\nu^* + c\cos^2\nu^* \quad (64)$$

where the +ve and -ve signs apply to the detection of protons and neutrons respectively. This expression has been used to calculate the cross-section for photo-energy above 100 MeV.

2.3.2 A Brief Summary of the Computer Programme

The main steps taken in order to evaluate equation (57) are outlined as follows:

I. The photon energy is calculated for a set of specified angle and energy for the outgoing particle for a particular set of pair momentum variables, i.e. K, ψ and ϕ. The calculation can be performed by means of conservation of momentum and energy equations (24) and (28), i.e.

$$\omega = F(K, \psi, \phi, E_N, \theta_N) \quad .$$

II. Intensity of bremsstrahlung $B(\omega)$ for the specified photon energy in part (I) was calculated for photon-induced reactions by means of extreme relativistic formula of Bethe and Heitler[73, 74] and for electron-induced reactions by using the DWBA formalism[75].

III. The momentum distribution of a correlated neutron and proton pair, G(K), can be evaluated by choosing either the square well or harmonic oscillator potentials for a specified value of K using equation (55) (for a particularly chosen shell).

IV. Free deuteron differential cross sections, $\frac{d\sigma}{d\Omega_N^*}(\omega', \nu_N^*)$, for photo energies less than 80 MeV were constructed by interpolation between the calculated cross-section according to the Partovi formula[69] and for the photon energy range above 100 MeV a least squares fit to Kose et al.[72] angular distribution data provides the necessary expression for the cross-section of photo-

disintegration of the deuteron. An interpolation between the Partovi calculations and the measurements of Kose et al. was made in the photon energy range 80-100 MeV (see section 2.3.1).

V. Calculation of two total Jacobians by using the formalism discussed in section (2.2.3), (see Appendix B) was made and the integration on d^3k ($d^3k = k^2dk\ \sin\psi d\psi d\phi$) then carried out. The final calculation of the double differential cross-sections could be determined with the values of pseudo-Levinger constant calculated as given in section (2.2.2) for a particularly chosen shell.

2.4.Ø. Conclusion and Further Objectives

The immediate consequences of the approach mentioned in this chapter can be classified into two categories:

a) Calculation of the total and double differential cross-section without a floating factor has been achieved for the cases of interest, i.e. pure square well and harmonic oscillator potentials, for the (γ, np) process.

b) Comparison of the evaluated proton double differential cross-section with experimental data,[71] for the case of pure square well potential, overestimates data by a small factor 4 (in the region less than 60 MeV (Fig. 2.7). In a similar comparison using the harmonic oscillator potential the calculation overestimates data by a large factor 8 (in the region less than 60 MeV (Fig. 2.9)). The calculated results also show that both of the potentials cases are not capable of reproducing the data in the region above 60 MeV. The interesting point is the difference in the use of these two potentials which is about a factor of 2 in the resulting double differential cross-section (Figure 2.10).

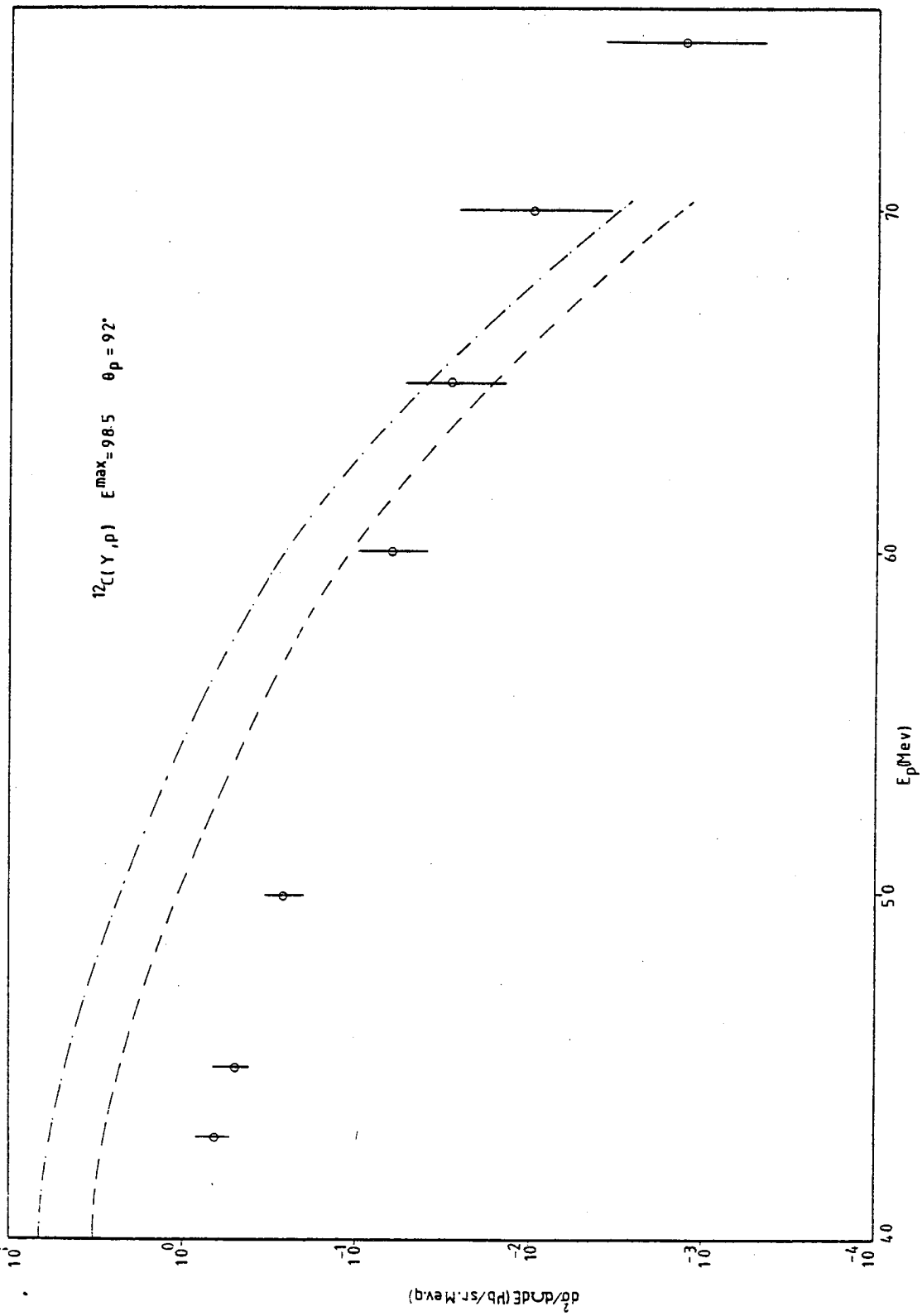

Figure 2.10: The calculated results in Fig. 2.7 (broken curve) and in Fig. 2.9 (dash-dotted curve) are compared with experimental data[71] (empty circle).

The double differential cross-section was also evaluated using for the G(K) a simple Gaussian distribution (refer to equation (53) and Fig. 2.8, top right corner curve). This cross-section is compared with the above mentioned data (Fig. 2.11) where a normalization factor in the form of Levinger constant $L = 2$ and a factor $\frac{NZ}{A}$ are incorporated (the oscillator parameter $\alpha = 109$ MeV/c).

A comparison can also be made between the double differential cross-section that results from either a pure square well or harmonic oscillator potential and the double differential cross-section evaluated using the previously referred Gaussian distribution for G(K) (Fig. 2.12).

The objective of this chapter was to provide a new approach for the calculation of the final (double differential cross-section in the process for the (γ,np) reaction. The final state interactions were ignored in this type of calculation because the chosen target was a light one and in this situation the outgoing particles are not that much sensitive to secondary collisions with the other target nucleons.

The main objective of the next chapter is to introduce a formalism in order to take final state interactions into consideration for medium and heavy target nuclei where the final state interaction becomes important. As a natural extension of this investigation emission of complex particles, e.g. α-partice, as part of the final stage in the (γ,np) reaction will also be considered.

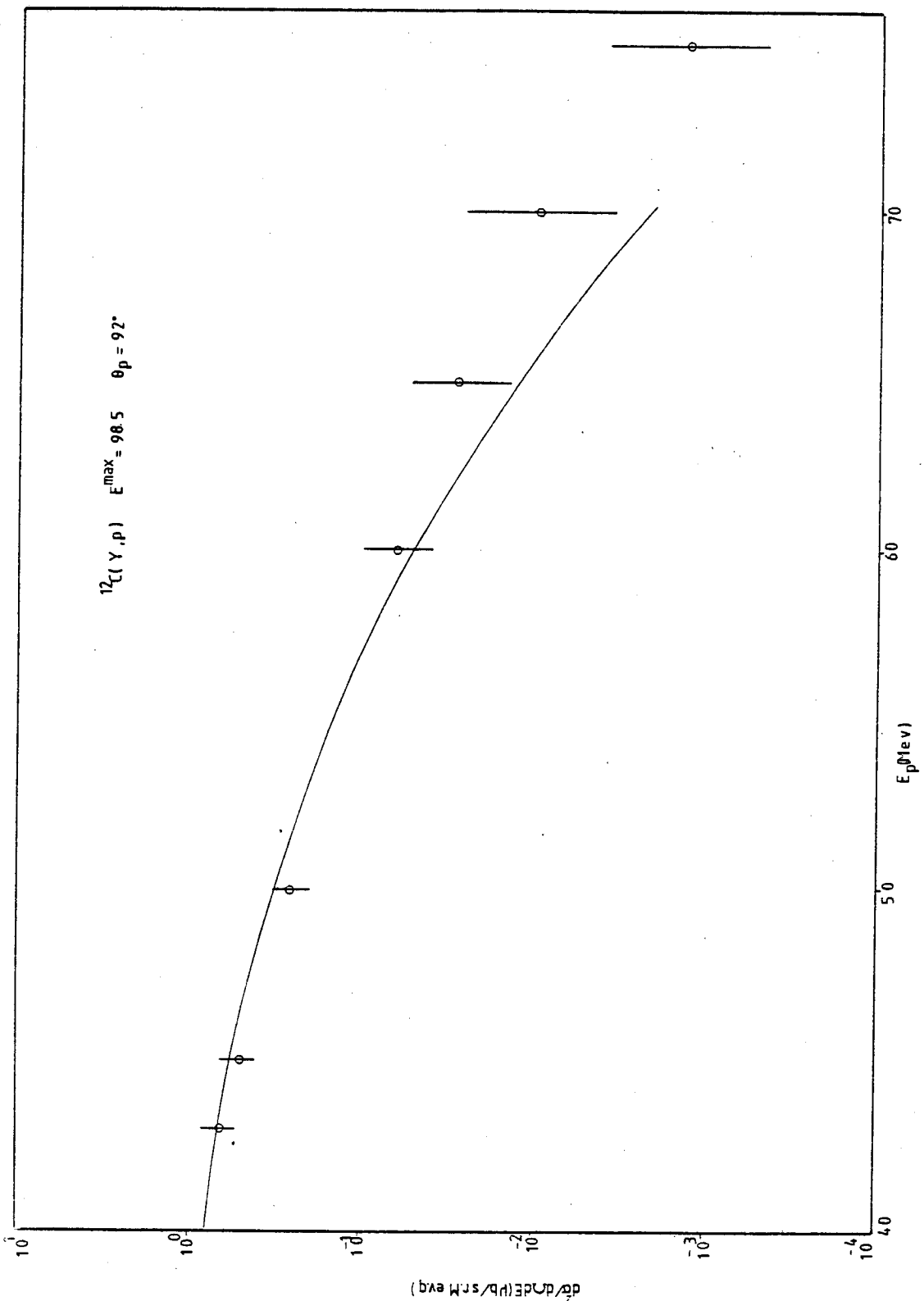

Figure 2.11: Comparison of calculated double differential cross-section using the floating factor Levinger L = 2 (see section 2.4.0) with experimental data[71] (empty circle).

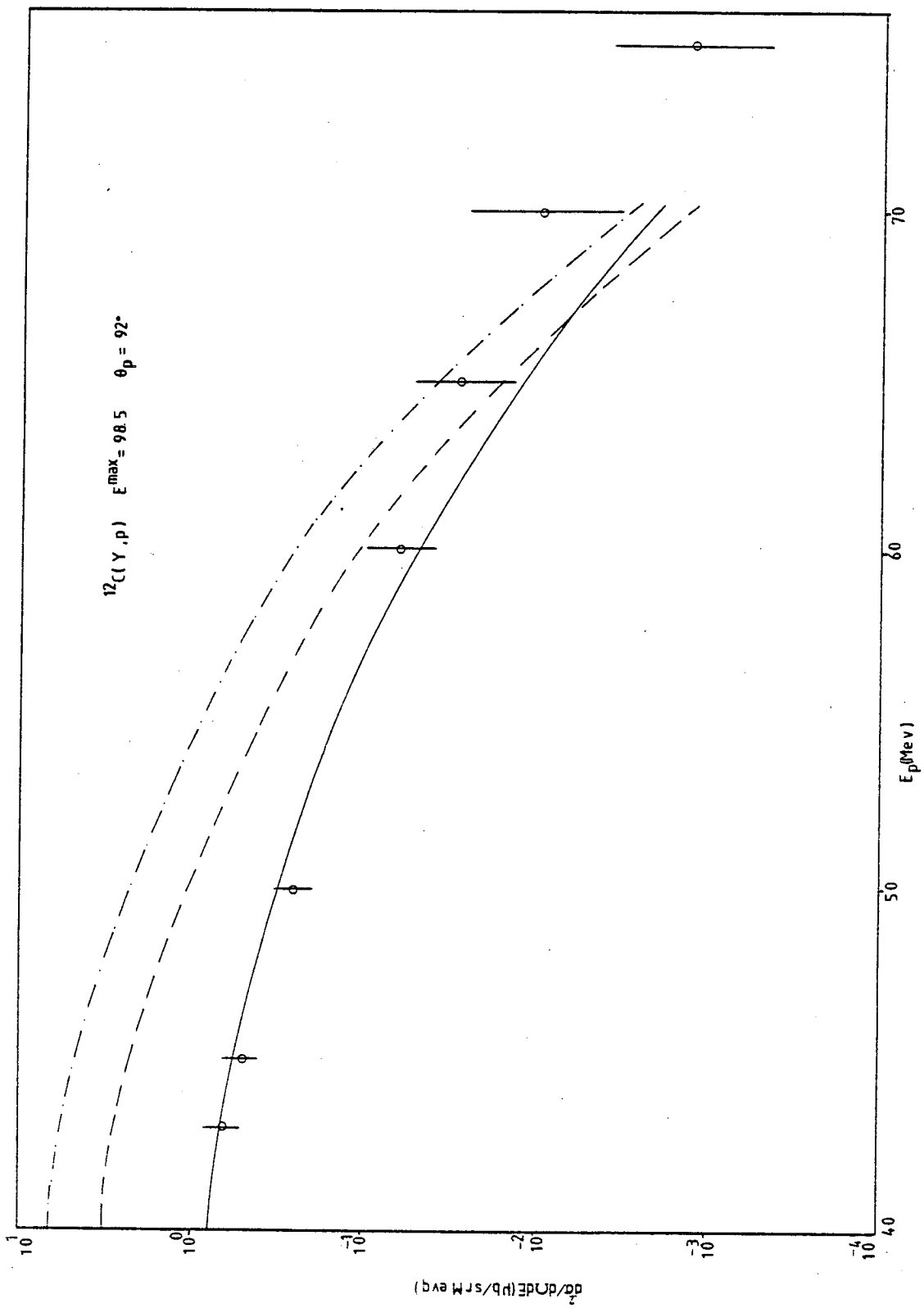

Figure 2.12: The calculated results in Fig. 2.7 (broken curve) and in Fig. 2.9 (dash-dotted curve) together with the results in Fig. 2.11 (full curve) are compared with the experimental data[71].

CHAPTER III

QUASI-FREE SCATTERING MODEL

3.1.Ø Introduction

The quasi-free scattering model [6] for particle induced reactions providing pre-compound energy distribution of emitted particles will be explained in this chapter. This model was chosen from among all the pre-compound models (see Chapter I) because of its success in producing the energy distribution of particles emitted prior to the equilibrium state for the nucleus.

The central assumption which this model is based on is the use of quasi-free scattering mechanism. To this end the model will be referred to as the QFS model. There are two types of nucleon induced reactions which are of interest in the present study. In the first type the emission of nucleons is the prime interest, while in the second type the emission of α-particles is of interest. The reason for studying these reactions is that it provides a direct link for the investigation of the energy distribution of reaction of the types 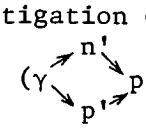 , 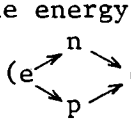 , see diagrams 3.1(A) and 3.1(B).

In section (3.2.Ø), the description of the principles governing the QFS model for (Nucleon, Nucleon') reactions will be given, then the formulation of the QFS model for (N,N') reaction will be presented in section (3.2.1). The principles of the QFS model for the case of (Nucleon-Alpha) reactions will be discussed in section (3.3.Ø) and the related formulation for this case will be given in section (3.3.1). Finally, in section (3.4.Ø) a formalism will be developed for the specific photo-nuclear induced (γ, p) and (e, α) reactions using the QFS model.

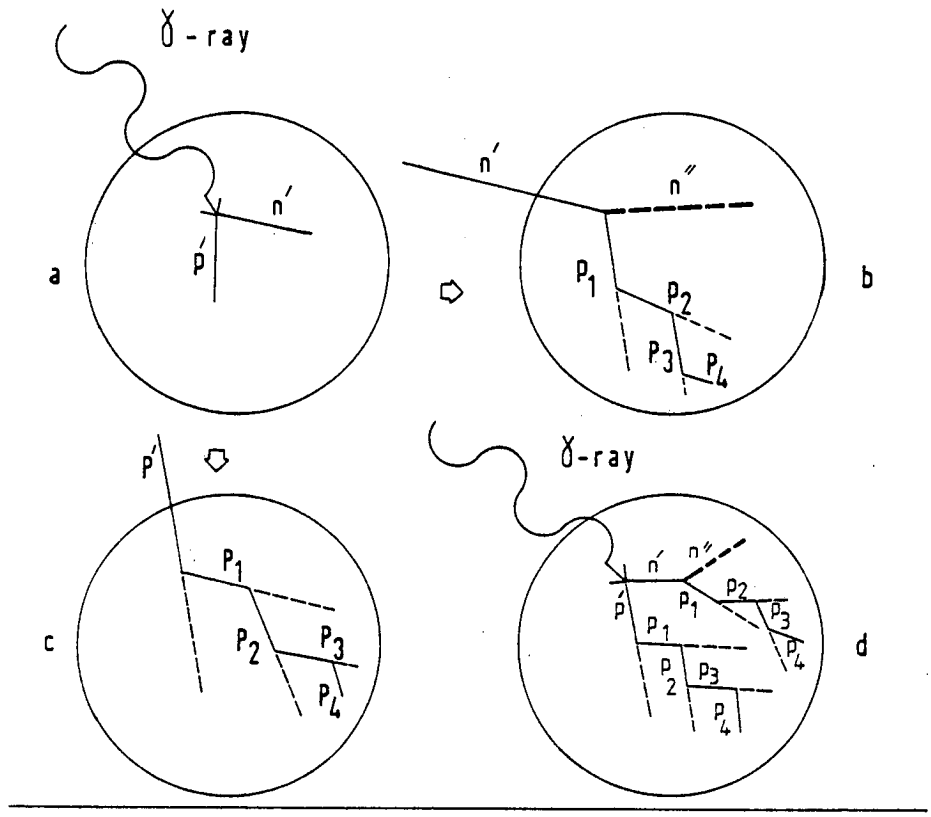

Diagram 3.1(A)

a) Collision of γ-ray with a correlated neutron and proton

b) The process of collision between neutron and proton inside the nucleus (The QFS model is used).

c) The process of collision between proton and proton inside the nucleus. (The QFS model is used).

d) The reaction of type (γ,p) can be explained by linking γ-induced reaction (a) to the nucleon-induced reactions b) and c) for considering the final state interaction mechanism, i.e. (γ → n' → p) (γ → p' → p)

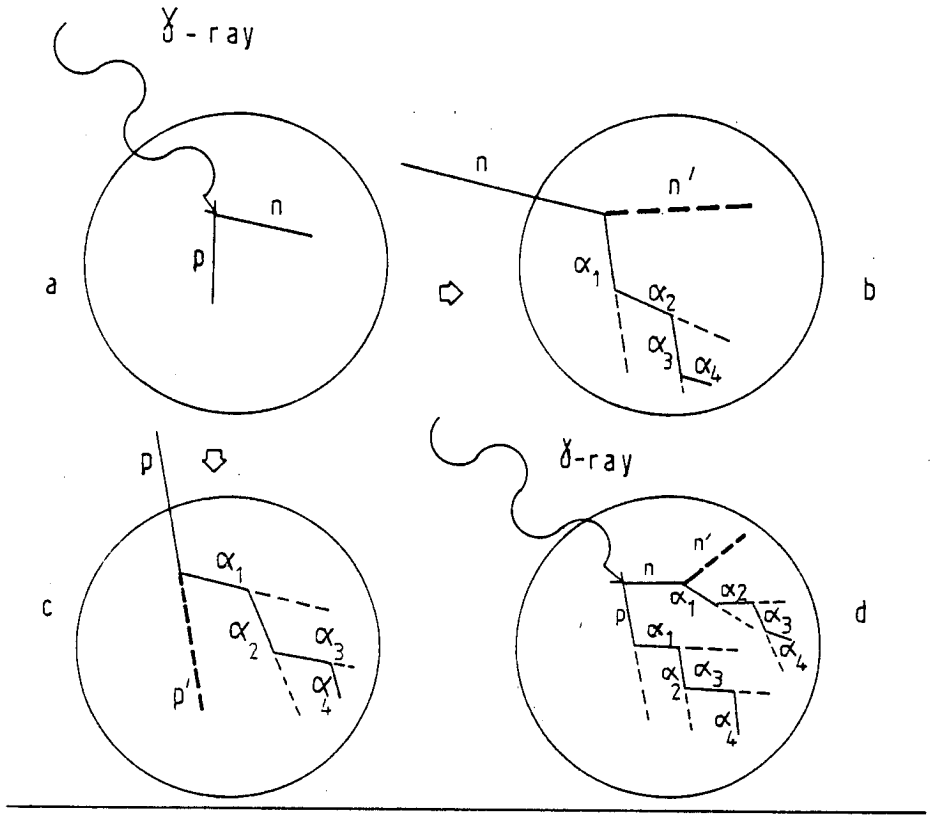

Diagram 3.1(B)

a) Collision of γ-ray with a correlated neutron and proton.

b) The process of collision between neutron and α-particle inside the nucleus (The QFS model is used).

c) The process of collision between proton and α-particle inside the nucleus. (The QFS model is used).

d) The reaction of type (γ,α) can be discussed by linking γ-induced reaction (a) to the nucleon-induced reactions (b) and (c) for considering the final state interactions, i.e. $(\gamma \nearrow \begin{matrix} n \searrow \\ p \nearrow \end{matrix} \alpha)$. It is noticeable that the process of collision between n or p with nucleon and subsequently with α-particles, has not been shown in (b), (c) and (d) (see section 3.3.0).

3.2.Ø Principle of the Quasi-Free Scattering Model for (Nucleon-Nucleon') Reactions

The basis of the quasi-free scattering model for nucleon induced reactions are as follows:

I) The reaction of the nucleon with the target nucleus is viewed microscopically as proceeding through a series of two-body collisions between the projectile nucleon and the nucleons within the target. Blann et al.[6] assumed this to conform to Fermi gas model momentum distribution.

II) At time t_o when the nucleus is in the ground state, the nucleon enters the potential well of the target nucleus. The two-body collisions of the projectile nucleon with all possible nucleons in the target are computed using free nucleon-nucleon angular distributions to determine the energy distributions of the projectile nucleon in the well after collision.

III) Phase space arguments are applied to the calculation of the emission rate versus the internal transition rate of the projectile nucleon (see diagram 3.2).

IV) The result after the first interaction at time t_1 is a projectile nucleon energy distribution in the nuclear well, and an emission spectrum for the inelastically scattered projectile nucleon. The struck nucleon energy distribution inside the nucleus and its emission spectrum has been taken into account.

V) As this process is repeated the projectile nucleon continues to lose energy to the nucleons until equilibrium is obtained.

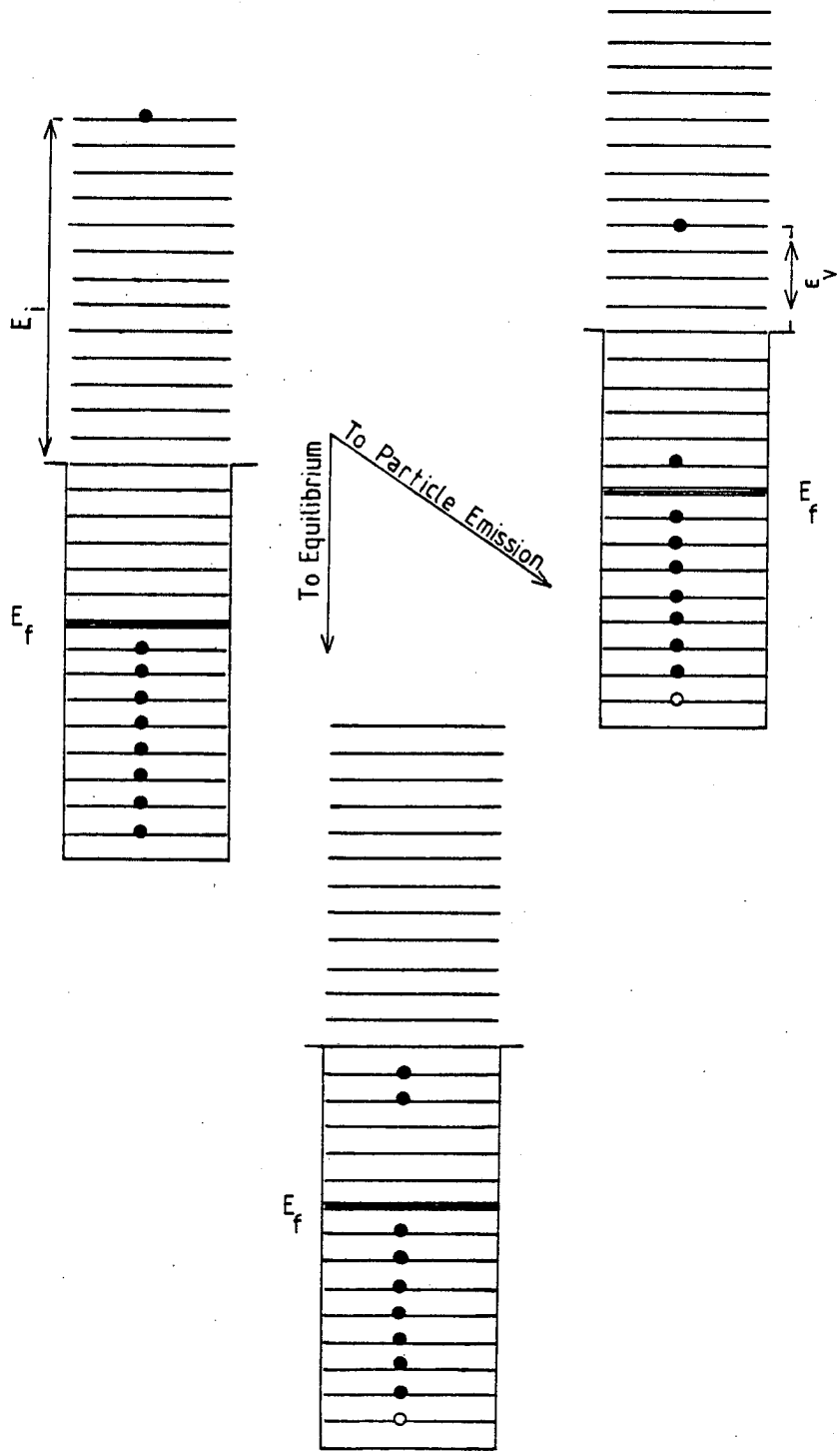

Diagram 3.2: Pictorial representation of the ideas of the two-body interaction toward an equilibrium and the possibility of emission of particles. Full circle is particle and empty circle is hole.

In the next section the above principles will be formulated in order to calculate the energy distribution for (Nucleon-Nucleon') reactions.

3.2.1 Related Formulation for (N, N') Reactions

One can divide the potential well of the target nucleus into 1 MeV bins, then an incident nucleon of laboratory energy E_i enters the potential well of the target nucleus with Fermi energy E_f. For convenience the energy of the incident nucleons is measured from the bottom of the nuclear well, (see diagram 3.3).

$$E_i' = E_i + E_f + BE_n \qquad (1)$$

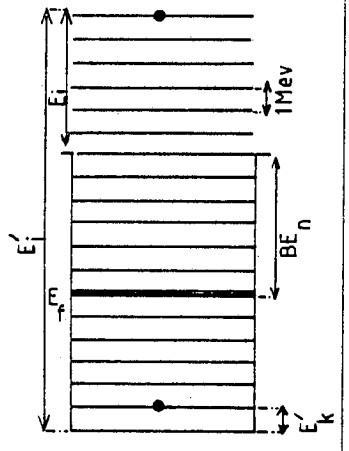

Diagram 3.3

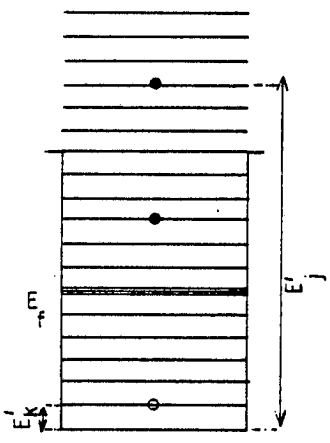

Diagram 3.4

where $E_f + BE_n$ = well depth, BE_n is the binding energy of the nucleon to the target nucleus. The process of two-body collisions between a nucleon above the Fermi energy and one below the Fermi energy will result in two nucleons above the Fermi energy. These energies will be defined by E'_j. The nucleons in the Fermi sea are specified by energy E'_k (see diagram 3.4).

The total emission probability can be expressed as the ratio

of the transition rate into the continuum to the total transition rate. The assumption made is that the emission probability is governed by phase space considerations and is dependent only on the energy of the particle being emitted and the energies of the nucleons in the well.

The kinetic energy spectrum is a result of nucleon emission from all possible E_j'. The total probability for emitting a nucleon with energy ε_ν is given by:

$$P_\nu(\varepsilon_\nu) = \frac{\lambda_c(\varepsilon_\nu)}{\lambda_c(\varepsilon_\nu) + \sum_{k=1}^{E_f} \lambda_{kj}} \qquad (2)$$

where ε_ν is the laboratory energy at which the nucleon with a possible E_j' energy is emitted into the continuum, (see diagram 3.5).

$$\varepsilon_\nu = E_j' - (E_f + BE_n) \quad . \qquad (3)$$

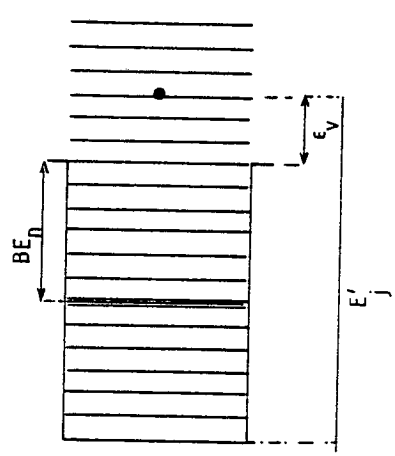

Diagram 3.5

The intranuclear transition rate for a nucleon of energy E_j' interacting with a nucleon of energy E_k' is denoted by λ_{kj} and the summation is taken over all nucleons in the nuclear well with energy $E_k' = 1$ MeV to E_f. The term λ_{kj} can be derived by using the standard rate expression for a beam of particles incident on a thin target of nuclear matter[76], i.e.

$$\lambda_{kj} = [\sigma_{kj} \; \nu_j' \; g_k'] \; /V \tag{4}$$

where σ_{kj} is the Pauli allowed nucleon-nucleon scattering cross-section and ν_j' the velocity of the nucleon with energy E_j' in the nuclear well. g'_k is the number of nucleon states per MeV at an energy E_k' in the target nucleus below the Fermi energy where it is normalized to the nuclear volume V. The term $\lambda_c(\varepsilon_\nu)$ is the rate for emission into the continuum of particles with channel energy ε_ν which is situated above the Fermi energy. The emission rate into the continuum is given by applying phase space considerations and it takes the following form[76]:

$$\lambda_c(\varepsilon_\nu) = \left[\frac{\sigma_{inv}(\varepsilon_\nu)\nu_\nu}{\Omega}\right]\left[\frac{\omega_c(\varepsilon_\nu)}{g_j'}\right] \tag{5}$$

where $\sigma_{inv}(\varepsilon_\nu)$ is the inverse cross-section for particle ε_ν, and Ω is the volume in which the free particle phase space states are normalized. The velocity of nucleon with energy ε_ν outside the nuclear well is ν_ν and finally, $\omega_c(\varepsilon_\nu)$ is the continuum state density[6,76], i.e.,

$$\omega_c(\varepsilon_\nu) = (4\pi\Omega(2m)^{3/2}/h^3)\varepsilon_\nu^{1/2} \tag{6}$$

where m is the nucleon mass. The quantity g_j' is the number of nucleon states per MeV at an energy E_j' in the nuclear well[41].

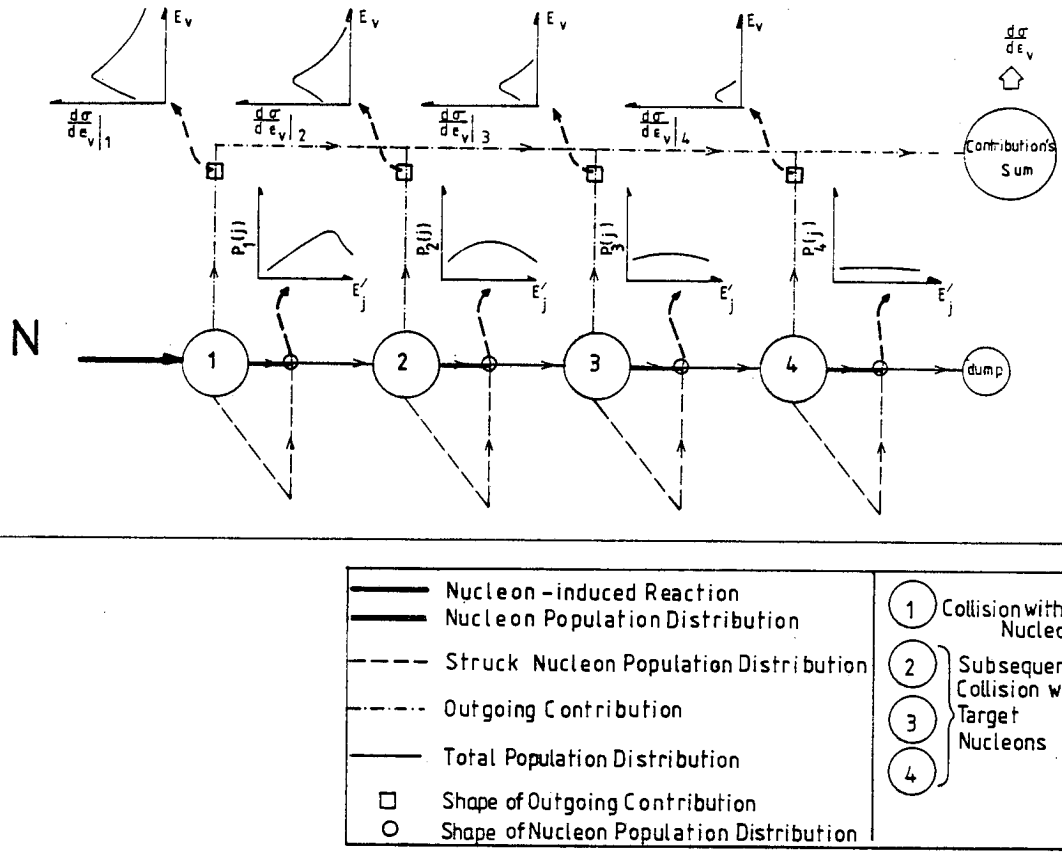

Diagram 3.6: The schematic representation of the (N,N') reaction using the Q.F.S. model.

The total probability, $P_\nu(\varepsilon_\nu)$ can be multiplied by the number of nucleons at E_j' and the total reaction cross-section σ_R results in an absolute cross-section for nucleon emission of energy (see diagram 3.6), i.e.

$$\left[\frac{d\sigma}{d\varepsilon_\nu}\right]_1 = \sigma_R \cdot \left[\frac{\lambda_c(\varepsilon_\nu)}{\lambda_c(\varepsilon_\nu) + \sum_{k=1}^{E_f} \lambda_{kj}}\right] \cdot P_1(j) \qquad (7)$$

where $p_1(j)$ in the number of nucleons with energy E_j' at time t_1 (see 3.2.Ø) for the first interaction. In equation (7) indices j and ν are connected to each other by equation (3).

The nucleons which are not emitted have their energy redistributed in the nuclear well according to the free nucleon-nucleon scattering kinematics, resulting in an energy distribution of nucleons with $E_j' > E_f$. The calculation of $p_2(j)$ and the number of nucleons at E_j' will provide one with energy distribution for emitted particles after the second interaction (see diagram 3.6):

$$\left[\frac{d\sigma}{d\varepsilon_\nu}\right]_2 = \sigma_R \cdot \left[\frac{\lambda_c(\varepsilon_\nu)}{\lambda_c(\varepsilon_\nu) + \sum_{k=1}^{E_f} \lambda_{kj}}\right] \cdot P_2(j) \qquad (8)$$

one can generally write

$$\frac{d\sigma}{d\varepsilon_\nu} = \sigma_R \sum_{S=1}^{N} \left[\frac{\lambda_c(\varepsilon_\nu)}{\lambda_c(\varepsilon_\nu) + \sum_{k=1}^{E_f} \lambda_{kj}}\right] \cdot P_S(j) \qquad (9)$$

where σ_R is in mb and energy spectrum in ^{mb}/MeV. In equation (9) the term $P_S(j)$, i.e. population versus excitation energy, which resulted from the two-body scattering sequence, is computed using a

recursion equation , i.e.

$$P_{S+1}(L) = \sum_{j,j\geq L} P_S(j) \left(1 - \frac{\lambda_c(\varepsilon_\nu)}{\lambda_c(\varepsilon_\nu) + \sum_{k=1}^{E_f} \lambda_{kj}}\right) \frac{\lambda_+(j \to L)}{\lambda_+(j)} \qquad (10)$$

where $\lambda_+(j \to L)$ denotes[76] the intranuclear transition rate for a nucleon of energy E_j' with nucleons below the Fermi energy E_f such that the final energy is E_L'. The term $\lambda_+(j)$ is equal to $\sum_{k=1}^{E_f} \lambda_{kj}$, the total intranuclear transition rate.

In the next section the above formalism will be critically discussed in order to get a clear view about the problems facing the treatment of (N, N') reaction by the QFS model.

3.2.2 Discussion Concerning (N, N') Reaction Using Quasi-Free Scattering Model.

The QFS model discussed in sections (3.2.Ø) and (3.2.1) for the case of (N, N') has been reasonably successful[6,76,77] in producing angle integrated experimental data (Fig. 3.1).

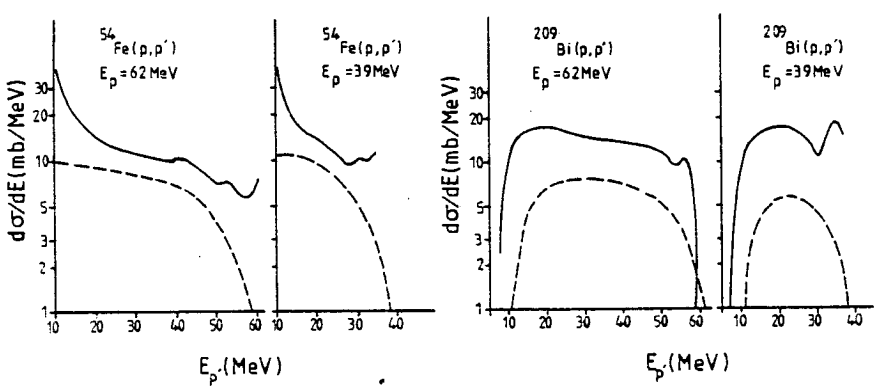

Figure 3.1: Calculation of the energy spectra for 62 and 39 MeV protons on ^{209}Bi and ^{54}Fe. Solid curves: experimental results. Broken curves: Calculated results using the Q.F.S. model. See ref. (76) for details.

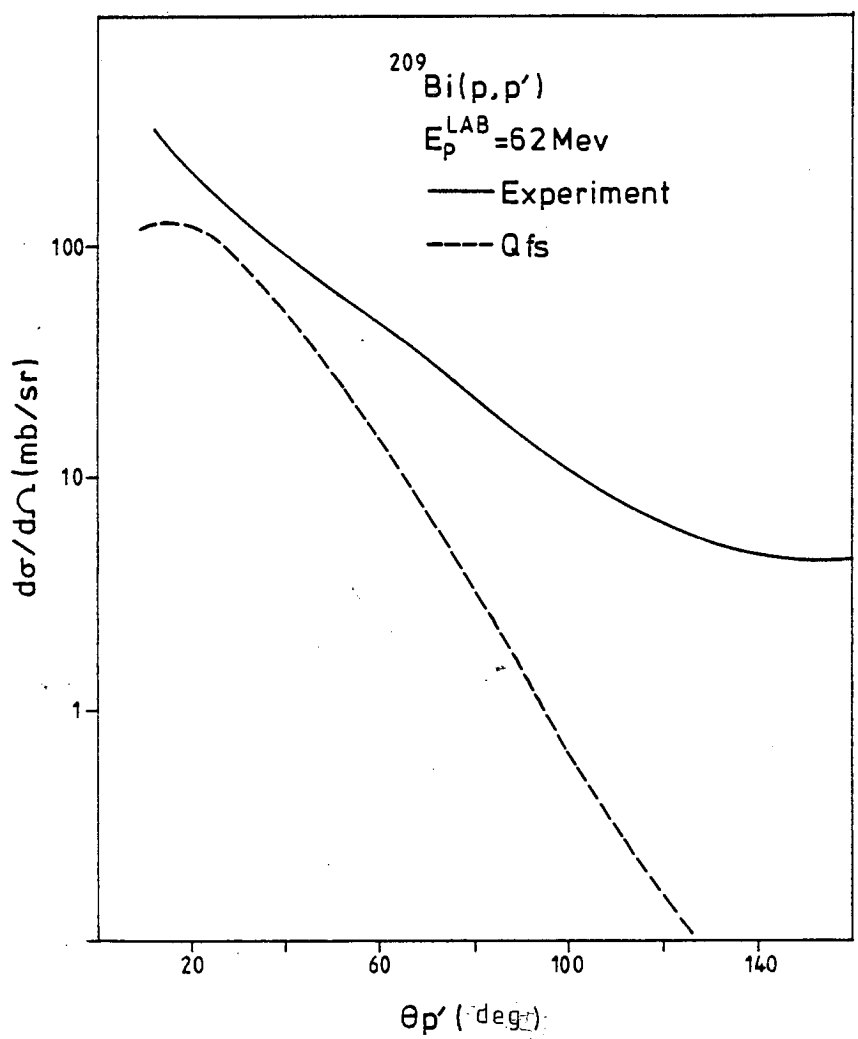

Figure 3.2: Calculation of the $\frac{d\sigma}{d\Omega}$ for 62 MeV protons on ^{209}Bi.
Solid curve: experimental results.
Broken curve: calculated results using the Q.F.S. model. See ref. (78) for details.

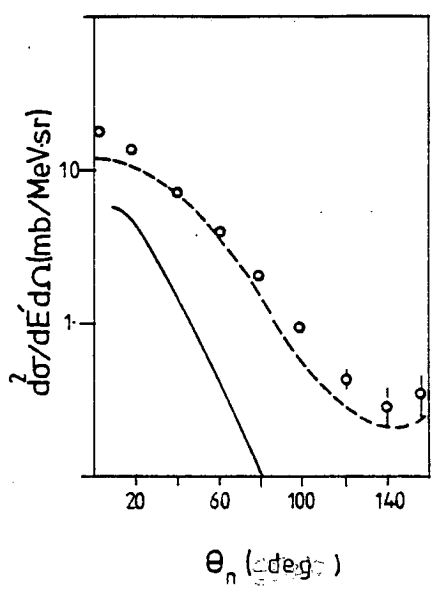

Figure 3.3: Calculation of $\frac{d^2\sigma}{dEd\Omega}$ compared to experimental data. Empty circle: experimental data. Broken curve: Tamura et al. [52a, 52c] calculated results. (The outgoing energy is $E_n = 31 \pm 2.5$ using ^{208}Pb (p,n)). Full curve: calculated results using the Q.F.S. Model. See ref. 78 for details.

However there are two central assumptions in the QFS model which need more attention. These two assumptions are as follows:

I) The free nucleon-nucleon scattering cross-section has been used in the QFS model and from dynamics of the elementary nucleon-nucleon collision, the internal transition rates are determined.

II) The principle of detailed balance has been incorporated by using inverse cross-section in the calculation of emission probability.

The validity of these two fundamental assumptions can be examined by considering angular distribution for (N, N') type reactions.

The comparison between calculated and experimental spectra after integration over angle can be quite misleading as an indication of the validity of the model. Therefore the comparison with angular distribution strongly confirms the strength and weakness of the QFS model. To this end the QFS model was appropriately extended by Keuser[78]. The angular distribution for (N, N') reactions produced the data quite successfully in an angle area of up to 70° (Fig. 3.2). However, there is a marked discrepancy between measured and calculated cross-sections which fall off too sharply above 70°.

Moreover the angular distribution for (N, N') reaction was compared[78] to the quantum mechanical approach of Tamura et al.[52a,c] (see Chapter I) for a better assessment of the QFS model (Fig. 3.3). The success of Tamura et al.'s approach in producing the experimental data suggests further investigation on the validity of the central assumptions which the QFS model is based on. In particular, the residual interactions which are approximated by the free nucleon cross-sections.

In the present study the investigation of $(\gamma,N' \Rightarrow N',N)$ provides further evidences for the strength and weakness of the QFS model (see chapter 4).

The next section is devoted to the study of energy spectrum for α-particles resulting from the (N,α) reaction.

3.3.Ø Principles of the Quasi-Free Scattering Model for (Nucleon-Alpha) Reactions

The application of the QFS model for (N,α) reactions can basically be evaluated using the same concept mentioned for the (Nucleon-Nucleon') reactions (see (3.2.Ø)). However, there are differences in principle. The process for (N,α) reactions can be schematically presented by diagram 3.7.

In the following, the steps taken to produce the energy spectrum for (N,α) reactions will be explained:

a) The process of interaction of the nucleon with a target nucleus proceeds through a sequence of two-body collisions between the projectile nucleon and an α-like cluster with the probability ϕ, diagram 3.7. However, there is a probability of $(1 - \phi)$ for collision of a projectile nucleon with a target nucleon, diagram 3.7.

b) The two-body collisions of the projectile nucleon with all possible α-like clusters can be calculated, using free nucleon-alpha particle angular distributions to determine the energy distributions of α-cluster in the well after collision (Box (1), diagram 3.7). Blann et al.[6,76] assumed a range of energy Δ_α in the target nucleus (see diagram 3.8) over which the nucleons cluster to an α-structure and are uniformly distributed below effective Fermi energy E_f^{α} (see section 3.3.1 , and also diagram 3.8). The reason for such a range of energy Δ_α for α-particle

has been given on the basis that the α-particle is localised in a region near to the surface of the potential well. This assumption can be supported by alpha-transfer reactions and elastic scattering of α-particles[79]. This assumption will be further discussed in section (3.3.2).

c) The Pauli allowed α-particle energy distribution resulting after averaging over Δ_α and all collision angles, then will behave as a second generation projectile with an energy distribution. The calculation then proceeds with subsequent (α, α') interactions resulting in a contribution denoted by (A) (diagram 3.7), (also see Part 4 for (α , α') interactions).

d) The nucleon partner from the initial fraction ϕ of (N, α) interactions (diagram 3.7 arrow denoted by N_1) may also further interact with an α-like structure. Then the subsequent (α, α') interactions give rise to a contribution (labelled (B)). This contribution originates from two subsequent (N, α) interactions, thus the collision probability is proportional to ϕ^2. Contribution (B) turned out to be small in all calculations performed.

e) The (Nucleon-Nucleon') interaction with probability $(1 - \phi)$, mentioned before in part (a), will give rise to pre-compound nucleon emission (arrow denoted by N_4 in diagram 3.7). However, the internally scattered nucleon from this branch and from part (d), i.e. N_2 arrows will also have a probability of scattering with an α-like structure. This probability is assumed to be equal to ϕ, independent of nucleon energy. The subsequent (α, α') interactions will contribute to the pre-equilibrium α-emission, a component further on referred to as (C).

f) The reactions of (α, α') nature will be dealt with on the basis of interaction of an alpha particle with nucleons inside the nuclear well, which results in (i) an alpha particle energy distribution; (ii) a nucleon energy distribution in the nuclear potential and, (iii) an emission spectra for the alpha particle. As this process is repeated, the above mentioned contributions to the total α-emission, (A), (B) and (C) will be produced.

g) The α-pre-equilibrium emission spectra resulting from the subsequent (α, α') calculation can be compared on an absolute scale by means of the normalization constants, $\phi\sigma_R$ for contribution (A), $\phi(1 - \phi)\sigma_R$ for contribution (C) and $\phi^2\sigma_R$ for contribution (B). These are added up to give the yield of α-particles emitted during the equilibrium cascade.

Principles mentioned above will be formulated in the next section where the ambiguities of how to treat the alpha state densities in the continuum and in the nuclear well will be discussed. The questions such as what is the energy of an alpha particle inside the nuclear well, how the possibility of alpha break-up should be treated and, finally, the treatment of the Pauli allowed nucleon-alpha scattering cross-section will also be considered.

3.3.1 Related Formulation for (N,α) Reactions

A similar expression to equation (9) can be written for the total emission spectrum of α-particles into continuum summed over all collision periods (section 3.2.1), (see diagrams 3.7 and 3.8).

$$\frac{d\sigma}{d\varepsilon_\alpha} = \sigma_R \sum_{S=1}^{N} \left[\frac{\lambda_c(\varepsilon_\alpha)}{\lambda_c(\varepsilon_\alpha) + \sum_{k=1}^{E_f} \lambda_{k\alpha_j}} \right] . (1 - B_j^\alpha).P_S(j) \qquad (11)$$

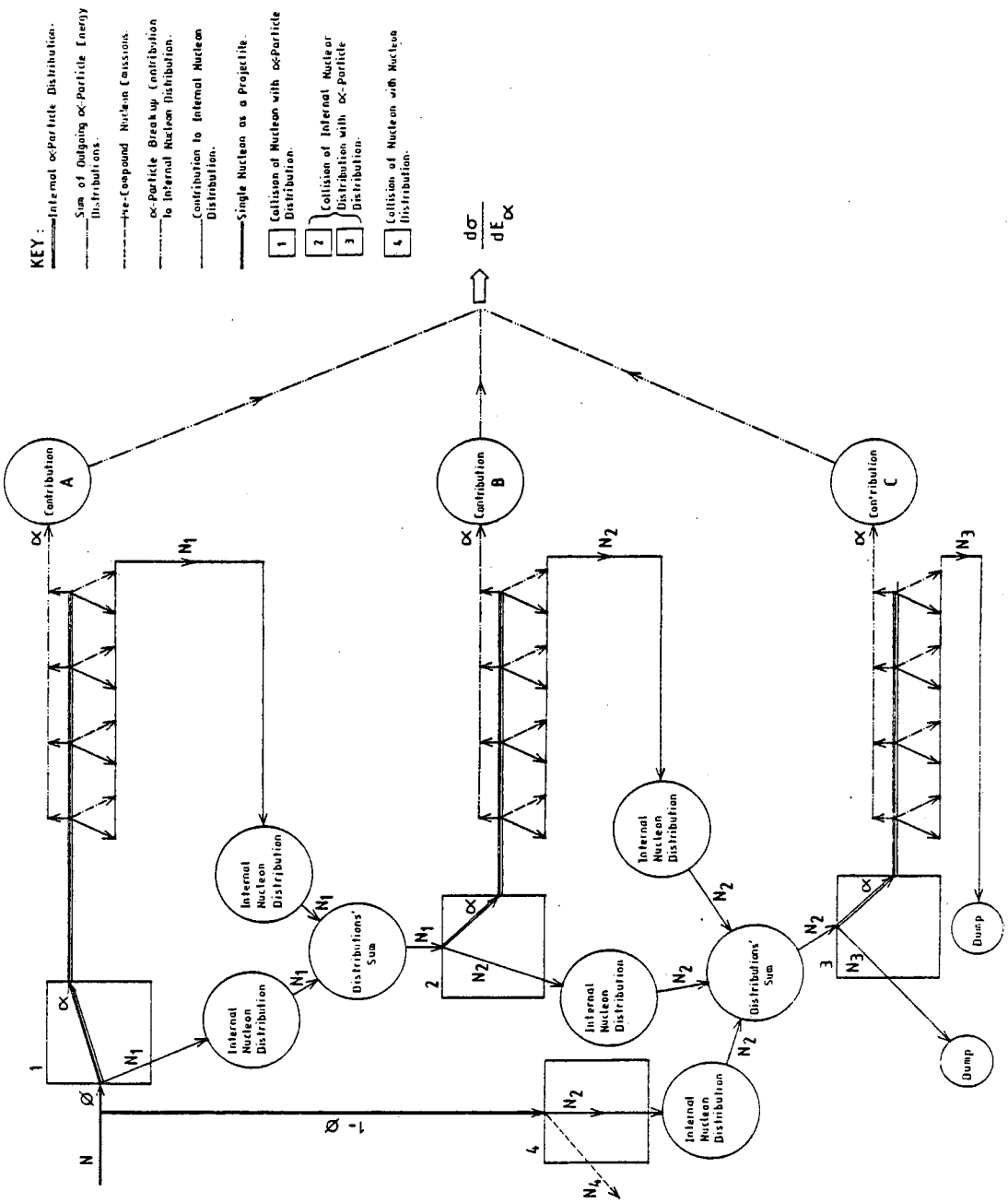

Diagram 3.7: The schematic representation of (N,α) reaction using the Q.F.S. model.

where the term inside the bracket is the overall alpha particle emission probability and $\lambda_{k\alpha_j}$ is the intranuclear rate for an alpha particle interacting with a nucleon in the nuclear well. The rate at which the alpha particle undergoes transitions into the continuum is calculated by a similar expression mentioned in section (3.2.1) (i.e., the application of detailed balance principle, eq. (5)):

$$\lambda_c(\varepsilon_\alpha) = \left[\frac{\sigma_{inv}(\varepsilon_\alpha)\nu'_\alpha}{V}\right]\left[\frac{\omega_c(\varepsilon_\alpha)}{g'_{\alpha_j}}\right] \qquad (12)$$

where all the terms in equation (12) conceptually carry the same explanations as equation (5) in section (3.2.1). However terms $\omega_c(\varepsilon_\alpha)$ and g'_{α_j} need clarification, as will be given below. The term $\lambda_{k\alpha_j}$ mentioned in equation (11) can be given by an analogous expression to Eq.(4), section (3.2.1), i.e.:

$$\lambda_{k\alpha_j} = [\sigma^P_{k\alpha_j}\ \nu'_\alpha\ g'_k] / V \qquad (13)$$

where $\sigma^P_{k\alpha_j}$ is total Pauli allowed cross-section for interaction of an alpha particle with energy E'_α with a nucleon at energy E'_k. The velocity of an α-particle with energy E'_{α_j} in the nuclear well is ν'_α. The remaining terms have been specified in equation (4), section (3.2.1). One can evaluate $\omega_c(\varepsilon_\alpha)$ by treating the α-particle as a single particle and then to apply phase space arguments. The number of alpha states per MeV at an energy E'_{α_j} i.e. g'_{α_j}, can also be given by

$$g'_{\alpha_j} = \int_{E'_{\alpha_j} - \frac{1}{2}}^{E'_{\alpha_j} + \frac{1}{2}} \omega'(E)dE$$

where $\omega'(E'_{\alpha_j})$ is the cluster state density inside the nucleus and is given by: $\omega'(E'_{\alpha_j}) = [2\pi V (2M)^{3/2}/h^3](E'_{\alpha_j})^{\frac{1}{2}}$. The reduction by $\frac{1}{2}$ from the nucleon expression is a result of the alpha particle spin of zero (see section 3.3.2). In the above analysis a question that arises is about the energy of alpha particles, i.e. E'_{α_j}. In the nucleon case the energy of the nucleon in the well was treated by adding the laboratory energy to the nuclear well depth. Since an alpha particle is made up of four nucleons, the energy of the alpha particle in the nuclear well is set equal to the laboratory energy of the alpha particle plus four times the nuclear well depth, i.e.,

$$E'_{\alpha_j} = \varepsilon_\alpha + 4\varepsilon_f^n + 4\overline{BE}_n \qquad (15)$$

where $4(\varepsilon_f^n + \overline{BE}_n)$ is the depth of the nuclear well and $\overline{BE}_n$ is the average nucleon binding energy ($\overline{BE}_n = (28.3 + BE_\alpha)/4$, with 28.3 MeV the energy required to break the alpha particle into its constituent nucleons). The effective Fermi energy, mentioned in (3.3.Ø) part b, can now be defined by $E_f^\alpha = 4\varepsilon_f^n + 28.3$, where ε_f^n in a local density approximation takes a value equal to 8 MeV suggested by Blann et al.[6] (see diagram 3.8 and section 3.3.2). Therefore one can write for E'_{α_j} using equation (15):

$$E'_{\alpha_j} = \varepsilon_\alpha + E_f^\alpha + BE_\alpha \quad . \qquad (16)$$

There are three remaining factors to be clarified in equation (11) $P_S(j)$, B_j^α as alpha break-up factor, and, Pauli factor for the alpha particle. The latter has been suggested to provide a realistic

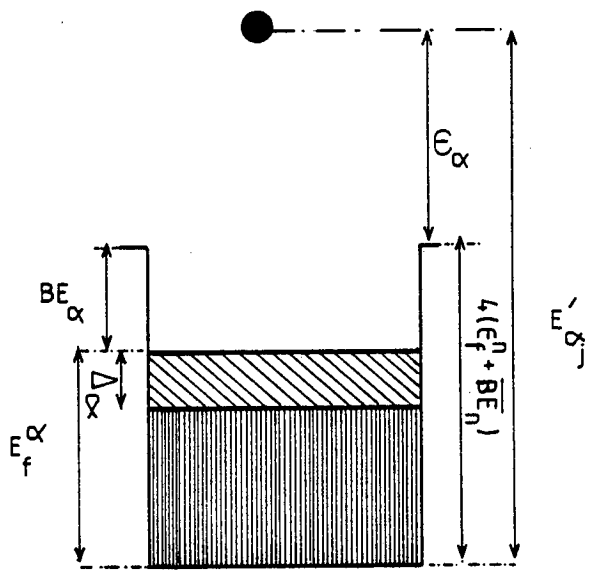
ϵ_α
BE_α
Δ
E_f^α
$4(\epsilon_f^n + \overline{BE}^n)$
$E_j^{\alpha'}$

Diagram 3·8

derivation of $\lambda_{k\alpha_j}$, i.e. the intranuclear rate.

The quantity $P_S(j)$ in equation (11) can be given by a similar expression to (10) for the case of (N, α) reactions.

$$P_{S+1}(L) = \sum_{jj \geq L} (1 - B_j^{\alpha}) P_S(j) \left(1 - \frac{\lambda_c(\varepsilon_\alpha)}{\lambda_c(\varepsilon_\alpha) + \sum_{k=1} \lambda_{k\alpha_j}} \frac{E_f}{}\right) \times$$

$$\times \frac{\lambda_+(j \to L)}{\lambda_+(j)} \qquad (17)$$

where the only difference with equation (10) is about the factor $(1 - B_j^{\alpha})$ which takes α-particle break-up into account, i.e. if α-clusters break up into nucleon degree of freedom during one collision period.

The break-up factor B_j^{α} is a parameter which adjusts the absolute cross-section of the emission spectrum. Therefore this factor behaves as a reduction factor for the number of alpha particles in the nuclear well. It is then reasonable to include B_j^{α} to modify $P_S(j)$ to allow some fraction of the population to dissipate due to break-up during each collision.

Finally the Pauli exclusion factor has been introduced in order to correct the energy integrated Pauli allowed cross-section for elastic (α,N) scattering in the nuclear environment, i.e. $\sigma^P_{k\alpha_j}$, eq. (13),

$$\sigma^P_{k\alpha_j} = \int_{\alpha_{U_1}}^{\alpha_{U_2}} F_{\alpha_U} \left[\frac{d\sigma(k, \alpha_j)}{d\varepsilon}\right]_{\alpha_U} d\varepsilon \qquad (18)$$

where $\left[\frac{d\sigma(k, \alpha_j)}{d\varepsilon}\right]_{\alpha_U}$ is the angle averaged elastic scattering

differential cross-section for an α-cluster at energy α_j scattering with nucleons at energy E_k' $(E_k' \lesssim E_f)$ to give an ultimate alpha energy α_U. Factor F_{α_U} is the fraction of the differential cross-section which is estimated to be allowed for cluster scattering in nuclear matter due to the influence of the Pauli exclusion principle. When the alpha particle break-up, the available energy is distributed among the four nucleons, none of which may be below the Fermi energy E_f^{α}. On the basis of this principle F_{α_U} has been given by[6]

$$F_{\alpha_U} = \left[\frac{E'_{\alpha_j} - E_f^{\alpha}}{E'_{\alpha_j} - E_f^{\alpha} + 4\varepsilon_f^n} \right]^3$$

where F_{α_U} has been derived using the ratio of total configuration for which no particle is below the Fermi energy E_f^{α}, to total configuration for which particles are above as well as below Fermi energy.

3.3.2 Discussion Concerning (N, α) Reaction Using the Quasi-Free Scattering Model

The formalism discussed in section (3.3.Ø) and (3.3.1) for (N,α) reaction provides the energy spectrum for the outgoing α-particle. This angle-integrated spectrum has been compared[6, 76] with experimental data for different target nucleuses. The results were quite satisfactory (Fig. 3.4). However there are uncertainties in the QFS model for the case of (N,α) reactions.

In the following these weak points will be discussed:

a) In equations (12) and (14), $\omega_c(E_\alpha)$, the cluster state density outside the nucleus, and $\omega'(E'_{\alpha_j})$, the cluster state density

inside the nucleus, have been evaluated considering the α-particle as a single particle. The expressions for these state densities were derived directly from the phase space argument for the number of states in a Fermi gas. However, the α-particle is a boson. Therefore one can crudely accept the assumption of treating α-particle as a single particle and consequently applying the Fermi gas model. The conclusion is that the use of Fermi gas momentum distribution for an α-particle is quite ad hoc.

b) The calculation of energy spectrum for (N,N') reactions as discussed in section (3.2.1) obeys the requirement of the Pauli principle. For the (N,N') reaction these interactions for which either of the scattered pair of nucleons is left with less than the Fermi energy are forbidden. However, this requirement for the case of the final state α-particle energy in the (N,α) interaction needs some attention. There are four possibilities for dealing with α-particle final state energies:

I) The requirement that an α-particle is treated as a single particle and after any (N,α) interaction α-particles should be left with an energy greater than four times the nucleon Fermi energy. This procedure considers no break-up of α-particles.

II) An α-particle should be treated as a single particle and should be left with an energy greater than the nucleon Fermi energy following any collision. The break-up of α-particles has been neglected.

III) The possibility of having α-particles four times above a pseudo Fermi energy where this pseudo-Fermi energy can be determined by comparison with experimental data. In the QFS model this pseudo-Fermi energy is left as a free parameter and a range of values between 4 - 12 MeV has been suggested[6, 76] for it. If the possibility

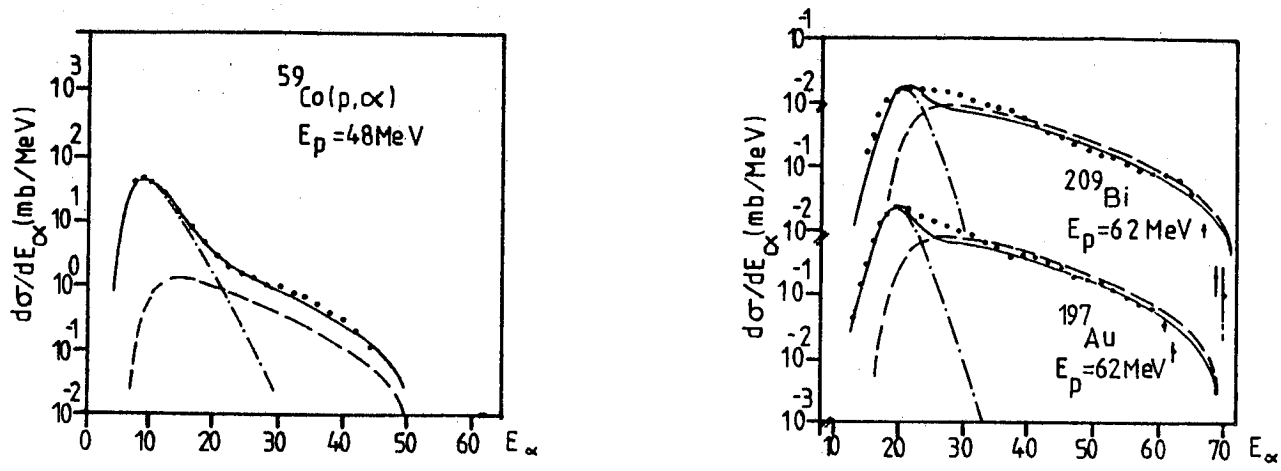

Figure 3.4: Calculation of $\frac{d\sigma}{dE_\alpha}$ energy spectra. Solid points: experimental results; dash-dotted curve: equilibrium component normalised to the experimental result. Dash curve: Q.F.S. model calculation with $\phi = 0.1$. Solid curve: sum of evaporation and best fitting Q.F.S. model contribution (ϕ varied). See ref. (6) for details.

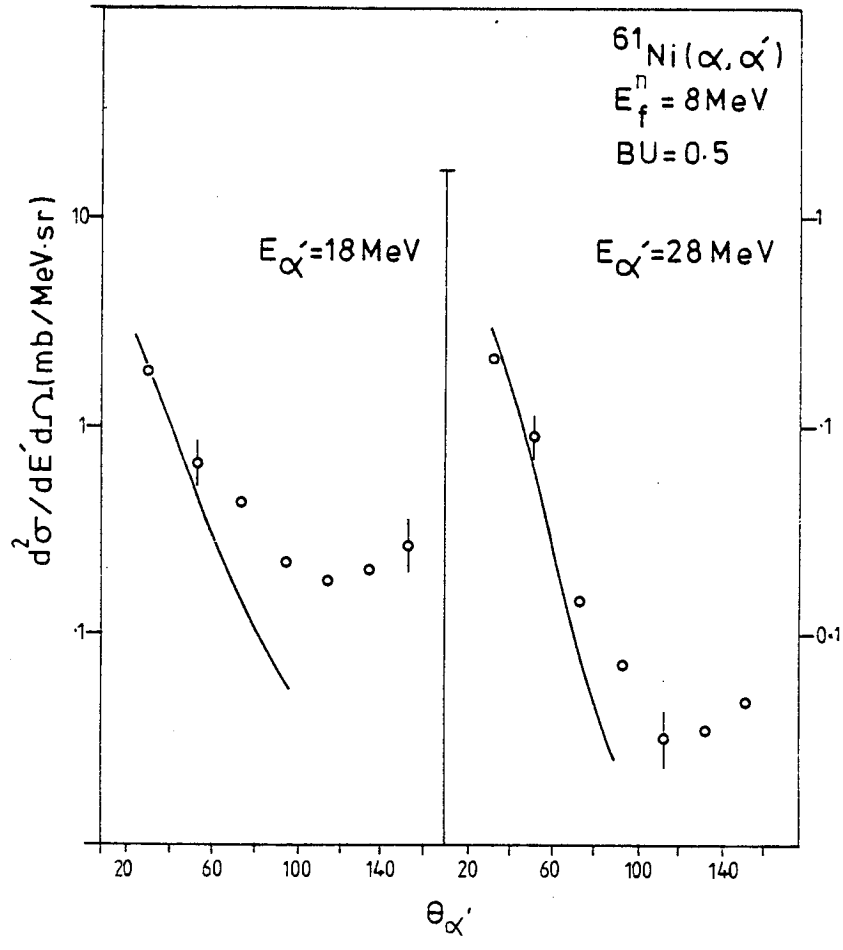

Figure 3.5: The curves represent absolute cross-section calculated in the Q.F.S. model. Empty circle: experimental data. See ref. 80 for details.

of alpha particle break-up is also taken into consideration, then an arbitrary factor F_{α_u} (Eq. 19) can be introduced to make the treatment of the Pauli principle more realistic.

IV) Because alpha particles are bosons, and therefore not subject to the Pauli principle, there can be no restriction in the final state energies of an alpha-particle, namely it can be any where above and below the Fermi sea.

The first and second procedures will greatly block the intranuclear transition rate and consequently the alpha emission probabilities will increase quite extensively. Consequently the absolute cross-sections of the calculated QFS alpha emission energy spectra will be greater than the experimental spectra. On the other hand, although in the third procedure the pseudo Fermi energy can be justified by comparison with experimental data, the treatment of the Pauli exclusion principle is also liable to criticism. This treatment can be criticised considering that there are possibilities for alpha break-up different from break-up to four particles. These possibilities could be alpha break-up into two correlated neutron and proton pairs and/or a proton with a triton which result in a change in value of F_{α_u} in equation (19). The last procedure, however, takes into account the boson nature of α-particles. The possibility of α-break-up into four nucleons can also be taken into account on the basis of the assumption that the resultant four nucleons enter vacant levels in the nucleus regardless of whether these levels are above or below the Fermi sea.

c) One of the parameters introduced in the QFS model is a range of energy Δ_α in the target nucleus, over which the nucleon clusters to an α-structure. Blann et al.[6] suggested that

clustering takes place in the region near the surface of the nucleus. This suggestion can be supported by the calculations of Brink and Castro[79]. They indicated that when nuclear matter is reduced to about one-third of its density at the centre of a heavy nucleus, it tends to coalesce into alpha clusters. This suggests that in the outer regions of the nucleus, where density is low, it is very likely that alpha clusters will be found.

d) It is obvious that an alpha particle in the nucleus is not the same as a free-alpha particle. The reason is that an α-particle in the nucleus is naturally distorted by the fields of the surrounding nucleons and may be violently changed by close interactions between them. Therefore a similar comparison with the Quantum mechanical model, as discussed in section (1.3.2), Chapter I, can provide valuable information on the validity of quasi-free scattering model for the (n,α) reactions.

e) The angular distribution of an outgoing α-particle, as a test of strength or weakness of the QFS model, can produce important information. Recently[80] a comparison of calculated α-particle angular distribution with experimental data has been done for reactions of type (α, α'). The results of this comparison (Fig. 3.5) show a marked discrepancy between measured and calculated cross-sections, from which the latter fall off too quickly. Although the QFS model neglects the refraction which the α-particle undergoes as it enters or leaves the nucleus, the consideration of these effects could not provide much better agreement with data.

f) There are other shortcomings in the treatment of reaction mechanism by the QFS model. In the case of (N,α) reactions the possibility of the pick-up of a triton by proton-induced reactions (N = P) has been ignored. The cross-sections from this case might

contribute to the highest energy portion of the alpha spectra. The hypothesis of triton pick-up has been treated by several calculations[81,82,52b], among them the multistep direct reaction approach by Tamura et al.[52b] which satisfactorily reproduced the continuous alpha spectra. In this context, Kalbach[82] has suggested that the pick-up mechanism could effectively supply the predominant contributions to the alpha spectra although Kalbach's calculation is based on the exciton model and the reliability of this calculation rests on the justification of the exciton model discussed in Chapter I.

g) Another weak point is the fact that Blann et al.[6] considered only the possibility of interactions of the alpha particles with nucleons with $E_k' < E_f$ of the target nucleus. Interactions between alpha-particles and excited nucleons or between two α-particles are neglected. In the former case the mass of alpha is much greater than the nucleon mass, the alpha preserves most of its energy. If, on the other hand, interaction takes place between two alpha particles, the loss of energy will result in a reduction in the energy of the outgoing alpha particle.

The above considerations gave a better picture of the problems of the QFS model, while the present study will give further assessment of the QFS model.

In the following section the QFS model will be used to produce a formalism suitable for considering the final state interactions in photon-induced reactions.

3.4.Ø Development of the Necessary Formalism to be Used in Photon-Induced Reactions

The success of the QFS model, as discussed in this chapter in treating the (Nucleon-Nucleon') or (Nucleon-Alpha cluster) interactions during the equilibration cascade, enables one to calculate the probability of emission per MeV of scattered nucleon projectile or knocked-out α-particle into continuum for a specified nucleon projectile. Therefore using equation (9) one can write for the ultimate probabiliy for emitting a nucleon with energy ε_ν after S interactions by:

$$P(\varepsilon_\nu, E_i) = \sum_{S=1}^{N} \left[\frac{\lambda_c(\varepsilon_\nu)}{\lambda_c(\varepsilon_\nu) + \sum_{k=1}^{E_f} \lambda_{k_j}} \right] \cdot P_S(j) \qquad (20)$$

where ν denotes neutron or proton and $P(\varepsilon_\nu, E_i)$ is the emission probability of a particle with energy E_ν. E_i is projectile energy in the laboratory system. For the case of nucleon-alpha cluster interaction, the ultimate probability for emission of alpha particles is given by using equation (11):

$$P(\varepsilon_\alpha, E_i) = \sum_{S=1}^{N} \left[\frac{\lambda_c(\varepsilon_\alpha)}{\lambda_c(\varepsilon_\alpha) + \sum_{k=1}^{E_f} \lambda_{k\alpha_j}} \right] (1 - B_j^\alpha) . P_S(j) . \qquad (21)$$

The objectives of the next chapter are to use these emission probabilities, equation (20) and (21), in order to calculate the energy distribution for reactions such as (γ, p) and (e,α). These calculations will then be compared to experimental data for ^{60}Ni.

CHAPTER IV

THE SYNTHESIS OF THE QUASI-DEUTERON AND QUASI-FREE SCATTERING MODELS

4.1.Ø Introduction

It is well known that the final state interactions are essential when the nucleus is probed with photons. The primary generated photonucleon will make collisions with the rest of the nucleons inside the nucleus, therefore changing the energy spectrum of the initial outgoing particles, Although the consideration of final state interactions is less important for light nuclei, it produces a significant effect for medium and heavy nuclei.

Accordingly, the purpose of this chapter to combine the quasi-deuteron and quasi-free-scattering models. These two models were discussed in Chapters II and III respectively. To this end the formalism developed in Chapter III (section 3.4.Ø) will be effectively used in order to take account of the final state interactions for $(\gamma, N' \Rightarrow (N',N)$ and $(e,N \Rightarrow N,\alpha)$ reactions using ^{60}Ni.

In section (4.2.Ø) the necessary formalism for the folding of the quasi-deuteron and the quasi-free-scattering models will be given. Then in section (4.3.Ø), the calculation of energy spectra for $(\gamma,N' \Rightarrow N',N)$ will be presented. Finally, in section (4.4.Ø) the calculation of energy spectra for $(e,N \Rightarrow N,\alpha)$ will be considered.

4.2.Ø Formalism for the Folding Quasi-Deuteron and Quasi-Free-Scattering Model

In Chapter II, equation (57) was derived for the purpose of calculating the double differential (γ, np) cross-section for a particular shell. This equation is rewritten here for convenience.

$$\left[\frac{d^2\sigma}{d\Omega_N dE_N}\right]_\beta = L'_\beta \; N_\beta \; Z_\beta \int \vec{dK} \; G_\beta(K) \left[\frac{d\sigma}{d\Omega^*_N}\right]_d \; B(\omega) J_{tot}$$

where N = proton or neutron (for the remaining terms refer to section 2.2.3). This equation assumes that the primary photonucleons will leave the nucleus without undergoing collisions.

Equations (20) and (21) which were developed in Chapter III will be used here but with different rotation:

$$P(E_\nu, E_N) = \sum_{S=1}^{M} \left[\frac{\lambda_c(E_\nu)}{\lambda_c(E_\nu) + \sum_{k=1}^{E_f} \lambda_{kj}}\right] \cdot P_S(j) \qquad (1)$$

$$P(E_\alpha, E_N) = \sum_{S=1}^{M} \left[\frac{\lambda_c(E_\alpha)}{\lambda_c(E_\alpha) + \sum_{k=1}^{E_f} \lambda_{k\alpha_j}}\right] (1 - B_j^\alpha) . P_S(j). \qquad (2)$$

The quantities $P(E_\nu, E_N)$ and $P(E_\alpha, E_N)$ are the probabilities for emitting a nucleon with energy E_ν, and for emitting an α-particle with energy E_α, respectively (E_N is the projectile energy with N = proton or neutron).

Formally, the synthesis of the double differential cross-sections for the $A(\gamma, np)A-2$ process with the probabilities for emitting particles with energy $\hat{E}$ at solid angle $\hat{\Omega}$ can be written as:

$$\frac{d^2\sigma}{d\hat{\Omega}d\hat{E}} = \int\int \frac{d^2\sigma}{d\Omega_N dE_N} \cdot P(\hat{E},\hat{\Omega};\ E_N,\ \Omega_N)\ dE_N\ d\Omega_N \quad . \tag{3}$$

In this equation, the double differential cross-section for photonucleon emission with energy E_N at solid angle Ω_N is given by $\frac{d^2\sigma}{d\Omega_N dE_N}$. This photonucleon then will make cascade collisions where the probability for emitting a particle with energy $\hat{E}$ at solid angle $\hat{\Omega}$ is given by $P(\hat{E},\ \hat{\Omega}\ ;\ E_N,\ \Omega_N)$.

In the present study, equation (3) is replaced by the following expression assuming that the cross-sections are isotropic, i.e. $d\hat{\Omega} = d\Omega_N$ (see section 4.3.4 for further discussion).

$$\frac{d^2\sigma}{d\hat{\Omega}\ d\hat{E}} = \int \frac{d^2\sigma}{d\Omega_N dE_N} \cdot P\ (\hat{E};\ E_N)\ dE_N \quad . \tag{4}$$

In this equation, a primary generated photonucleon with energy E_N makes cascade collisions. Where the probability for emitting a particle with energy $\hat{E}$ is given by $P(\hat{E};\ \hat{E}_N)$.

Equation (4) can now be restructured for the case of $(\gamma,\ N)$ reactions by substituting $\frac{d^2\sigma}{d\Omega_N dE_N}$ with $\left[\frac{d^2\sigma}{d\Omega_n dE_N}\right]_\beta$, using equation (57) (derived in Chapter II) and substituting $P(\hat{E};\ E_N)$ with $P(E_\nu;\ E_N)$ using equation (1). Therefore equation (4) takes its new form of:

$$\left[\frac{d^2\sigma}{d\Omega_\nu dE_\nu}\right]_\beta = \int \left[L_\beta'\ N_\beta\ Z_\beta \int d\vec{K}\ G_\beta(K)\ \frac{d\sigma}{d\Omega^*_N}\ B(\omega)\ J_{tot}\right] \times \left[\sum_S \left(\frac{\lambda_c(E_\nu)}{\lambda_c(E_\nu) + \sum_{k=1}^{E_f} \lambda_{kj}}\right) \cdot P_S(j)\right] dE_N \tag{5}$$

where the quantities in the two right hand side brackets are E_N

dependent. Expression (5) will be used for the calculation of energy spectra of $(\gamma \nearrow^{n'}_{p'} \searrow P)$ or generally (γ, p) reactions using ^{60}Ni (see section 4.3.Ø).

For the case of $(e \nearrow^{n}_{p} \searrow \alpha)$ or generally (e,α) reactions a similar expression to (5) can be written, i.e.:

$$\left[\frac{d^2\sigma}{d\Omega_\alpha dE_\alpha}\right]_\beta = \int \left[L'_\beta N_\beta Z_\beta \int d\vec{K}\, G_\beta(K) \frac{d\sigma}{d\Omega^*_N} B(\omega)\, J_{tot}\right] \times$$

$$\left[\sum_S \left(\frac{\lambda_c(E_\alpha)}{\lambda_c(E_\alpha) + \sum_{k=1}^{E_f} \lambda_{k\alpha_j}}\right)(1 - B_j^\alpha).P_S(j)\right] dE_N \qquad (16)$$

where the quantities in the two right hand side brackets are E_N dependent. Equation (6) will be used to calculate the energy spectra of (e,α) reactions using ^{60}Ni (see section 4.4.Ø).

The calculated results using equations (5) and (6) will then be summed over the shell's indices β where the summed quantities over β are denoted by $\left[\frac{d^2\sigma}{d\Omega_\nu dE_\nu}\right]_F$ and $\left[\frac{d^2\sigma}{d\Omega_\alpha dE_\alpha}\right]_F$. Later in section (4.3.Ø) and (4.4.0) these two final results will be compared with the experimental data.

4.3.Ø The Calculation of Energy Spectra for (γ,p) Using ^{60}Ni

4.3.1 Introduction

In this section the energy spectra for (γ,p) will be evaluated by the use of:

a) A compound nucleus formalism for evaluating compound

contributions (see section 4.3.2 and Appendix C).

b) A formalism derived in section (4.2.Ø) for calculating pre-compound contributions (see section 4.3.3). Then the theoretically calculated results for (γ,p) energy spectra will be compared with the experimental data obtained by the Edinburgh group[83] (see section 4.3.4).

4.3.2 The Calculation of Compound Nucleus Component for (γ,p) Process

In this section the calculation of compound nucleus contribution to the (γ,p) energy spectrum will be presented (the details of compound nucleus formalism are given in Appendix C). For this purpose, the following expression is used:

$$\frac{d\sigma}{dE_p}(E_\gamma) = \int_{Q_n}^{30} \frac{d\bar{\sigma}}{dE_p}(E_\gamma)\, K(E_e,E_\gamma).E_\gamma^{-1}\, dE_\gamma \qquad (7)$$

where $K(E_e, E_\gamma).E_\gamma^{-1}$ defines the bremsstrahlung spectrum of real photons and it is calculated by using a formula suggested by Bethe and Heitler[73, 74]. In equation (7) $\frac{d\bar{\sigma}}{dE_p}(E_\gamma)$ can be expressed by:

$$\frac{d\bar{\sigma}}{dE_p}(E_\gamma) = \bar{\sigma}_n(E_\gamma)\, \frac{\sum_{s'\ell'} T_{\ell'}(E_\gamma, E_p)}{\sum_{s''\ell''} T_{\ell''}(n)} \qquad (8)$$

In this equation $\bar{\sigma}_n(E_\gamma)$ is taken from reference (84) for ^{60}Ni and the branching ratios for proton and neutron.

Channels, i.e. $\frac{\sum_{s'\ell'} T_{\ell'}(E_\gamma, E_p)}{\sum_{s''\ell''} T_{\ell''}(n)}$ are calculated using a certain computer code[85,86]. Then the calculation of the proton energy

spectra is carried out up to a photon energy of 30 MeV (equation (7)). This energy corresponds to a reasonable upper limit of the giant resonance region in medium weight and heavy nuclei. The calculated result is shown in Figures (4.12) and (4.19).

4.3.3 Pre-compound Contributions for (γ, p) Process

The approach presented in section (4.2.Ø) for the calculation of double differential cross-sections will be adopted for calculating $\left[\frac{d^2\sigma}{d\Omega_p dE_p}\right]_\beta$ for (γ,p) reactions (see diagram 4.1). To this end, the shell model configuration will be used and the contributions to final $\left[\frac{d^2\sigma}{d\Omega_\nu dE_\nu}\right]_F$ from different shells will be calculated.

The main feature for the present calculation is that the calculation of $\left[\frac{d^2\sigma}{d\Omega_p dE_p}\right]_F$ invokes no floating parameter like the Levinger constant. This is contrary to such similar studies as the modified exciton and Monte Carlo Cascade models[3,4] (see section 1.1.Ø). Instead the values calculated for pseudo-Levinger constant (Tables 8(a) and 8(b)) using ^{60}Ni will be effectively incorporated in the present approach. These pseudo-Levinger constants are calculated by using two potentials (square well and harmonic oscillator potentials) as discussed in section (2.2.2).

In the following two subsections the evaluation of $\left[\frac{d^2\sigma}{d\Omega_p dE_p}\right]_F$ for the case of square well potential and for the case of harmonic oscillator potential will be given in turn.

4.3.3.1 Square Well Potential Case for (γ,p) Process

The pre-compound contributions to (γ,p) energy spectrum are calculated using expression (5) (section 4.2.Ø). In this equation the different terms are calculated as follows:

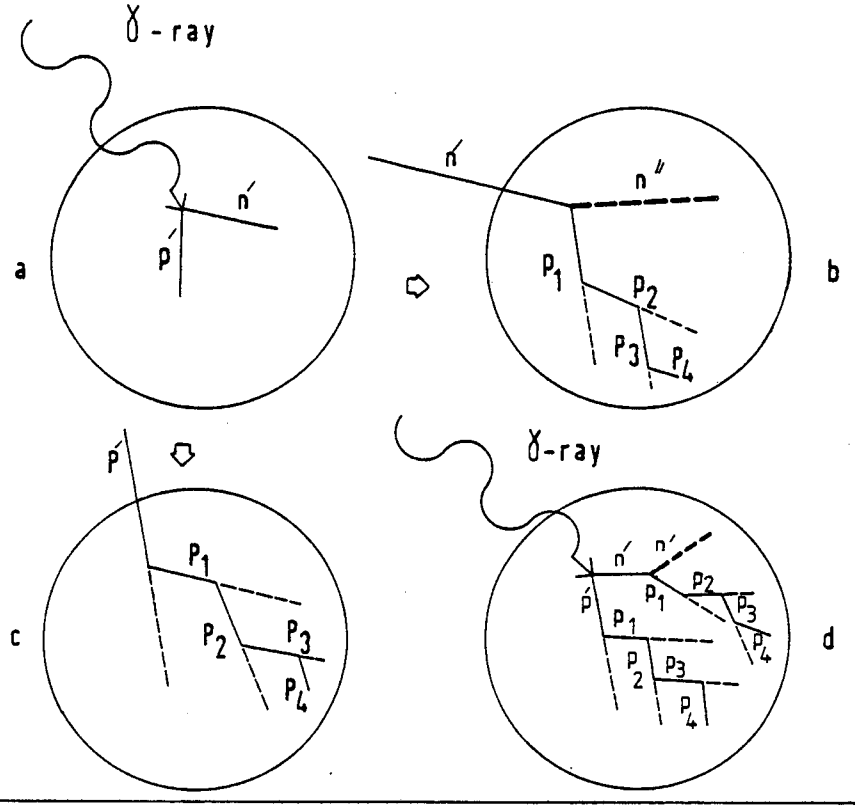
γ - ray
a
n´
p´
n´
n´´
p1
p2
p3
p4
b
p´
p1
p2
p3
p4
c
γ-ray
n´
n´
p´
p1
p2
p3
p4
p1
p2
p3
p4
d

Diagram 4.1

1) The pseudo-Levinger constant L_β' for different principle and non-principle shells are calculated using square well potential. These coefficients can be seen in Table (8), Chapter II.

2) The number of contributing correlated pairs $N_\beta Z_\beta$ for each shell are evaluated using the procedure mentioned in Chapter II, section (2.2.2).

3) For momentum distributions of the correlated neutron and proton pairs, expression (55) in Chapter II is used where the wavefunctions for square well potential are incorporated (refer to Figures 4.1 to 4.5 where these momentum distributions are shown by broken lines.

4) For the photodisintegration of deuteron cross-sections $\frac{d\sigma}{d\Omega^*_N}$ the procedure described in section (2.3.Ø) is incorporated.

5) The spectrum for bremsstrahlung $B(\omega)$ is calculated by the means of extreme relativistic formula of Bethe and Heitler[73,74].

6) By calculating the total Jacobian using the formalism discussed in Chapter II, section (2.2.3), the first right hand side bracket in expression (5) is evaluated employing the computer programme discussed in section (2.3.Ø). Then the process of calculating the primary photo-protons double differential cross-sections is carried out and the results restored. A similar process for primary photo-neutrons is carried out and the results are again stored. Subsequently the calculated proton and neutron double differential cross-sections are multiplied by the probabilities for emitting the nucleon. These probabilities will be discussed in part (7).

7) Probabilities for emitting a particle with an energy E_ν are calculated for different energies of primary generated photo-

Figures 4.1 - 4.5: The shell dependent quasi-deuteron momentum distributions, using ^{60}Ni; the broken curves are calculated using square well associated wavefunctions and the full curves are calculated using harmonic oscillator associated wavefunctions.

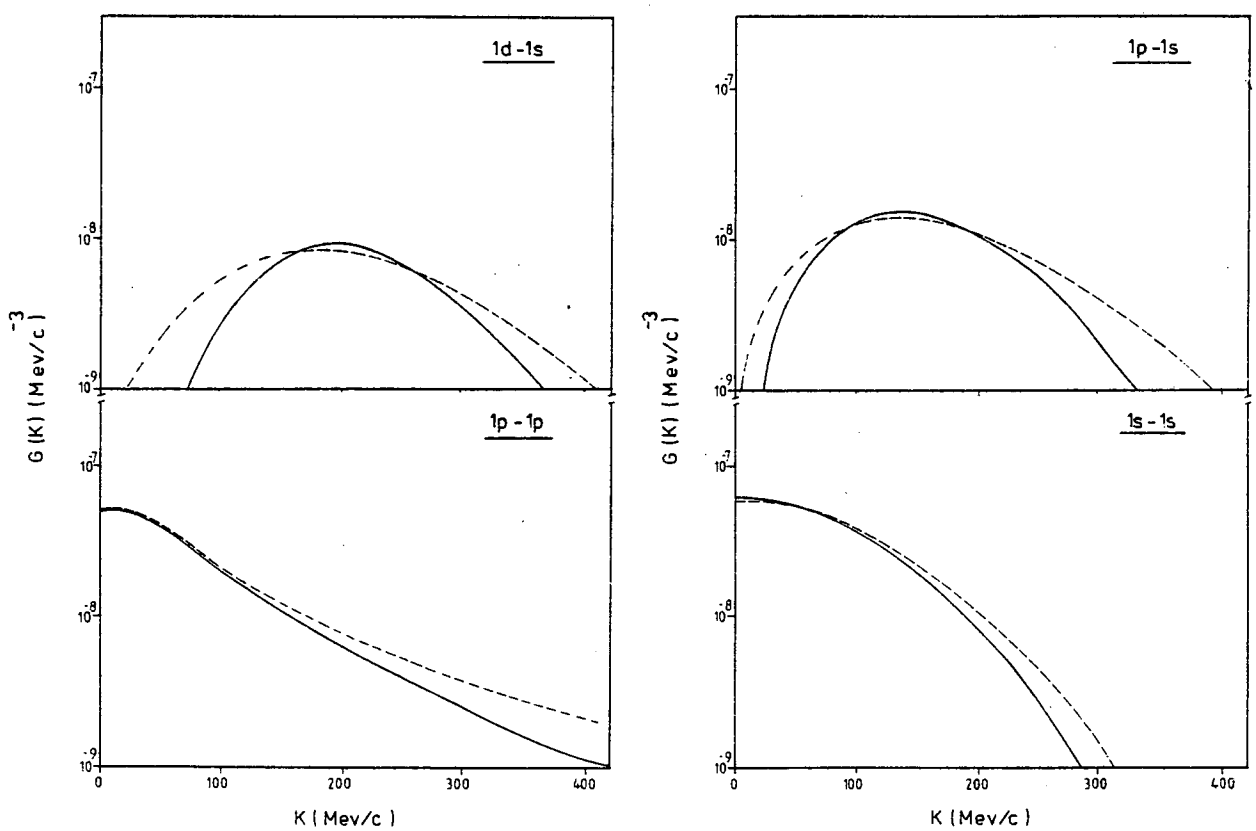

Fig. 4.1

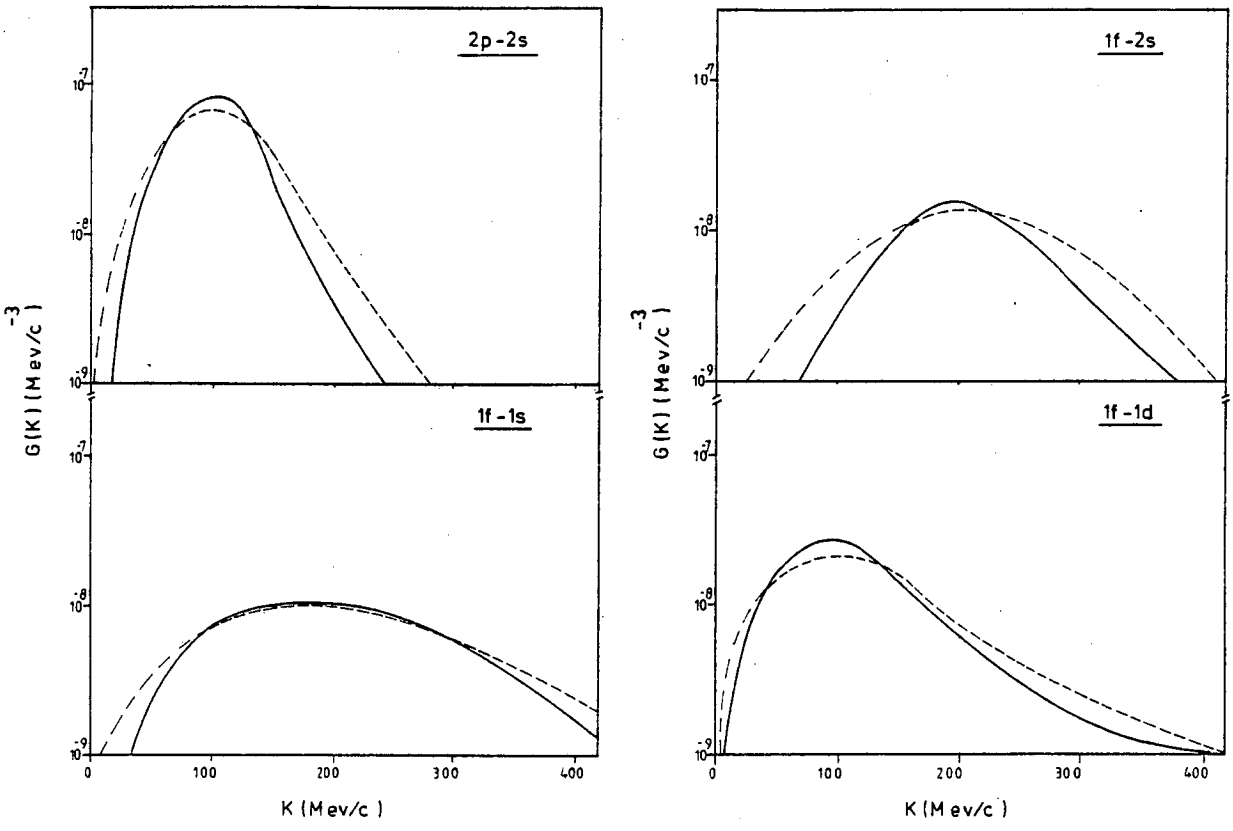
2p-2s
1f-2s
1f-1s
1f-1d
G(K) (Mev/c)^-3
K (Mev/c)
0
100
200
300
400

Fig. 4.2

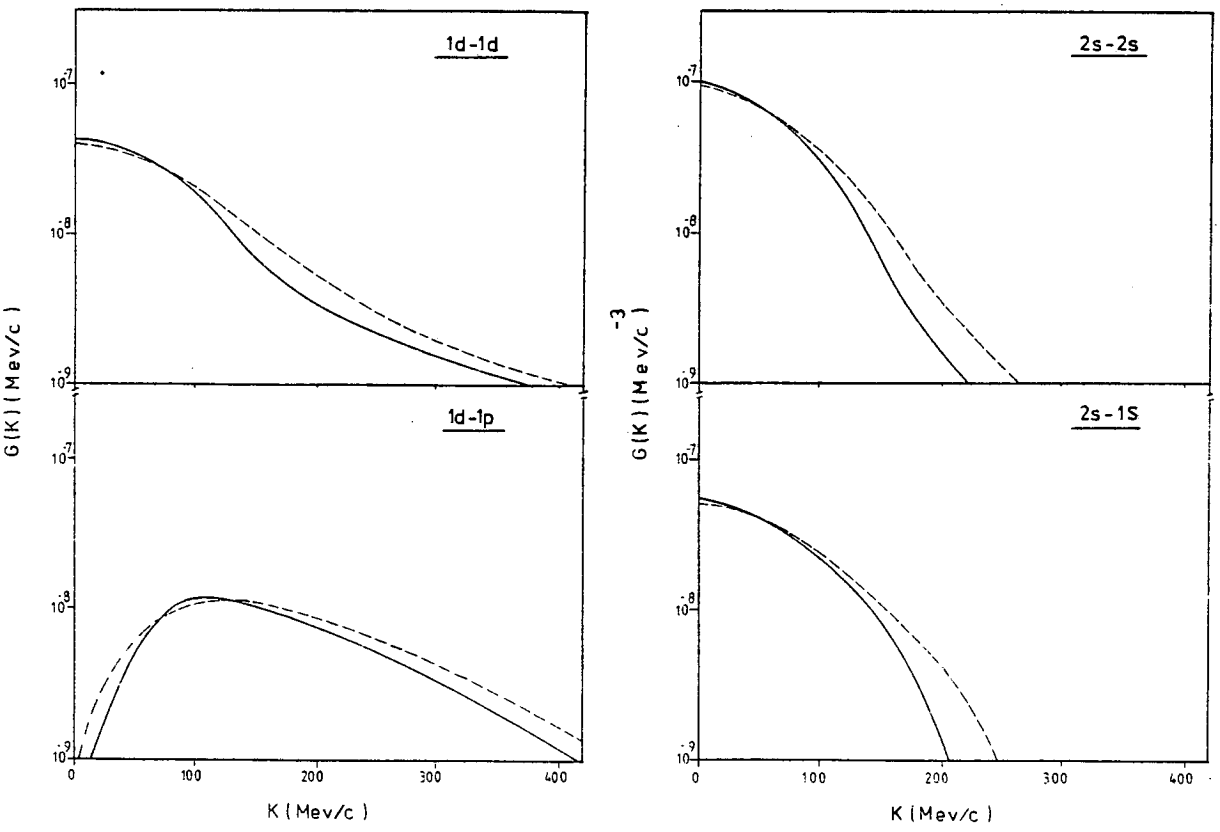
1d-1d
2s-2s
1d-1p
2s-1S
G(K) (Mev/c)^-3
K (Mev/c)
0
100
200
300
400

Fig. 4.3

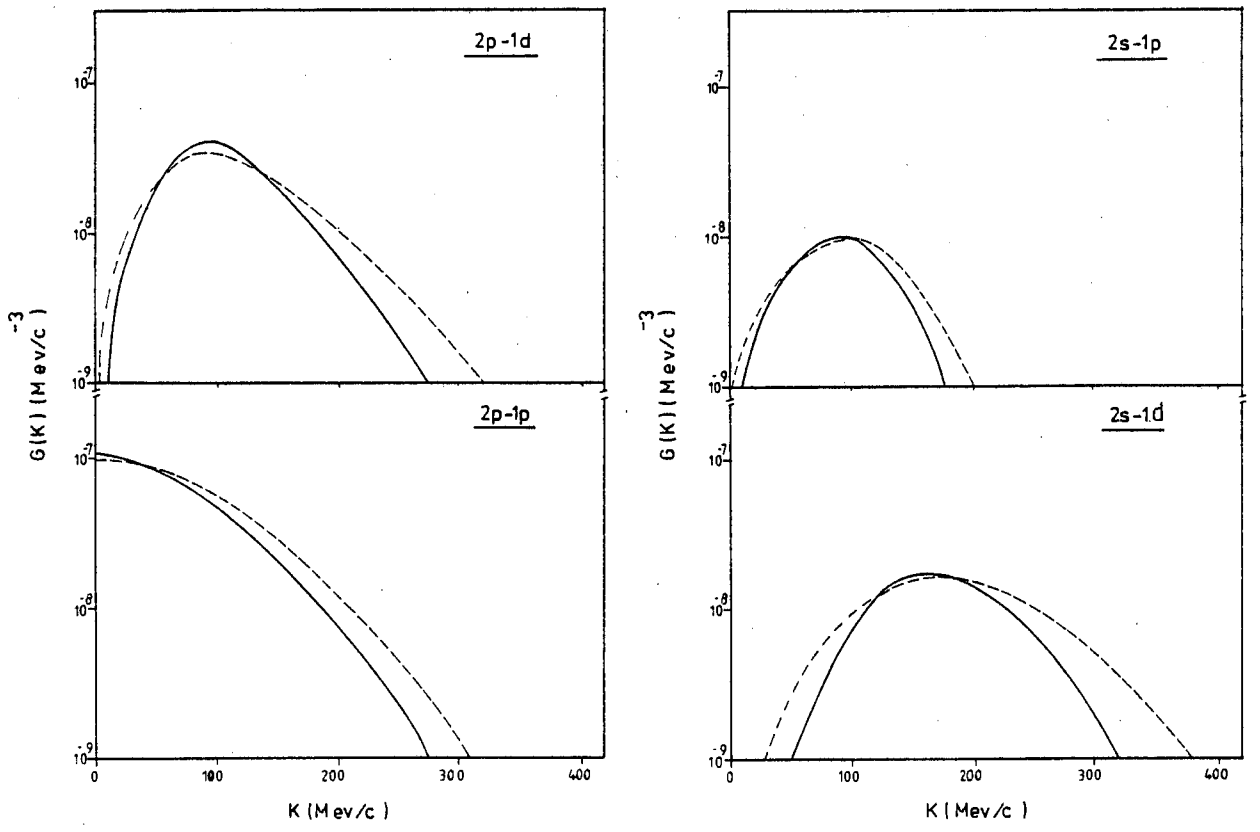
2p-1d
2p-1p
2s-1p
2s-1d
G(K) (Mev/c)^-3
K (Mev/c)
0
100
200
300
400

Fig. 4.4

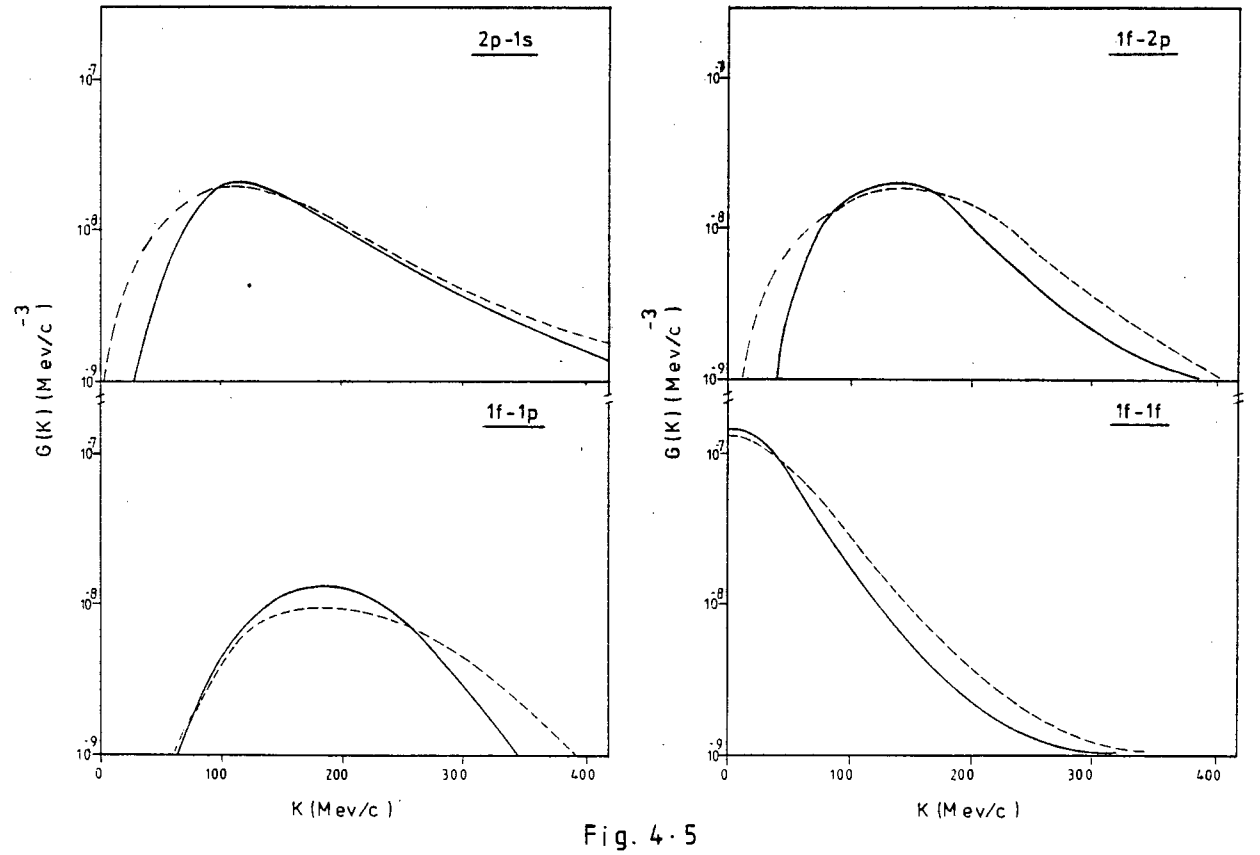
2p-1s
1f-1p
1f-2p
1f-1f
G(K) (Mev/c)^-3
K (Mev/c)
0
100
200
300
400

Fig. 4.5

nucleons using the quasi-free-scattering model (see Chapter III). The results of this process are then stored.

8) Then the calculation of $\left[\frac{d^2\sigma}{d\Omega_p dE_p}\right]_\beta$ is carried out by integrating equation (5) over the energy ranges of the primary photonucleons. The process of calculating $\left[\frac{d^2\sigma}{d\Omega_p dE_p}\right]_\beta$ is schematically shown in diagram 4.1. The results of the calculation for different shells are presented in Figures 4.6 to 4.11.

9) The final results are evaluated by summing over different shell's indices β, i.e. $\sum_\beta \left[\frac{d^2\sigma}{d\Omega_p dE_p}\right]_\beta$. These results are then compared with the experimental data as shown in Fig. 4.12.

It is obvious that the results of the theoretically calculated (γ, p) pre-compound overestimate the experimental data. For further discussion see section (4.3.4).

4.3.3.2 Harmonic Oscillator Potential Case for (γ, p) Process

The calculation of pre-compound contributions to (γ, p) energy spectrum using the harmonic oscillator potential is similar to the square well potential case. However the following terms in equation (5) are differently calculated for the case of harmonic oscillator potential.

1) The pseudo-Levinger constant L_β' for different principal and non-principal shells are evaluated using harmonic oscillator potential. These coefficients can be seen in Table 8(b), Chapter II.

2) For momentum distributions of the correlated neutron and proton pairs equation (55) in Chapter II is used where the wavefunctions associated with the harmonic oscillator potential are

Figures 4.6 - 4.10: The (γ,p) Pre-compound Contributions using ^{60}Ni

curve (1) is $\sum_{\beta} \left[\frac{\alpha^2\sigma}{d\Omega_p dE_p}\right]_{\beta}$.

Figure 4.11: Addition of curve (1) in Figures 4.6 to 4.10 in order to compare with data.

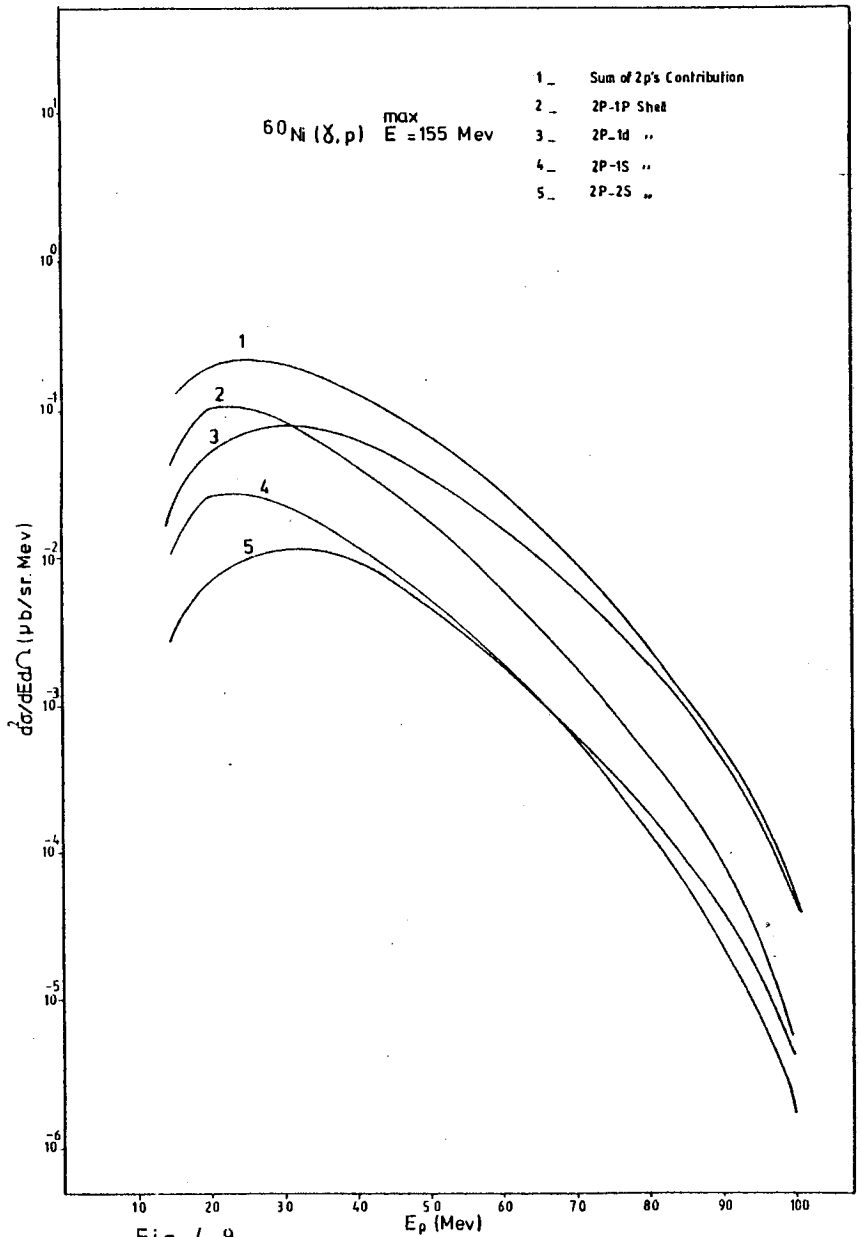
1 _ Sum of 2p's Contribution
2 _ 2P-1P Shell
3 _ 2P-1d ,,
4 _ 2P-1S ,,
5 _ 2P-2S ,,
60Ni (γ, p) Emax = 155 Mev
d²σ/dEdΩ (μb/sr. Mev)
Ep (Mev)

Fig. 4·8

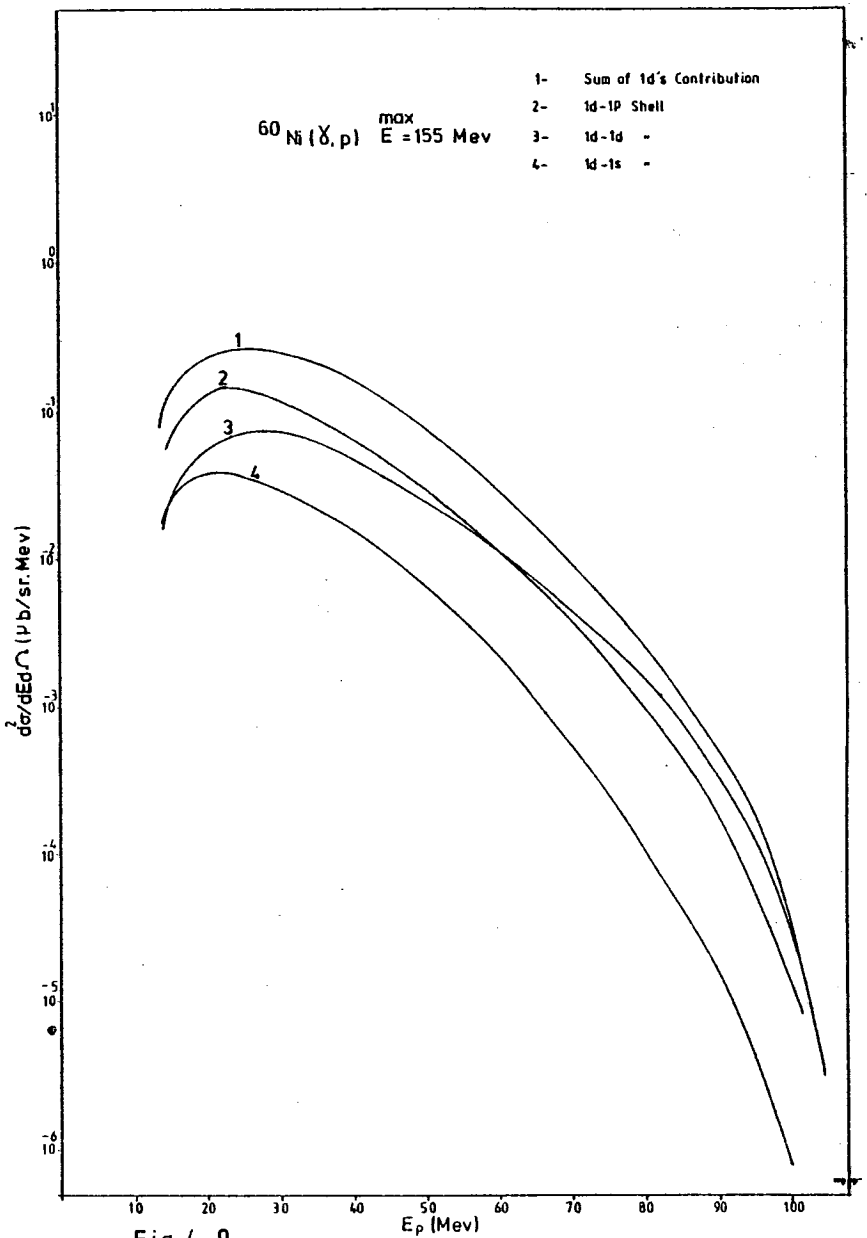
1- Sum of 1d's Contribution
2- 1d-1P Shell
3- 1d-1d "
4- 1d-1s "
60Ni (γ, p) Emax = 155 Mev
d²σ/dEdΩ (μb/sr. Mev)
Ep (Mev)

Fig. 4·9

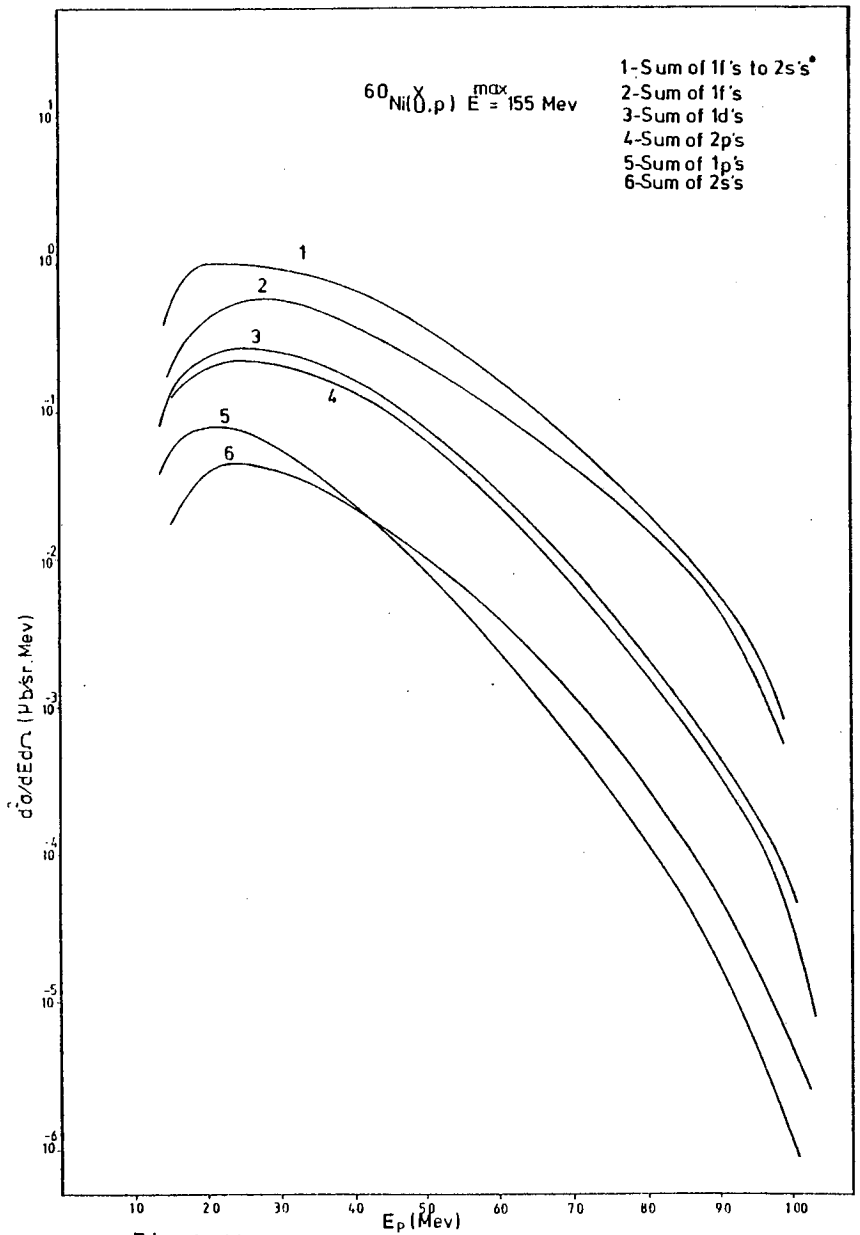

Fig. 4.11

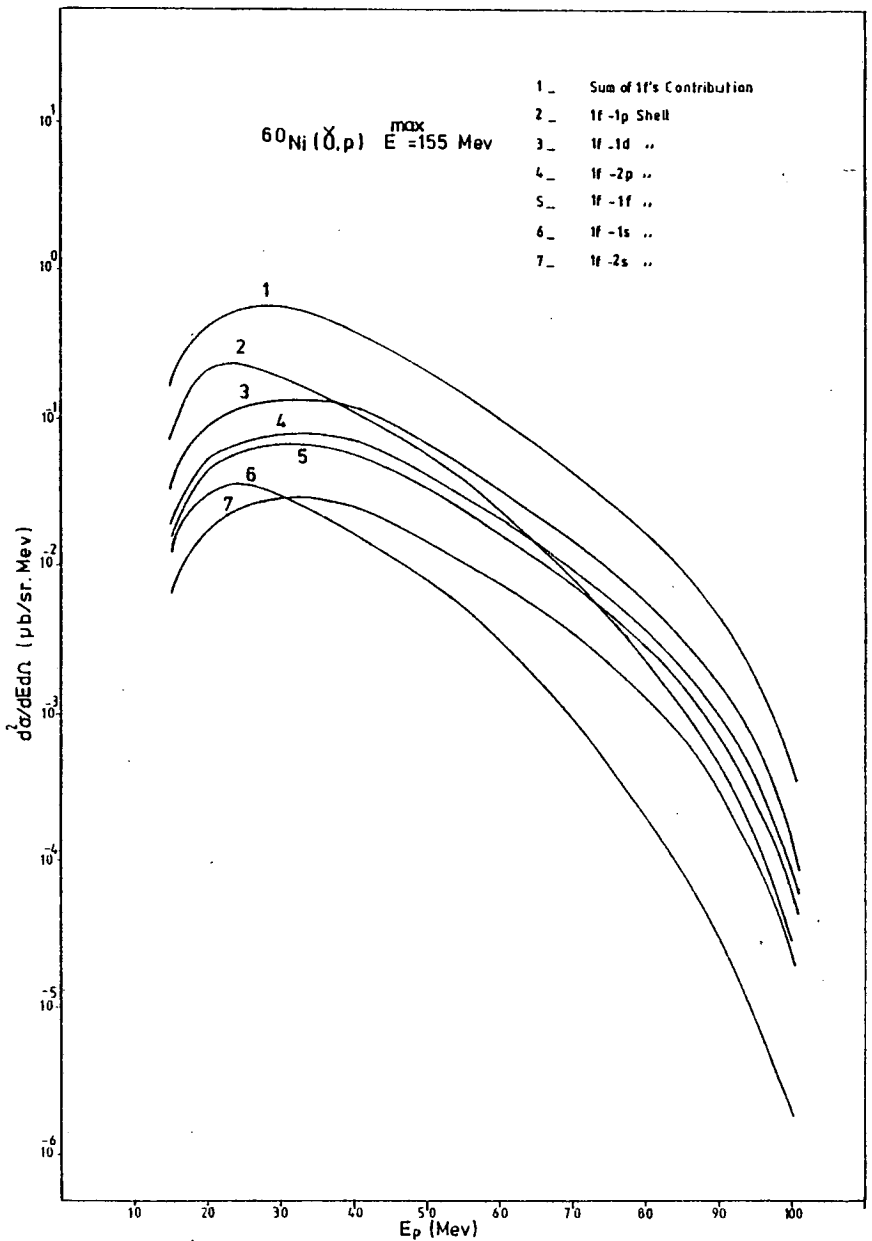

Fig. 4.10

Figure 4.12: The calculated (γ,p) compound and pre-compound results compared with the experimental data.

* : Square (sq.) well potential.

ǂ : Experimental data[83] taken at angle 90^{o}.

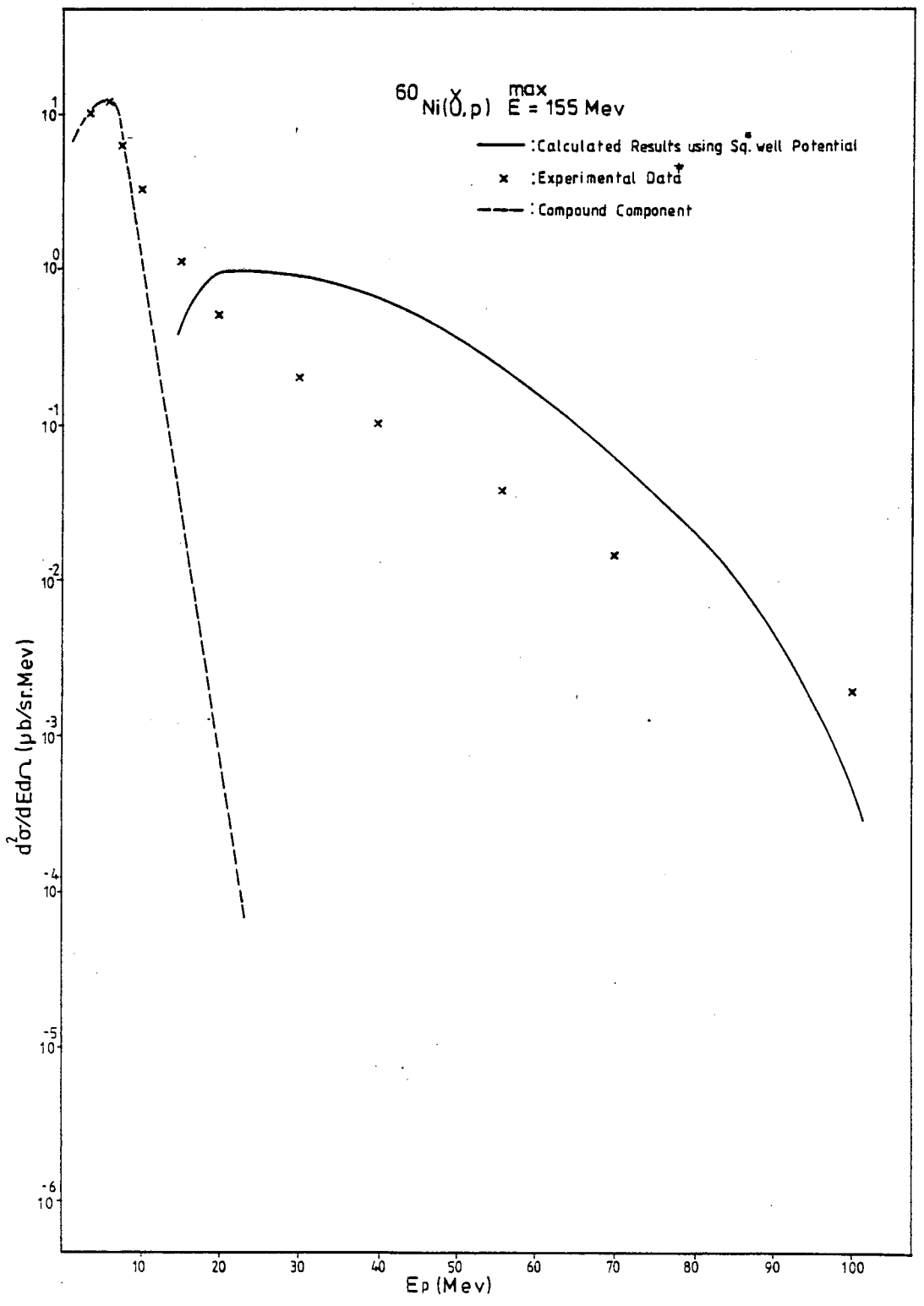
^{60}Ni(γ,p) E^{max} = 155 Mev
: Calculated Results using Sq. well Potential
: Experimental Data
: Compound Component
$d^2\sigma/dE d\Omega$ (μb/sr.Mev)
Ep (Mev)
10
20
30
40
50
60
70
80
90
100

Figures 4.13 - 4.17: The (γ,p) pre-compound contribution using ^{60}Ni; curve (1) is $\sum_{\beta}\left[\frac{d\sigma^2}{d\Omega_p dE_p}\right]_{\beta}$.

Figure 4.18: Addition of curve (1) in Figures 4.13 to 4.17 in order to compare with data.

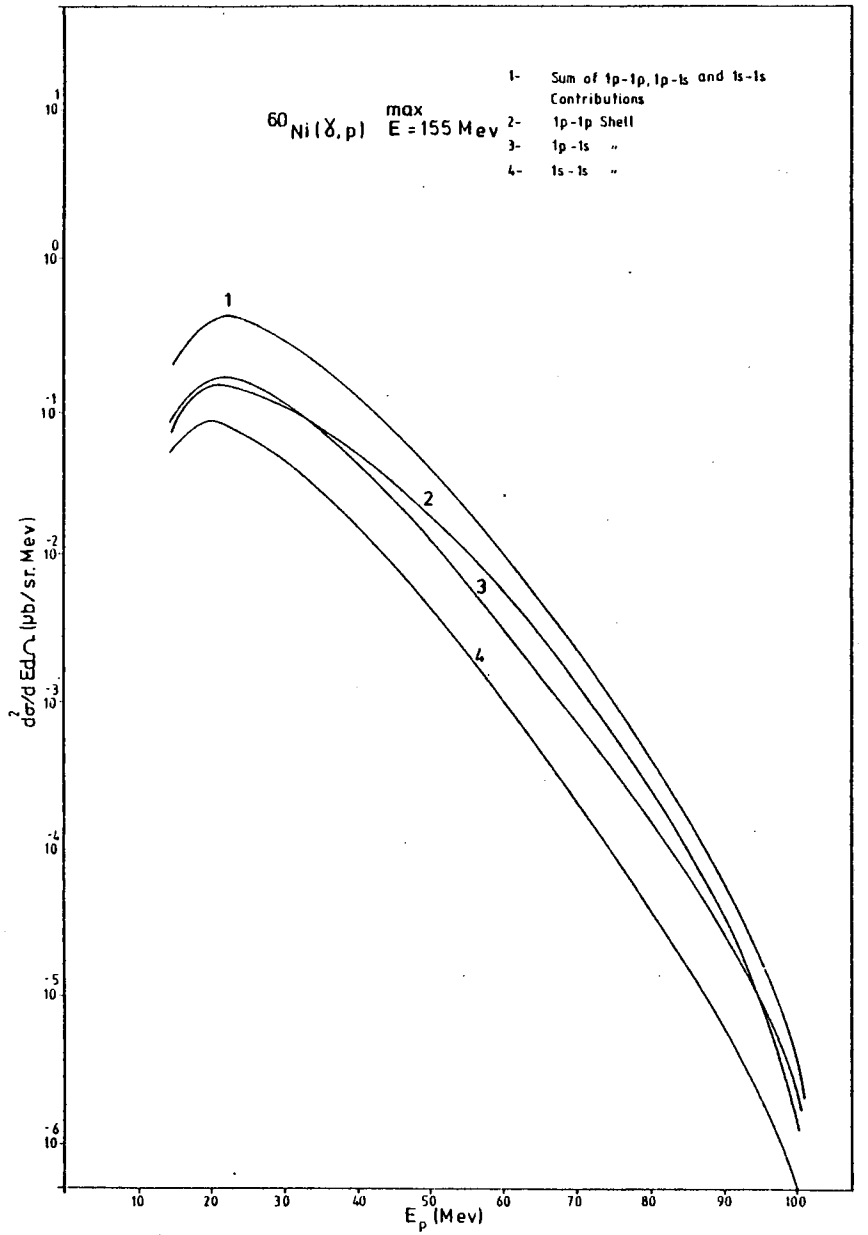

Fig. 4.13

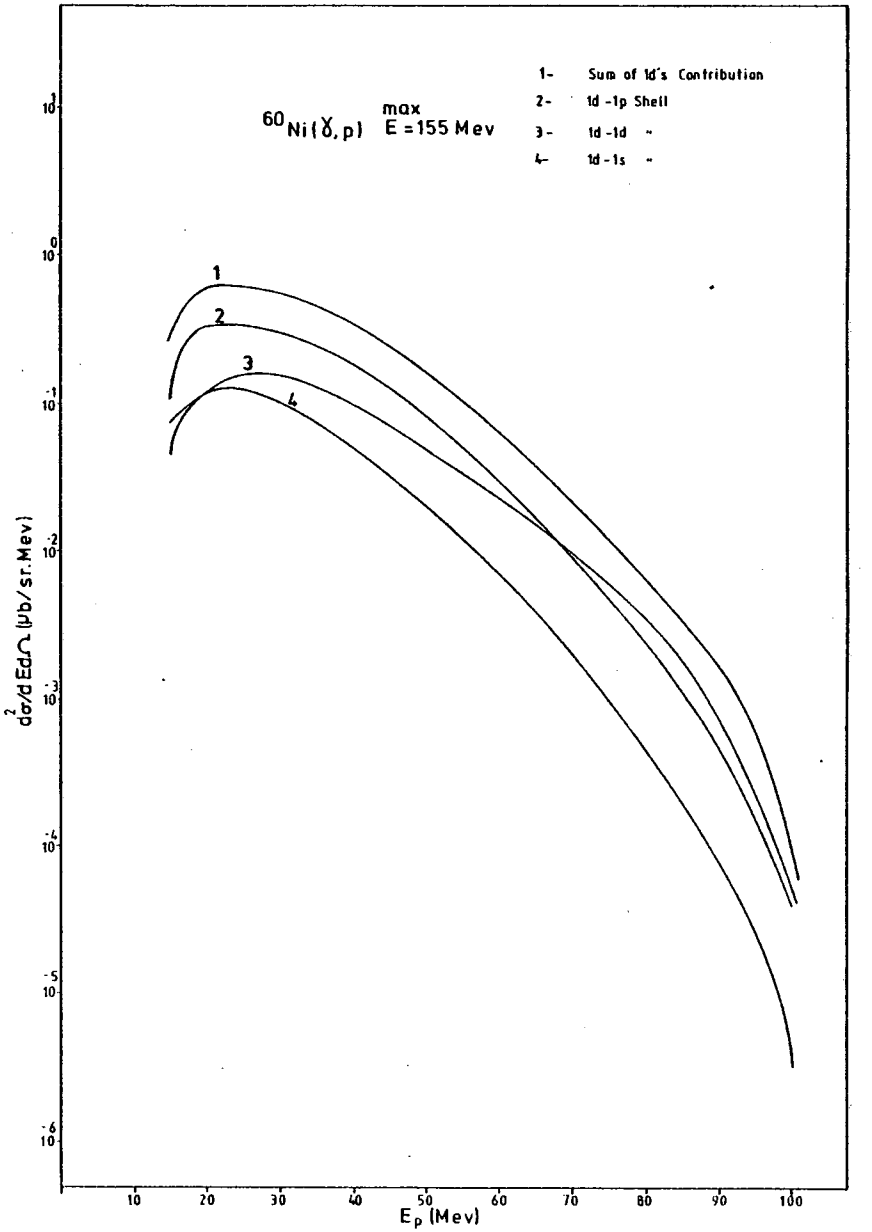

Fig. 4.14

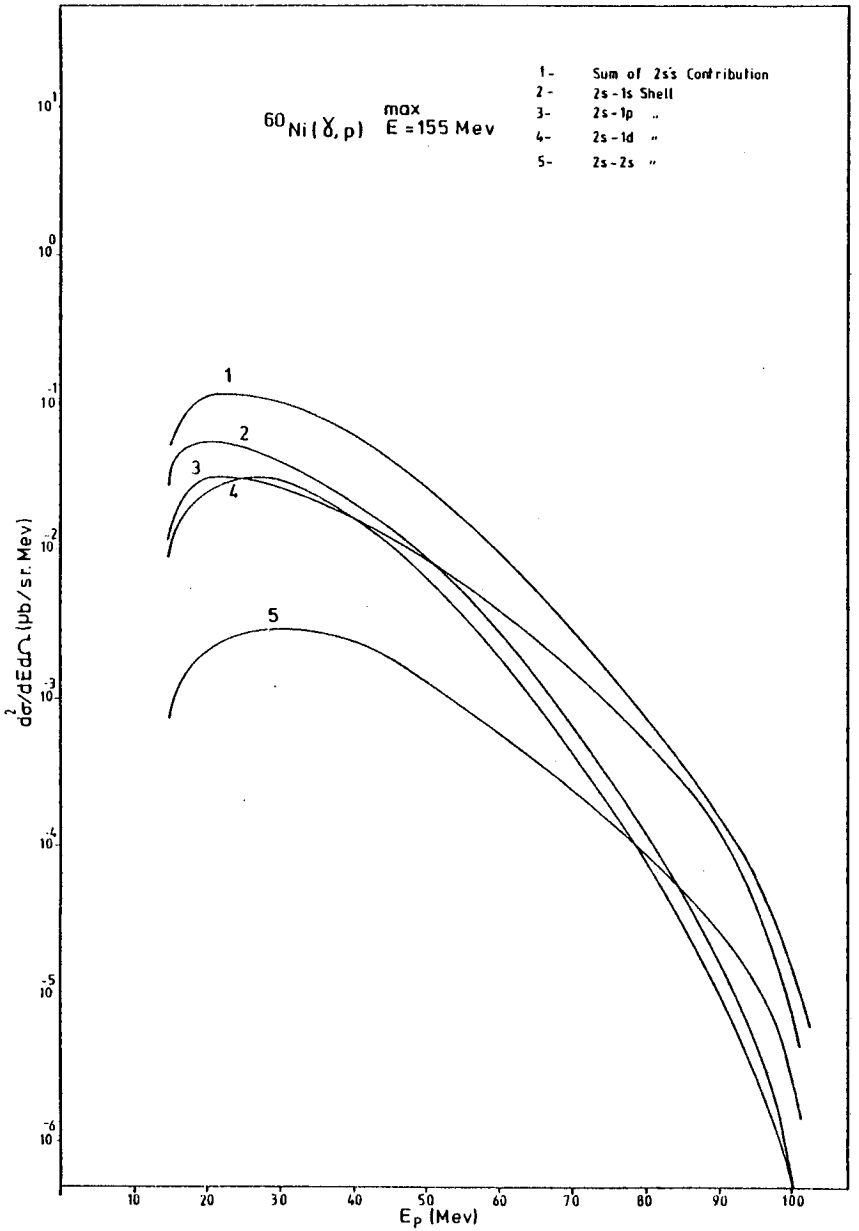

Fig. 4.15

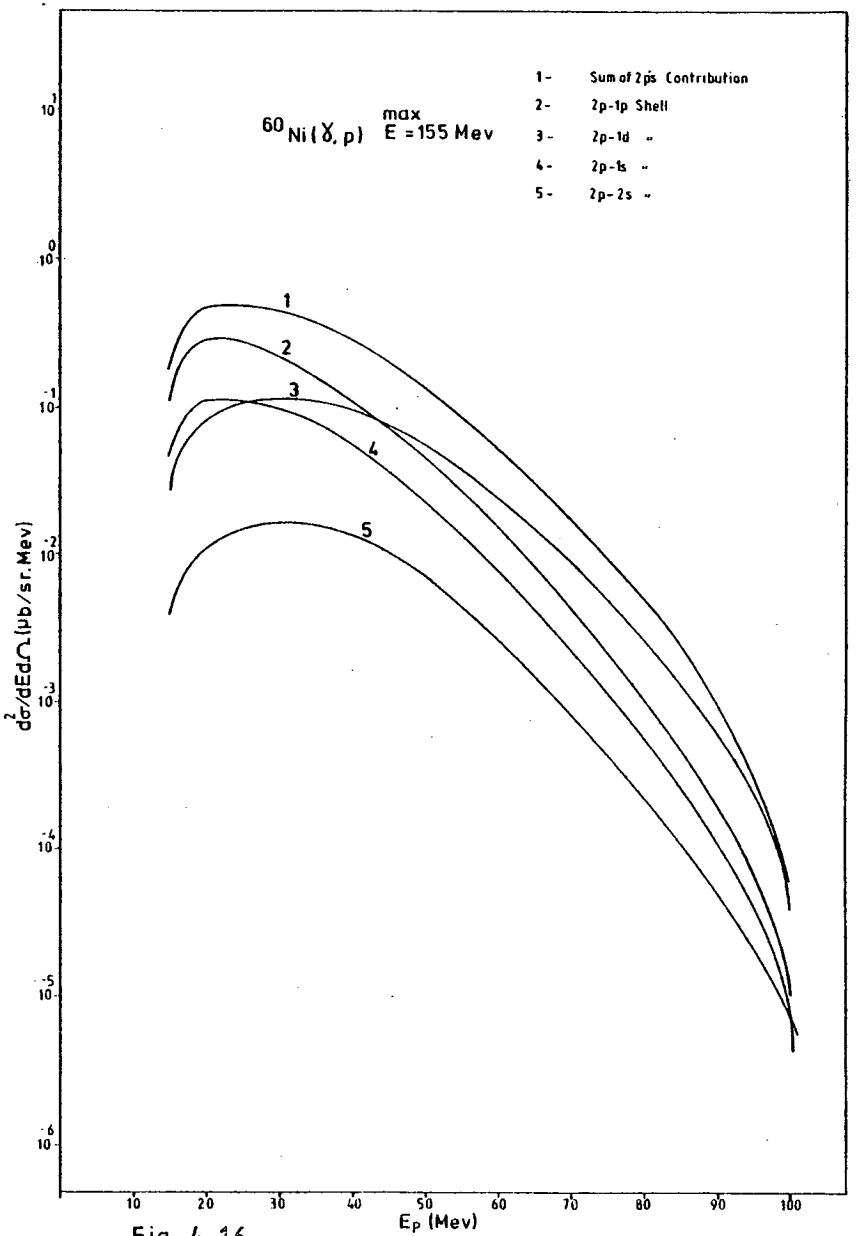

Fig. 4.16

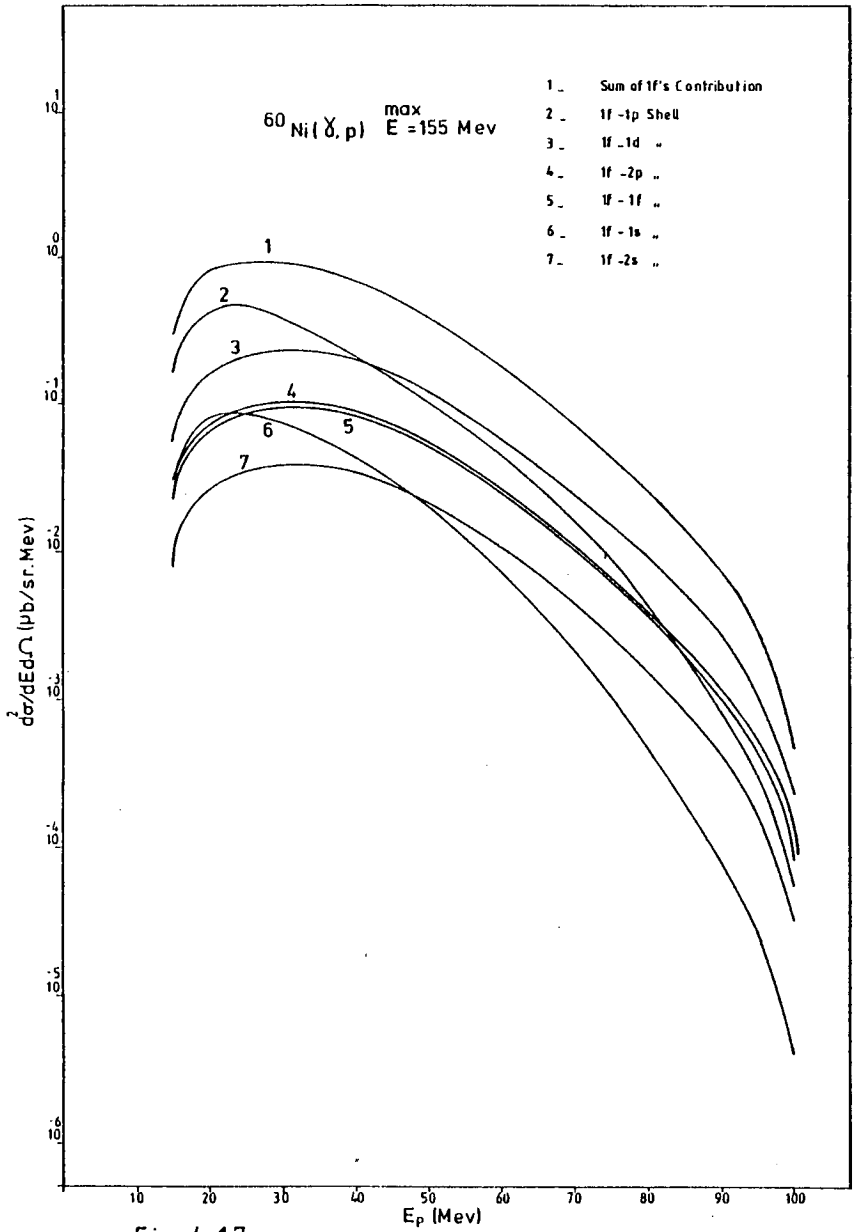

Fig. 4.17

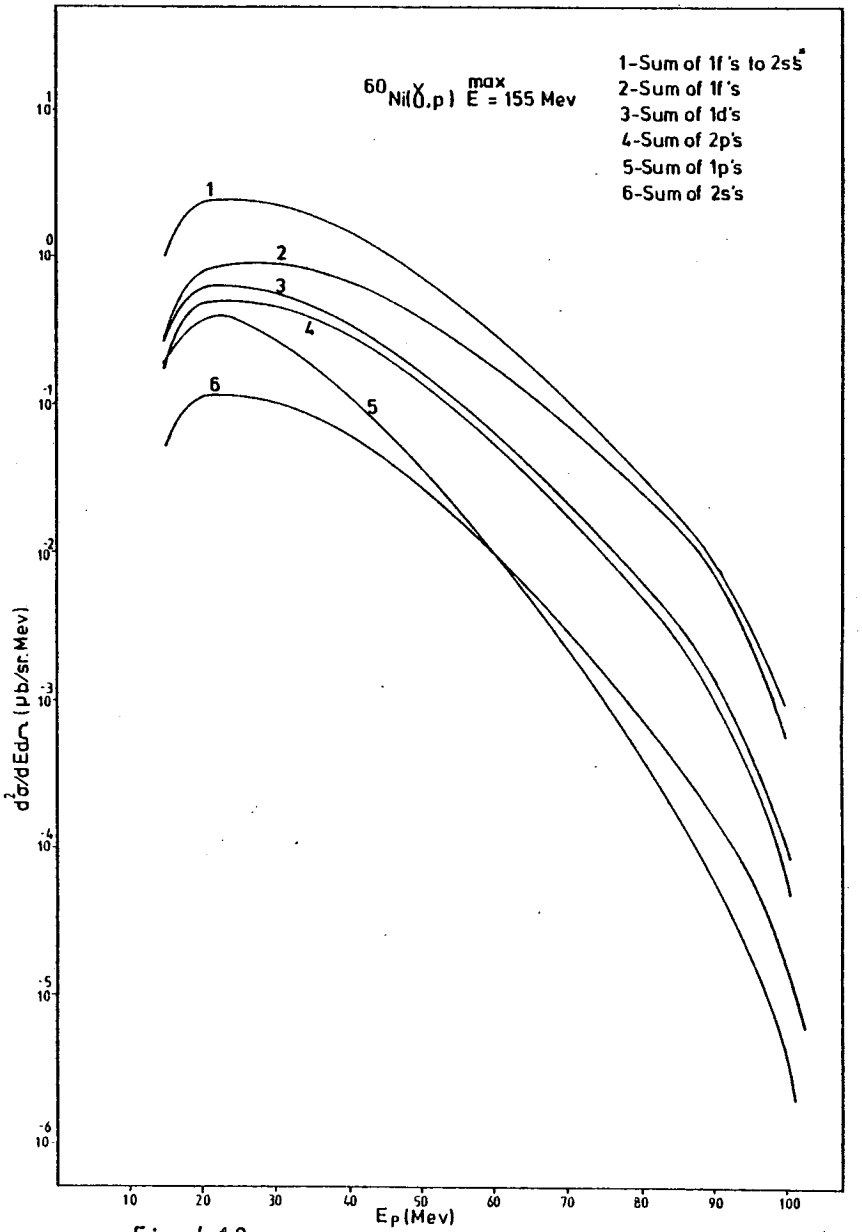

Fig. 4·18

employed. These momentum distributions are shown in Figures 4.1 to 4.5 by full lines.

3) Then the calculation of $\left[\frac{d^2\sigma}{d\Omega_p dE_p}\right]_\beta$ is carried out using a similar procedure as mentioned in section (4.3.3.1). The results of the calculation for different shells are presented in Figures 4.13 to 4.18.

4) The final results are evaluated by summing over different shell's contributions. Then these results are compared with the experimental data as shown in Figure 4.19.

The calculated results using harmonic oscillator, too, clearly indicate an over-estimation of the experimental data. In section (4.3.4) the two sets of energy spectrum for (γ,p) calculated by the use of each of the two different potentials (i.e square well and harmonic oscillator) will be discussed in relation to the experimental data.

4.3.4 Conclusion Related to (γ, p) Reactions

Results of the calculation of $\left[\frac{d^2\sigma}{d\Omega_p dE_p}\right]$ for (γ,p) using ^{60}Ni presented in sections (4.3.3.1) and (4.3.3.2) are compared with each other in this section (Fig. 4.20a). It should be emphasized that these calculations have been attempted without redress to arbitrary variable parameters. It is clear however that these calculations over-estimate the experimental results. Therefore, the immediate questions which can be posed are about the sources of these over-estimations (Fig. 4.20a, curves (1) and (2)), i.e.

a) is the quasi-free scattering model inappropriate for the consideration of the final state interactions when $(\gamma,N' \Rightarrow N',N)$ reactions are considered?

Figure 4.19: The calculated (γ,p) compound and pre-compound results are compared with the experimental data.

* : Harmonic Oscillator (H.O.)

ǂ : Experimental data[83] taken at angle 90^{o}.

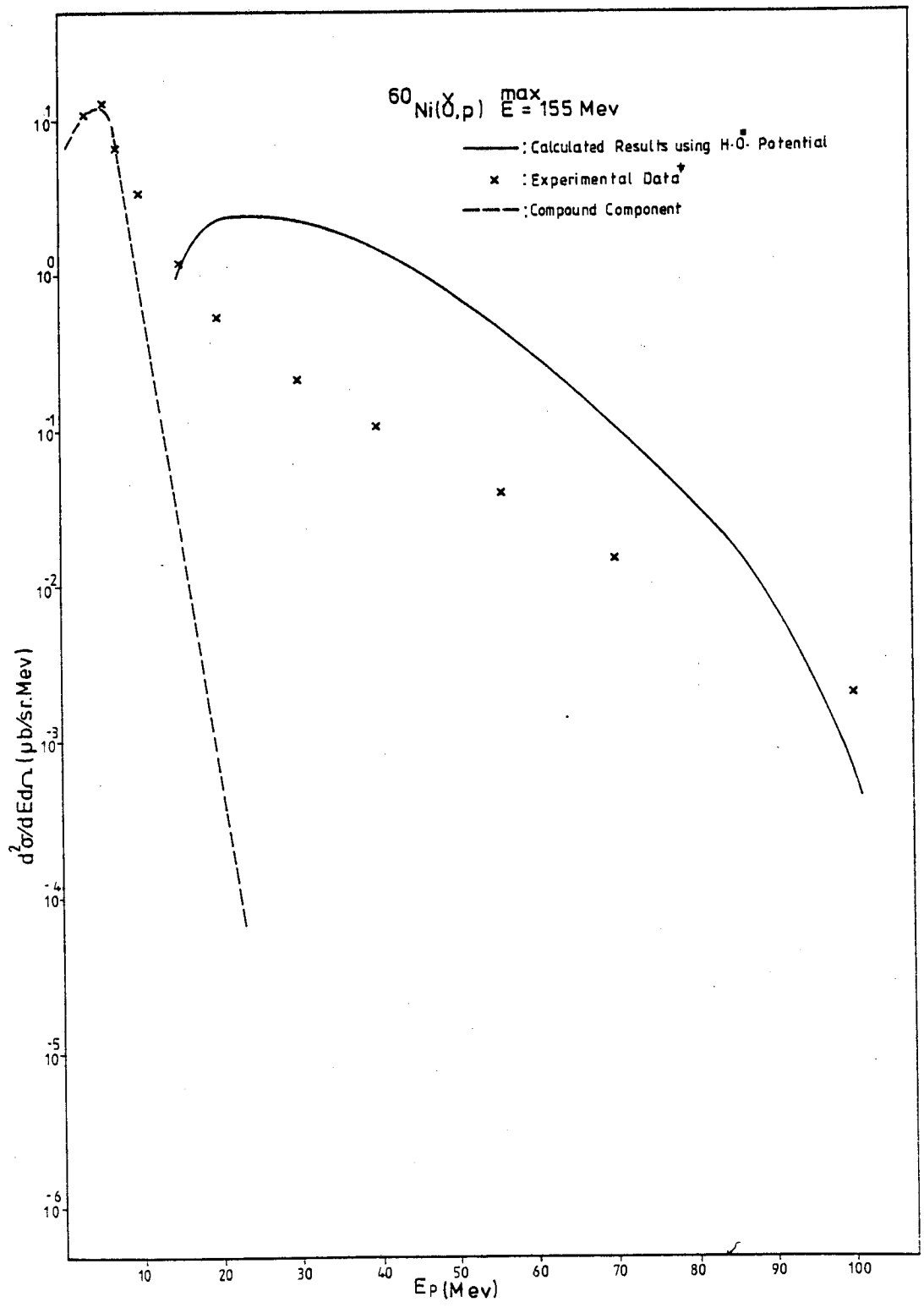
$^{60}Ni(\gamma,p)$ E^{max} = 155 Mev
: Calculated Results using H·O· Potential
: Experimental Data*
: Compound Component
$d^2\sigma/dEd\Omega$ (μb/sr.Mev)
Ep (Mev)
1
0
-1
-2
-3
-4
-5
-6
10
20
30
40
50
60
70
80
90
100

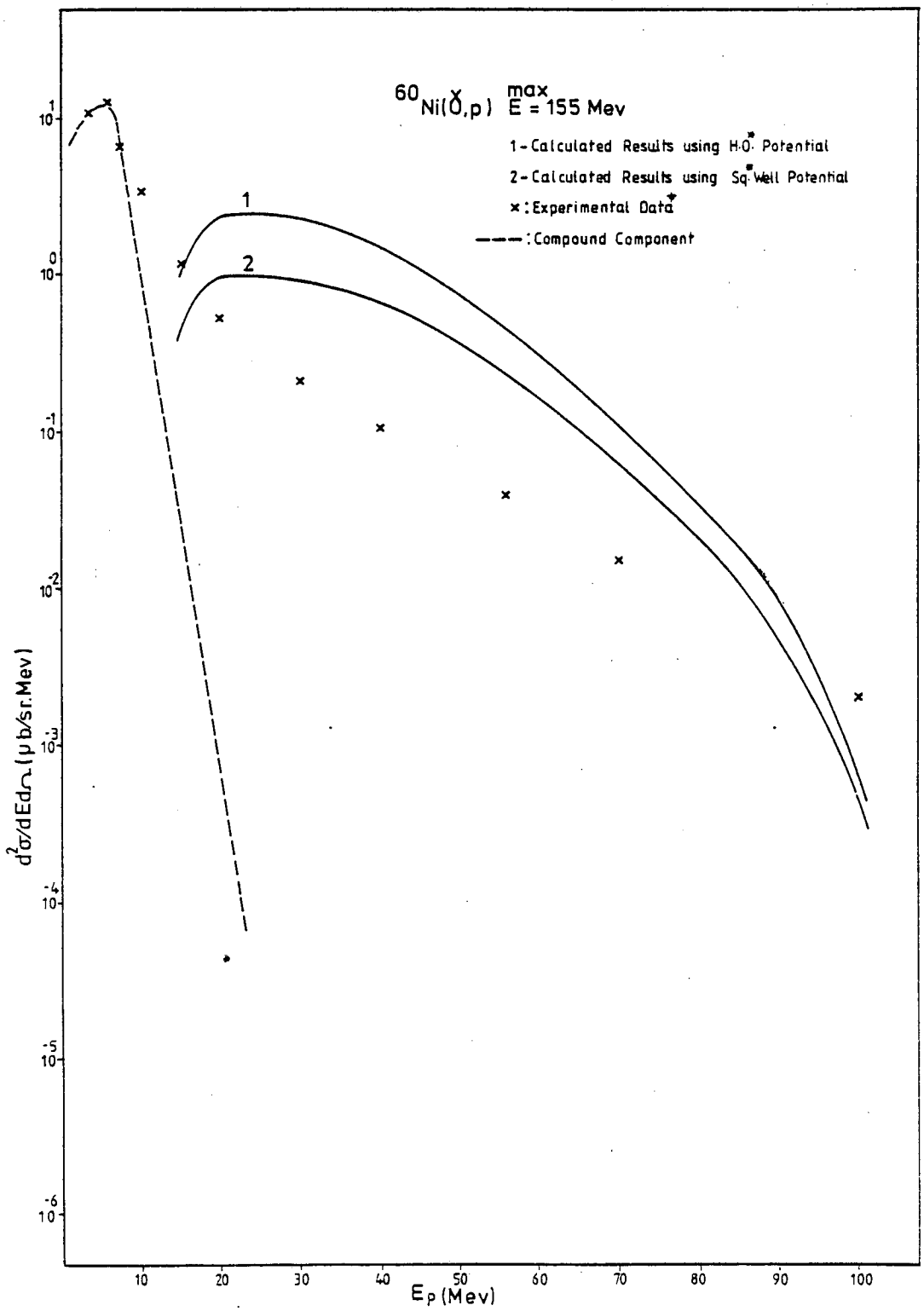

Figure 4.20a: The calculated results in Fig. 4.12 for square well and in Fig. 4.19 for harmonic oscillator potentials are compared with the experimental data.

* : Square (Sq.) well and Harmonic Oscillator (H.O.)

‡ : Experimental data[83] taken at angle 90°.

b) is the quasi-deuteron model improperly considered in the derivation of double differential cross-section for primary generated photo-nucleons?

These two fundamental questions will be discussed below.

The quasi-free scattering model in different calculations has proved to be a successful model, capable of producing energy spectra (see Fig. 3.1, Chapter III). These investigations for (P,P') reaction using ^{209}Bi and ^{54}Fe indicate that the calculated results slightly underestimate the data. Concerning angular distribution, the quasi-free scattering model presents a partial successful picture in reproducing data (see Figures 3.2 and 3.3, Chapter III).

In the calculation of $\left[\frac{d^2\sigma}{d\Omega_p dE_p}\right]_F$, the primary generated photo-nucleons are assumed to make collisions without changing their initial angle. Consequently, the emission probability, $P(E_p; E_N)$ is considered instead of $P(\hat{E}, \hat{\Omega}; E_N, \Omega_N)$ (see section 4.2.Ø). This is due to the incorporated quasi-free scattering model which was not capable of producing $P(\hat{E}, \hat{\Omega}; E_N, \Omega_N)$. It can be said that the consideration of a more realistic emission probability, i.e. $P(\hat{E}, \hat{\Omega}; E_N, \Omega_N)$ can improve the accuracy of $\left[\frac{d^2\sigma}{d\Omega_p dE_p}\right]_F$, particularly in high energy outgoing particles.

On the basis of the above discussion it is possible to argue that the quasi-free scattering model is appropriate for the consideration of the final state interactions. Further, the weak points of this model for (N,N') reaction and a more adequate emission probabilities seem not to be responsible for data overestimation.

Calculation of the double differential cross-sections for the primary photo-generated protons (as discussed in Chapter II, using ^{12}C) indicated that the calculated results overestimate the experimental

data at $E_p < 60$ MeV for the two cases of interest (a factor of four and a factor of eight for square well and harmonic oscillator potentials, respectively.) In this type of calculation the final state interactions were ignored due to the insensitivity of light nuclei. For the calculation of (γ,p) double differential cross-sections using ^{60}Ni, it is appropriate to compare the results of (γ,p) with and without final state interactions (Fig. 4.20b). This figure indicates that the consideration of the final state interactions will increase the cross-sections for particles with low outgoing energies, while the effect of the final state interactions decrease the cross-sections for particles with high outgoing energies.

The above discussion indicates that the calculations of (γ, p) double differential cross-sections for ^{12}C and ^{60}Ni without final state interactions already overestimate the experimental data. Therefore the source of overestimation of data by the theoretical calculation can be interpreted as the failure of the possibility to express the photonuclear cross-section for the reaction proceeding through the two-particle absorption mechanism in terms of the deuteron photodisintegration cross-section ($E_\gamma \lesssim 150$). This can be supported by the fact that at the energies below the meson production threshold ($E_\gamma \lesssim 150$ MeV, $\lambda \gtrsim 1.3F$). We are concerned with both small and large nucleon separations ($r \gtrsim 1.3F$). It is also well known that the quasi-deuteron model is justified for the region $E_\gamma \gtrsim 200$ (the photon wavelength is less than $(1F)$, where the exchange cross-sections, σ_d^{exch} is dominant (Fig. 4.21). Therefore it can be argued that if the quasi-deuteron model is to be employed for the region $E_\gamma \lesssim 150$ MeV. Only the exchange cross-sections, σ_d^{exch}, should be used. This idea has been investigated in Chapter II by

Figure 4.20b: Curves (1) and (2) calculated results presented in Fig. 4.20a and curves (3) and (4) calculated results without considering final state interactions in (γ,p) process.

* : Square (sq.) well and Harmonic Oscillator (H.O).

ǂ : Experimental data[83] taken at angle 90^{o}.

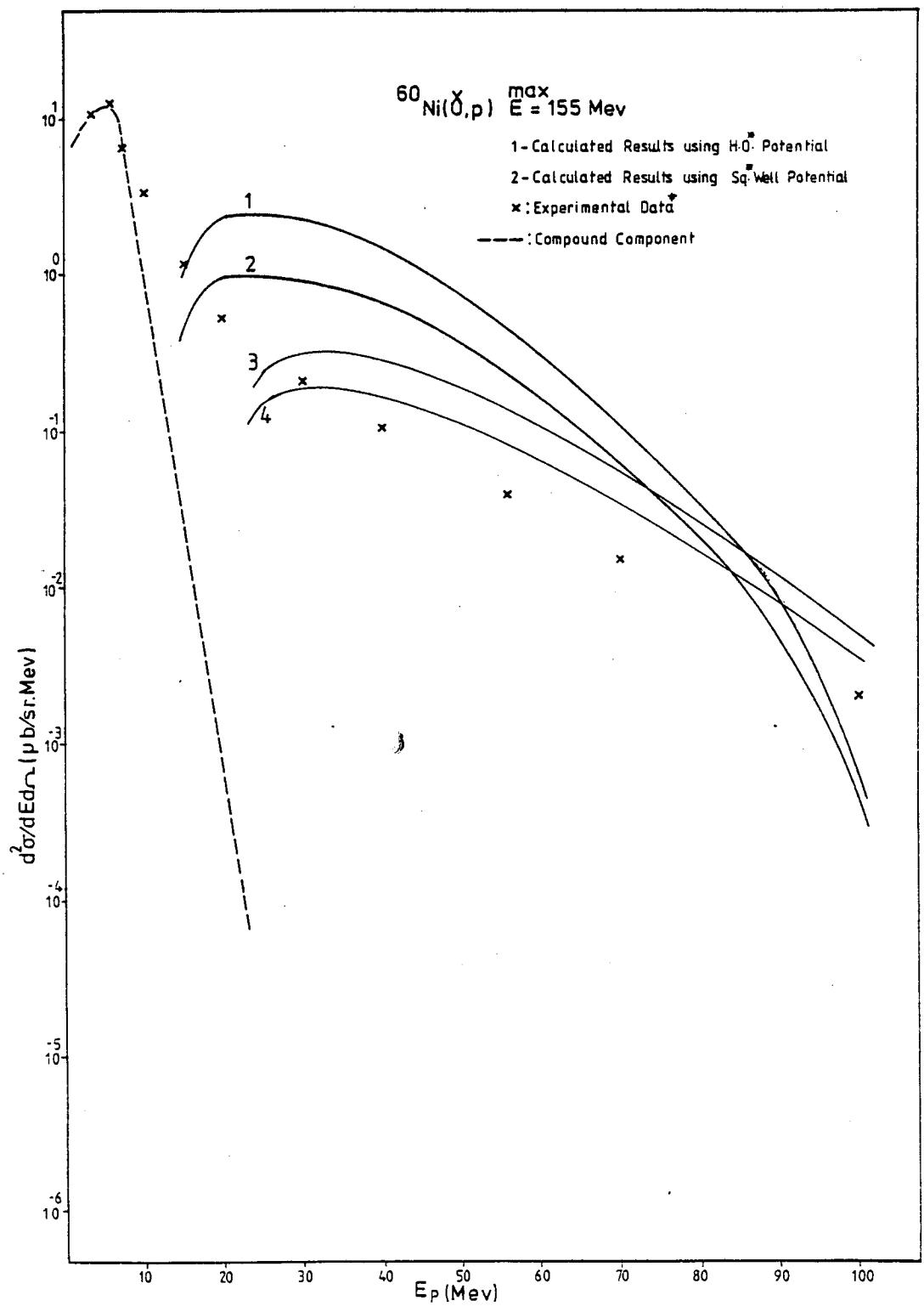
$^{60}Ni(\gamma,p)$ E^{max} = 155 Mev
1 - Calculated Results using H.O. Potential
2 - Calculated Results using Sq. Well Potential
× : Experimental Data
——— : Compound Component
1
2
3
4
$d^2\sigma/dEd\Omega$ (μb/sr.Mev)
E_p (Mev)

Fig. 4·20b

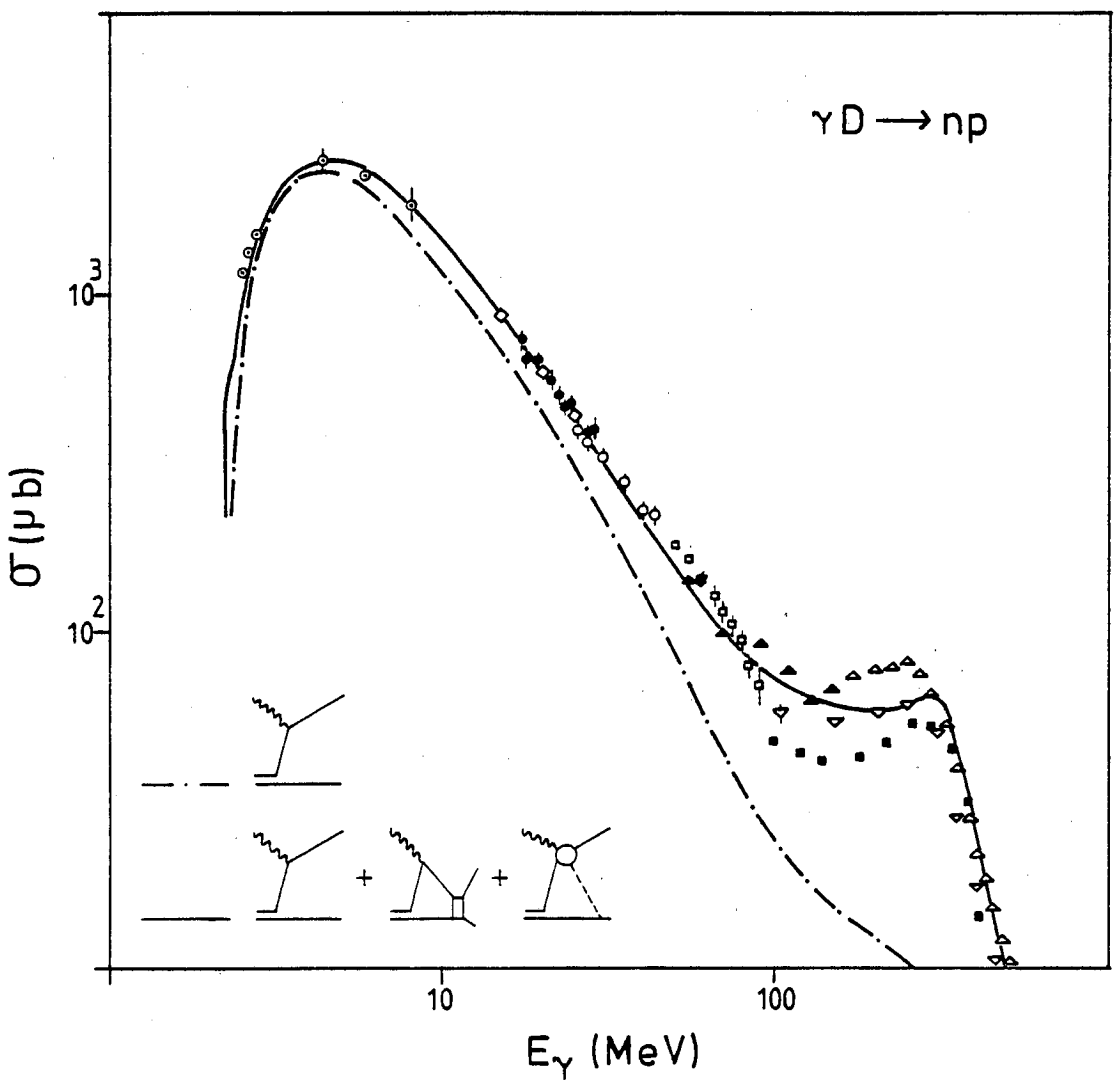

Figure 4.21: The deuteron total photo-absorption cross-section is plotted against the energy of the incoming photon. Dash-dotted curve: The constructed cross-section using the amplitude corresponding to the photon interaction with the nucleon (proton or neutron). Full curve: sum of dash-dotted curve, the meson exchange current and NN scattering vertices. For details of data given in Fig. 4.21 and further information, refer to ref. 14.

calculating total photo-absorption cross-section for ^{12}C and ^{16}O. The conclusion reached in section (2.2.2.4) indicates that the use of $\sigma_d^{exch.}$ instead of σ_d will improve the reproduction of data for the region $E_\gamma \lesssim 150$ MeV.

Accordingly, in order to get a closer agreement between the theoretical calculations and the experimental data (Fig. 4.20a), a conversion factor for the replacement of σ_d by $\sigma_d^{exch.}$ will be evaluated using the values given for σ_d and σ_d^{exch} corresponding to different photon energies. These values are given in Table 4.1.

E_γ (MeV)	$\sigma_d(E_\gamma)$ (μb)	$\sigma_d^{exch.}(E_\gamma)$ (μb)
20	590	38.8
30	370	37.5
40	231	33.8
50	154	31.2
80	88	25.5
100	70	23.2
120	62	21.6
140	54	20.7

Table 4.1: The $\sigma_d^{exch}(E_\gamma)$ cross section, computed by Laget[14] and $\sigma_d(E_\gamma)$ the total photo-disintegration cross-section (table taken from reference 10a).

The values given in Table 4.1 for $\sigma_d(E_\gamma)$ and $\sigma_d^{exch}(E_\gamma)$ can be compared to each other in order to evaluate an average value for the conversion factor mentioned above, i.e. ~ 0.11.

Subsequently, the two curves (1) and (2) in Figure 4.20 are multiplied by the deduced conversion factor. The results can be

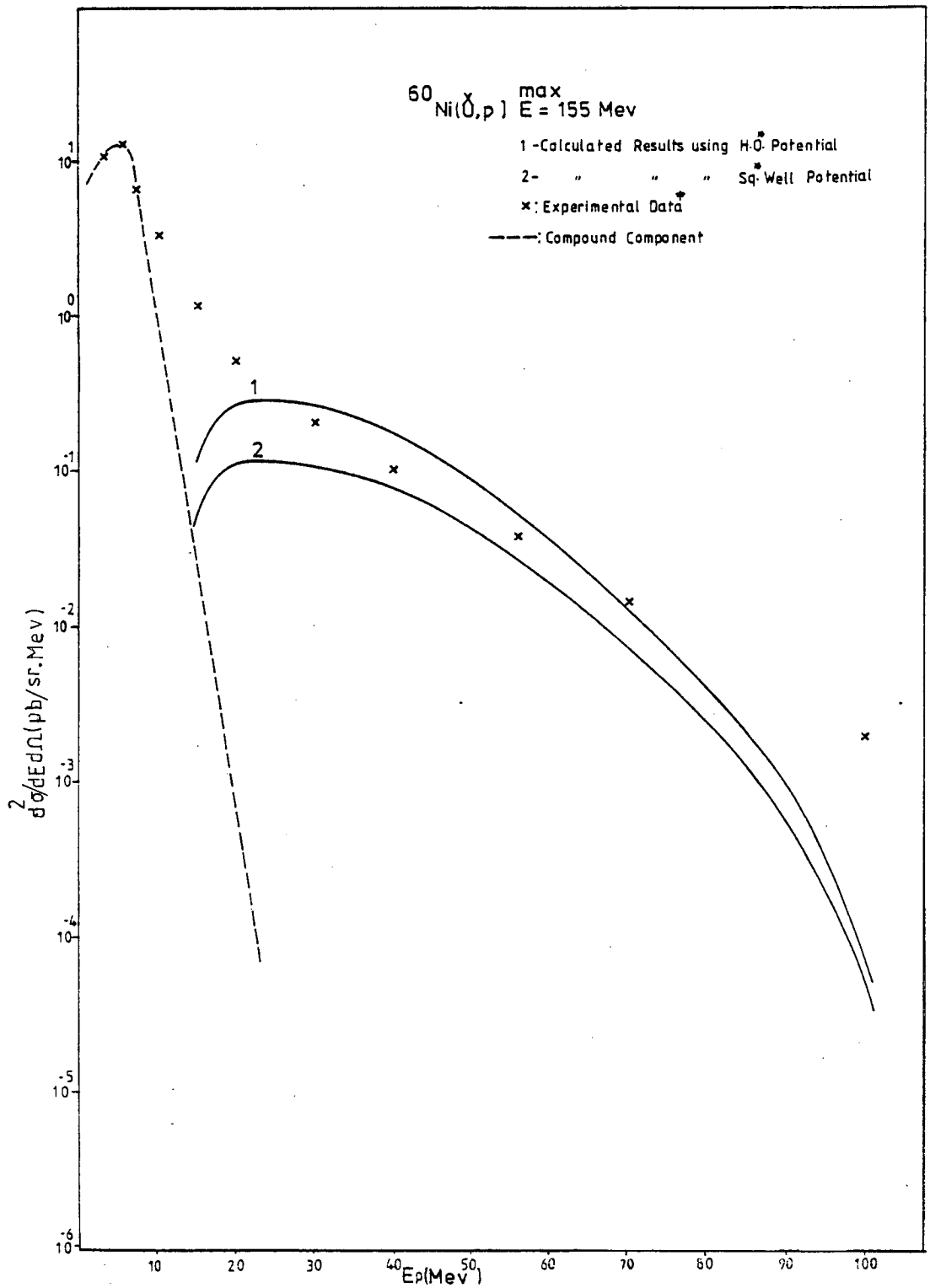

Figure 4.22: The pre-compound calculated results in Fig. 4.20a are multiplied by the conversion factor deduced in sub-section 4.3.4 and are compared with data (see Fig. 4.20a caption for more information).

seen in Figure 4.22, where a reasonable agreement is achieved below $E_p \lesssim 70$ MeV between the theoretically calculated results and the experimental data. The calculated results, however, indicate that more fundamental calculations are needed to confirm the validity of the argument concerning the replacement of the total photo-disintegration cross-section of the deuteron with the exchange part.

The last point to be noted in Figure 4.20a concerns the poor reproduction of the data for $E_p > 70$ MeV, which is probably due to a direct reaction component for the (γ, p) process.

4.4.Ø The Calculation of Energy Spectra for the (e,α) Process Using ^{60}Ni

4.4.1 Introduction

The correlation of protons and neutrons into small clusters, particularly alpha particles, has been investigated by different methods. Electromagnetic induced reaction is one of the processes that has been used in order to investigate the alpha particle clustering. It is on this basis that the calculation of energy spectrum for the (e, α) process using ^{60}Ni will be carried out in this section. To this end the following procedure is adopted.

a) The calculation of compound nucleus component,

b) The calculation of pre-compound contributions to energy spectra using the formalism proposed in section (4.2.Ø), equation (6).

In the following two sections the compound and pre-compound

contributions to the (e, α) energy spectra will be considered.

4.4.2 The Calculation of Compound Nucleus Component for the (e,α) Process

The (e,α) compound nucleus component is calculated using the following expression:

$$\frac{d\sigma}{dE_\alpha}(E_e, E1) = \int_{-Q_n}^{30} \frac{d\bar{\sigma}}{dE_\alpha}(E_\gamma) N^{E1}(E_e, E_\gamma).E_\gamma^{-1}\, dE_\gamma \qquad (9)$$

where $\frac{d\bar{\sigma}}{dE_\alpha}(E_\gamma)$ is given by

$$\frac{d\bar{\sigma}}{dE_\alpha}(E_\gamma) = \bar{\sigma}_n(E_\gamma) \frac{\sum_{s'\ell'} T_{\ell'}(E_\gamma, E_\alpha)}{\sum_{s''\ell''} T_{\ell''}(n)} \qquad (10)$$

The remaining quantities are introduced in Appendix (C). In equation (9) the virtual photon spectrum $N^{E1}(E_e, E_\gamma)$ is calculated, using the DWBA formalism[75], where the assumption of a pure dipole resonance excitation process is used. In equation (10) the values adopted for $\bar{\sigma}_n(E_\gamma)$ are taken from Berman[84] for ^{60}Ni and the transmission coefficients $T_{\ell'}(E_\gamma, E_\alpha)$ and $T_{\ell''}(n)$ are given by a computer code[85,86]. The calculation of $\frac{d\sigma}{dE_\alpha}(E_e, E1)$ is then carried out by obtaining the alpha to neutron branching ratio at 1 MeV excitation energy intervals and integrating expression (9). The resultant energy spectra is shown in Figures 4.29 and 4.36.

4.4.3 Pre-Compound Contributions for the (e,α) Process

According to the formalism suggested in section (4.2.Ø), equation (6), a shell model approach is adopted for the calculation of (e,α) pre-compound energy spectrum. In this approach the different contributions to (e,α) pre-compound energy spectra will be calculated by following the cascade processes for electro-nucleons inside the nucleus. These electrolnucleons are created due to the absorption of virtual photons by (np) pairs on different shells. Cascade processes for electro-nucleons are shown in diagram 4.2.

The probability for collision between an electro-nucleon and a preformed α-cluster, ϕ, is assumed to be a floating parameter. In the nucleon-induced calculation[6, 87], i.e. (N, α) reactions, there is a variation in the value of the preformation factor. This means that ϕ appears to decrease to some extent with increasing A from 0.10 in the medium mass region to 0.075 in the mass region above A = 200. Blann et al.[6] have performed the quasi-free scattering calculation for (N,α) reaction with a set of parameters, i.e. a pseudo Fermi energy ε_f^n = 4 MeV and ϕ = 0.10. It must be emphasized that this set of parameter values is not unique; for example, spectra of almost the same degree of agreement may be obtained[6] for ε_f^n = 8 MeV, with ϕ = 0.03 (see Chapter III for an explanation of the pseudo Fermi energy). In the present study the calculation of α-particle emission probabilities is carried out using ε_f^n = 8 MeV and ϕ = 0.03 (see section 4.4.4).

In the following two subsections the results of calculation of (e,α) pre-compound for the two cases of study, i.e. square well and harmonic oscillator potentials will be presented.

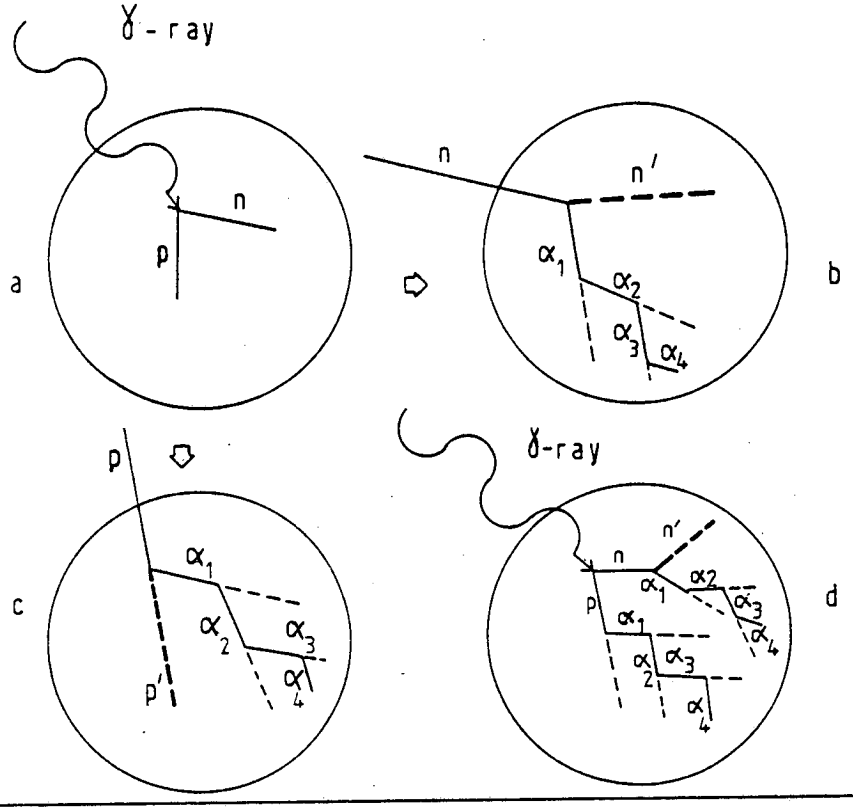
γ - ray
n
p
a
n
n'
α1
α2
α3
α4
b
p
p'
α1
α2
α3
α4
c
γ-ray
n
n'
α1
α2
α3
α4
p
α1
α2
α3
α4
d

Diagram 4. 2

4.4.3·1 Square Well Potential Case for (e,α) Process

In order to calculate the (e,α) spectrum, equation (6) is used where the different quantities are calculated according to the following procedure:

1) The pseudo-Levinger constants L'_β are presented in Table 8(a), Chapter II. These values will be used with the corresponding number of contributing correlated pairs, $N_\beta Z_\beta$.

2) The momentum distribution of (np) pairs G(K) and the quantity $\frac{d\sigma}{d\Omega^*_N}$ will be evaluated using the approach mentioned in section (4.3.3.1).

3) B(ω), the spectrum for electrons is calculated using the DWBA formalism[75].

4) The first right-hand-side bracket in expression (6) is therefore evaluated using the computer programme discussed in section (2.3.Ø). The calculation of double differential cross-sections for the primary photo-nucleon will then be followed by the evaluation of the probabilities for the emission of alpha particles. These probabilities are calculated by using the second right-hand-side bracket in equation (6).

5) Then the calculation of $\left[\frac{d^2\sigma}{d\Omega_\alpha dE_\alpha}\right]_\beta$ is carried out by integrating equation (6) over the energy ranges of primary photo-nucleons. The process of calculating $\left[\frac{d^2\sigma}{d\Omega_\alpha dE_\alpha}\right]_\beta$ is shown schematically in diagram 4.2. Results of the calculation for different shells are presented in Figures 4.23 to 4.28.

6) The final results, i.e. $\sum_\beta \left[\frac{d^2\sigma}{d\Omega_\alpha dE_\alpha}\right]_\beta$ is then compared with the experimental data as shown in Figure 4.29.

The theoretically calculated results for (e,α) pre-compound double differential cross-sections clearly overestimate the experimental

Figure 4.23 - 4.27: The (e,α) pre-compound contributions using ^{60}Ni; curve (1) is $\sum_{\beta} \left[\frac{d^2\sigma}{d\Omega_\alpha dE_\alpha}\right]_\beta$.

Figure 4.28: Addition of curve (1) in Figures 4.23 to 4.27 in order to compare with data.

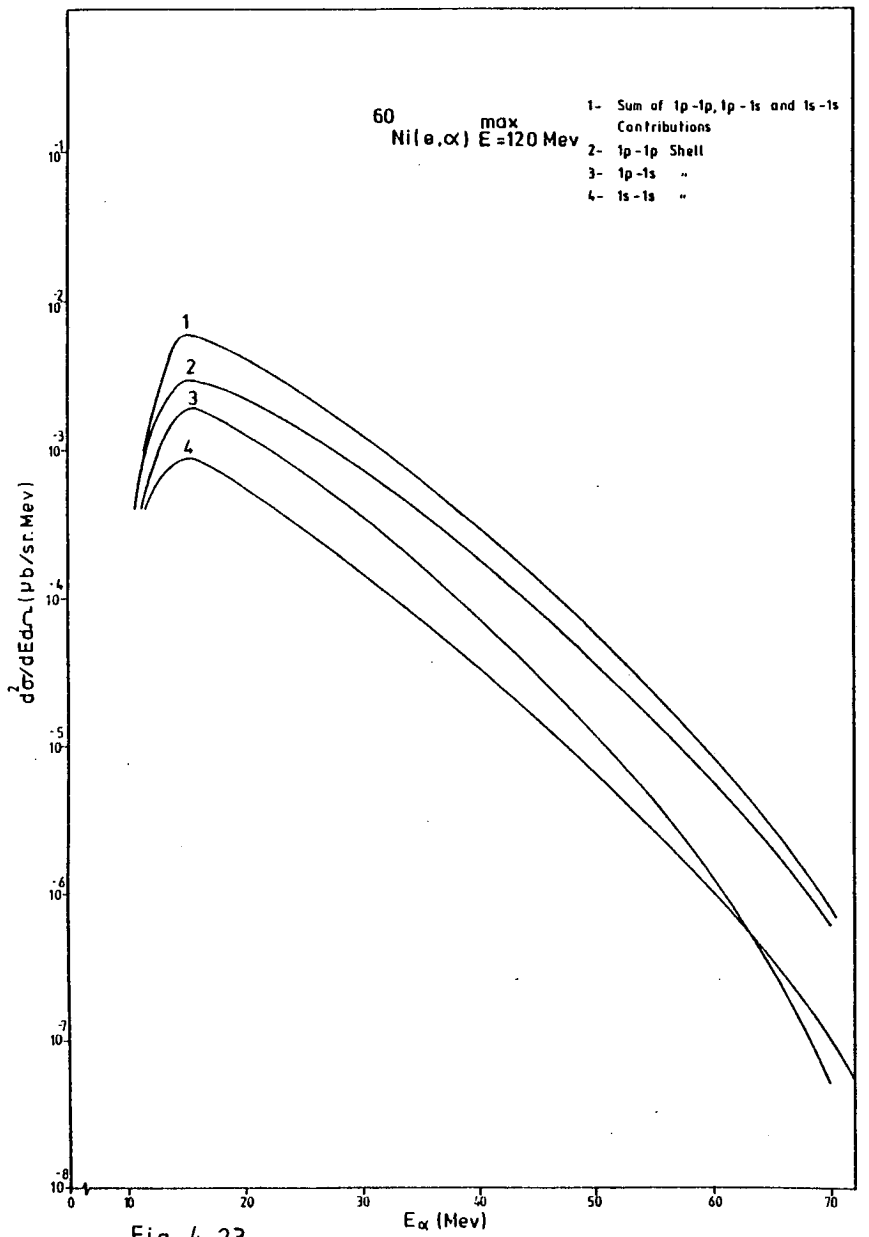

Fig. 4.23

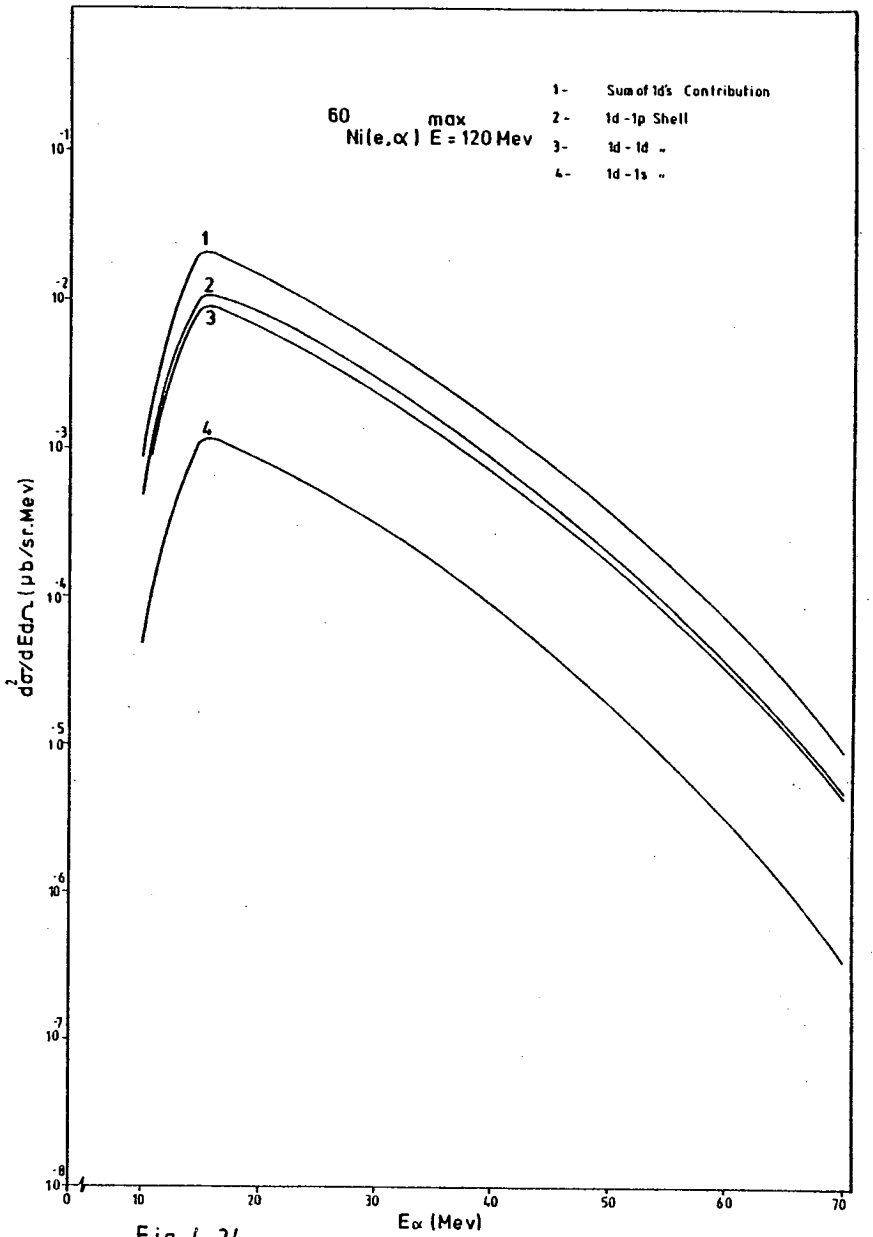

Fig. 4.24

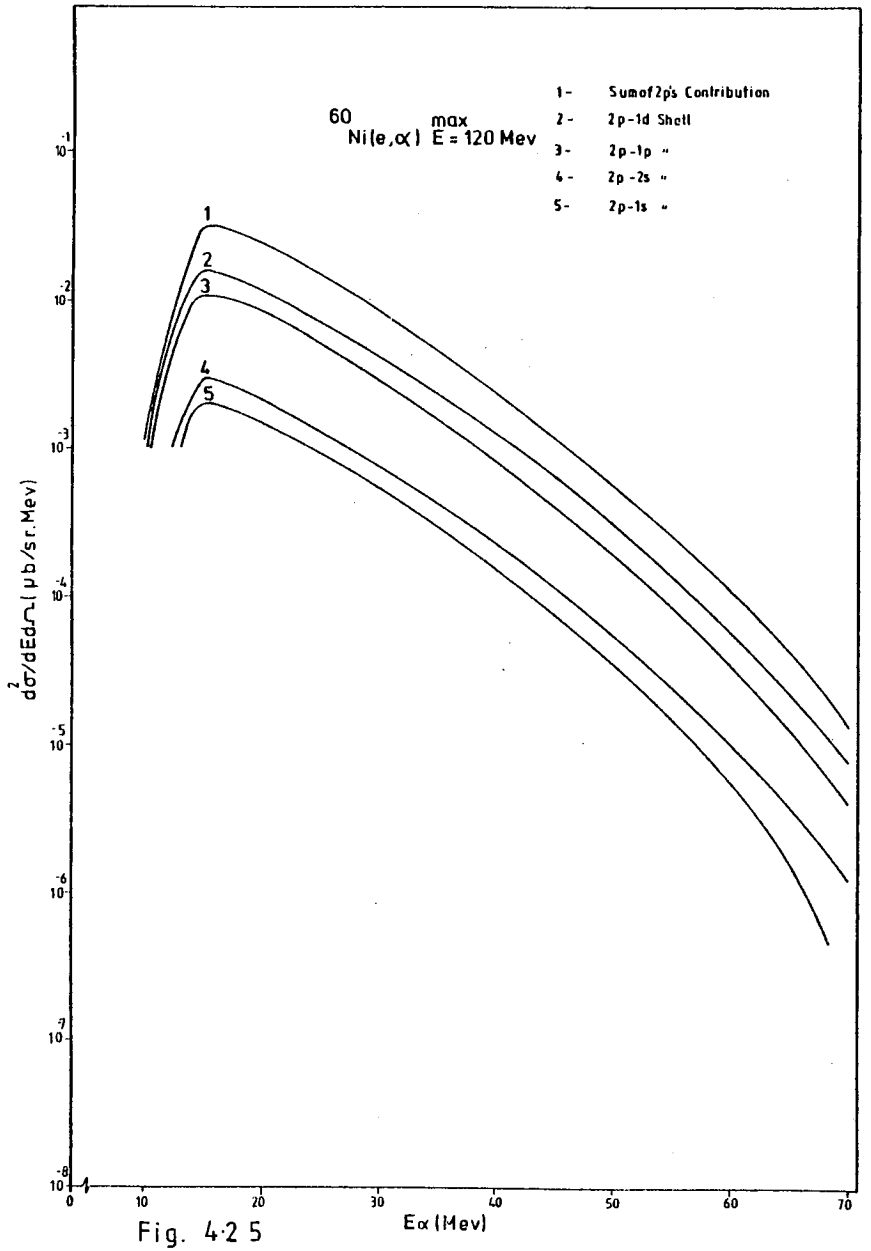

Fig. 4·2 5

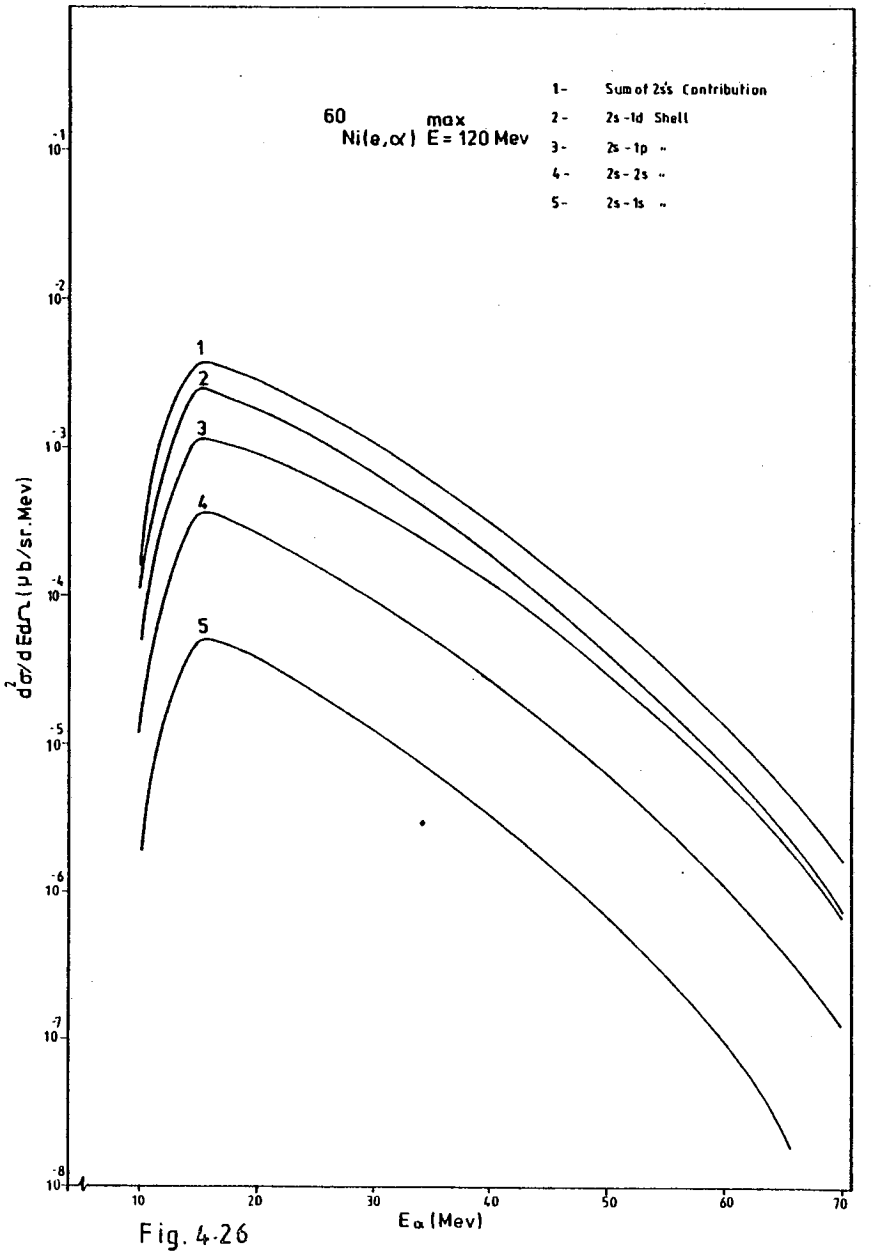

Fig. 4·26

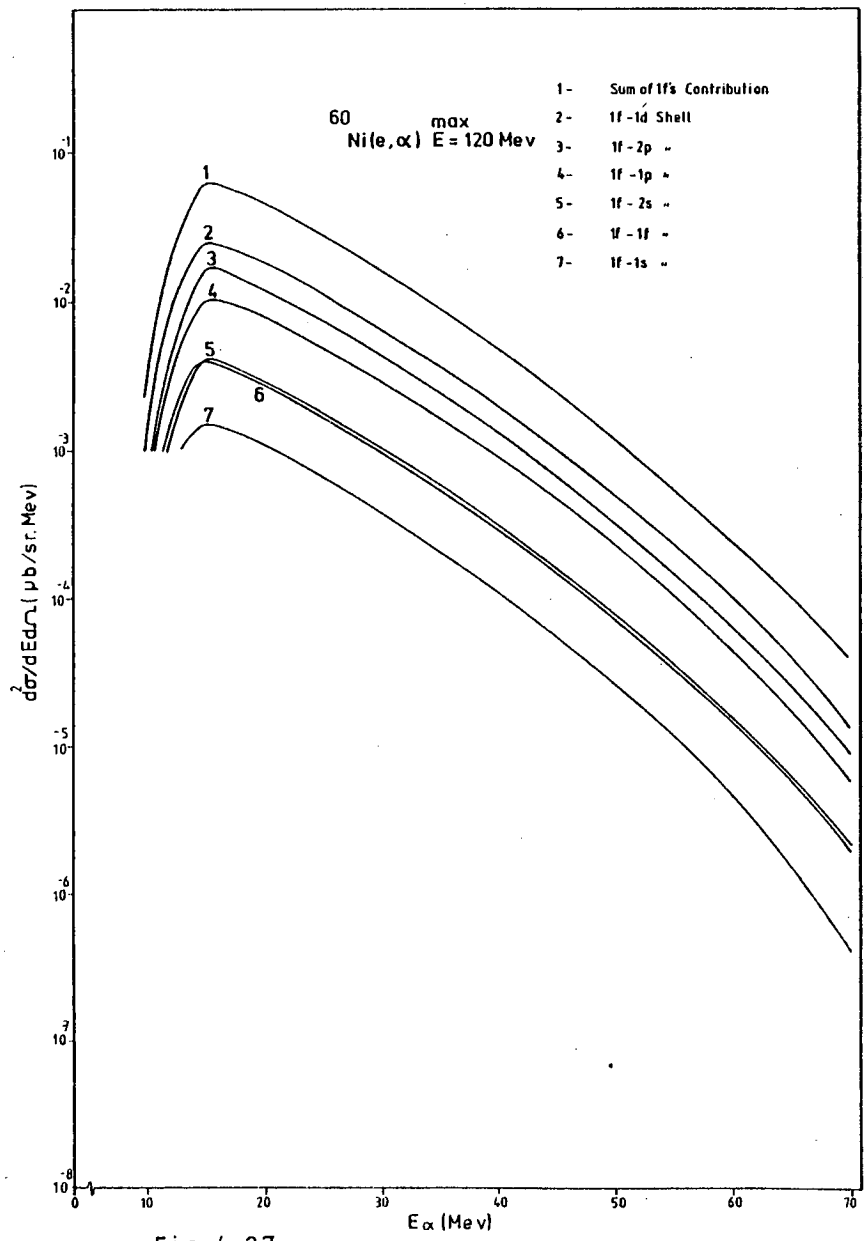

Fig. 4·27

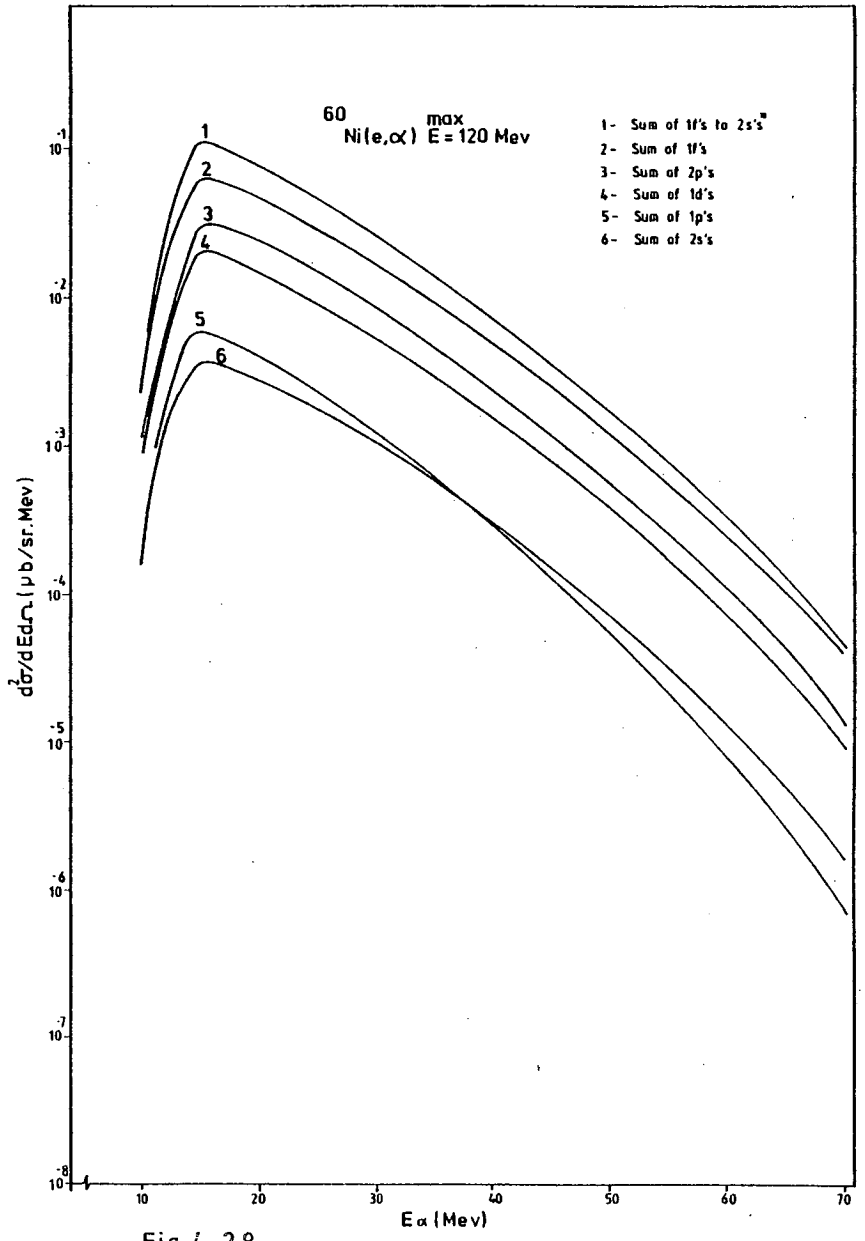

Fig. 4·28

Figure 4.29: The calculated (e,α) compound and pre-compound results are compared with the experimental data.

* : Square (Sq.) well potential.

ǂ : Experimental data[1] taken at angle 30°.

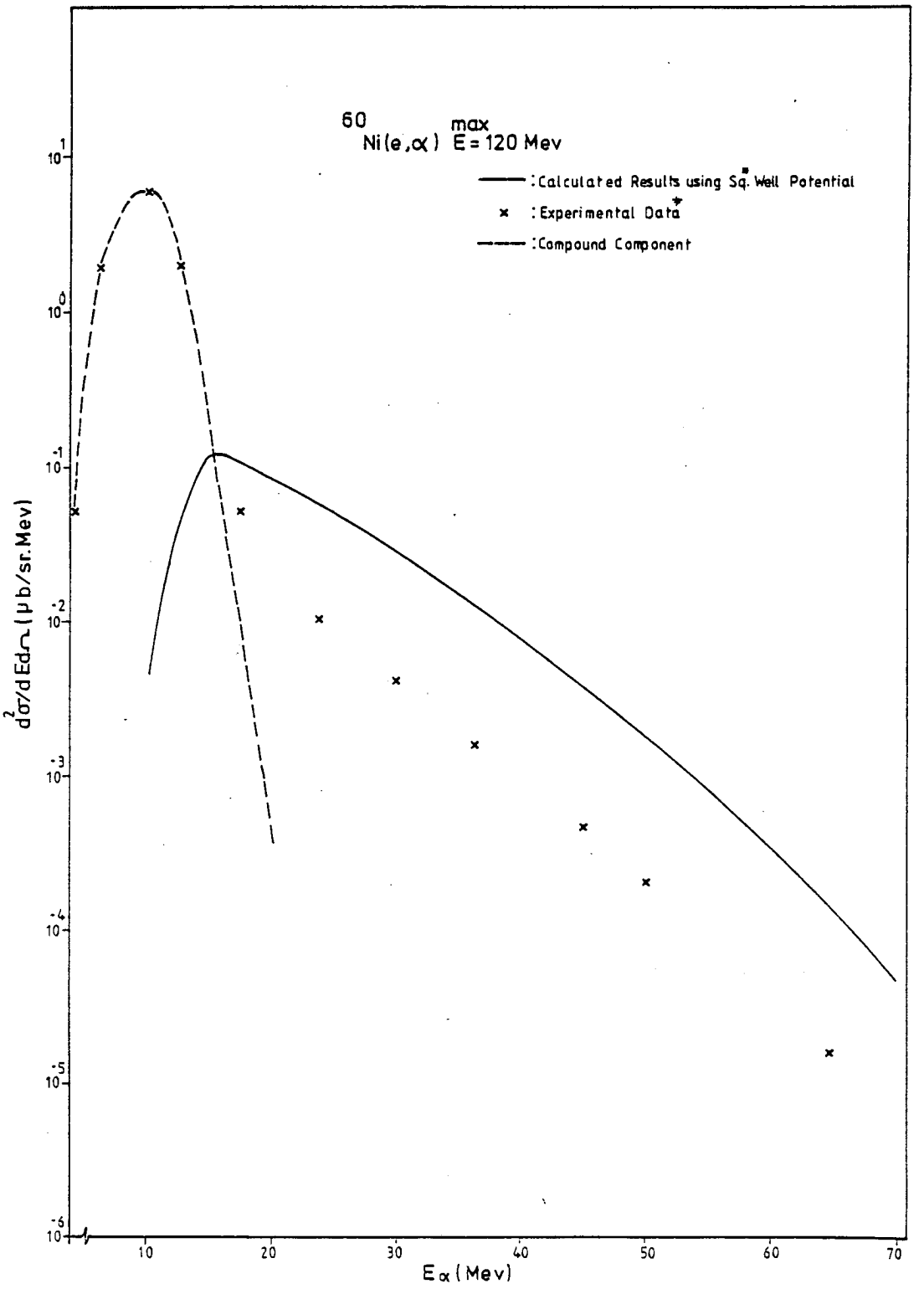
60 max
Ni(e,α) E = 120 Mev
: Calculated Results using Sq. Well Potential
: Experimental Data
: Compound Component
d²σ/dEdΩ (μb/sr.Mev)
Eα (Mev)
10
20
30
40
50
60
70

data. In section (4.4.4) this point will be discussed further.

4.4.3.2 Harmonic Oscillator Potential Case for the (e,α) Process

The pre-compound contribution to the (e,α) energy spectrum is evaluated using the harmonic oscillator potential. Although the procedure for calculating (e,α) pre-compound contributions is similar to the square well potential case, the following terms in equation (6) are calculated differently:

1) In equation (6), the values for L_β' are taken from Table 8(b) and the momentum distributions for (np) pairs from Figures 4.1 to 4.5 (see section 4.3.3.2).

2) Then the calculation of $\left[\frac{d^2\sigma}{d\Omega_\alpha dE_\alpha}\right]_\beta$ is carried out using a similar procedure as that mentioned in section (4.4.3.1). The results of the calculation for different shells are presented in Figures 4.30 to 4.35.

3) The final results are obtained by summing over the shell's indices, β, i.e. $\sum_\beta \left[\frac{d^2\sigma}{d\Omega_\alpha dE_\alpha}\right]_\beta$. These results are then compared with the experimental data as shown in Figure 4.36.

The pre-compound contributions to (e,α) again clearly overestimate the experimental data. In section (4.4.4) the sources of this overestimation will be investigated.

4.4.4 Conclusion Related to (e,α) Reactions

A comparison between the results of the calculation of $\left[\frac{d^2\sigma}{d\Omega_\alpha dE_\alpha}\right]$ with the experimental data (Fig. 4.37) indicates a noticeable disagreement for the pre-compound component. In section (4.3.4) a similar problem was observed for the (γ,p) process. It is likely that the sources of these overestimations for (γ,p) and (e,α) processes are similar. In order to investigate more about the causes of overestimation of data (in Figure 4.37), two fundamental questions

Figure 4.30 - 4.34: The (e,α) pre-compound contributions using ^{60}Ni; curve (1) is $\sum_{\beta} \left[\frac{d^2\sigma}{d\Omega_\alpha dE_\alpha}\right]_\beta$.

Figure 4.35: Addition of curve (1) in Figures 4.30 to 4.34 in order to compare with data.

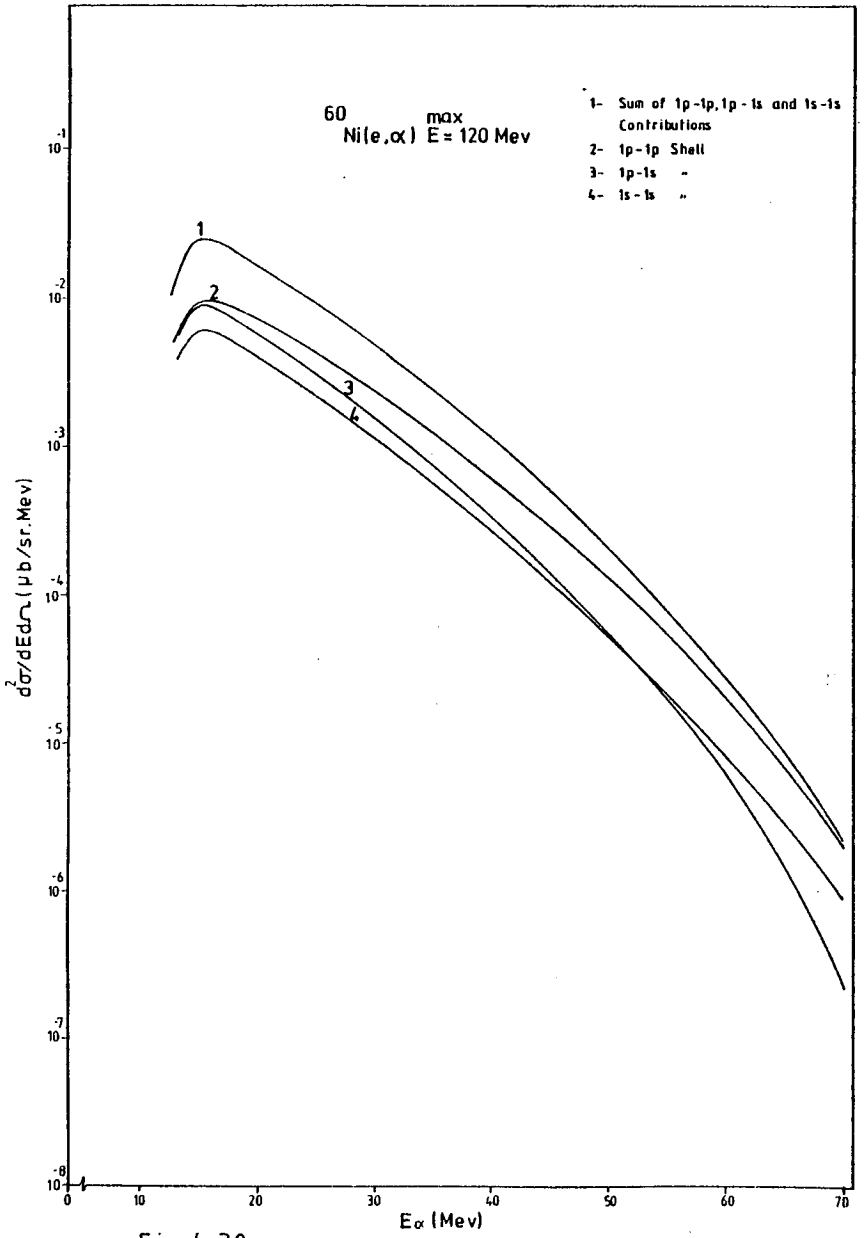

Fig. 4·30

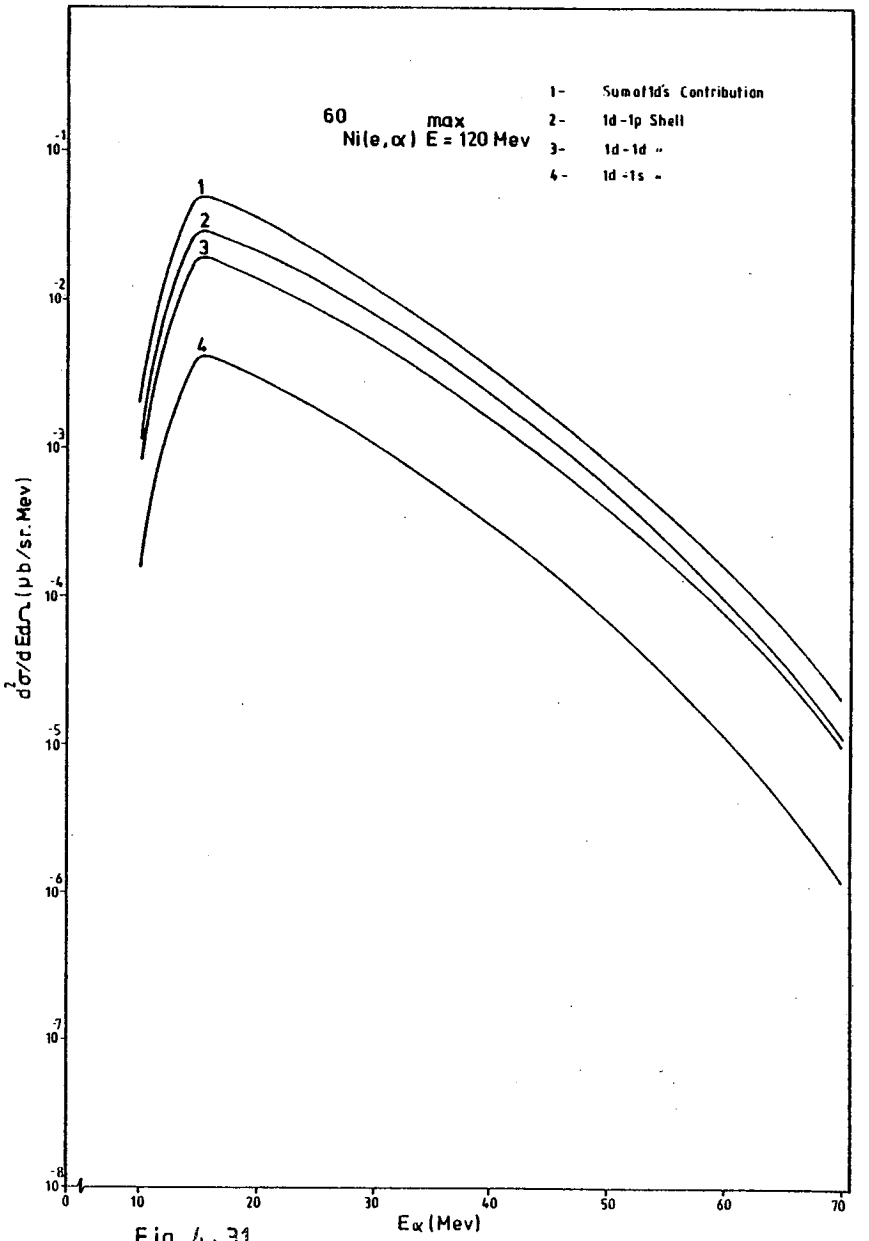

Fig. 4·31

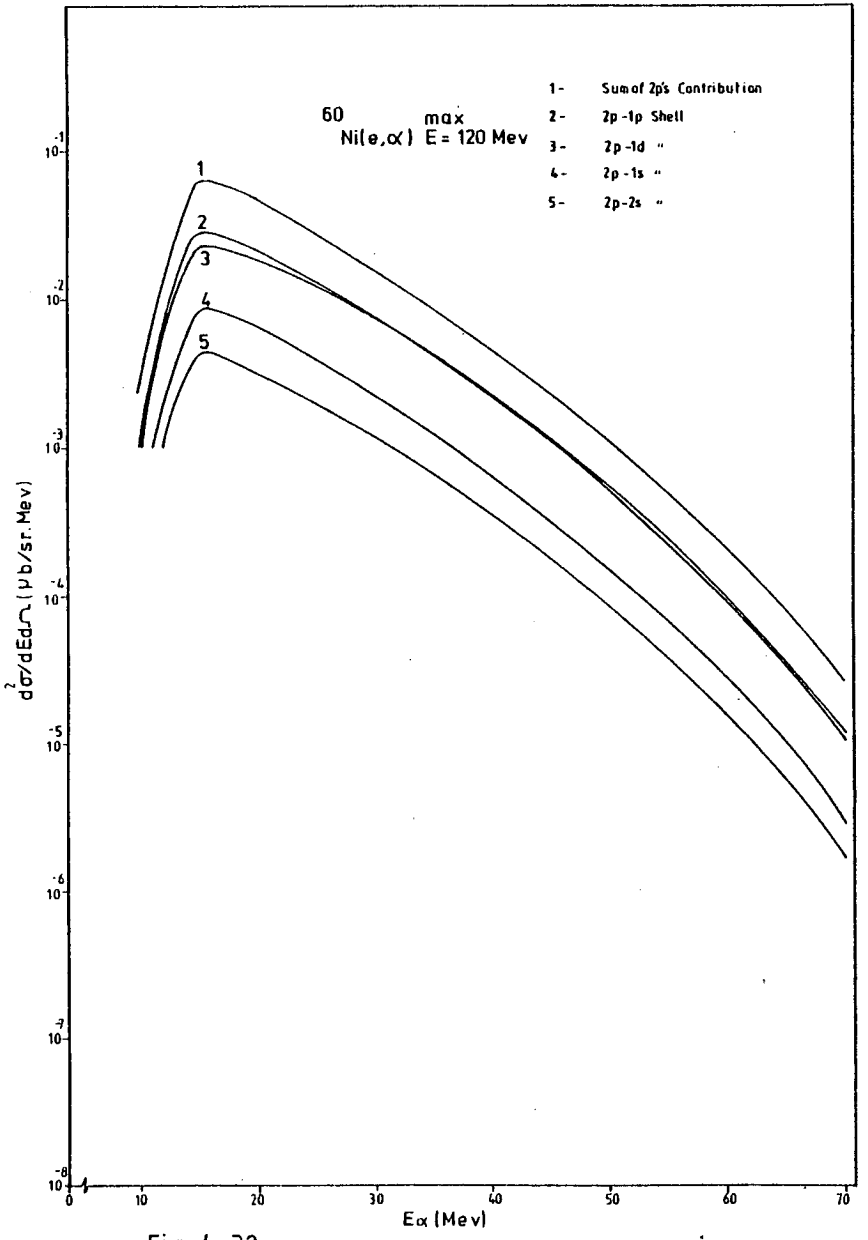

Fig. 4·32

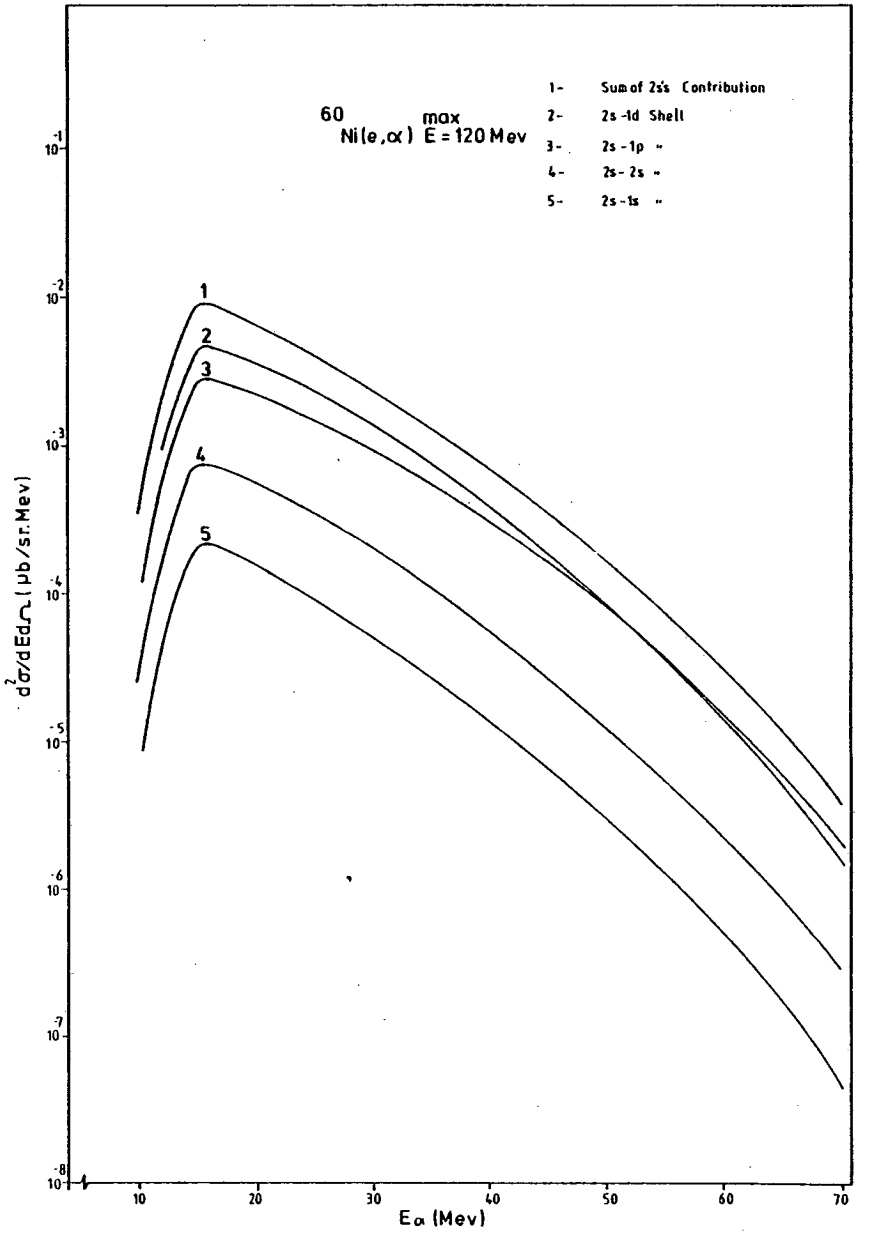

Fig. 4·33

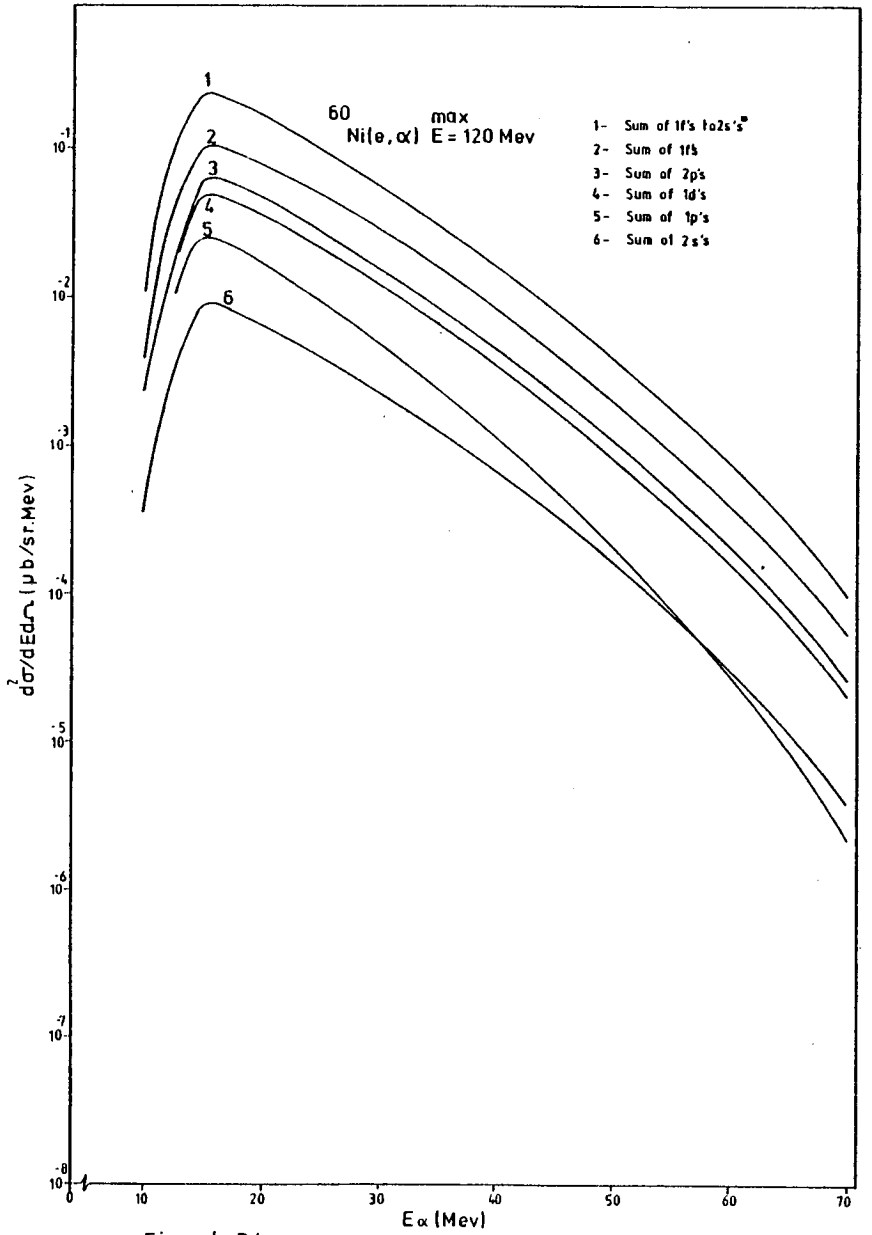

Fig. 4.34

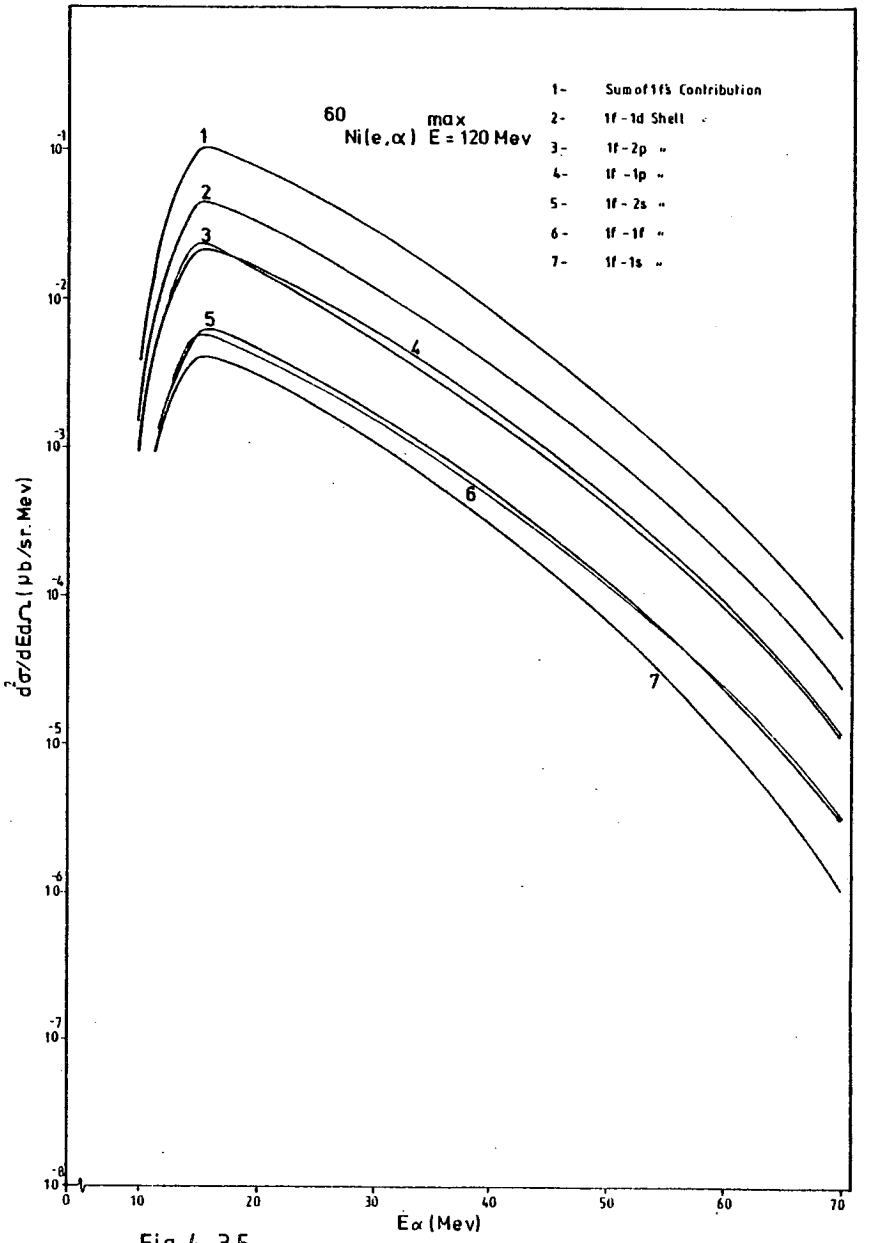

Fig 4.35

Figure 4.36: The calculated (e,α) compound and pre-compound results are compared with the experimental data.

* : Harmonic Oscillator (H.O.)

ǂ : Experimental data[1] taken at angle 30^{o}.

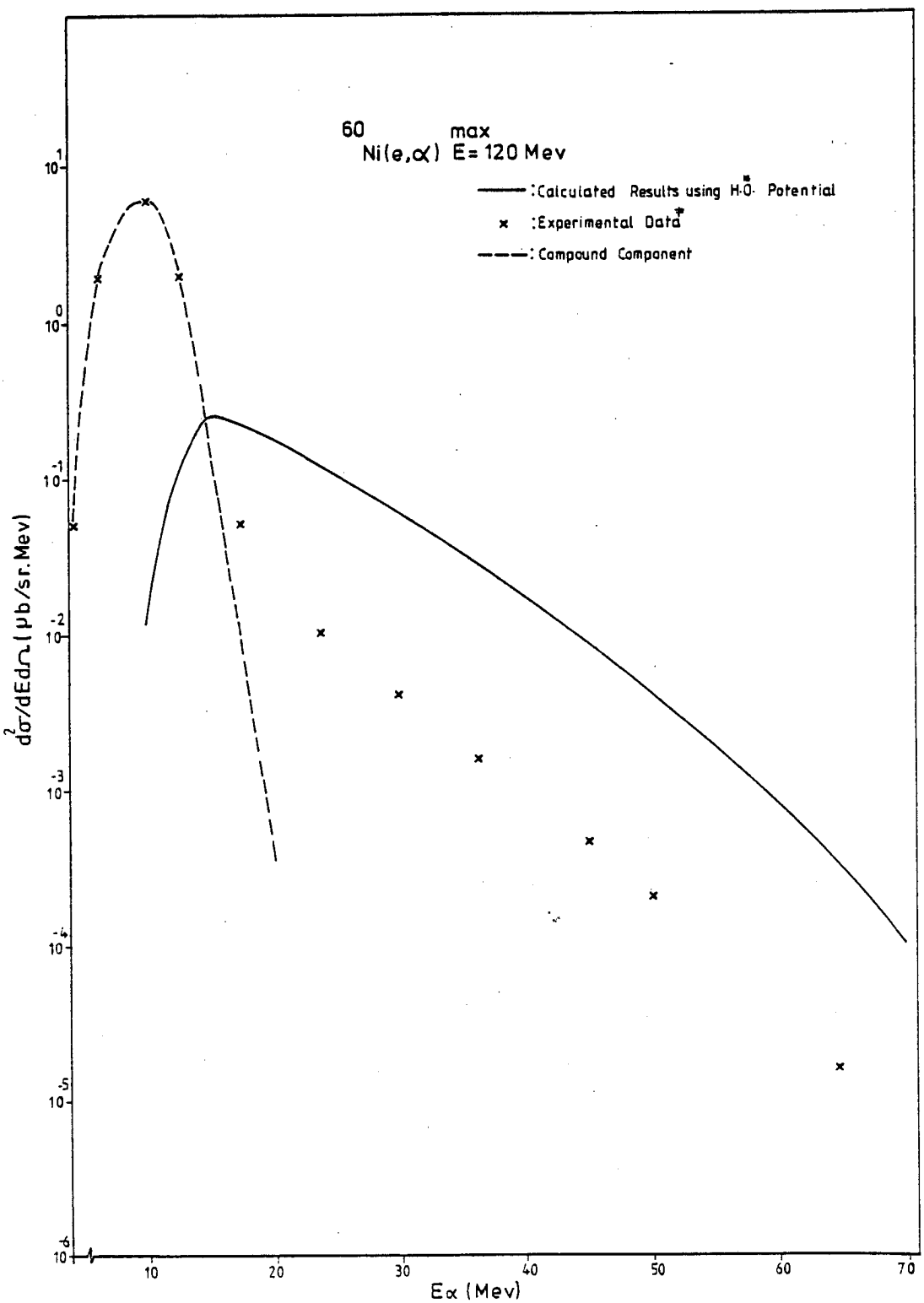
60 max
Ni(e,α) E= 120 Mev
: Calculated Results using H.O. Potential
: Experimental Data*
: Compound Component
d²σ/dEdΩ (μb/sr.Mev)
Eα (Mev)
10
20
30
40
50
60
70

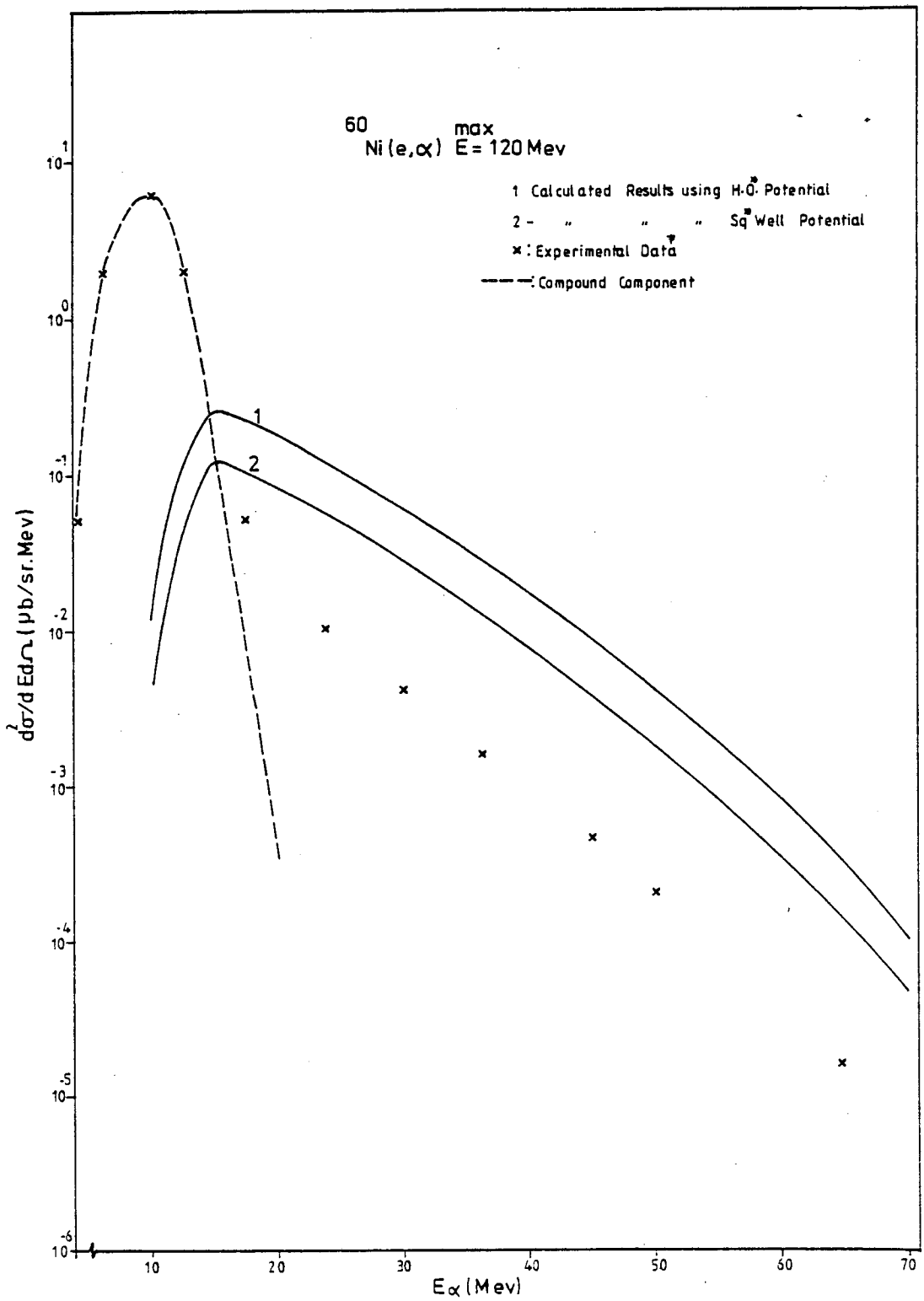

Figure 4.37: The calculated results in Figure 4.29 for Square Well and in Fig. 4.36 for Harmonic Oscillator potentials are compared with the experimental data.

* : Square (Sq.) Well and Harmonic Oscillator (H.O.)

ǂ : Experimental data[1] taken at angle 30°.

will be considered with respect to the reactions of (e,N $\Rightarrow$ N,α) type.

a) is the quasi-free scattering model inappropriate for the consideration of the final state interactions when (e,N $\Rightarrow$ N,α) reactions are considered?

b) if the quasi-deuteron model can be reconstructed on the basis of the argument given in section (4.3.4), what is the conversion factor mentioned in section (4.3.4) for (e,α) reactions using E_e = 120 MeV?

These questions will be tackled below.

In Chapter III, the quasi-free scattering model with different uncertainties, particularly for the (N,α) process, were investigated. As was mentioned there, if a proper set of free parameters are chosen for the quasi-free scattering mode, then this model is successfully capable of producing the experimental data concerning (N,α) energy spectra. There are three free parameters which must be considered:

i) the pseudo Fermi energy ε_f^n,

ii) free parameter for the break-up factor B_j^α

iii) free parameter for the probability of collision with an alpha particle ϕ.

In the present study a tested set of values for ε, B_j^α and ϕ are used, i.e. ε_f^n = 8 MeV, B_j^α = 0.5 and ϕ = 0.03. Considering this set of values the final results are shown in Figure 4.37. In order to reach a closer agreement with the experimental data a new set of free parameters can be employed; for example, ε_f^n = 8 MeV, B_j^α = 0.9 and ϕ = 0.015. However this set of data demands that α- particles should break up with a 90% probability (the suggested[6] range for B_j^α is given between 0.5 - 0.7) during collision with

nucleons. This indicates that the problem of overestimation, as shown in Figure 4.37, can not be solved by changing the realistic set of parameters, i.e. ε_f^n = 8 MeV, B_j^α = 0.5 and ϕ = 0.03, with a lesser realistic one.

Although the quasi-free scattering model for (N,α) reactions involves a great deal of uncertainties, on the basis of the above discussion it can be concluded that the model is appropriate to be considered for the final state interactions when (e,N) ⇒ (N,α) reactions are investigated. Further, it is likely that the sources of overestimation of data by the theoretical calculation can be found in the (e,N) part of the synthesised model.

In section 4.3.4 a similar problem concerning overestimation of (γ,p) data by theoretical calculation was considered. The conclusion reached in section 4.3.4 will be effectively used in the present section. To this end a conversion factor ∿ 0.12 is calculated using Table 4.1 and considering E_e = 120 MeV. The two curves in Figure 4.37 are multiplied by the deduced conversion factor. The results can be seen in Figure 4.38, where a reasonable agreement is achieved between the theoretically calculated results and the experimental data.

The close agreement between calculated results and the experimental data, however, must not conceal a more fundamental investigation about the validity of the replacement of the σ_d with σ_d^{exch} and a more rigorous calculation of double differential cross-sections.

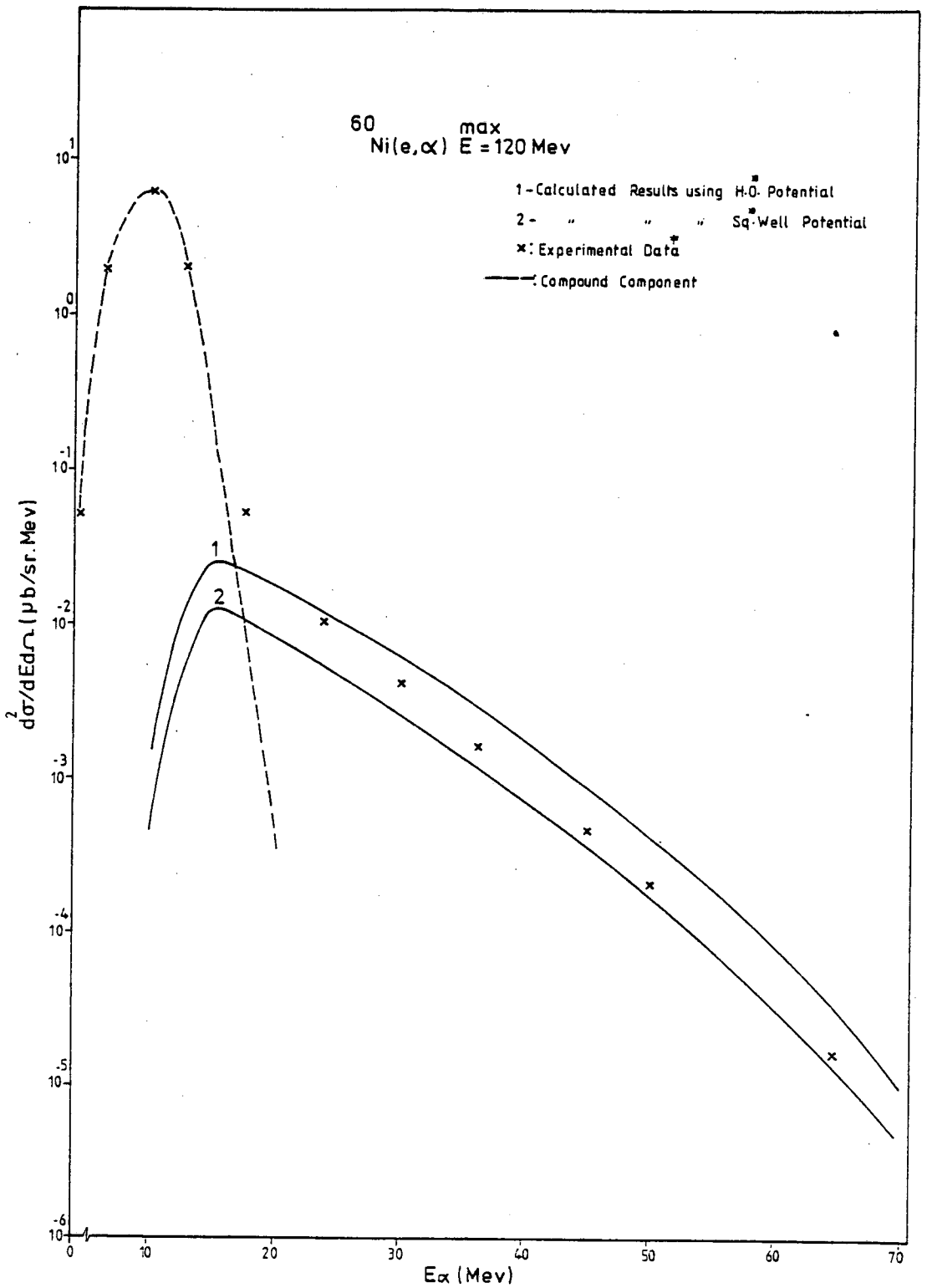

Figure 4.38: The pre-compound calculated results in Fig. 4.37 are multiplied by the conversion factor deduced in sub-section 4.4.4 and are compared with data (see Fig. 4.37 caption for more information).

CHAPTER V

CONCLUSIONS

In this study a new approach is proposed for the calculation of pre-compound nucleon and α-particle energy spectra resulting from photo-nuclear reactions at energies below the meson production threshold.

In order to investigate more realistically the photo-absorption process, the shell model configuration has been used in contrast to the Fermi gas model originally suggested for the quasi-deuteron model. To this end the Levinger constant has been replaced by a so-called "pseudo-Levinger constant" which is theoretically calculated and it is shell dependent (for further information see section 2.2.2.4, Chapter II). Consequently, the evaluation of the double differential cross-section for the (γ, np) process has been carried out without using a floating factor. The process of final state interactions of photo-generated nucleons has been taken into account by calculating the probabilities for particle emission using the quasi-free scattering model.

The calculation of double differential cross-section for the (γ, np) process has been initially performed for ^{12}C. For this light nuclei the process of final state interactions is assumed not to be of great import. The comparison between the evaluated proton double differential cross-section with the experimental data results in an overestimation of the data (E_p < 60 MeV) by a factor of $\sim$ 4 and a factor of $\sim$ 8, using square well and harmonic oscillator potential, respectively. For the region E_p > 60 MeV, however, the

calculations underestimate the data. The latter result is not unexpected because of direct reaction events.

The study of the (γ, np) process is then extended to the medium weight nuclei where ^{60}Ni has been chosen for this purpose. The calculated (γ,p) double differential cross-section, without considering the final state interactions, compared with the experimental data indicate that the data lies close to the theoretical results when the square well and harmonic oscillator potentials are used. However, in the ^{60}Ni case study the process of final state interactions is carrying great weight. Therefore, a synthesised model, consisting of the quasi-deuteron and quasi-free scattering, has been constructed effectively to take into account the final state interactions. This synthesised model is then capable of considering the two processes of 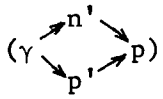 and 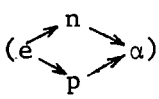 . The calculated results markedly overestimate the experimental data.

As regards the (γ, p) process using ^{12}C and ^{60}Ni, the study of the origin of overestimation of data by theoretical calculation can be interpreted by the following arguments:

a) The evaluation of (γ, p) double differential cross-section for the ^{12}C case study ignoring the final state interactions indicates that the overestimation of data is likely to be due to the failure of expressing the photo-nuclear cross-section for the reaction proceeding through the two-particle absorption mechanism in terms of the deuteron photo-disintegration cross-section (E_γ < 150 MeV).

b) Considering the ^{60}Ni case study, the calculated (γ, p) double differential cross-sections, without taking the final state interactions into account, already lie close to the experimental data.

While considering the final state interactions the data lies markedly below the theoretically calculated results. If the advantages and disadvantages of the quasi-free scattering model responsible for taking into account the final state interactions are closely considered, it becomes obvious that the quasi-free scattering model reproduces the (N, N') experimental energy spectra quite satisfactorily (these points have been discussed in full detail in Chapter III). As regards the experimental angular distribution, the quasi-free scattering model successfully reproduces the data in the forward angles. This is in spite of the fact that the (N, N') experimental angular distribution data is only partially reproduced by this model in the backward angles. Therefore it can be argued that it is unlikely that the overestimation of (γ, p) data by the theoretical calculation is due to the failure of the quasi-free scattering model. While it is possible that the origin of this overestimation is the failure of using total deuteron photodisintegration cross-section in the quasi-deuteron model, i.e. in the initial interactions $(\gamma \nearrow n' \searrow p')$ as the first part of the $(\gamma \nearrow n' \searrow p \nearrow p')$ process.

As regards the $(e \nearrow n \searrow p \nearrow \alpha)$ process using ^{60}Ni the study of the origin of overestimation of data by theoretical calculation can be explained by considering the strength and weakness of quasi-free scattering model regarding (N, α) reactions. The success of this model in producing experimental energy spectra for (N, α) reaction is supported by its reasonable reproduction of experimental angular distribution data at forward angles. This is in spite of the fact that at backward angles the reproduction of data is partially successful (these points have been discussed in full

detail in Chapter III). Therefore it is possible to argue that the source of overestimation of data by theoretical calculation is unlikely to be the use of the quasi-free scattering model. While there is a possibility that due to the failure of the initial interaction ($(e \rightarrow {}^{n}_{p}$) as the first part of the ($e \rightarrow {}^{n}_{p} \rightarrow \alpha$) process) the problem of overestimation of data has occurred.

On the basis of the above discussion it is possible to argue that for the ^{12}C and ^{60}Ni case studies, the source of overestimation of data by theoretical calculation is likely to be the use of the total photo-disintegration cross-section of the deuteron in the quasi-deuteron model. The possibility that this cross-section can be replaced by a more realistic term, the meson exchange part, is an idea which was discussed in Chapter II and IV in some detail and needs further investigation.

The synthesised model proposed in this study compared to the similarly suggested models[3, 4] conveys more information concerning the analysis of photo-induced pre-compound nucleon and α-particle energy spectra, but a more fundamental theory describing the electromagnetic perturbed nuclei, with the consequence of multi-step particle emission possibilities is needed.

APPENDIX A QUASI-DEUTERON MODEL FORMALISM

The formalism described in sub-section 2.2.1 has been derived by Levinger[5] where the wavefunction for the ground state of the nucleus, with proton (1) very close to neutron (2), assumed to be:

$$\psi_\alpha(1, 2, 3, \ldots, A) = \psi_K(\vec{R})\psi_k(\vec{r})\psi_\beta(3, \ldots, A). \qquad (A - 1)$$

The quasi-deuteron wavefunction $\psi_k(\vec{r})$, where r is the distance between the proton and neutron, can be written

$$\psi_k(r) = (4\pi)^{\frac{1}{2}}[\sin(kr + \delta)/\sin\delta - \eta]/(a^2 + k^2)^{\frac{1}{2}}\nu^{\frac{1}{2}}r \qquad (A - 2)$$

where η is a function which is appreciable only inside the range of the nuclear forces. Further ν is the nucleus volume and k is the wave number, i.e. $k = \frac{1}{2}|\vec{K}_1 - \vec{K}_2|$. $\vec{K}_1$ and $\vec{K}_2$ are momentums of proton and neutron. The theory of the effective range of nuclear forces gives $\cot\delta \simeq -\alpha/k$ with α^{-1} the scattering length.

For the high energy photoeffect, ψ_k at small r with $kr << 1$ can be expanded by:

$$\psi_k(r) \simeq (4\pi/\nu)^{\frac{1}{2}}(\alpha^2 + k^2)^{-\frac{1}{2}}\, r^{-1}(1 - \alpha r - \eta). \qquad (A - 3)$$

The wavefunction of the deuteron ground state is

$$\psi_d(r) \simeq [2\alpha/(1 - \alpha r_o)]^{\frac{1}{2}}\, r^{-1}(1 - \alpha r - \eta) \qquad (A - 4)$$

where r_o is the effective range. Assuming that the wavefunction $\psi_\beta(3, \ldots, A)$ in equation (A - 1) is the same for both initial and final states and using the effective range theory the photo-electric cross-section of the quasi-deuteron can be written by:

$$\frac{\sigma_{qd}}{\sigma_d} = \left[\frac{\psi_k}{\psi_d}\right]^2 = \frac{2\pi(1 - \alpha r_o)}{\alpha(\alpha^2 + k^2)\nu} \quad . \qquad (A - 5)$$

APPENDIX B JACOBIAN FORMALISM

The Jacobian determinate expresses how the n-dimensional volume element $dy_1 \ldots dy_n$ differs from the element $dx_1 \ldots dx_n$:

$$\frac{\partial(x_1 \ldots x_n)}{\partial(y_1 \ldots y_n)} \equiv \begin{vmatrix} \frac{\partial x_1}{\partial y_1} & \frac{\partial x_2}{\partial y_1} & \cdots & \frac{\partial x_n}{\partial y_1} \\ \cdot & & & \\ \cdot & & & \\ \cdot & & & \\ \frac{\partial x_1}{\partial y_n} & \cdots & \cdots & \frac{\partial x_n}{\partial y_n} \end{vmatrix} \qquad \text{(B-1)}$$

The volume element $dx_1 \ldots dx_n'$ can therefore be transformed to the volume element $dy_1 \ldots dy_n$ by:

$$dx_1 \ldots dx_n = \frac{\partial(x_1 \ldots x_n)}{\partial(y_1 \ldots y_n)} \, dy_1 \ldots dy_n \; . \qquad \text{(B-2)}$$

It is also possible to write the following equation between $f(x_1 \ldots x_n)$ and $g(y_1 \ldots y_n)$:

$$g(y_1 \ldots y_n) \equiv f(x_1 \ldots x_n) \, \frac{\partial(x_1 \ldots x_n)}{\partial(y_1 \ldots y_n)} \qquad \text{(B-3)}$$

On the basis of the above formalism the Jacobian $J_1 \equiv \frac{d(\cos \nu_p^*)}{d(\cos \nu_p')}$ which was introduced in section 2.2.3.2, equation (33) is written as:

$$J_1 = \frac{\eta'^2_p (1 - \eta^{*2})}{[(1-\eta'_p \eta^* \cos \nu'_p)^2 - (1-\eta'^2_p)(1-\eta^{*2})]^{\frac{1}{2}} (\eta'_p - \eta^* \cos \nu'_p)} \; . \qquad \text{(B-4)}$$

This expression is derived using the following equation:

$$\cos \nu_p^* = \frac{\cos \nu_p' - \eta^*/\eta_p'}{[(\cos\nu_p' - \eta^*/\eta_p') + \sin^2\nu_p'(1 - \eta^{*2})]^{\frac{1}{2}}} \qquad \text{(B-5)}$$

where $\eta^* = \frac{\omega'}{\omega' + 2m'}$ and $\eta_p' = \frac{k_p'}{E_p' + m'}$ (the ω' and m' were introduced in section 2.2.3.2).

The Jacobian $J_2 = \frac{\partial\omega}{\partial\omega'}$, which was introduced in section 2.2.3.2, equation (36), is derived by the use of the following equation given for the photon energy in the rest system:

$$\omega' = \omega\gamma(1 - \eta \cos \psi) \quad . \qquad \text{(B-6)}$$

Therefore,

$$J_2 = \frac{1}{\gamma(1 - \eta \cos\psi)} \qquad \text{(B-7)}$$

where $\gamma = (1 - \eta^2)^{-\frac{1}{2}}$ and $\eta = \frac{K}{(K^2 + 4m'^2)^{\frac{1}{2}}}$ (see section 2.2.3.2 for explanation of K and ψ).

The Jacobian $J_3 \equiv \frac{\partial\omega'(E_p', \nu_p')}{\partial E_p'}$ was given in section 2.2.3.2, equation (37) is derived as

$$J_3 = \frac{\omega'(1 - \frac{E_p'}{k_p'} \cos \nu_p')}{k_p' \cos \nu_p' - E_p'} \qquad \text{(B-8)}$$

where the rest-system energy-momentum conservation equations (see equation (38), section 2.2.2.3) are effectively used.

The Jacobian $J_4 \equiv \dfrac{d(\cos \nu'_p)}{d(\cos \theta'_p)} \cdot \dfrac{k_p}{k'_p}$ was introduced in equation (43), section 2.2.2.3 is derived by

$$J_4 \equiv \left[\frac{d(\cos \nu'_p)}{d(\cos \theta'_p)}\right] \cdot \left[\frac{dE'_p \, d(\cos \theta'_p)}{dE_p \, d(\cos \theta_p)}\right] \quad . \tag{B-9}$$

The first bracket can be written by

$$\frac{d(\cos \nu'_p)}{d(\cos \theta'_p)} = \frac{\cos \psi' \sin \theta'_p - \cos \theta'_p \sin \psi' \cos(\Delta)}{\sin \theta'_p} \tag{B-10}$$

where the relation between $\cos \nu'_p$ and $\cos \theta'_p$ is used, i.e.

$$\cos \nu'_p = \cos \theta'_p \cos \psi' + \sin \theta'_p \sin \psi' \cos(\Delta) \; . \tag{B-11}$$

In equations (B-10) and (B-11), the angle Δ is the difference between the azimuthal angle of the photon and proton azimuthal angle in the rest system. For the second bracket in equation (B-9) the relativistic invariance

$$\frac{d\vec{k}_p}{\varepsilon} = \frac{d\vec{k}'_p}{\varepsilon'} \tag{B-12}$$

is used where ε and ε' are total energy. This equation can be written by

$$\frac{k^2 dk_p \, d(\cos \theta_p)}{\varepsilon_p} = \frac{k'^2 dk'_p \, d(\cos \theta'_p)}{\varepsilon'_p} \quad . \tag{B-13}$$

then

$$k_p dE_p d(\cos \theta) = k'_p \, dE_p d(\cos \theta'_p) \tag{B-14}$$

where the $k_p dk_p = \varepsilon \, d \, \varepsilon_p = \varepsilon dE_p$ is used. Therefore

$$dE'_p \, d(\cos\theta'_p) = \frac{k_p}{k'_p} \, dE_p \, d(\cos\theta_p) \, . \qquad \text{(B-15)}$$

Thus, equation (B-9) takes its new form by substituting equations (B-15) and (B-10) in (B-9):

$$J_4 = \frac{k_p}{k'_p} \left[\frac{\cos\psi' \sin\theta'_p - \cos\theta'_p \sin\psi' \cos(\Delta)}{\sin(\theta'_p)} \right] \qquad \text{(B-16)}$$

The Jacobian $J_5 \equiv \frac{dK}{dE'_p}$ can be derived by the use of the the following procedure, i.e. by writing:

$$J_5 = \left[\frac{dK}{dE_p}\right] \left[\frac{dE_p}{dE'_p}\right] \qquad \text{(B-17)}$$

where the first bracket can be evaluated by using the conservation of momentum equation in the Laboratory system (see diagram A in section 2.2.3.2 and equation (24)). The second bracket can be evaluated by using the Lorentz transformation for energy, i.e.

$$E_p' = \gamma[E_p - k_p \eta(\cos\theta_p \cos\psi + \sin\theta_p \sin\psi \cos\phi)] \qquad \text{(B-18)}$$

In the formalism given in this Appendix the Lorentz transformation for momentum and energy were used where formally the pre-transformations can be written by:

$$\hat{E}' = \gamma(\hat{E} - \vec{\eta} \cdot \vec{\hat{K}}) \qquad \text{(B-19)}$$

$$= \gamma(\hat{E} - \eta\hat{K} \cos(\theta_\eta - \theta_{\hat{K}})).$$

and for momentum

$$\hat{\vec{K}}' = \hat{\vec{K}} + \vec{\eta}\,\gamma\left(\frac{\gamma}{\gamma+1}\,\vec{\eta}\cdot\hat{\vec{K}} - \hat{E}\right) \qquad \text{(B-21)}$$

where the primed and unprimed quantities are referred to rest and laboratory system.

APPENDIX C COMPOUND NUCLEUS FORMALISM

The Hauser-Feshbach expression for the reaction cross-section $\bar{\sigma}_{cc'}$ averaged over compound nucleus fluctuations, for an entrance channel c and exit channel c' is given by

$$\bar{\sigma}_{cc'} = \frac{\pi}{K_c^2} \sum_{J\pi} \left[\frac{(2J+1)}{(2J_c+1)(2j+1)} \cdot \{ \sum_{s\ell} T_\ell(c) \} \cdot \frac{\sum_{s''\ell''} T_{\ell'}(c')}{\sum_{s''\ell''} T_{\ell''}(c'')} \right] \qquad (C-1)$$

where the unprimed quantities refer to the incoming channel, c, single primed quantities to the outgoing channel of interest, c', and double primed quantities to all possible outgoing channels c''. The quantum numbers of each channel c are given by $c = (\alpha, J_c, j, s, \ell, J, M_j, \pi)$ where α labels the pair of particles in their state of excitation. J_c and j are intrinsic spins of the particles (e.g. target nucleus and projectile), s is the channel spin ($\underline{s} = \underline{J}_c + \underline{j}$), J the total angular momentum ($\underline{J} = \underline{\ell} + \underline{s}$). M_J its components (assumed to be averaged over) and π is the total parity. The wavenumber of the incident channel is given by K_c, and T_ℓ are transmission coefficients. The $\bar{\sigma}_{cc'}$ for each compound nucleus state of spin J and parity π can be factorised into (Bohr assumption):

$$\bar{\sigma}^{J\pi}_{cc'} = \bar{\sigma}^{J\pi}_{cN}(c) \frac{\sum_{s'\ell'} T_{\ell'}(c')}{\sum_{s''\ell''} T_{\ell''}(c'')} \,. \qquad (C-2)$$

where $\bar{\sigma}^{J\pi}_{cN}(c)$ is the cross-section for the formation of the compound nucleus. The second term is a branching ratio which gives the probability that the compound nucleus will decay by channel c'.

In the case of photo absorption mechanism, $\sigma_{cN}(c)$ is just the Giant dipole resonance (GDR) total photon absorption cross-section (assuming $J^{\pi} = 1^{-}$, and no direct or pre-equilibrium GDR decays). Therefore the equation (C - 2) yields

$$\bar{\sigma}_{\gamma,n} = \bar{\sigma}_{cN}(\gamma) \frac{\sum_{s'\ell'} T_{\ell'}(n)}{\sum_{s''\ell''} T_{\ell''}(c'')} \qquad (C\text{-}3)$$

where $\bar{\sigma}_{cN}(\gamma)$ is the total photo-neutron cross-section. For the cases, for example (γ, p) and (e, α), a similar expression can be written, i.e.

$$\bar{\sigma}_{\gamma,p} = \bar{\sigma}_{\gamma,n} \frac{\sum_{s'\ell'} T_{\ell'}(p)}{\sum_{s''\ell''} T_{\ell''}(n)} \qquad (C\text{-}4)$$

and for (e,α),

$$\bar{\sigma}_{\gamma,\alpha} = \bar{\sigma}_{\gamma,n} \frac{\sum_{s'\ell'} T_{\ell'}(\alpha)}{\sum_{s''\ell''} T_{\ell''}(n)} \qquad (C\text{-}5)$$

Equations (C-4) and (C-5) can then be written in the appropriate form for the proton and α-particle energy distribution, i.e.

$$\frac{d\bar{\sigma}}{dE_p}(E_\gamma) = \bar{\sigma}_n(E_\gamma) \frac{\sum_{s'\ell'} T_{\ell'}(E_\gamma, E_p)}{\sum_{s''\ell''} T_{\ell''}(n)} \qquad (C\text{-}6)$$

and for (e,α)

$$\frac{d\bar{\sigma}}{dE_\alpha}(E_\gamma) = \bar{\sigma}_n(E_\gamma) \frac{\sum_{s'\ell'} T_{\ell'}(E_\gamma, E_\alpha)}{\sum_{s''\ell''} T_{\ell''}(n)} \; . \qquad (C\text{-}7)$$

REFERENCES

1) A.G. Flowers, Ph.D. Thesis, University of Edinburgh (1979).

2) P.G. Thorely, Ph.D. Thesis, University of Edinburgh (1980).

3) T.A. Gabriel and R.G. Alsmiller, Phys. Rev. 182, 1035 (1969).

4) J.R. Wu and C.C. Chang, Phys. Rev., C16, 1812 (1977).

5) J.S. Levinger, Phys. Rev. 84, 43 (1951).

6) A. Mignerey, M. Blann and W. Scobel, Nucl. Phys. A287, 301 (1977).

7) J.M. Eisenberg and W. Greiner, Nuclear Theory, Vol. 2 (1976).

8) G. Ricco, International School on Electro- and Photo-Nuclear Reactions I, S. Costa and C. Schaerf, Eds., Lecture Notes in Physics, Vo. 61 (Springer-Verlag, Berlin, 1977) p. 223.

9) B. Ziegler, Lecture Note in Physics, 86, 101 (1978).

10) [a] A. Leprêtre, H. Beil, R. Begère, P. Carlos, J. Fagot, A. Deminiac and A.V. Veyssière, Nucl. Phys. A367, 237 (1981).

[b] P. Carlos, H. Beil, R. Bergère, B.L. Berman, A. Leprêtre, and A. Veyssière, Nucl. Phys. A378, 317 (1982).

11) D.J.S. Findlay, D.J. Gibson, R.O. Owens and J.L. Matthews, Phys. Lett. 79B (1978) 356.

12) [a] H. Goringer and B. Schoch, Phys. Lett. 97B, 41 (1980).

[b] M. Sené, Ph.D. Thesis, University of Edinburgh, (1982).

13) J.S. Levinger, Phys. Lett. 82B, 181 (1979).

14) J.M. Laget, Nucl. Phys. A312, 265 (1978).

15) J.L. Matthews, Ph.D. Thesis, M.I.T. (1967).

16) K. Gottfried, Nucl. Phys. 5, 557 (1958).

17) T.J. Kopaleishvili and Jibuti, Nucl. Phys. 44, 34 (1963).

18) S. Fujii, Nuovo Cimento 25, 995 (1962).

19) A. Reitan, Nucl. Phys. 36, 56 (1962).

20) E. Østgaard, Nucl. Phys. 64, 289 (1965).

21) E. Bramanis, Nucl. Phys. A175, 17 (1971); A193, 323 (1972).

REFERENCES (Contd.)

22) H. Hebach, A. Wortberg and M. Gari, Nucl. Phys. A267, 425 (1976).

23) M. Gari and H. Hebach, Phys. Rept. 72, 1 (1981)

24) J.M. Laget, Nucl. Phys. A358, 275 (1981).

25) C.T. Noguchi and F. Parts, Phys. Rev. C14, 1133 (1976).

26) C.T. Noguchi and F. Parts, Phys. Rev. Lett., Vol. 33, 1168 (1974).

27) W. Weise and M.G. Huber, Nucl. Phys. A162, 330 (1971).

28) M. Fink, H. Hebach and H. Kummel, Nucl. Phys. A186, 353 (1972).

29) A. Malecki and P. Picchi, Nuovo Cimento Lett. 8, 16, (1973).

30) B. Schoch, Phys. Rev. Lett. 41, 80 (1978).

31) G.G. Taran, Yad. Fiz. 7, 478 (1968) [Sov. J. Nucl. Phys. 7, 301 (1968)].

32) N. Bohr, Nature 137, 344 (1936).

33) R. Serber, Phys. Rev. 72, 1114 (1947).

34) V.A. Sidorov, Nucl. Phys. 35, 253 (1962).

35) J.M. Miller, Proceedings of the International Conference on Nuclear Physics, Vol. 2, 597 (1973).

36) J.J. Griffin, Phys. Rev. Lett. 17, 478 (1966).

37) M. Blann, Phys. Rev. C17, 1871 (1978).

38) E. Gadioli, E. Gadioli Erba and G. Tagliaferri, Phys. Rev. C17, 2238 (1978).

39) H. Feshbach, A. Kerman, and S. Koonin, Ann. Phys. (N.Y.) 125, 429 (1980).

40) M. Blann, Ann. Rev. Nucl. Sci. 25, 123 (1975).

41) A. Mignerey, Ph.D. Thesis, Rochester, U.S.A., unpublished (1975).

42) M. Blann, A. Mignerey and W. Scobel, Nukleonika 21, 335 (1976).

43) C. Kalbach, Phys. Rev. C23, 124 (1981).

44) A. Ferrero, E. Gadioli, E. Gadioli Erba, I. Iori, N. Molko and L. Zetta, Z. Phys. A293, 123 (1979).

REFERENCES (Contd.)

45) K. Chen, Z. Fraenkel, G. Friedlander, J.R. Grover, J.M. Miller and Y. Shimamoto, Phys. Rev. 166, 949 (1968).

46) H.W. Bertini, Phys. Rev. C5, 2118 (1972); C6, 631 (1972).

47) A. Galossky, R.R. Doering, D.M. Patterson and H.W. Bertini, Phys. Rev. C14, 748 (1976).

48) A.S. Iljinov, V.I. Nazaruk and S.E. Chigrinov, Nucl. Phys. A268, 513 (1976).

49) H.C. Chiang and J. Hüfner, Nucl. Phys. A349, 466 (1980).

50) R.J. Glauber and G. Marthiae, Nucl. Phys. B21, 135 (1970).

51) W.Q. Chao, F. Hachenberg and J. Hüfner, Nucl. Phys. A384, 24 (1982).

52) [a] T. Tamura, T. Udagawa, D.H. Feng and K.K. Kan, Phys. Lett. 66B, 109 (1977).

[b] T. Tamura, T. Udagawa, and H. Lenke, Phys. Rev. C26, 379 (1982).

[c] T. Tamura and Udagawa, Phys. Lett. 78B, 189 (1978).

53) R. Weiner and M. Westrom, Phys. Rev. Lett. 34, 1523 (1975)

54) N. Stetle, M. Westrom, R.M. Weiner, Private communication (1981).

55) A.G. Flowers, D. Branford, J.C. McGeorge, A.C. Shotter, P.J. Thorley, C.H. Zimmerman, R.O. Owens and J.S. Pringle, Phys. Rev. Lett. 43, 323 (1979).

56) L. Westerberg, D.G. Sarantites, D.C. Hensley, R.A. Dayras, M.L. Halbert and J.H. Barker, Phys. Rev. C18, 796 (1978).

57) J. Goldberg in Peyrou Festschrift, Ed. by Armenteros, Burger and Prentki, Geneva, p. 51 (1978).

58) G.D. Harp and T.M. Miller, Phys. Rev. C3, 1847 (1971).

59) C.K. Cline and M. Blann, Nucl. Phys. A172, 225 (1971).

60) D. Agassi, H.A. Weidenmüller and G. Mantzouranis, Phys. Reports C22, 147 (1975).

61) G. Mantzouranis, H.P. Weidenmüller and D. Agassi, Z. Phys. A276, 145 (1976).

62) G. Mantzouranis, Phys. Rev. C14, 2018 (1976).

REFERENCES (Contd.)

63) P. Madler and R. Reif, Nucl. Phys. A373, 27 (1982).

64) P. Madler and R. Reif, Nucl. Phys. A337, 445 (1980).

65) R. Bonelli, M. Camnasio, L. Colli Milazzo and P.E. Hodgson, Phys. Rev. C24, 71 (1981).

66) O.A.P. Tavares, J.D. Pinheiro Filho, V. Di Napoli, J.M. Martins and M.L. Terranova, Nuovo Cim. Lett. 27, 358 (1980).

67) J. Ahrens, B. Borchert, K.H. Czock, H.B. Eppler, H. Gimm, H. Gundrum, M. Kröning, P. Riehn, G. Sita Ram, A. Zieger and B. Ziegler, Nucl. Phys. A251, 479 (1975).

68) H. Schier and B. Schoch, Nucl. Phys. A229, 93 (1974).

69) F. Partovi, Ann. Phys. 27, 79 (1964).

70) Y.S. Kim, Phys. Rev. 129, 1293 (1963).

71) J.L. Matthews, W. Bertozzi, S. Kowalski, C.P. Sargent and W. Turchinetz, Nucl. Phys. A112, 654 (1968).

72) A. Kose, W. Paul, K. Stockhurst and K.H. Kissler, Zeit. Phys. 202, 364 (1967).

73) H.W. Koch and J.W. Motz, Rev. Mod. Phys. 31, 920 (1959).

74) J.L. Matthews and R.O. Owens, Nucl. Instr. and Meth., 111, 157 (1973)

75) W.W. Gargaro and D.S. Onley, Phys. Rev. C4, 1032 (1971).

76) W. Scobel, A. Mignerey and M. Blann, Nucl. Phys. A273, 125 (1976).

77) P. Plischke, W. Scobel and M. Borman, Z. Physik, A281, 245 (1977).

78) H. Keuser, Diplomarbeit, Bonn, Germany, unpublished (1980).

79) P.E. Hodgson, Growth Points in Nuclear Physics, Vol. 1, p. 140 (1980).

80) J. Bisplinghoff, M. Blann, H. Keuser, Proceedings of the International Workshop on "Reaction Models for Continuous Spectra of Light Particles", Bad Honnef (1978).

81) R. Bonetti, L. Milazzo Colli and G.M. Braga Marcazzan, J. Phys. G: Nucl. Phys. 4, 1903 (1978).

82) C. Kalbach, Z. Physik A283, 401 (1977).

83) P.G. Thorely, Edinburgh Nuclear Structure Group, unpublished data (1981).

REFERENCES (Contd.)

84) B.L. Berman and S.C. Fultz, Rev. Mod. Phys. 47, 713 (1975).

85) N. Shikazono and T. Terasawa, Nucl. Phys., A250, 260 (1975).

86) P.J. Dalimore, Australian National University, Report No. ANU-P/512 (1970).

87) J.J. Hogan, Z. Physik A295, 169 (1980).